# 論文 / 著書情報
# Article / Book Information

| | |
|---|---|
| 題目(和文) | |
| Title(English) | Injectable Enzymatically Crosslinked hydrogel Systems for Drug Delivery and Tissue Engineering |
| 著者(和文) | LEE Fan |
| Author(English) | Lee Fan |
| 出典(和文) | 学位:博士(工学),<br>学位授与機関:東京工業大学,<br>報告番号:乙第4132号,<br>授与年月日:2016年6月30日,<br>学位の種別:論文博士,<br>審査員:早川　晃鏡,柿本　雅明,手塚　育志,高田　十志和,石曽根　隆,芹澤　武 |
| Citation(English) | Degree:Doctor (Engineering),<br>Conferring organization: Tokyo Institute of Technology,<br>Report number:乙第4132号,<br>Conferred date:2016/6/30,<br>Degree Type:Thesis doctor,<br>Examiner:,,,,, |
| 学位種別(和文) | 博士論文 |
| Type(English) | Doctoral Thesis |

# INJECTABLE ENZYMATICALLY CROSSLINKED HYDROGEL SYSTEMS FOR DRUG DELIVERY AND TISSUE ENGINEERING

**FAN LEE**

## Abstract

Hydrogels are physically/chemically crosslinked natural/synthetic polymers; they are widely used as biomaterials for drug delivery and tissue engineering. In particular, injectable hydrogel systems have drawn a lot of attention because of the elimination of surgical implantation. Although several *in situ* crosslinking strategies have been developed for the formation of injectable hydrogels, the crosslink density and gelation rate of most existing systems cannot be independently tuned. Crosslink density is an important parameter because it affects the rate of hydrogel degradation, the rate of drug release, and the viability, proliferation and differentiation of encapsulated cells. On the other hand, the gelation rate of an injectable hydrogel system should be tunable based on the application requirement.

In this thesis, injectable hydrogel systems composed of polymer-phenol conjugates were developed for various biomedical applications. First, a hydrogel system composed of hyaluronic acid-tyramine (HA-Tyr) conjugates was designed. The HA-Tyr conjugates were crosslinked by the oxidative coupling of tyramine moieties in the presence of horseradish peroxidase (HRP) and hydrogen peroxide ($H_2O_2$). It was shown that HRP predominantly controlled the gelation rate of the hydrogel, while $H_2O_2$ controlled the crosslink density. The HA-Tyr hydrogel system was applied for the delivery of interferon-α2a (IFN-α2a) and trastuzumab, which are therapeutic proteins used in cancer treatment. The aim was to reduce the injection frequency of the proteins *via* sustained release from hydrogels, while not compromising the therapeutic outcome. Two methods were developed to achieve sustained release of the proteins from the hydrogels. First, the crosslink density of hydrogel was varied to control the release rate of proteins. Second, electrostatic interactions between the proteins and the hydrogel were employed to immobilize the proteins in the hydrogel, and the release was regulated by hydrogel degradation. Using mice xenograft models of human cancers, it was demonstrated that the sustained release of proteins from hydrogels more effectively inhibited tumor growth than bolus injections.

In addition, a dextran-tyramine (Dex-Tyr) hydrogel, which was formed by HRP-mediated crosslinking reaction and contained poly(ethylene glycol) (PEG) microdomains, was developed for the sustained delivery of PEGylated IFN-α2a (PEG-IFN-α2a). It was shown that the release rate could be tuned by the PEG domain size, which in turn was controlled by the gelation rate. Remarkably, a one-time administration of PEG-IFN-α2a-loaded hydrogel

provided sustained delivery of the protein for 3 months, and prevented liver injury as effectively as weekly administration of the protein in a humanized mice model of hepatitis C.

Besides protein delivery, the enzymatically crosslinked HA-Tyr hydrogel system was also used in tissue engineering applications. The goal of tissue engineering is to construct tissues from a combination of cells and scaffold materials. One of the challenges associated with tissue engineering is the insufficient vascularization of the tissue construct, which compromises the survival of embedded cells after transplantation. To address this challenge, two methods of vascularizing HA-Tyr hydrogels were developed. First, an interpenetrating polymer network (IPN) hydrogel composed of fibrin and HA-Tyr was formed. Compared to fibrin gels, the IPN hydrogels demonstrated improved structural stability against cell-induced contraction and degradation by proteases, while maintaining cell proliferation and capillary network formation. Second, an Arg-Gly-Asp (RGD) peptide containing phenol moieties ($Ph_2$-PEG-RGD) was designed for *in situ* conjugation into the HA-Tyr network during HRP-mediated crosslinking reaction. Conjugation of the peptide significantly improved cell adhesion, migration and capillary network formation in the hydrogel. *In vivo* study confirmed that functional vasculature could be formed in the peptide-conjugated hydrogels within two weeks post-injection. In addition, the HA-Tyr hydrogel system was investigated as a 3D culture system for the propagation of human embryonic stem cells, which are the most promising cell source for tissue engineering.

Lastly, a bioactive hydrogel composed of HA-(-)-epigallocatechin-3-gallate (HA-EGCG) conjugates was developed as an injectable and degradation-resistant system. EGCG is a green tea catechin that is known for various health benefits, therefore the conjugation of EGCG to HA would endow the resulting conjugates with the bioactivities of EGCG. Indeed, HA-EGCG conjugates exhibited radical scavenging, anti-proliferative and enzyme-inhibiting properties. Moreover, it was shown that the $H_2O_2$ produced by EGCG autoxidation in aerobic condition could serve as the oxidant in the HRP-mediated coupling of EGCG. Thus the addition of HRP alone induced the gelation of a solution HA-EGCG conjugates within a few minutes. Moreover, HA-EGCG hydrogels degraded slower *in vivo* compared with HA-Tyr hydrogels, which was attributed to the enzyme-inhibiting properties of EGCG moieties. Furthermore, it was demonstrated that hydrogels could be formed through EGCG coupling *via* quinone formation even in the absence of HRP. The HRP-free gelation is a promising alternative approach to form injectable hydrogels composed of polymer-phenol conjugates, as it circumvented the safety concern associated with HRP due to its plant origin.

**Acknowledgement**

First, I would like to express my sincere gratitude to Dr Motoichi Kurisawa, who introduced me to the field of biomaterials back in 2005, and has been a mentor since. Thank you very much for opening the door to biomaterials research, which to this day I am thrilled to be part of, and for your patience, guidance and encouragement in the last ten years. Second, I would like to thank Professor Teruaki Hayakawa for his tremendous support in my pursuit for PhD. I am indebted to you for your kindness and help. Indeed, without your invaluable support and advice, none of this would have been possible. I would also like to express my heartfelt gratitude to IBN directors, Professor Jackie Y. Ying and Ms Noreena AbuBakar. Thank you very much for your constant support and encouragement over the years, and for providing a wonderful research environment at IBN.

I would like to thank my co-workers who I have worked closely with, Dr Joo Eun Chung, Dr Lishan Wang, Dr Keming Xu, Dr Ki Hyun Bae, Dr Gao Shu Jun, and Dr Jaehong Lim. Thank you very much for all the help you have rendered to me, the fruitful discussions and helpful comments. This thesis would not be in its present form without you. I would also like to thank Dr Susi Tan, Dr Liang Kun, Dr Atsushi Yamashita, Nunnarpas Yongvongsoontorn, Chixuan Liu, Dr Li Li and Dr Ng Sheng Yong. Thank you all for the various ways you have helped me, for your company in the lab and the laughers we shared. I also want to thank Dr Michael Reithofer for the help and training in NMR measurement, and Dr Su Seong Lee for access to LC-MS.

I would like to thank the undergraduate research students who I had the privilege to mentor, especially Seow Wan Yi, Sui Har Choy, Clara Fu, Janice Jang, and Esther Peh. Thank you for the assistance you have provided. I thank also the collaborators and co-authors who have contributed to the publications, including Dr Hirohisa Yano, Dr Karthikeyan Narayanan, Dr Chan Du, Dr Andrew C.A. Wan, Dr Qingfeng Chen, Dr Choong Tat Keng, Sue Yee Tan and Yee Joo Tan. I thank JNC Corporation (Tokyo, Japan) for the generous supply of hyaluronic acid. This research was funded by the Institute of Bioengineering and Nanotechnology (Biomedical Research Council, A*STAR, Singapore).

Last but not the least; I would like thank my beloved fiancée, Jolene, my ever-supportive family and church friends, for all your prayers and encouragement. I am blessed to have you in my life.

*February 2016*

## Table of Content

# Chapter 1

# General Introduction

## 1.1. Introduction

Hydrogels are crosslinked polymeric networks capable of retaining water. Both natural and synthetic polymers have been used to form hydrogels. The polymers are crosslinked through either physical interactions or chemical bonds, resulting in a network that swells in water while maintaining a defined 3D structure. The amount of water in a hydrogel is generally greater than 50% of the total weight [1]. In some cases hydrogels can absorb water up to several thousand times of the weight of the polymer used to form the gel [2]. The high water content results in a transparent material, which is an important feature in the development hydrogel-based contact lens composed of crosslinked poly(hydroxyethyl methacrylate) (pHEMA). This is credited as the pioneering work of hydrogels in the biomedical field [3, 4]. Because hydrogel is similar to soft tissues in terms of its rubbery nature, it causes little mechanical and frictional irritation to the surrounding tissues when placed in the body. Therefore, hydrogels have also been used for *in vivo* applications, such as a coating on the inner surface of blood vessels to minimize thrombosis following surgery-induced tissue injuries [5], and as a barrier between tissues to prevent post-operative adhesion formation [6]. In the last few decades, hydrogels have emerged as one of the main class of biomaterials for drug delivery and tissue engineering

### 1.1.1. Hydrogels in protein delivery

The aqueous environment within a hydrogel is particularly suitable for the encapsulation of proteins, which are prone to denaturation in non-aqueous environment. Therefore hydrogels have been employed as a delivery system for therapeutic proteins [1, 7-10]. The first protein to be administered for therapeutic purposes was insulin, for the treatment of diabetes mellitus. Initially, insulin was isolated from animal pancreases; however, limited availability of animal pancreases and immune response to animal proteins restricted the usage of this protein. Subsequently, recombinant DNA technology was developed, which made possible the large-scale production of human insulin for widespread use. Currently, there are more than 130 therapeutic proteins or peptides approved by the US Food and Drug Administration (FDA), and more than 70% of which are produced recombinantly [11]. These therapeutic proteins are used to treat a variety of illnesses, including cancer, hemophilia A, hepatitis C, multiple sclerosis and osteoporosis [11]. New screening libraries for peptide-based drugs [12] and novel protein engineering methods for modulation of protein properties (such as efficiency, stability and specificity) are currently under research [13]. These efforts

pave the way for the discovery of novel therapeutic proteins. Nevertheless, the method of administrating these delicate biomolecules remains to be optimized before the benefits can be fully realized.

Presently, therapeutic proteins are administered mainly through the parenteral routes *via* intravenous, subcutaneous or intramuscular injections. However frequent injections are required to maintain the concentration of proteins within the therapeutic window as the proteins are rapidly cleared from the blood stream through renal filtration and proteolysis. For instance, interferon-α (IFN-α), a cytokine that is used to treat hepatitis C, has a short circulating half-life of 6−8 h in human [14]. As a result, frequent injections (thrice-weekly) are needed throughout the entire course of therapy, which can be up to 6 months or more. Frequent injections cause considerable patient discomfort, lack of compliance, as well as increased cost of treatment due to the requirement for trained medical personnel [15]. These drawbacks prompted the development of technologies that could extend the half-life of therapeutic proteins *in vivo*, including post-production modifications such as PEGylation [16]; and the encapsulation of proteins in drug delivery systems (DDS), such as liposomes, microspheres, and more recently, hydrogels [1, 8].

The concept of protein delivery using hydrogels is to incorporate therapeutic proteins within the crosslinked polymeric network, which limits the mobility of the proteins and results in slow release from the hydrogel over an extended period of time. Consequently, the half-life of the proteins in the body is increased and the frequency of injection can be decreased. Furthermore, the crosslinked polymeric network could protect the incorporated proteins from proteolytic degradation by minimizing exposures to proteases. Nevertheless, only a limited number of hydrogel systems have been tested in animal models, and even less has reached clinical trials. One of the challenges in using hydrogels for protein delivery is to introduce the hydrogels non-invasively into the body. While preformed hydrogels require invasive techniques to be implanted in the body, injectable hydrogel systems allow the gel precursors to be injected as an aqueous solution using a syringe, which is then followed by gelation *in situ*. It is important that hydrogels are formed rapidly after injection, because leakage of the proteins to the surrounding tissue can occur if the gelation rate is too slow. Other challenges associated with protein delivery using hydrogels include the suppression of burst release and the extension of release duration.

### 1.1.2. Hydrogels in tissue engineering

In addition to protein delivery, hydrogels are also used as scaffolds for tissue engineering [17-24]. The primary aim of tissue engineering is to construct tissues from a combination of cells and scaffold materials, the latter serve to support the cells in a 3D environment and provide appropriate mechanical and/or biological cues. The engineered tissues are either placed directly in the patient's body, or allowed to mature *ex vivo* prior to transplantation. Once transplanted, the engineered tissues can promote healing of damaged or diseased tissues, or achieve therapeutic effects through restoration of tissue functions (this is also known as regenerative medicine). An example of engineered tissues is the skin substitute Dermagraft®, which is approved by the FDA in the United States for the treatment of diabetic foot ulcers. Dermagraft® is composed of human neonatal fibroblasts seeded on a biodegradable poly(lactic-*co*-glycolic acid) (PLGA) mesh [25]. Besides *in vivo* applications, engineered tissues can also be used for the testing of drug metabolism and toxicity *in vitro*.

Hydrogel is an attractive scaffold material for tissue engineering because the aqueous 3D environment is suitable for cell encapsulation. Cohesion between hydrogel and the surrounding tissue can be achieved by first filling the irregularly-shaped wound with an aqueous mixture of gel precursors and cells, and then initiate gelation *in situ*. Moreover, injectable hydrogel systems allow clinicians to administer the gel precursors and cells into the patient non-invasively, unlike preformed porous scaffolds made of synthetic polymers which require surgical implantation. By controlling the stiffness of the hydrogel and incorporating ECM-derived growth factors, proteins or bioactive peptides, a hydrogel can recapitulate both the mechanical as well as the biological aspects of the native tissue. Presently, pancreatic islets encapsulated in hydrogels are in clinical trials for the treatment of type 1 diabetes mellitus [26]. Significant efforts in engineering cartilage tissue using hydrogels are also underway [27]. One of the challenges of tissue engineering is the formation of a vascular network within the tissue construct, which is essential in the engineering thick and complex tissues, because blood vessels are required in the transportation of nutrients and other biomolecules to ensure the viability of the embedded cells [28]. In addition, cell source is another bottle neck in tissue engineering. At the moment, stem cells are the most promising source as they have unlimited self-renewal capability [29] and can differentiate into specialized cell types. However, the large-scale expansion of stem cells without animal-derived components remains a challenge.

## 1.2. Polymers used to form biodegradable hydrogels

In the engineering of tissues for the replacement of defective body parts, hydrogel serves as a temporary scaffold to support the cells in a 3D environment until it is replaced by the ECM secreted by the embedded cells. Hence hydrogels should be biodegradable to allow eventual resoprtion by the body. For protein delivery application, biodegradable hydrogels are also desirable because they can facilitate the release of incorporated proteins through network degradation, which eliminates the need for surgical retrieval of the hydrogels. Both synthetic and natural polymers have been used to form biodegradable hydrogels.

### 1.2.1. Synthetic polymers

One of the most commonly used synthetic polymers for hydrogel formation is poly(ethylene glycol) (PEG) (Fig. 1-1a and b), which is a water-soluble polyether. A wide range of PEG molecular weight is available in linear and branched geometry. PEG degrades very slowly *in vivo*, hence it has been co-polymerized with polyesters such as poly(lactic acid) (PLA), poly(lactic-*co*-glycolic acid) (PLGA) or poly(*ε*-caprolactone) (PCL) to form diblock or triblock copolymers (Fig. 1-1c, d and e) that are biodegradable through hydrolysis of the ester bonds. An advantage of PEG-polyester block copolymers is that they exhibit spontaneous temperature-induced physical gelation, which is attributed to micelle formation and association [30]. However, one concern associated with PLGA block copolymer is that the degraded products (lactic acid and glycolic acid) can reduce the local pH of the surrounding environment, resulting in decreased cell viability [31] or denaturation of incorporated proteins [32]. Alternatively, PEG hydrogel can be made biodegradable by introducing matrix metalloproteinase (MMP)-sensitive peptide as the crosslinkers [33].

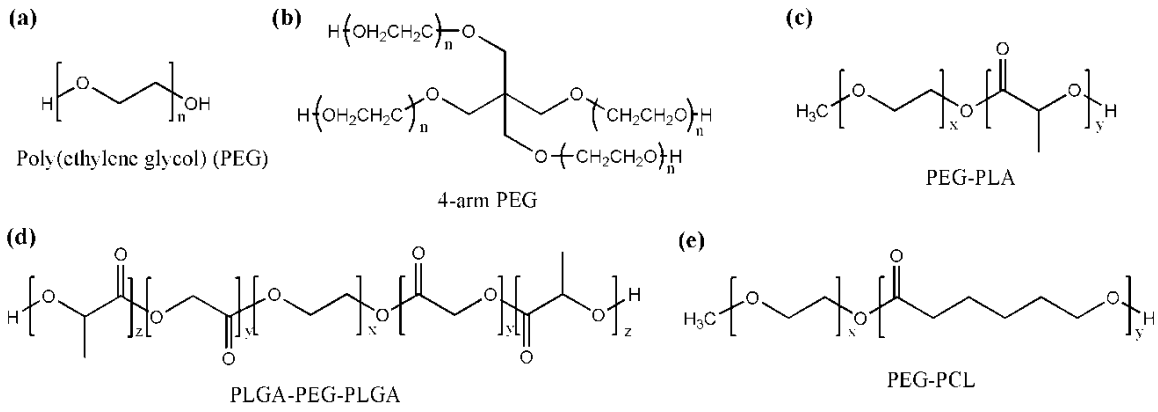


**Fig. 1-1. Chemical structures of commonly used synthetic polymers for hydrogel formation.**

### 1.2.2. Natural polymers

Natural polymers used to form hydrogels are broadly divided into two categories− polysaccharides and proteins. Commonly used polysaccharide-based polymers for hydrogel formation include hyaluronic acid (HA), alginate, dextran and chitosan (Fig. 1-2). Commonly used protein-based polymers include collagen, gelatin and fibrin. Unlike synthetic polymers which are typically degraded by hydrolysis of ester bonds, natural polymers are degraded mainly by enzymes. Natural polymers are more advantageous than synthetic polymers in terms of their biological properties. For instance, collagen and HA are major components of the ECM and possess inherent biological properties that are desirable for tissue engineering applications. Collagen interacts with integrins and HA interacts with CD44; these cell-matrix interactions facilitate cell adhesion and/or elicit cellular pathways. Among the natural polymers, HA is one of the most widely used to form hydrogels because of its availability, biodegradability, viscoelastic property and versatility in chemical modifications [34]. Importantly, HA is a FDA-approved material for osteoarthritis treatment *via* intra-articular injection. The following section provides a summary of HA, including its biological functions, clinical uses and methods of chemical modification.

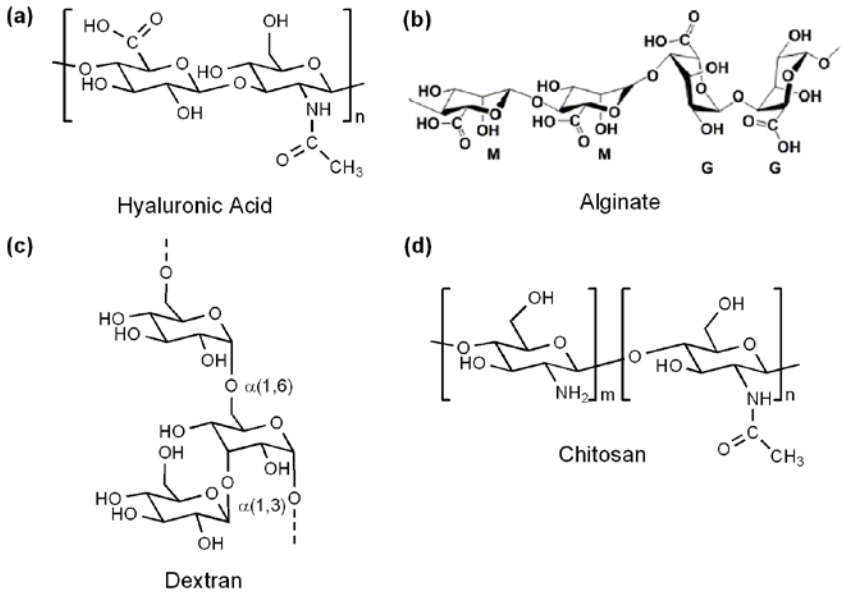


**Fig. 1-2. Chemical structures of commonly used polysaccharides for hydrogel formation. (a) Hyaluronic acid (HA), (b) alginate [35] (M = β-D-mannuronic acid, G = α-L-guluronic acid), (c) dextran and (d) chitosan.**

### 1.2.3. Hyaluronic acid

Hyaluronic acid (HA) is a unbranched, non-sulfated glycosaminoglycan (GAG) composed of repeating disaccharide units of β-1,4-D-glucuronic acid and β-1,3-*N*-acetyl-D-glucosamine

(Fig. 1-2a). HA is also known as sodium hyaluronate because both in physiological condition and in most commercial products, HA is found in the form of sodium salt. HA was first isolated from bovine vitreous by Karl Meyer in 1934 [36], since then HA has been identified in various human and non-human tissues (Table 1-1). HA is present at the ECM of connective tissues in all vertebrates. In human, about half of the body's HA is found in the skin, and high concentrations are present in the synovial fluid, vitreous humor of the eye and umbilical cord. Besides vertebrates, HA is also present in some bacteria, e.g. in the capsules of *Streptococcus pyogenes*. The HA capsules bind to CD44 receptors on the surface of keratinocytes, facilitating the attachment of bacteria during the initial colonization [37, 38]. HA is absent in fungi, plants and insects [39].

**Table 1-1.** Concentration of HA in different tissues [39]

| Tissue or body fluid | Concentration (μg/ml) | Remarks |
|---|---|---|
| Rooster comb | 7500 | The animal tissue with by far the highest HA content |
| Human umbilical cord | 4100 | Contains primarily HA with a relatively high molar mass |
| Human joint (synovial) fluid | 1400-3600 | The volume of the synovial fluid increases under inflammatory conditions. This leads to a decreased HA concentration. |
| Bovine nasal cartilage | 1200 | Often used as a cartilage model in experimental studies |
| Human vitreous body | 140-340 | HA concentration increases upon the maturation of this tissue |
| Human dermis | 200-500 | Suggested as a "rejuvenating" agent in cosmetic dermatology |
| Human epidermis | 100 | HA concentration is much higher around the cells that synthesize HA |
| Rabbit brain | 65 | HA is supposed to reduce the probability of occurrence of brain tumors |
| Rabbit heart | 27 | HA is a major constituent in the pathological matrix that occludes the artery in coronary restenosis |
| Human thoracic lymph | 0.2-50 | The low molar mass of this HA is explained by the preferential uptake of the larger molecules by the liver endothelial cells |
| Human urine | 0.1-0.3 | Urine is also an important source of hyaluronidase |
| Human serum | 0.01-0.1 | HA concentrations increase in serum from elderly people as well as in patients with rheumatoid arthritis and liver cirrhosis |

In human, HA is synthesized by a family of enzymes located in the plasma membrane, known as HA synthase (HAS) [40]. There are three enzymes in the HAS family (HAS1-3) that differ in their catalytic activity, with HAS3 being the most catalytically active [41]. Newly synthesized HA is extruded directly into the ECM, where HA is a major constituent

[42]. The molecular weight of HA in the human body ranges from $10^4$ to $10^7$ Da. HA is catabolized locally by internalization and degradation within the tissues, or drained into the lymphatic systems for metabolic degradation. HA that is returned into the blood vasculature is cleared by sinusoidal endothelial cells in the liver [43]. The enzymes responsible for the degradation of HA in the body are known as hyaluronidase. The three main types of hyaluronidase are HYAL1, HYAL2 and PH-20 [41, 44]. HYAL1 is a lysozomal enzyme, but is also found in serum and urine at low concentrations [44]. It cleaves HA into small fragments of 2-10 disaccharide units. HYAL2 is a glycophosphatidylinositol (GPI)-anchored protein found at the plasma membrane, it cleaves HA to around 50 disaccharide units [41]. PH-20 is mammalian sperm plasma-membrane protein, it helps the sperm to traverse the HA-rich layer surrounding an egg during fertilization [44].

#### 1.2.3.1. Biological roles of HA

HA plays important roles in the body despite its simple molecular structure. Unlike other GAGs, HA is not covalently linked to a core protein but serves as a template for the binding of aggrecan, an ECM proteoglycan. HA-aggrecan aggregates, together with collagen, confer the load bearing property of the cartilage. Cellular events, such as proliferation and migration, have been shown to depend on the concentration of HA in the ECM. For instance, increase in HA concentration leads to a hydrated matrix that allow cells to divide and migrate [45]. During wound healing, HA concentration in the milieu of a fibrin clot increases, which help to stabilize the volume and structure of the fibrin clot [46]. In addition to its hydrating and space-filling functions, HA also plays important biosignaling roles through interactions with cell surface receptors, such as CD44, receptor for hyaluronate-mediated motility (RHAMM), HA receptor for endocytosis (HARE), and lymphatic vessel endothelial hyaluronan receptor (LYVE-1) [47]. Among the different receptors, CD44 is the most extensively studied and is known to be involved in cell differentiation, proliferation, and migration. HA-CD44 interaction is also implicated in tumor progression and metastasis [48]. Interestingly, interactions between HA and its receptors elicit different and often opposing cellular processes depending on the molecular weight of HA. For instance, native high molecular weight HA is anti-angiogenic and inhibits endothelial cell proliferation and capillary formation [41]. On the contrary, HA oligomers (3-10 disaccharide units; 1-4 kDa) promote angiogenesis through stimulation of collagen synthesis [49], endothelial cell proliferation, migration, and capillary sprout formation [41, 49]. HA oligomers produced by reactive oxygen species that are present at the sites of injury or inflammation have also been shown to

induce the expression of proinflammatory cytokines [41, 50]. For example, 28 kDa HA induced the production of biologically active interleukin-12 by elicited macrophages; whereas1000 kDa HA did not induce the same response [51].

#### 1.2.3.2. Clinical applications of HA

The water-retaining and viscoelastic properties of HA makes it a suitable material for various medical and cosmetic applications. For instance, intra-articular (i.a.) injection of HA for the treatment of knee osteoarthritis (OA), also known as viscosupplementation, was performed as early as in the 1970s [52]. Several clinical trials conducted in the past few decades suggested that i.a. injections of HA is effective in relieving pain, albeit with a delayed onset compared to i.a. injection of steroids [52-54]. The typical treatment regime composed of 3 to 5 weekly injections, providing pain relief for up to 6 months [53, 54]. The mechanism through which HA provides pain relief is not fully understood. However, research suggested that HA inhibits nociceptor activation, promotes GAGs synthesis and modulates the expressions of proinflammatory cytokines and proteases [53, 55]. Table 1-2 lists some of the commercially available HA products for OA treatment. HA has also used in ophthalmology, as it is the major component of the vitreous humor. Exogenous HA is applied during eye surgeries to replace the lost vitreous volume, and to protect the corneal endothelium from mechanical trauma. In addition, HA has been incorporated in artificial tear formulations for the treatment of dry eye syndrome [56]. HA has also been applied for wound healing applications [39], and lightly crosslinked HA is used as dermal filler to augment facial wrinkles and scars [57]. HA in commercial products is extracted from rooster's comb, however, contamination with animal proteins/pathogens is a major concern. More recently, HA is being produced by bacterial fermentation, which is free from animal pathogens [58]. Producing HA with uniform molecular weight is the subject of current research.

**Table 1-2.** Commercially available HA products for the treatment of osteoarthritis

| | **SUPARTZ** | **HYGLAN** | **SYNVISC** | **SYNVISC ONE** |
|---|---|---|---|---|
| Manufacturer | Seikagaku Corporation | Fidia Farmaceutical | Genzyme Corporation | |
| HA MW (kDa) | 620 - 1,170 | 500 - 730 | Hylan A – 6,000, Hylan B – hydrated gel | |
| HA concentration | 1.0% | 1.0% | 0.8% | |
| Dose per syringe | 2.5 ml | 2 ml | 2 ml | 6 ml |
| Injection regimen | Once a week for 3-5 wks | Once a week for 3-5 wks | Once a week for 3 wks | One injection |

### 1.2.3.3. Chemical modifications of HA

HA has been chemically modified to produce derivatives for different biomedical applications. Different functional groups, drugs and peptides could be introduced or conjugated to HA by various chemistries [34, 58]. The carboxyl [59] and hydroxyl [60] groups, and the reducing end of HA [61], are the main sites for chemical modification. The most widely used chemistry is the activation of the carboxyl groups by 1-ethyl-3-(3-dimethylaminopropyl)-carbodiimide hydrochloride (EDC·HCl) for amide bond formation in aqueous condition. The reaction is typically carried out at acidic pH to protonate the carbodiimide nitrogen. Protonated EDC reacts with the carboxyl group to form *O*-acylisourea intermediate, which is unstable and readily rearranges to form a stable but unreactive *N*-acylurea. In the presence of a primary amine, the *O*-acylisourea intermediate undergoes nucleophilic attack by the amine to form an amide bond [59]. To minimize the formation of *N*-acylurea, *N*-hydroxysuccinimide (NHS) [62] or 1-hydroxybenzotriazole (HOBt) [63] are often added to form HA-ester intermediate. The HA-ester intermediate is more stable than the *O*-acylisourea intermediate and can also undergo nucleophilic attack by primary amine. The degree of substitution (DS), defined as the number of substituted carboxyl groups in every 100 disaccharide units, using EDC chemistry is dependent on the pKa of the primary amine. Amine with high pKa value will result in low DS due to protonation of the amine at pH below the pKa. The DS could be improved by first forming HA-ester intermediates at acidic environment, then add the primary amine compound at a neutral pH to facilitate conjugation. Alternatively, the reaction can be performed in organic solvent which minimizes hydrolysis of the unstable *O*-acylisourea intermediate. In this case HA needs to be first converted from sodium salt to the acidic form or tetrabutylammonium salt in order be solubilized in organic solvent. However the conversion to acidic form requires treatment with strong acid and may results in HA degradation [64].

Amide bond formation between the carboxyl group of HA and primary amine can also be achieved using 2-chloro-1-methylpyridinium iodide (CMPI). The reaction is usually done in aqueous/organic mixture or in pure organic solvent such as DMF or DMSO, hence HA needs to be converted to the acidic form or tetrabutylammonium salt. CMPI reacts with carboxyl group of HA to form a pyridinium intermediate, which then reacts with primary amine to form amide bond. The DS of L-alanine ethyl ester is reported to be 100% when the reaction was carried out in DMF using HA tetrabutylammonium salt [65]. The modified HA showed diminished degradability by hyaluronidase due to the high degree of modification. A

combination of 2-chloro-dimethyoxy-1,3,5-triazine (CDMT) and *N*-methylmorpholinium (NMM) has also been utilized for amidation of HA. Reaction is carried out in a mixture of water and organic solvent mixture to allow dissolution of both HA and CDMT. CDMT reacts with the carboxyl group of HA to form a triazine-activated ester, which readily reacts with primary amine to form amide bond. DS between 3-20% was achieved depending on the pKa and solubility of the primary amine [66]. More recently, 4-(4,6-dimethoxy-1,3,5-triazin-2-yl)-4-methylmorpholinium chloride (DMTMM) has been utilized to form amide bond in aqueous environment. The efficiency of DMTMM is much greater than EDC, with the DS reaching as high as 75% [67].

## 1.3. Injectable (*in situ* forming) hydrogel systems

A major advancement in hydrogel technology is the development of *in situ* crosslinking mechanisms which renders the system injectable by allowing an aqueous mixture of gel precursors and bioactive agents to be administered using a syringe [68, 69]. Once inside the body, the gel precursors are crosslinked by physical or chemical bonds *in situ*. The facile procedure and minimized invasiveness of an injectable hydrogel system are preferable over conventional preformed hydrogels that require invasive techniques for implantation. In physical crosslinking, reversible physical interactions between polymer chains, such as ionic, substrate-ligand or hydrophobic interactions are employed to induce gelation. Although physically crosslinked hydrogels do not involve chemical reactions that could potentially affect the integrity of the bioactive agents to be encapsulated, the *in vivo* stabilities are often compromised due to interactions with physiological molecules or mechanical stress in the body [70, 71]. In contrast, chemically crosslinked hydrogels have superior mechanical properties, which render them with structural stability. The following section provides a review on the existing strategies to form chemically crosslinked hydrogels *in situ.* For each of the crosslinking strategy, the method of tuning the mechanical property and gelation rate is highlighted, and the advantages and limitations are discussed.

### 1.3.1. *In situ* chemical crosslinking strategies

#### 1.3.1.1. Disulfide bond formation

Polymers containing thiol groups can form intra- and/or intermolecular disulfide bonds by oxidation, thereby producing a crosslinked network *in situ*. The advantages of disulfide bond formation are that the reaction is mild and can be induced by simply exposure to air. A major

drawback of disulfide-mediated gel formation is the slow rate of gelation. As a result, a high thiol substitution degree is often required in order to form hydrogels quickly. However, extensive modification to a natural polymer may results in irreversible changes to its native properties, such as degradability. Alternatively, gelation could also be accelerated by increasing the pH of the medium, because more thiols were converted to the reactive thiolates at higher pH. For instance, a solution of thiol-modified hyaluronic acid (Fig. 1-3; 3% w/v and DS = 58%) showed no obvious increase in viscosity after 30 min at pH 6, but gelation occurred within 15 min at pH 7 and above [72]. Nevertheless, the gelation time of injectable hydrogel systems should be within a few minutes, especially for drug delivery applications. Hence oxidizing agent such as hydrogen peroxide ($H_2O_2$) is frequently added to further accelerate the formation of disulfide bonds [73, 74]. Nevertheless, only 25-50% of thiols were converted to disulfide bonds after oxidization by $H_2O_2$, and no free thiols could be detected. The result suggested that only some of the thiols participated in the crosslinking reaction, and majority was converted to other products, such as sulfenic or sulfonic acids [73]. The rate of disulfide bond formation is influenced by other factors, including the pKa of the thiol moiety, temperature and oxygen level of the reaction medium.

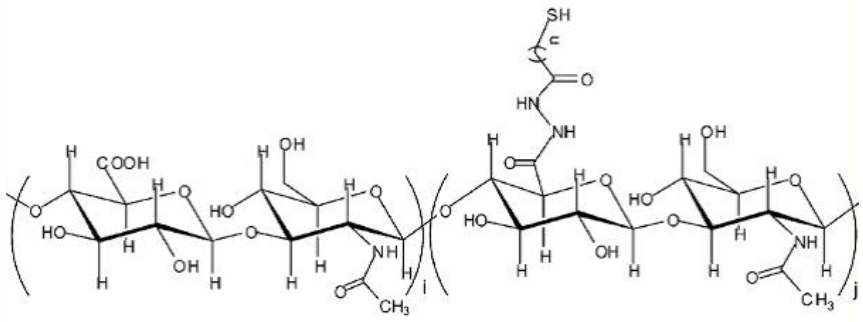


**Fig. 1-3. Thiol-containing HA derivative for hydrogel formation through disulfide bond [72]. Reprinted with permission from Shu XZ, Liu Y, Luo Y, Roberts MC, Prestwich GD, Disulfide cross-linked hyaluronan hydrogels, *Biomacromolecules* 3:1304-11. Copyright 2002 American Chemical Society.**

Oxidation of thiol groups can occur during conjugation of thiol moieties to polymers, resulting in unintended/premature crosslinking. This can be prevented by performing the synthesis under inert conditions, such as nitrogen or argon atmosphere. Alternatively, synthesis performed at pH less than 5 can minimize the formation of thiolate anions, the reactive form of thiol, thus preventing the formation of disulfide bonds [75]. Also, post-synthesis reduction of disulfide bonds can be achieved by the addition of reducing agents, such as dithiothreitol (DTT), to regenerate the thiol groups. Due to the tendency of thiols in

forming disulfide bonds, thiol-modified polymers are unstable when stored in aqueous form. Therefore inert or acidic conditions, or oxygen scavengers, are needed for long-term storage. Protected thiol group in the form of thioacetate has been developed to overcome the stability issue during storage. However, deprotection in alkaline condition is needed to yield the free thiols [76]. More recently, thiol-disulfide exchange reaction was introduced to form disulfide crosslinked hydrogels. HA derivative containing pyridyl dithiol reacts with a dithiol crosslinker to form hydrogels *via* thiol-disulfide exchange (Fig. 1-4) [77]. Hydrogels were formed within 10 to 15 min at 37°C based on tube-inversion method. The range of storage modulus (G') obtained by varying the feed ratio of the dithiol crosslinker was narrow, between 100-300 Pa.

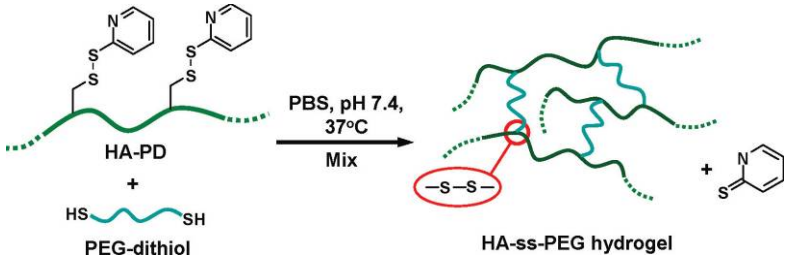


**Fig. 1-4. Disulfide crosslinked HA hydrogel formed via thiol-disulfide exchange between pyridyl disulfide-modified HA (HA-PD) and PEG-dithiol [77]. Reprinted with permission from Choh SY, Cross D, Wang C, Facile synthesis and characterization of disulfide-cross-linked hyaluronic acid hydrogels for protein delivery and cell encapsulation, *Biomacromolecules* 12:1126-36. Copyright 2011 American Chemical Society.**

### 1.3.1.2. Michael-type addition reaction

Michael-type addition reaction is the addition of a non-enolate nucleophile, such as amines and thiols, to the $\beta$ carbon of a carbon-carbon double bond that is conjugated with an electron withdrawing and resonance stabilizing group (Fig. 1-5a) [78]. Because Michael-type addition can take place rapidly under mild reaction conditions and does not produce toxic byproducts, it has been utilized to form injectable, chemically crosslinked hydrogels. Michael acceptors that have been employed to form hydrogels include acrylate [21, 79], vinyl sulfones [33, 80, 81] and maleimides [82] (Fig. 1-5b). Thiol is the most widely used Michael donor in hydrogel preparation. However, thiol can form disulfide bonds by air oxidation, which lowers the effective concentration of thiol available for Michael-type addition reaction. Therefore oxygen-free medium is needed to minimize disulfide bond formation.

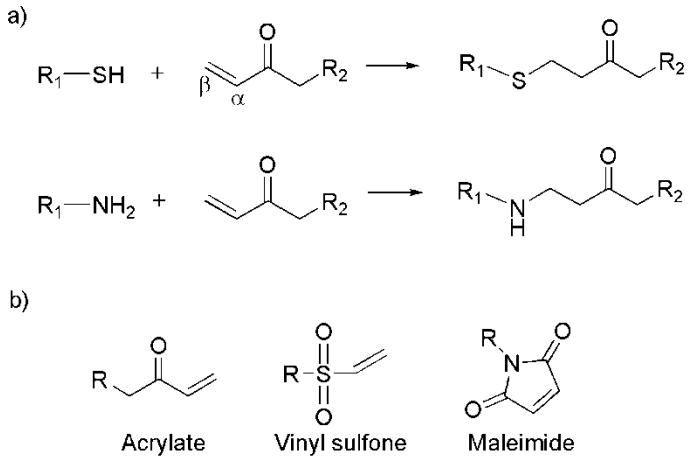


**Fig. 1-5. a) Schematic depicting Michael-type addition reaction using thiol or amine. b) Common Michael acceptors used to form injectable hydrogels.**

Similar to disulfide crosslinked hydrogels, the gelation rate of hydrogels that uses thiol as the Michael donor depends on the amount of thiolate anion, which in turn depends on pH and temperature. For instance, Elbert *et al.* showed that a mixture of PEG-triacrylate (three-arm PEG, each PEG chain terminates with an acrylate group) and PEG-dithiol, at a total PEG concentration of 10% (w/v), had a gel point of 22 min at pH 7 and decreased to 6 min at pH 8.2 [79]. The gel point was defined as the crossover between storage modulus (G') and loss modulus (G''). Gel point was furthered reduced to less than a 1 min by using a solution of PEG-octaacrylate (eight-arm PEG, each PEG chain terminates with an acrylate group) and PEG-dithiol at a total PEG concentration of 40% (w/v). BSA-loaded PEG-multiacrylate/PEG-dithiol hydrogel released the protein over a period of several days. Shu *et al.* developed thiol-modified HA, which formed hydrogels through Michael-type addition reaction with various *α,β*-unsaturated esters and amides of PEG (Fig. 1-6). It was found that PEG-diacrylate (PEGDA) was the most reactive crosslinker, with a gelation time of 5 min based on the tube-inversion method [21]. Thiol to acrylate ratio of 2:1 was needed to ensure the incorporation of all the PEGDA into the hydrogel; however, about 6% of the incorporated PEGDA contained a free acrylate group (single end anchorage). Thiol to acrylate ratio of 3:1 was needed for all the acrylate groups to be reacted. Fibroblasts encapsulated in the crosslinked HA hydrogel remained viable and proliferative over a period of 28 days culture *in vitro*. Nie *et al.* showed that the gelation time of hydrogels composed of maleimide-functionalized heparin and thiol-functionalized PEG could be tuned by controlling the degree of functionalization of maleimide and the concentration of the gel precursors. However, the G' of the hydrogel was changed concurrently [82]. Similar observation was made by Tae *et al.* using thiol-modified

heparin and PEG-diacrylate; changes in the degree of thiolation and gel precursor concentration affected both the gelation rate and the G' [83].

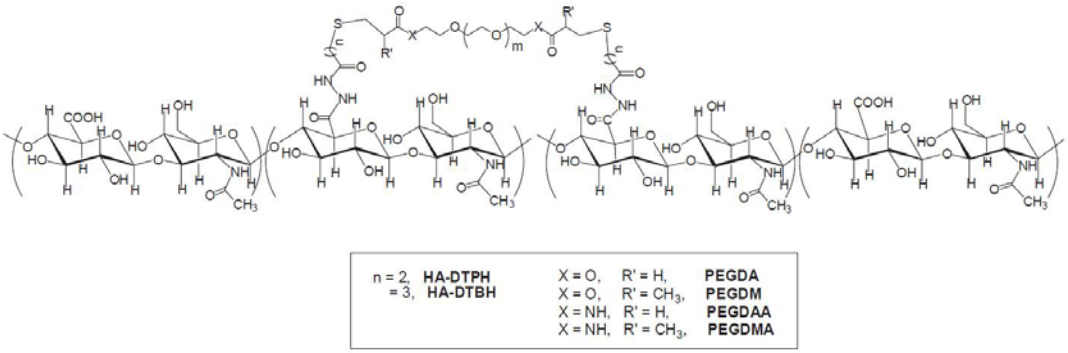


**Fig. 1-6. Structures of α,β-unsaturated esters and amides of PEG crosslinked with thiolated HA [21]. HA-3-thiopropanoyl hydrazide derivative (HA-DTPH) HA-4-thiobutanoyl hydrazide (HA-DTBH), PEG-diacrylate (PEGDA), PEG-dimethacrylate (PEGDM), PEG-diacrylamide (PEGDAA) and PEG-dimethacrylamide (PEGDMA).**

### 1.3.1.3. Photo-initiated radical polymerization

A photopolymerizable hydrogel system consists of photopolymerizable gel precursors, crosslinkers, photoinitators and a UV or visible light source. Photocrosslinkable gel precursors can be either monomers or macromers; the latter are more commonly used for *in situ* forming hydrogels because of the potential cytotoxicity associated with monomeric compounds [84]. Crosslinkers are typically lower in molecular weight compare to the gel precursors and have two acrylate end groups. Photoinitiators used in biomedical applications can be divided into two groups based on the mechanism of photolysis: photocleavage and hydrogen abstraction. Photocleavage produces radicals by homolytic cleavage of molecular bonds upon light exposure. An example of such is 2-hydroxy-1-[4-(hydroxyethoxy)phenyl]-2-methyl-1-propanone, or commonly known as Irgacure 2925. Hydrogen abstraction is the abstraction of hydrogen from an H-donor molecule upon UV exposure that generates a ketyl radical and a donor radical. An example of such is isopropylthioxanthone. The radicals generated from either photocleavage of hydrogen abstraction attack the carbon-carbon double bond in the acrylate groups of the gel precursors and initiate the polymerization process.

Leach *et. al.* developed a glycidyl methacrylate-modified HA which formed a gel upon UV exposure in the presence of the photoinitiator Irgacure 2959 and *N*-vinyl pyrrolidinone (NVP) [85]. NVP was added to accelerate the rate of polymerization. Hydrogels were formed after 1 min of illumination. As the degree of methacrylate substitution increased from 5 to

11%, the G' increased modestly from 109 to 155 Pa. Increased cytotoxicity was associated with increased Irgacure 2959 concentrations and a diluted photoinitiator was needed to prevent cytotoxicity. Park *et. al.* reported a photopolymerized hydrogel system composed of methacrylated-HA and poly(etheylene glycol) diacrylate (PEG-DA), the latter served as the crosslinker [86]. Hydrogels were formed rapidly upon illumination in the presence of eosin Y (photosensitizer), triethanolamine (initiator) and NVP. The complex modulus (G*) reached plateau within 1 min. The concentration of PEG-DA and the molecular weight of the HA derivatives were varied in order to modulate the mechanical property of the hydrogels.

The advantage of photo-initiated polymerization over redox-initiated polymerization is the spacial and temporal control of the crosslinking process, because photoinitiators produce free radicals only upon exposure to a light source [17]. Moreover, photopolymerized hydrogels could be formed rapidly. However, the concentration of photoinitiators, the intensity of the light source and duration of irradiation should be kept to the minimum to avoid cytotoxicity [87]. A potential disadvantage of photo-initiated radical polymerization is that the intense light may irreversibly conjugate encapsulated protein to the hydrogel *via* Michael addition reaction between the lysine amino acids and the methacrylated gel precursors [88]. Although the gel precursors can be injected as a solution, they must be exposed to light to form hydrogels, and the introduction of light source may involve invasive techniques.

#### 1.3.1.4. Schiff base formation

Hydrogels formed through Schiff base formation requires two components, an aldehyde-modified polymer/crosslinker and an amine-modified polymer/crosslinker. Upon mixing of the two components, Schiff base is formed by nucleophilic attack of the amine groups on the electrophilic carbon of the aldehyde groups. The rate of crosslinking is dependent on the pH of the reaction medium. At high pH values, the fraction of unprotonated amines available for Schiff base formation increases, hence accelerates the rate of gelation [89]. Hydrazide is particularly suitable for Schiff base-mediated *in situ* crosslinking reaction. This is because the amino groups of hydrazide have a low pKa of 2-3, therefore they are unprotonated nucleophiles under physiological condition [90]. Schiff base formation between hydrazide and aldehyde resulted in hydrazone bond (Fig. 1-7).

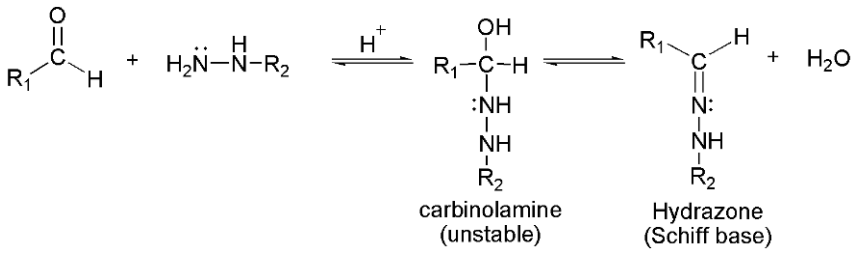


**Fig. 1-7. Schiff base formation between hydrazide and aldehyde.**

Luo *et. al.* prepared a hyaluronic acid-adipic dihydrazide derivatives (HA-ADH, DS = 55%), which crosslinked with poly(ethylene glycol)-propiondialdehyde (PEG-diald) to form a gel within 60 sec (Fig. 1-8) [91]. Rapid gelation was also observed when HA-ADH was reacted with aldehyde-modified HA [63]. Gelation time was controlled by adjusting the gel precursor concentration and decreased from 5 to 1 min as the concentration of the HA derivatives increased from 1 to 2% (w/v). The HA-aldehyde derivative was synthesized by ring opening at the proximal hydroxyl groups using sodium periodate. However, oxidation with sodium periodate resulted in a significant reduction in the molecular weight of HA. Hydrogels formed by Schiff base formation tends to have poor mechanical property. Despite having a high degree of ADH substitution, HA-ADH (DS = 48%) crosslinked with various aldehyde-modified polysaccharides resulted in hydrogels with low G' (maximum of 300 Pa) [92]. A dose-dependent reduction in cell viability in the presence of aldehyde-modified gel precursors was observed [92]. This may be a concern when Schiff base formation is used to form hydrogels for cell encapsulation.

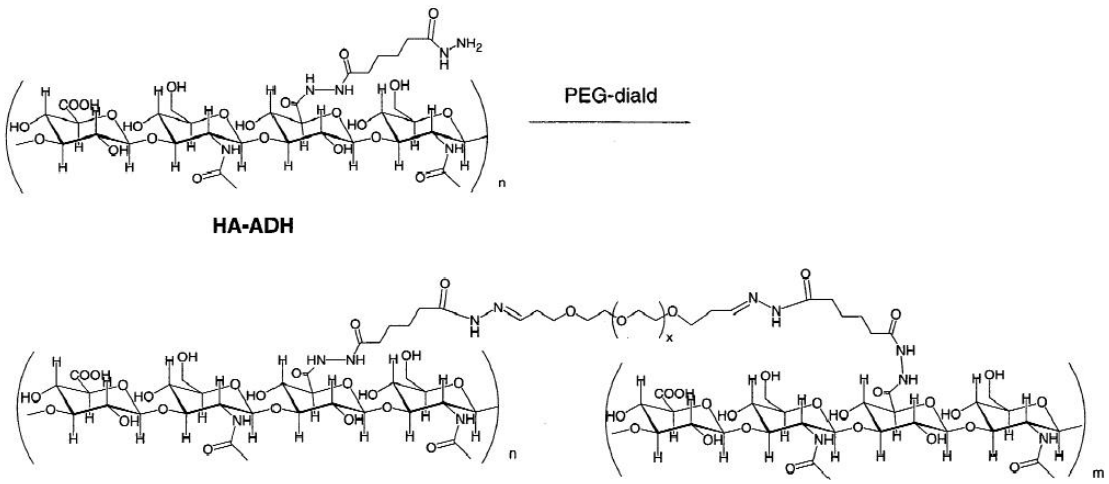


**Fig. 1-8. Hyaluronic acid-adipic dihydrazide derivatives (HA-ADH) crosslinked with poly(ethylene glycol)-propiondialdehyde (PEG-diald) [91]. Reprinted from Journal of Controlled Release, 69, Luo Y,**

**Kirker KR, Prestwich GD, Cross-linked hyaluronic acid hydrogel films: new biomaterials for drug delivery, 169-84, Copyright 2000, with permission from Elsevier.**

### 1.3.1.5. Click chemistry

Click chemistry, specifically the copper(I)-catalyzed azide-alkyne cycloaddition (CuAAC), is a highly efficient reaction that can occur at physiological condition (Fig. 1-9) [93]. Not only is CuAAC more efficient than the 1,3-dipolar Huisgen cycloaddition between azide and alkyne, the product of CuAAC is also regioseletive, consisting solely of 1,4-regioisomers of 1,2,3-triazoles. Malkoch *et. al.* described a PEG-based hydrogel system composed of diacetylene-functionalized and tetraazide-functionalized PEG derivatives [94]. Hydrogels were formed rapidly by mixing the PEG derivatives in the presence of copper sulfate with sodium ascorbate as reducing agent. When diacetylene-functionalized and tetraazide-functionalized PEG derivatives were mixed at 2 to 1 ratio, i.e. acetylene to azide ratio of 1:1, only 0.2% of functional groups remained unreacted. The result suggested that click-mediated crosslinking reaction is highly efficient and formed nearly perfect network with very few dangling ends.

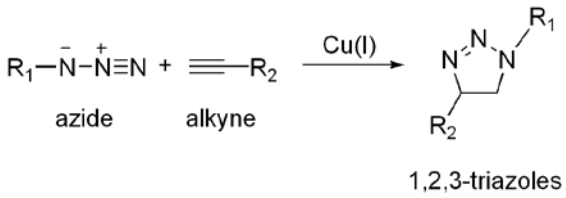


**Fig. 1-9. Copper(I)-catalyzed azide-alkyne cycloaddition (CuAAC).**

Crescenzi *et. al.* developed a hyaluronic acid hydrogel system composed of HA-azido and HA-propargylamide derivatives (Fig. 1-10) [95]. No information on the degree of substitution of azide and propargylamide was provided. Upon addition of CuCl, gel points (G' = G'') were reached between 130 to 160 sec. The degree of crosslinking, i.e. the number of triazoles formed in every 100 disaccharide units, were determined to be from 8 to 21. HA-azido derivatives had also been utilized to form hydrogels with different dialkyne crosslinkers in the presence of $CuSO_4$ and ascorbic acid [96]. Both the gelation rate and G' values increased with increasing concentration of HA-azido derivatives. G' increased from 1520 Pa to 6700 Pa as the concentration of HA-azido derivatives increased from 2 to 10% (w/v). Interestingly, it was found that $CuSO_4$ concentration affected only the gelation rate but not the G' value. One drawback with CuAAC-mediated crosslinking reaction is the presence of copper in the

resulting gels, which is undesirable for injectable systems as the copper may causes cytotoxicity.

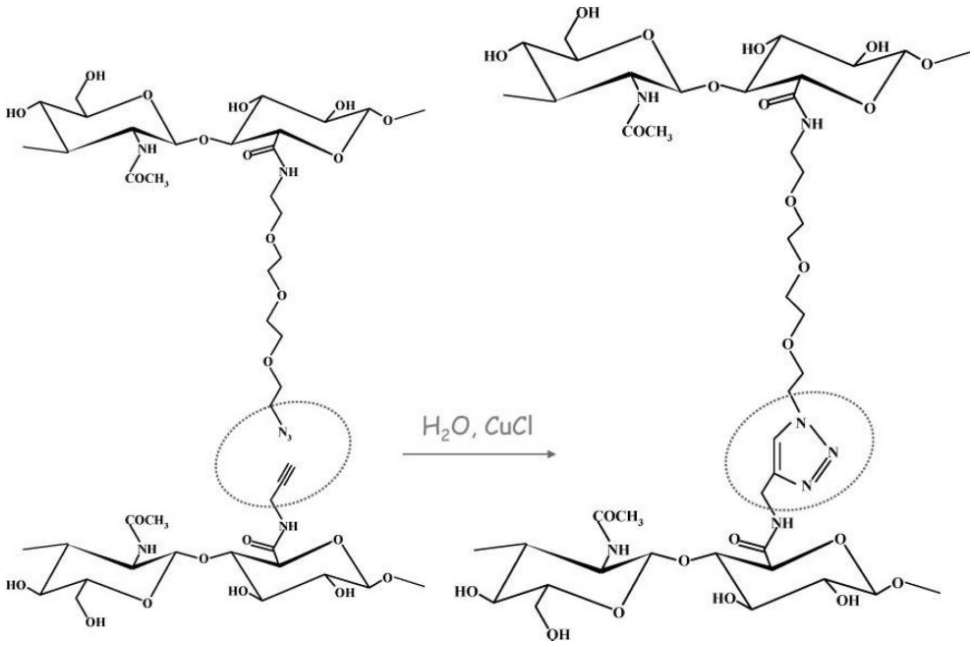


**Fig. 1-10. HA hydrogels formed by click chemistry [95]. Reprinted with permission from Crescenzi V, Cornelio L, Di Meo C, Nardecchia S, Lamanna R, Novel hydrogels via click chemistry: synthesis and potential biomedical applications, *Biomacromolecules* 8:1844-50. Copyright 2007 American Chemical Society.**

### 1.3.1.6. Genipin

Genipin is a chemical compound extracted from *Gardenia jasminoides*. Due to its low concentration in gardenia fruits, genipin is manufactured from geniposide by using beta-glucosidase [97]. Genipin is water-soluble and much less toxic than glutaraldehyde. It can act as a crosslinker for polymers containing amine groups, e.g. chitosan and gelatin, to form blue-colored fluorescent hydrogels. Several different crosslinking mechanisms for genipin have been proposed. The fastest mechanism is a nucleophilic attack on the C3 of genipin by an amine group followed by a nucleophilic substitution of the ester group of genipin by a second amine group to form an amide (Fig. 1-11). The gelation time of genipin-crosslinked chitosan was shown to be inversely proportional to genipin concentration [98]. Gel point (G' = G") decreased from 8 to 2 min as the concentration of genipin increased from 0.1 to 0.15% (w/v). The increase in genipin concentration also increased the crosslink density of the resulting hydrogels, as reflected by an increase of G'. Genipin has also been used to increase the crosslink density of HA hydrogels formed by Schiff base reaction between HA-aldehyde and ethylamine-conjugated HA [99].

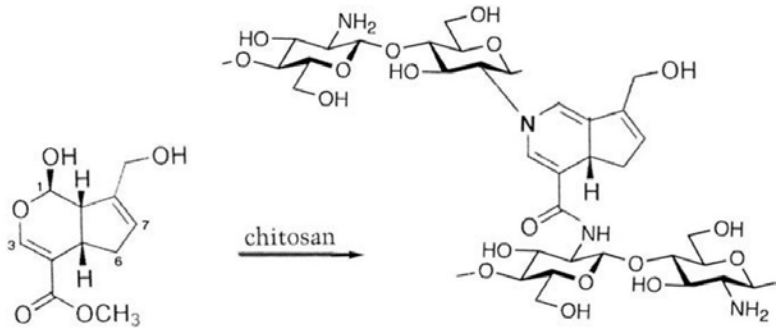


**Fig. 1-11. Crosslinking of chitosan by genipin [97]. Reprinted from *Carbohydrate Polymers*, 77, Muzzarelli RAA, Genipin-crosslinked chitosan hydrogels as biomedical and pharmaceutical aids, 1-9, Copyright 2009, with permission from Elsevier.**

### 1.3.1.7. Redox-initiated radical polymerization

Ammonium persulfate (APS) and *N,N,N',N'*-tetramethylethylenediamine (TEMED) were commonly used as aqueous redox initiators for radical polymerization. APS and TEMED generate free radicals which react with acrylate groups that lead to polymerization. The concentration of the redox initiators greatly affect the gelation time. Sarvestani *et. al.* studied the gelation kinetics of poly(lactide-*co*-ethylene-*co*-fumarate) (PLEOF) macromers using methylene bisacrylamide as the crosslinker and APS and TEMED as the redox initiators (Fig. 1-12) [100]. It was shown that the gel point decreased from more than 30 min to less than 5 min as the concentrations of both APS and TEMED increased from 0.005M to 0.02M. The G' also increased when APS and TEMED concentrations increased from 0.005M to 0.01M, but decreased from 0.01M to 0.02M, possibly due to intramolecular crosslinking of the vinyl groups of the bisacrylamide, resulting in the reduction of elastically-active crosslinking.

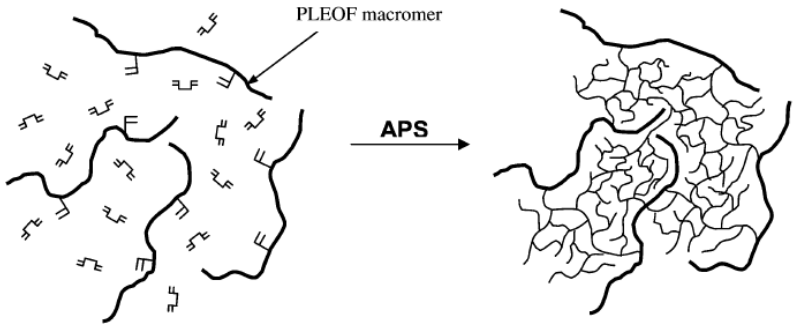


**Fig. 1-12. Schematic depicting the formation of poly(lactide-co-ethylene-co-fumarate) (PLEOF) hydrogel crosslinked by bisacrylamide using APS as the initiator [100]. Reprinted with permission from Sarvestani AS, He X, Jabbari E, Viscoelastic characterization and modeling of gelation kinetics of injectable in situ cross-linkable poly(lactide-co-ethylene oxide-co-fumarate) hydrogels, *Biomacromolecules* 8:406-15. Copyright 2007 American Chemical Society.**

One major concern with redox-initiated polymerization is the cytotoxicity effects of the initiators. Using oligo(poly(ethylene glycol) fumarate) (OPF) as the gel precursor material, Temenoff *et. al.* tested the cytotoxicty of various initiator combinations at different concentrations [101]. It was found that although a combination of sodium persulfate and ascorbate-2-phosphate showed the highest cytocompatibility; however, the system did not form fully crosslinked hydrogel. A combination of 20 mM APS and ascorbic acid ensured complete crosslinking and minimum cytotoxicity.

### 1.3.2. Limitations of existing injectable and chemically crosslinked hydrogel systems

A limitation of existing injectable and chemically crosslinked hydrogel systems is that the crosslink density and gelation rate cannot be tuned in a facile and independent manner. Crosslink density is an important property of a hydrogel because it directly influences the rates of hydrogel degradation and drug release, and the rates of cell proliferation and migration within the gel matrix [6]. Moreover, recent research on cell-matrix interactions showed that matrix stiffness plays a vital role on cell functions, tissue morphogenesis and stem cell differentiation [6, 13]. The stiffness of a hydrogel is dependent on the crosslink density and often expressed in terms of storage modulus (G'). Thus the tuning of crosslink density is essential in tailoring a hydrogel's mechanical strength for a specific application. In addition to crosslink density, gelation rate is another important property of an injectable hydrogel system. For drug delivery applications, hydrogels should be formed rapidly after injection to prevent the uncontrolled diffusion of gel precursors and drugs to the surrounding tissues [14]. For tissue engineering applications, a moderate rate of gelation would be more desirable to allow time for the gel precursors to fill the irregularly shaped defects, thereby achieving cohesion between the hydrogel and the surrounding native tissue [15].

As described in the preceding section, the crosslink density of most injectable and chemically crosslinked hydrogel systems is varied *via* the degree of substitution (DS) of the crosslinking moiety or the concentration of gel precursors (polymers and/or crosslinkers). Changes in these parameters would alter the gelation rate as well (Fig. 1-13). Likewise, the tuning of gelation rate is limited to varying the DS of the crosslinking moiety or the polymer/crosslinker concentrations [16, 17], which inevitably change the crosslink density and cause undesirable modifications to the degradation and drug release profiles. Moreover, to increase the DS of the crosslinking moiety, extensive chemical modification to the polymer is often required, which could lead to irreversible changes to the polymer's native property,

such as biodegradability for natural polymers. For instance, the degradability of HA by hyaluronidase was compromised when the DS of the carboxyl groups of HA was increased [102]. Therefore, an injectable hydrogel system that allows the facile and independent tuning of crosslink density and gelation rate, without extensive modification to the polymer or changes in the gel precursor concentration, would be a useful system for drug delivery and tissue engineering applications (Fig. 1-14).

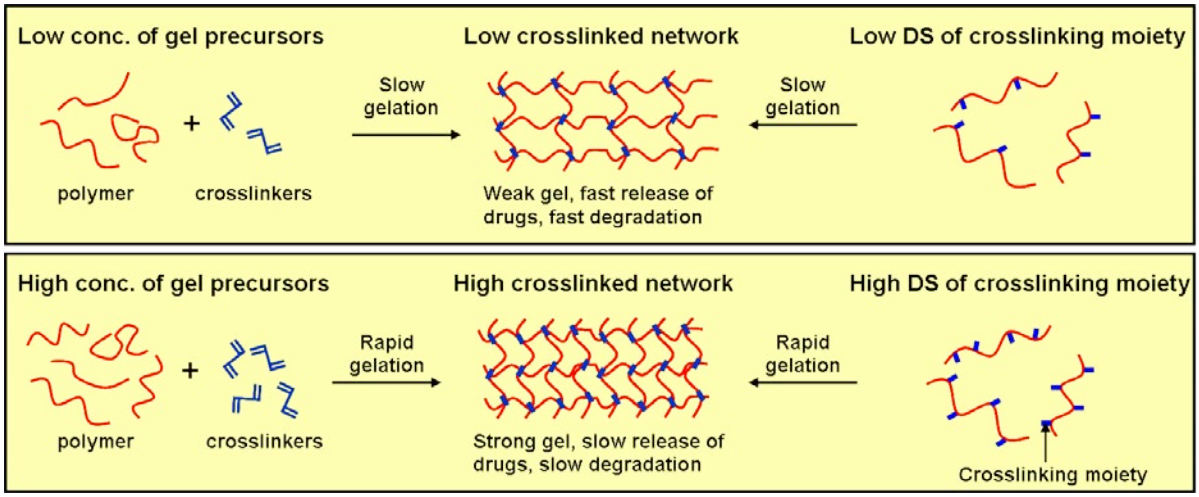


**Fig. 1-13. Changing the polymer and/or crosslinker concentrations affects both the mechanical property and gelation rate of the resulting hydrogels.**

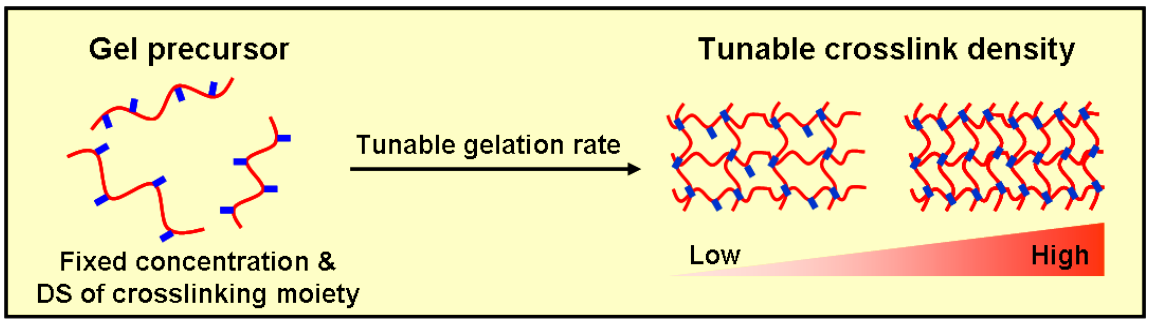


**Fig. 1-14. A hydrogel system with independent tuning of gelation rate and crosslink density.**

## 1.4. Objectives of this study

Previously our laboratory has reported an injectable hydrogel system composed of hyaluronic acid-tyramine (HA-Tyr) conjugates [103]. The HA-Tyr conjugates were crosslinked *in situ* by the oxidative coupling of tyramine moieties in the presence of horseradish peroxidase (HRP) and hydrogen peroxide ($H_2O_2$). Building upon this work, the present study seeks to achieve the following objectives by further developing the HA-Tyr

hydrogel system and designing new hydrogel systems composed of different polymer-phenol conjugates:

- Independent tuning the gelation rate and crosslink density
- Sustained delivery of therapeutic proteins, namely, interferon-α2a, trastuzumab and PEGylated interferon-α2a, for liver cancer, breast cancer and hepatitis C treatment, respectively
- Formation of vascularized hydrogels for tissue engineering applications, and 3D propagation of human embryonic stem cells in hydrogels
- Formation of an injectable and bioactive hydrogel system that does not require the addition of exogenous $H_2O_2$

## 1.5. Outline of the thesis

In **Chapter 1**, an overview on hydrogel and its application in protein delivery and tissue engineering, and the pros and cons of various polymers and *in situ* crosslinking strategies for the formation of injectable hydrogels, are provided. The biological roles and clinical applications of hyaluronic acid (HA), one of the most commonly used polymers in hydrogels, is described. In addition, the limitations of existing injectable and chemically crosslinked hydrogel systems are discussed. Lastly, the objectives of this study are stated. **Chapter 2** details the synthesis, purification and characterization of HA-Tyr conjugates. In the presence of HRP and $H_2O_2$, HA-Tyr conjugates crosslinked *in situ* through the oxidative coupling of tyramine moieties, forming a chemically crosslinked hydrogel. The effects of HRP and $H_2O_2$ on the gelation rate and crosslink density were examined. Then, α-amylase, a model protein, was incorporated in the hydrogel, and the effect of crosslink density on the rate of protein release and the activity of released proteins were characterized. Next, the HA-Tyr hydrogel was employed as a delivery system for interferon-α2a (IFN-α2a) for liver cancer treatment. IFN-α2a is a cytokine with anti-viral and anti-cancer activities. Sustained release of IFN-α2a over a period of 24 h was achieved by tuning the hydrogel crosslink density. The pharmacokinetics and anti-tumor effect of IFN-α2a delivered using hydrogels were compared with bolus injections through a series of *in vitro* and *in vivo* experiments.

In order to extend the release duration to more than 24 h, interactions between proteins and hydrogels are required to reduce the release rate. **Chapter 3** investigates whether

electrostatic interactions between positively charged proteins (lysozyme) and the negatively charged HA-Tyr hydrogel could immobilize the proteins within the hydrogel. Degradation of hydrogels in the presence of hyaluronidase, which facilitated the release of immobilized proteins, was characterized. Then, trastuzumab, a positively charged monoclonal antibody used in breast cancer therapy, and hyaluronidase were incorporated together in HA-Tyr hydrogels. Trastuzumab was immobilized in the hydrogel through electrostatic interactions, and the release rate depended on the concentration of hyaluronidase. It was demonstrated that sustained release of up to 4 weeks could be achieved through controlled degradation of the hydrogel by hyaluronidase. The anti-tumor effect of trastuzumab delivered by HA-Tyr hydrogels was investigated in a mice xenograft model of human breast cancer, and compared with bolus injections. **Chapter 4** describes yet another method to deliver proteins for an extended period of time using hydrogels. Specifically, a dextran-tyramine (Dex-Tyr) hydrogel containing poly(ethylene glycol) (PEG) microdomains was developed for the sustained release of PEGylated proteins. PEGylated proteins contain covalently attached PEG chains, which effectively extend the circulating half-life of the proteins. It was found that PEGylated IFN-α2a (PEG-IFN-α2a) preferentially partition in the PEG microdomains, which prevented rapid diffusion of the proteins out of the hydrogel. The release profiles and pharmacokinetics were examined and compared with protein administered as a solution. Furthermore, the therapeutic efficacy of PEG-IFN-α2a delivered by the hydrogel was evaluated in a humanized mice model of hepatitis C.

In addition to protein delivery, the HA-Tyr hydrogel system was investigated as a scaffold for tissue engineering applications. One of the challenges in tissue engineering is the formation of a vascular network within the tissue construct, which is essential for the transportation of nutrients and other biomolecules to ensure the viability of the embedded cells. **Chapter 5** reports the formation of an interpenetrating polymer network (IPN) composed of fibrin and HA-Tyr hydrogel. Fibrin is widely used as a tissue engineering scaffold, but it has poor mechanical properties and degrades rapidly. By varying the crosslink density of HA-Tyr network, IPN hydrogels with different G' were formed, which were more resistant to cell-induced contraction and degradation by proteases as compared to fibrin gels alone. The formation of capillaries within the IPN hydrogels was also investigated. **Chapter 6** describes the design and synthesis of an Arg-Gly-Asp (RGD) peptide flanked by two phenol moieties for *in situ* conjugation into HA-Tyr hydrogels. RGD-modified hydrogels were characterized in terms of cell adhesion, proliferation and migration. Moreover, the formation

of functional vasculature in the hydrogels was examined by injecting hydrogels containing human umbilical vein endothelial cells (HUVECs) and human fibroblasts into the subcutaneous tissue of mice. Another challenge associated with tissue engineering is the cell source. Human embryonic stem cells (hESCs) are a promising cell source as they have unlimited self-renewal capability and can differentiate into any cell type. The current methods of hESCs propagation, however, are not suitable for large-scale production and clinical applications due to the requirement of animal-derived components, such as fetal bovine serum and Matrigel (a basement membrane extracted from Engelbreth-Holm-Swarm mouse sarcoma). **Chapter 7** explores the possibility of propagating hESCs in the 3D environment of HA-Tyr hydrogels using a chemically-defined culture medium containing no animal-derived components. The effects of crosslink density on the viability, proliferation and pluripotency of hESCs were investigated.

The formation of hydrogels by HRP-mediated crosslinking of polymer-phenol conjugates requires the addition of $H_2O_2$ as the oxidant. In order to simplify the gel formation process, a method of forming hydrogels without the need of exogenous $H_2O_2$ was developed. **Chapter 8** describes the design of an injectable hydrogel system composed of (-)-epigallocatechin-3-gallate (EGCG), a green tea catechin, as the crosslinking moiety. EGCG is well-known for its potential health benefits, including anti-inflammation and anti-cancer. Amine-functionalized EGCG dimers were synthesized and conjugated to HA, forming HA-EGCG conjugates. The HA-EGCG conjugates exhibited bioactivities that were not present in native HA, such as enzyme-inhibition, anti-prolfieration and radical scavenging. It was demonstrated that autoxidation of the EGCG moieties under aerobic condition produced $H_2O_2$ at a sufficiently fast rate, thus a hydrogel was formed by simply mixing HA-EGCG conjugates with HRP. Hydrogels were also formed *in situ* through EGCG quinone formation in the absence of HRP, which greatly simplifies the gel formation process and circumvents the safety concern associated with HRP due to its plant origin. Moreover, the HA-EGCG hydrogels were found to be resistant to hyaluronidase-mediated degradation due the presence of EGCG moieties.

Lastly, **Chapter 9** summarizes the findings presented in this thesis and addresses some of the concerns associated with HRP-mediated gelation. The significance of this study and the outlook of injectable hydrogels for protein delivery and tissue engineering are also discussed.

**References**

[1] Lee KY, Yuk SH. Polymeric protein delivery systems. Prog. Polym. Sci. 2007;32:669-97.

[2] Hoffman AS. Hydrogels for biomedical applications. Adv. Drug Del. Rev. 2012;64, Supplement:18-23.

[3] Lee SC, Kwon IK, Park K. Hydrogels for delivery of bioactive agents: A historical perspective. Adv. Drug Del. Rev. 2013;65:17-20.

[4] Hoffman AS. Hydrogels for biomedical applications. Adv. Drug Del. Rev. 2002;54:3-12.

[5] Hill-West JL, Chowdhury SM, Slepian MJ, Hubbell JA. Inhibition of thrombosis and intimal thickening by in situ photopolymerization of thin hydrogel barriers. Proc. Natl. Acad. Sci. U. S. A. 1994;91:5967-71.

[6] Yeo Y, Highley CB, Bellas E, Ito T, Marini R, Langer R, Kohane DS. In situ cross-linkable hyaluronic acid hydrogels prevent post-operative abdominal adhesions in a rabbit model. Biomaterials 2006;27:4698-705.

[7] Censi R, Di Martino P, Vermonden T, Hennink WE. Hydrogels for protein delivery in tissue engineering. J. Control. Release 2012;161:680-92.

[8] Vermonden T, Censi R, Hennink WE. Hydrogels for protein delivery. Chem. Rev. 2012;112:2853-88.

[9] Bae KH, Wang L-S, Kurisawa M. Injectable biodegradable hydrogels: progress and challenges. J. Mater. Chem. B 2013;1:5371-88.

[10] Qiu Y, Park K. Environment-sensitive hydrogels for drug delivery. Adv. Drug Del. Rev. 2012;64, Supplement:49-60.

[11] Leader B, Baca QJ, Golan DE. Protein therapeutics: a summary and pharmacological classification. Nat. Rev. Drug Discov. 2008;7:21-39.

[12] Watt PM. Screening for peptide drugs from the natural repertoire of biodiverse protein folds. Nat. Biotechnol. 2006;24:177-83.

[13] Marshall SA, Lazar GA, Chirino AJ, Desjarlais JR. Rational design and engineering of therapeutic proteins. Drug Discov. Today 2003;8:212-21.

[14] Harris JM, Chess RB. Effect of pegylation on pharmaceuticals. Nat. Rev. Drug Discov. 2003;2:214-21.

[15] R.J.Y. Ho, Gibaldi M. Biotechnology and Biopharmaceuticals: Transforming Proteins and Genes Into Drugs John Wiley & Sons, Hoboken, New Jersey; 2003. p. 339-74.

[16] Jevsevar S, Kunstelj M, Porekar VG. PEGylation of therapeutic proteins. Biotechnol. J. 2010;5:113-28.

[17] Drury JL, Mooney DJ. Hydrogels for tissue engineering: scaffold design variables and applications. Biomaterials 2003;24:4337-51.

[18] Bae JW, Choi JH, Lee Y, Park KD. Horseradish peroxidase-catalysed in situ-forming hydrogels for tissue-engineering applications. J. Tissue Eng. Regen. Med. 2014:doi: 10.1002/term.917.

[19] Lee KY, Mooney DJ. Hydrogels for Tissue Engineering. Chem. Rev. 2001;101:1869-80.

[20] Khademhosseini A, Langer R. Microengineered hydrogels for tissue engineering. Biomaterials 2007;28:5087-92.

[21] Zheng Shu X, Liu Y, Palumbo FS, Luo Y, Prestwich GD. In situ crosslinkable hyaluronan hydrogels for tissue engineering. Biomaterials 2004;25:1339-48.

[22] Nicodemus GD, Bryant SJ. Cell Encapsulation in Biodegradable Hydrogels for Tissue Engineering Applications. Tissue Eng. Part B Rev. 2008;14:149-65.

[23] Brandl F, Sommer F, Goepferich A. Rational design of hydrogels for tissue engineering: Impact of physical factors on cell behavior. Biomaterials 2007;28:134-46.

[24] Annabi N, Nichol JW, Zhong X, Ji C, Koshy S, Khademhosseini A, Dehghani F. Controlling the Porosity and Microarchitecture of Hydrogels for Tissue Engineering. Tissue Eng. Part B Rev. 2010;16:371-83.

[25] Verma S, Garkhal K, Mittal A, Kumar N. Biodegradable Polymers for Emerging Clinical Use in Tissue Engineering. Biodegradable Polymers in Clinical Use and Clinical Development: John Wiley & Sons, Inc.; 2011. p. 565-629.

[26] Qi M. Transplantation of Encapsulated Pancreatic Islets as a Treatment for Patients with Type 1 Diabetes Mellitus. Advances in Medicine 2014;2014:1-15.

[27] Kim IL, Mauck RL, Burdick JA. Hydrogel design for cartilage tissue engineering: a case study with hyaluronic acid. Biomaterials 2011;32:8771-82.

[28] Geckil H, Xu F, Zhang X, Moon S, Demirci U. Engineering hydrogels as extracellular matrix mimics. Nanomedicine (Lond) 2010;5:469-84.

[29] Brivanlou AH, Gage FH, Jaenisch R, Jessell T, Melton D, Rossant J. Setting standards for human embryonic stem cells. Science 2003;300:913-6.

[30] Li Y, Rodrigues J, Tomas H. Injectable and biodegradable hydrogels: gelation, biodegradation and biomedical applications. Chem. Soc. Rev. 2012;41:2193-221.

[31] Sung HJ, Meredith C, Johnson C, Galis ZS. The effect of scaffold degradation rate on three-dimensional cell growth and angiogenesis. Biomaterials 2004;25:5735-42.

[32] Estey T, Kang J, Schwendeman SP, Carpenter JF. BSA degradation under acidic conditions: a model for protein instability during release from PLGA delivery systems. J. Pharm. Sci. 2006;95:1626-39.

[33] Lutolf MP, Lauer-Fields JL, Schmoekel HG, Metters AT, Weber FE, Fields GB, Hubbell JA. Synthetic matrix metalloproteinase-sensitive hydrogels for the conduction of tissue regeneration: engineering cell-invasion characteristics. Proc. Natl. Acad. Sci. U. S. A. 2003;100:5413-8.

[34] Burdick JA, Prestwich GD. Hyaluronic Acid Hydrogels for Biomedical Applications. Adv. Mater. 2011;23:H41-H56.

[35] Pawar SN, Edgar KJ. Alginate derivatization: a review of chemistry, properties and applications. Biomaterials 2012;33:3279-305.

[36] Hardingham T. Solution Properties of Hyaluronan. In: Garg HG, Hales CA, editors. Chemistry and Biology of Hyaluronan: Elsevier Ltd; 2004. p. 1-18.

[37] Schrager HM, Albertí S, Cywes C, Dougherty GJ, Wessels MR. Hyaluronic acid capsule modulates M protein-mediated adherence and acts as a ligand for attachment of group A Streptococcus to CD44 on human keratinocytes. J. Clin. Invest. 1998;101:1708-16.

[38] Kang SO, Wright JO, Tesorero RA, Lee H, Beall B, Cho KH. Thermoregulation of capsule production by Streptococcus pyogenes. PLoS One 2012;7:e37367.

[39] Kogan G, Soltés L, Stern R, Gemeiner P. Hyaluronic acid: a natural biopolymer with a broad range of biomedical and industrial applications. Biotechnol. Lett. 2007;29:17-25.

[40] Camenisch TD, McDonald JA. Hyaluronan: is bigger better? Am. J. Respir. Cell Mol. Biol. 2000;23:431-3.

[41] Slevin M, Krupinski J, Gaffney J, Matou S, West D, Delisser H, Savani RC, Kumar S. Hyaluronan-mediated angiogenesis in vascular disease: uncovering RHAMM and CD44 receptor signaling pathways. Matrix Biol. 2007;26:58-68.

[42] Laurent TC, Fraser JR. Hyaluronan. FASEB J. 1992;6:2397-404.

[43] Lepperdinger G, Fehrer C, Reitinger S. Biodegradation of Hyaluronan. In: Garg HG, Hales CA, editors. Chemistry and Biology of Hyaluronan: Elsevier Ltd; 2004. p. 71-82.

[44] Lepperdinger Gn, Fehrer C, Reitinger S, Garg HG, Hales CA. Chapter 4 - Biodegradation of Hyaluronan. Chemistry and Biology of Hyaluronan. Oxford: Elsevier Science Ltd; 2004. p. 71-82.

[45] Toole BP. Hyaluronan in Morphogenesis and Tissue Remodeling. http://glycoforum.gr.jp/science/hyaluronan/HA08/HA08E.html

[46] Weigel PH, Fuller GM, LeBoeuf RD. A model for the role of hyaluronic acid and fibrin in the early events during the inflammatory response and wound healing. J. Theor. Biol. 1986;119:219-34.

[47] Oh EJ, Park K, Kim KS, Kim J, Yang J-A, Kong J-H, Lee MY, Hoffman AS, Hahn SK. Target specific and long-acting delivery of protein, peptide, and nucleotide therapeutics using hyaluronic acid derivatives. J. Control. Release 2010;141:2-12.

[48] Fuchs K, Hippe A, Schmaus A, Homey B, Sleeman JP, Orian-Rousseau V. Opposing effects of high- and low-molecular weight hyaluronan on CXCL12-induced CXCR4 signaling depend on CD44. Cell Death Dis. 2013;4:e819.

[49] Rooney P, Kumar S, Ponting J, Wang M. The role of hyaluronan in tumour neovascularization (review). Int. J. Cancer 1995;60:632-6.

[50] Bollyky PL, Falk BA, Wu RP, Buckner JH, Wight TN, Nepom GT. Intact extracellular matrix and the maintenance of immune tolerance: high molecular weight hyaluronan promotes persistence of induced CD4+CD25+ regulatory T cells. J. Leukoc. Biol. 2009;86:567-72.

[51] Hodge-Dufour J, Noble PW, Horton MR, Bao C, Wysoka M, Burdick MD, Strieter RM, Trinchieri G, Pure E. Induction of IL-12 and chemokines by hyaluronan requires adhesion-dependent priming of resident but not elicited macrophages. J. Immunol. 1997;159:2492-500.

[52] Migliore A, Granata M. Intra-articular use of hyaluronic acid in the treatment of osteoarthritis. Clin. Interv. Aging 2008;3:365-9.

[53] Moreland LW. Intra-articular hyaluronan (hyaluronic acid) and hylans for the treatment of osteoarthritis: mechanisms of action. Arthritis Res. Ther. 2003;5:54-67.

[54] Zhang W, Moskowitz RW, Nuki G, Abramson S, Altman RD, Arden N, Bierma-Zeinstra S, Brandt KD, Croft P, et al. OARSI recommendations for the management of hip and knee osteoarthritis, Part II: OARSI evidence-based, expert consensus guidelines. Osteoarthritis Cartilage 2008;16:137-62.

[55] Daher RJ, Chahine NO, Greenberg AS, Sgaglione NA, Grande DA. New methods to diagnose and treat cartilage degeneration. Nat. Rev. Rheumatol. 2009;5:599-607.

[56] Rah MJ. A review of hyaluronan and its ophthalmic applications. Optometry 2011;82:38-43.

[57] Fakhari A, Berkland C. Applications and emerging trends of hyaluronic acid in tissue engineering, as a dermal filler and in osteoarthritis treatment. Acta Biomater. 2013;9:7081-92.

[58] Schanté CE, Zuber G, Herlin C, Vandamme TF. Chemical modifications of hyaluronic acid for the synthesis of derivatives for a broad range of biomedical applications. Carbohydr. Polym. 2011;85:469-89.

[59] Kuo JW, Swann DA, Prestwich GD. Chemical modification of hyaluronic acid by carbodiimides. Bioconjug. Chem. 1991;2:232-41.

[60] Kenne L, Gohil S, Nilsson EM, Karlsson A, Ericsson D, Helander Kenne A, Nord LI. Modification and cross-linking parameters in hyaluronic acid hydrogels—Definitions and analytical methods. Carbohydr. Polym. 2013;91:410-8.

[61] Asayama S, Nogawa M, Takei Y, Akaike T, Maruyama A. Synthesis of Novel Polyampholyte Comb-Type Copolymers Consisting of a Poly(l-lysine) Backbone and Hyaluronic Acid Side Chains for a DNA Carrier. Bioconjug. Chem. 1998;9:476-81.

[62] Luo Y, Prestwich GD. Hyaluronic acid-N-hydroxysuccinimide: a useful intermediate for bioconjugation. Bioconjug. Chem. 2001;12:1085-8.

[63] Jia X, Colombo G, Padera R, Langer R, Kohane DS. Prolongation of sciatic nerve blockade by in situ cross-linked hyaluronic acid. Biomaterials 2004;25:4797-804.

[64] Wang X, Messman J, Mays JW, Baskaran D. Polypeptide grafted hyaluronan: synthesis and characterization. Biomacromolecules 2010;11:2313-20.

[65] Schanté C, Zuber G, Herlin C, Vandamme TF. Synthesis of N-alanyl-hyaluronamide with high degree of substitution for enhanced resistance to hyaluronidase-mediated digestion. Carbohydr. Polym. 2011;86:747-52.

[66] Bergman K, Elvingson C, Hilborn J, Svensk G, Bowden T. Hyaluronic acid derivatives prepared in aqueous media by triazine-activated amidation. Biomacromolecules 2007;8:2190-5.

[67] Nimmo CM, Owen SC, Shoichet MS. Diels-Alder Click cross-linked hyaluronic acid hydrogels for tissue engineering. Biomacromolecules 2011;12:824-30.

[68] Hatefi A, Amsden B. Biodegradable injectable in situ forming drug delivery systems. J. Control. Release 2002;80:9-28.

[69] Kretlow JD, Klouda L, Mikos AG. Injectable matrices and scaffolds for drug delivery in tissue engineering. Adv. Drug Del. Rev. 2007;59:263-73.

[70] LeRoux MA, Guilak F, Setton LA. Compressive and shear properties of alginate gel: effects of sodium ions and alginate concentration. J. Biomed. Mater. Res. 1999;47:46-53.

[71] Ramachandran S, Tseng Y, Yu YB. Repeated rapid shear-responsiveness of peptide hydrogels with tunable shear modulus. Biomacromolecules 2005;6:1316-21.

[72] Shu XZ, Liu Y, Luo Y, Roberts MC, Prestwich GD. Disulfide cross-linked hyaluronan hydrogels. Biomacromolecules 2002;3:1304-11.

[73] Shu XZ, Liu Y, Palumbo F, Prestwich GD. Disulfide-crosslinked hyaluronan-gelatin hydrogel films: a covalent mimic of the extracellular matrix for in vitro cell growth. Biomaterials 2003;24:3825-34.

[74] Sakloetsakun D, Hombach JM, Bernkop-Schnurch A. In situ gelling properties of chitosan-thioglycolic acid conjugate in the presence of oxidizing agents. Biomaterials 2009;30:6151-7.

[75] Bernkop-Schnurch A. Thiomers: a new generation of mucoadhesive polymers. Adv. Drug Del. Rev. 2005;57:1569-82.

[76] Goessl A, Tirelli N, Hubbell JA. A hydrogel system for stimulus-responsive, oxygen-sensitive in situ gelation. J. Biomater. Sci. Polym. Ed. 2004;15:895-904.

[77] Choh SY, Cross D, Wang C. Facile synthesis and characterization of disulfide-cross-linked hyaluronic acid hydrogels for protein delivery and cell encapsulation. Biomacromolecules 2011;12:1126-36.

[78] Mather BD, Viswanathan K, Miller KM, Long TE. Michael addition reactions in macromolecular design for emerging technologies. Prog. Polym. Sci. 2006;31:487-531.

[79] Elbert DL, Pratt AB, Lutolf MP, Halstenberg S, Hubbell JA. Protein delivery from materials formed by self-selective conjugate addition reactions. J. Control. Release 2001;76:11-25.

[80] Hiemstra C, Zhong ZY, van Steenbergen MJ, Hennink WE, Feijen J. Release of model proteins and basic fibroblast growth factor from in situ forming degradable dextran hydrogels. J. Control. Release 2007;122:71-8.

[81] Qiu B, Stefanos S, Ma J, Lalloo A, Perry BA, Leibowitz MJ, Sinko PJ, Stein S. A hydrogel prepared by in situ cross-linking of a thiol-containing poly(ethylene glycol)-based copolymer: a new biomaterial for protein drug delivery. Biomaterials 2003;24:11-8.

[82] Nie T, Baldwin A, Yamaguchi N, Kiick KL. Production of heparin-functionalized hydrogels for the development of responsive and controlled growth factor delivery systems. J. Control. Release 2007;122:287-96.

[83] Tae G, Kim YJ, Choi WI, Kim M, Stayton PS, Hoffman AS. Formation of a novel heparin-based hydrogel in the presence of heparin-binding biomolecules. Biomacromolecules 2007;8:1979-86.

[84] Nguyen KT, West JL. Photopolymerizable hydrogels for tissue engineering applications. Biomaterials 2002;23:4307-14.

[85] Leach JB, Bivens KA, Patrick CW, Schmidt CE. Photocrosslinked hyaluronic acid hydrogels: Natural, biodegradable tissue engineering scaffolds. Biotechnol. Bioeng. 2003;82:578-89.

[86] Park YD, Tirelli N, Hubbell JA. Photopolymerized hyaluronic acid-based hydrogels and interpenetrating networks. Biomaterials 2003;24:893-900.

[87] Williams CG, Malik AN, Kim TK, Manson PN, Elisseeff JH. Variable cytocompatibility of six cell lines with photoinitiators used for polymerizing hydrogels and cell encapsulation. Biomaterials 2005;26:1211-8.

[88] Mellott MB, Searcy K, Pishko MV. Release of protein from highly cross-linked hydrogels of poly(ethylene glycol) diacrylate fabricated by UV polymerization. Biomaterials 2001;22:929-41.

[89] Schacht E, Bogdanov B, Bulcke AVD, De Rooze N. Hydrogels prepared by crosslinking of gelatin with dextran dialdehyde. React. Funct. Polym. 1997;33:109-16.

[90] Bulpitt P, Aeschlimann D. New strategy for chemical modification of hyaluronic acid: Preparation of functionalized derivatives and their use in the formation of novel biocompatible hydrogels. J. Biomed. Mater. Res. 1999;47:152-69.

[91] Luo Y, Kirker KR, Prestwich GD. Cross-linked hyaluronic acid hydrogel films: new biomaterials for drug delivery. J. Control. Release 2000;69:169-84.

[92] Ito T, Yeo Y, Highley CB, Bellas E, Benitez CA, Kohane DS. The prevention of peritoneal adhesions by in situ cross-linking hydrogels of hyaluronic acid and cellulose derivatives. Biomaterials 2007;28:975-83.

[93] Lutz JF, Zarafshani Z. Efficient construction of therapeutics, bioconjugates, biomaterials and bioactive surfaces using azide-alkyne "click" chemistry. Adv. Drug Del. Rev. 2008;60:958-70.

[94] Malkoch M, Vestberg R, Gupta N, Mespouille L, Dubois P, Mason AF, Hedrick JL, Liao Q, Frank CW, et al. Synthesis of well-defined hydrogel networks using click chemistry. Chem. Commun. (Camb.) 2006:2774-6.

[95] Crescenzi V, Cornelio L, Di Meo C, Nardecchia S, Lamanna R. Novel hydrogels via click chemistry: synthesis and potential biomedical applications. Biomacromolecules 2007;8:1844-50.

[96] Testa G, Di Meo C, Nardecchia S, Capitani D, Mannina L, Lamanna R, Barbetta A, Dentini M. Influence of dialkyne structure on the properties of new click-gels based on hyaluronic acid. Int. J. Pharm. 2009;378:86-92.

[97] Muzzarelli RAA. Genipin-crosslinked chitosan hydrogels as biomedical and pharmaceutical aids. Carbohydr. Polym. 2009;77:1-9.

[98] Moura MJ, Figueiredo MM, Gil MH. Rheological study of genipin cross-linked chitosan hydrogels. Biomacromolecules 2007;8:3823-9.

[99] Tan H, Li H, Rubin JP, Marra KG. Controlled gelation and degradation rates of injectable hyaluronic acid-based hydrogels through a double crosslinking strategy. J. Tissue Eng. Regen. Med. 2011;5:790-7.

[100] Sarvestani AS, He X, Jabbari E. Viscoelastic characterization and modeling of gelation kinetics of injectable in situ cross-linkable poly(lactide-co-ethylene oxide-co-fumarate) hydrogels. Biomacromolecules 2007;8:406-15.

[101] Temenoff JS, Shin H, Conway DE, Engel PS, Mikos AG. In vitro cytotoxicity of redox radical initiators for cross-linking of oligo(poly(ethylene glycol) fumarate) macromers. Biomacromolecules 2003;4:1605-13.

[102] Schanté CE, Zuber G, Herlin C, Vandamme TF. Improvement of hyaluronic acid enzymatic stability by the grafting of amino-acids. Carbohydr. Polym. 2012;87:2211-6.

[103] Kurisawa M, Chung JE, Yang YY, Gao SJ, Uyama H. Injectable biodegradable hydrogels composed of hyaluronic acid-tyramine conjugates for drug delivery and tissue engineering. Chem. Commun. (Camb.) 2005:4312-4.

# Chapter 2

# Injectable Enzymatically-Crosslinked Hyaluronic Acid-Tyramine Hydrogel System with Tunable Gelation Rate and Crosslink Density for Protein Delivery

## 2.1. Introduction

Hydrogels are widely used as biomaterials for drug delivery [1-3]. In particular, injectable hydrogel systems have drawn a lot of attention because of the elimination of surgical implantation [4, 5]. Hydrogels are suitable for the delivery of protein drugs, as the aqueous environment within a hydrogel is ideal for the encapsulation of proteins that are prone to denaturation in non-aqueous environment. The crosslinked polymeric network limits the mobility of the proteins, resulting in the sustained release of encapsulated proteins from the hydrogel. Consequently, the half-life of the proteins in the body is increased and the frequency of injection can be decreased, which minimizes patient discomfort, improves patient compliance, and decreases the cost of treatment. However, the initial burst-release, short release duration, and incompletely release of encapsulated drugs, are some of the drawbacks associated that remained to be overcome.

In designing hydrogels for drug delivery, one must takes into consideration the crosslink density of the hydrogels. Crosslink density is an important parameter because it plays a significant role in controlling the drug release rate [6]. Thus, the ability to tune the crosslink density of an injectable hydrogel system in a facile manner is a valuable tool for the tailoring of drug release profiles. In addition to crosslink density, gelation rate is another important parameter of an injectable hydrogel system. For drug delivery application, hydrogels should form rapidly after injection to prevent the uncontrolled diffusion of gel precursors and drug molecules to the surrounding tissues [7]. This is because a sustained-release system typically contains a higher concentration of drugs than a bolus injection, and slow gelation could lead to a large amount of drugs diffusing away from the injection site and cause drug overdose. This drawback could hamper the therapeutic outcome and render the injectable hydrogel system unsuitable for the delivery of drugs with a narrow therapeutic index. Hence, the gelation rate of an injectable hydrogel system should be tunable in order to achieve rapid network formation, while avoiding clogging of the needle due to the increase in viscosity via *in situ* crosslinking. Unfortunately, the control of gelation rate of most injectable and chemically crosslinked hydrogel systems is limited to varying the gel precursor or crosslinker concentrations [8, 9], which inevitably changes the crosslink density that leads to undesirable modifications of the drug release profiles.

In this chapter, an injectable chemically crosslinked hydrogel system that allows the independent tuning of crosslink density and gelation rate in a facile manner is described.

Specifically, horseradish peroxidase (HRP), a heme-containing enzyme found in the root of horseradish (*Armoracia rusticana)*, was employed to form hydrogels *in situ* through the oxidative coupling of phenols in the presence of hydrogen peroxide ($H_2O_2$) [10, 11]. Our laboratory has previously reported the gelation of hyaluronic acid-tyramine conjugates (HA-Tyr) in the presence of HRP and $H_2O_2$ [12]. HA was chosen as the backbone polymer because of its excellent biocompatibility and biodegradability (Chapter 1). Herein, the concentrations of $H_2O_2$ and HRP were varied systematically. It was found that the crosslink density and gelation rate could be independently tuned by the concentrations of $H_2O_2$ and HRP, respectively. Subcutaneous injections of HA-Tyr conjugates revealed that as the gelation rate accelerated with increasing HRP concentration, the hydrogel became more localized to the injection site [13].

Next, we utilized the HA-Tyr hydrogel system for protein delivery. In order to incorporate proteins in the hydrogel matrix, proteins were mixed with HA-Tyr conjugates prior to the addition of HRP and $H_2O_2$. It was demonstrated that rapid gel formation, which was achieved by an optimal concentration of HRP, could enhance the protein encapsulation efficiency and minimize the uncontrolled diffusion of proteins after injection. Using a model protein, α-amylase, we demonstrated that the rate of protein release from hydrogels could be controlled by tuning the crosslink density of the hydrogel through the concentration of $H_2O_2$. Notably, by fixing the concentration of HRP, rapid gel formation was maintained even though the crosslink density was varied. Finally, we applied the HA-Tyr hydrogel system for the delivery of interferon-α2a (IFN-α2a). IFN-α is recommended for the treatment of chronic hepatitis C due to its antiviral activity [14, 15]. It has also been shown to reduce the incidence of hepatocellular carcinoma in patients with chronic hepatitis C [16]. Moreover, IFN-α inhibits the proliferation and induces the apoptosis of liver cancer cells *in vitro* [17, 18]. However, IFN-α has short circulating half-life of 6 to 8 h, hence frequent injections are required for hepatitis C treatment [19]. Herein, IFN-α2a was incorporated in HA-Tyr hydrogels with different crosslink densities. The release profiles and the anti-proliferation activity of released IFN-α2a were examined *in vitro*. Furthermore, the pharmacokinetics and tumor regression activity of IFN-α2a delivered by HA-Tyr hydrogels were evaluated in a mice xenograft model of human liver cancer.

## 2.2. Materials and methods

### 2.2.1. Materials

HA (90 kDa) was kindly donated by JNC Corporation (Tokyo, Japan). 1-Ethyl-3-(3-dimethylaminopropyl)-carbodiimide hydrochloride (EDC·HCl), *N*-hydroxysuccinimide (NHS), tyramine hydrochloride (Tyr·HCl), 5-aminofluorescein, α-amylase from *Bacillus amyloliquefaciens*, bovine serum albumin (BSA), hyaluronidase from bovine testes, and polyoxyethylene-sorbitan monolaurate (Tween 20) were all purchased from Sigma-Aldrich (Singapore). Hydrogen peroxide ($H_2O_2$) was from Lancaster and horseradish peroxidase (HRP, 100 U/mg) was from Wako Pure Chemical Industries. Polyclonal antibody to *Bacillus amyloliquefaciens* α-amylase (biotin) was purchased from Acris Antibodies. Streptavidin alkaline phosphate conjugated and *p*-nitrophenyl phosphate (*p*-NPP) were purchased from Chemicon. Interferon-α2a (IFN-α2a, $1 \times 10^8$ IU/mg protein) was purchased from Santa Cruz (CA, USA). VeriKine™ Human Interferon-Alpha ELISA kit was purchased from PBL Interferon Source (NJ, USA). Apo-ONE® homogeneous caspase-3/7 assay kit was purchased from Promega (Singapore). Alexa Fluor 680 conjugated BSA (SAIVI Alexa Fluor 680), fetal bovine serum (FBS), alarmarBlue assay kit, Alexa Fluor® 488 annexin V/Dead cell apoptosis kit for flow cytometry, and Image-iT™ live red caspase detection kit were purchased from Life Technologies (Singapore). Bicinchoninic acid (BCA) protein assay kit was purchased from Pierce (Singapore). Phosphate buffer saline (PBS, 150 mM, pH 7.3) was supplied by media preparation facility in Biopolis, Singapore.

### 2.2.2. Synthesis of HA-Tyr conjugate

HA-Tyr conjugates were synthesized as described previously [12] with modifications to the condensation agents and purification protocol, which more effectively remove the unreacted tyramine molecules. HA (1 g, 2.5 mmol of COOH) was dissolved in 100 ml of distilled water. To this solution tyramine hydrochloride (202 mg, 1.2 mmol) was added. EDC·HCl (479 mg, 2.5 mmol) and NHS (290 mg, 2.5 mmol) were then added to initiate the conjugation reaction. As the reaction proceeded, the pH of the mixture was maintained at 4.7 with 0.1 M NaOH. The reaction mixture was stirred overnight at room temperature and then the pH was brought to 7.0. The solution was transferred to dialysis tubes with molecular cut-off of 1000 Da. The tubes were dialyzed against 100 mM sodium chloride solution for 2 days, a mixture of distilled water and ethanol (3:1) for 1 day, and distilled water for 1 day, successively. The purified solution was lyophilized to obtain the HA-Tyr conjugates. The degree of substitution (DS, the number of tyramine molecules per 100 repeating units of HA) was calculated from $^1$H NMR measurement by comparing the ratio of the relative peak

integrations of phenyl protons of tyramine (peaks at 7.2 and 6.9 ppm) and the methyl protons of HA (1.9 ppm). The DS was 6.

### 2.2.3. Synthesis of fluorescent-labeled HA-Tyr conjugate

HA (1 g, 2.5 mmol of COOH) was dissolved in 100 ml of distilled water. To this solution, tyramine hydrochloride (162 mg, 0.93 mmol) and 5-aminofluorescein (81 mg, 0.23 mmol in 1.62 ml DMSO) were added. EDC·HCl (479 mg, 2.5 mmol) and NHS (290 mg, 2.5 mmol) were then added and the pH of the mixture was maintained at 4.7 with 0.1 M NaOH. The reaction was stirred overnight at room temperature and then brought to pH to 7.0. The solution was filtered with grade 1 Whatman cellulose filter paper to remove unconjugated aminofluorescein that had precipitated. The filtrate was collected into dialysis tubes of molecular cut-off 3500 Da. Then the dialysis and lyophilization procedures for HA-Tyr described above were followed. The degree of substitution of tyramine was calculated from $^{1}$H NMR and the degree of aminofluorescein conjugated was estimated by comparing the absorbance value at 490 nm of 1 mg/ml fluorescence-conjugated HA-Tyr solution to a set of aminofluorescein standards. The DS of tyramine and aminofluorescein were 4 and 0.4, respectively.

### 2.2.4. Formation and rheological measurement of HA-Tyr hydrogels

To form HA-Tyr hydrogels, HA-Tyr conjugates were dissolved in PBS at 1.75% (w/v). Then 5 μl each of HRP and $H_2O_2$ were added to 1 ml of HA-Tyr solution to initiate gelation. Various concentrations of HRP and $H_2O_2$ were used. Rheological measurements were performed with a HAAKE Rheoscope 1 rheometer (Karlsruhe, Germany) using a cone and plate geometry of 6 cm diameter and 0.903° cone angle. Immediately after adding HRP and $H_2O_2$ to HA-Tyr conjugates, the mixture was vortexed and applied to the bottom plate. The upper cone was then lowered to a measurement gap of 0.024 mm and a layer of silicon oil was carefully applied around the cone to prevent solvent evaporation during the experiment. The measurements were taken at 37 °C in the dynamic oscillatory mode with a constant deformation of 1% and frequency of 1 Hz. To avoid slippage of samples during the measurement, a roughened glass bottom plate was used. The measurement parameters were determined to be within the linear viscoelastic region in preliminary experiments. Measurement was allowed to proceed until the storage modulus (G') reached plateau. Then, a frequency sweep was performed with a constant shear stress predetermined to induce a 10%

deformation at 1 Hz. Also, a strain sweep of increasing deformation from 1 to 100% was performed at 1 Hz.

### 2.2.5. Swelling ratio, crosslink density and mesh size of HA-Tyr hydrogels

Swelling ratios were determined for slab-shaped HA-Tyr hydrogels. To form the slab-shaped HA-Tyr hydrogels, lyophilized HA-Tyr was dissolved in PBS at a concentration of 1.75% (w/v). Five μl of HRP was added to 1 ml of HA-Tyr solution to give a final concentration of 0.124 U/ml. Crosslinking was initiated by adding 5 μl of different concentrations of $H_2O_2$ solution to give final concentrations of 160, 291, 437, 582 and 728 μM. The mixture was vortexed vigorously before it was injected between two parallel glass plates clamped together with 1 mm spacing. The crosslinking reaction was allowed to proceed at 37 °C for 1 h. Round hydrogel disks with diameters of 1.6 cm were then cut out from the hydrogel slab using a circular mold. The hydrogel disks were swollen in PBS at 37 °C for at least 24 h. The swollen disks were then gently blotted dry with Kimwipe and weighed to obtain the swollen weight. The disks were then lyophilized to obtain the dry weight. The swelling ratio is defined as a ratio of the swollen weight to the dried weight.

The volumetric swelling ratio (Qv), average molecular weight between crosslinks ($M_c$) effective crosslink density ($\nu_e$) and mesh size ($\xi$) were calculated based on previously reported methods [20]. $Q_V$ was calculated by the following equation:

$$Q_V = 1 + \frac{\rho_P}{\rho_S}(Q_M - 1),$$

where $\rho_p$ and $\rho_S$ are the density of the dried polymer (1.229 g/cm$^3$) and water, respectively.

$M_c$ was derived from the following equation using:

$$Q_V^{5/3} \cong \frac{\bar{\nu} M_C}{V_1}(0.5 - \chi),$$

where $\bar{\nu}$ is the specific volume of the dry polymer (0.814 cm$^3$/g), $V_1$ is the molar volume of water (18 mol/cm$^3$) and $\chi$ is the Flory polymer-solvent interaction parameter, which was assumed to be 0.473. Then $\nu_e$ and $\xi$ were calculated with the following equations:

$$\nu_e = \frac{\rho_p}{M_C}$$

$$\xi = 0.1748\sqrt{M_C}Q_V^{1/3}$$

### 2.2.6. Morphology study of HA-Tyr hydrogels

HA-Tyr hydrogels formed in glass vials with 0.124 U/ml of HRP and 437, 582 and 728 μM of $H_2O_2$ were swelled in MilliQ water for 24 h to reach swelling equilibrium before cutting into thin slices (2 mm x 5 mm x 8 mm) using a sharp surgical blade. The samples were frozen rapidly by plunging them into liquid nitrogen slush and then freeze-dried for two days. Scanning electron microscopy (SEM) images of the lyophilized samples were taken using FEI Company Quanta 200 (Oregon, USA) equipped with a gaseous secondary electron detector in low vacuum mode.

### 2.2.7. Effects of gelation rate on gel formation and protein encapsulation *in vivo*

To examine the effect of gelation rate on hydrogel formation *in vivo*, nonobese diabetic/severe combined immunodeficiency (NOD/SCID) mice were used immediately after euthanization. After shaving the dorsal sides, each mouse was injected subcutaneously with 400 μl of 1.75% (w/v) fluorescence-labeled HA-Tyr with 728 μM $H_2O_2$ and different concentrations of HRP (0, 0.031 and 0.124 U/ml). Two hours after injection, the locations of fluorescent HA-Tyr hydrogels were detected using GE's eXplore Optix fluorescence imaging machine (Waukesha, WI) equipped with a 470 nm excitation laser. After fluorescence imaging, incisions were made to expose the site of injections and digital photographs were taken.

To examine the effect of gelation rate on protein encapsulation, adult female BALB/c nude mice was injected subcutaneously with 300 μl of 1.75 % (w/v) fluorescent HA-Tyr solution containing 80 μg of Alexa 680 conjugated BSA. The $H_2O_2$ concentration was 728 μM and the HRP concentration was 0, 0.031 or 0.124 U/ml. An hour later, fluorescence images of the mice were taken using the IVIS imaging system (Caliper Life Science, Massachusetts, USA) to determine the location of HA-Tyr conjugates (GFP filter set, $\lambda_{ex}$ = 445-490 nm, $\lambda_{em}$ = 515-575 nm, exposure time = 0.05 second) and the proteins (Cy5.5 filter set, $\lambda_{ex}$ = 615-665 nm, $\lambda_{em}$ = 695-770 nm, exposure time = 0.01 second). For both detections,

the binning of the CCD camera was set to 8; field of view (FOV) was 20 cm and the aperture of the lens on the camera was set to f/8. The care and use of laboratory animals were performed according to the protocol approved by the Institutional Animal Care and Use Committee (IACUC) at the Biological Resource Center (BRC) in Biopolis, Singapore.

### 2.2.8. Release of α-amylase from HA-Tyr hydrogels

HA-Tyr hydrogels loaded with 0.25 mg/ml of α-amylase were prepared by mixing 500 μl of HA-Tyr (3.5 % (w/v)) with 500 μl of protein solution (0.5 mg/ml). Then 5 μl each of HRP and $H_2O_2$ (final concentrations of HRP: 0.124 U/ml and $H_2O_2$: 437, 582 or 728 μM) was added and the mixture was vortexed gently before injected between two parallel glass plates clamped together with 1 mm spacing. Gelation was allowed to proceed at 37 °C for one hour at which G' would have reached plateau according to the rheology results. Round gel disks with diameter of 1.6 cm were then cut out from the hydrogel slab using a circular mold. Each disk was sandwiched between a plastic net and immersed in 20 ml of PBS. The samples were incubated at 37 °C on an orbital shaker at 100 rpm. At selected time points, 200 μl of the release medium was drawn and stored in a microcentrifuge tube containing 200 μl of 0.1 mg/ml BSA in PBS to prevent non-specific adsorption of the model proteins to the plastic surface of the microcentrifuge tubes. Two hundred μl of PBS was added to maintain the total release medium at 20 ml. The collected samples were stored at -20 °C.

Protein concentrations were determined by enzyme-linked immunosorbant assay (ELISA), which was carried out at room temperature. The washing procedure between each step was carried out by a plate washer (Amersham Bioscience), which was programmed to wash the wells three times with 300 μl of washing buffer (100 mM PBS containing 0.05 % Tween-20). One hundred μl of the samples thawed to room temperature was added to the wells of a 96-well MaxiSorb ELISA plate (NUNC). The proteins in the samples were bound to the well by incubation for 1.5 h and then the wells were washed. After washing, the wells were blocked with 200 μl of blocking buffer (BSA 2 % (w/v) in PBS) for 30 minutes to saturate the protein-binding sites and then the wells were washed. Then, 100 μl of biotinylated anti-α-amylase (2 μg/ml) antibodies diluted in blocking buffer were added to the wells and incubated for 1 h. After washing, 100 μl of streptavidin-alkaline phosphatase diluted in PBS was added and incubated for 1 h and then the wells were washed. Finally, 100 μl of *p*-NPP was added to each well and the plate was incubated until sufficient color had developed (approximately 80 min).

The absorbance at 405 nm was measured using Tecan Infinite 200 microplate reader. The amount of proteins contained in each sample was calculated by comparing to a set of protein standards. It was observed that the ELISA signal of a solution of α-amylase (2.66 μg/ml) in PBS at 37 °C decreased linearly with time and was reduced by 30 % at the end of 24 h. This might be due to adsorption of α-amylase to glass surface or denaturation of the protein. In order to compensate for the loss in signal, the amount of released α-amylase estimated by ELISA was adjusted according to the percentage loss observed in the controls.

Rheological measurements of the hydrogels incorporated with proteins were performed with a HAAKE Rheoscope 1 rheometer (Karlsruhe, Germany) using a cone and plate geometry of 3.5 cm diameter and $0.949^{o}$ cone angle. The measurements parameters were the same as described above.

### 2.2.9. Activities of α-amylase released from HA-Tyr hydrogels

Hydrogel disks (thickness: 1 mm, diameter: 8 mm) containing 5 mg/ml of α-amylase were degraded in 5 ml of 200 U/ml of hyaluronidase in PBS with 0.05 % (w/v) $NaN_3$ at 37 °C on an orbital shaker at 150 rpm. After 24 h, no visible sign of the hydrogels was observed. The activity of the α-amylase released into the degradation solution was determined by EnzChek Ultra Amylase Assay Kit (Invitrogen). Briefly, the degradation solutions containing the released α-amylase were diluted 200-folds with PBS. Fifty μl of the diluted samples were added to the wells of a 96-well fluorescence plate and then 50 μl of the substrates were added. The plate was incubated for 10 minutes on an orbital shaker at room temperature and then the fluorescence intensity ($\lambda_{ex}$ = 485 nm, $\lambda_{em}$ = 530 nm) was measured using the Tecan Infinite 200 microplate reader. The activities retained were determined by comparing to the activities of control protein solutions, which had been incubated for 24 h at 37 °C.

### 2.2.10. Release of IFN-α2a from HA-Tyr hydrogels

Hydrogels incorporated with IFN-α2a were prepared such that the final concentrations of HA-Tyr conjugates, IFN-α2a, HRP and $H_2O_2$ were 1.75% (w/v), $2.5 \times 10^5$ IU/ml, 0.124 U/ml, and 437 or 728 μM respectively. The gel mixture was injected between two parallel glass plates clamped 1.5 mm apart. Gelation was allowed to proceed at 37 °C for 2 h. Hydrogel disks, 1.6 cm in diameter, were then cut from the hydrogel slab using a circular mold. Each disk was placed in a plastic net and immersed in 20 ml of buffer solution (PBS with 0.5%

BSA). At selected time points, 200 μl of the media was withdrawn and replaced with an equal volume of fresh buffer solution to maintain a constant total volume. The collected samples were stored in LoBind tubes (Eppendorf, Germany) at 4 °C until analysis. Protein concentrations were determined by ELISA. Rheological measurement was performed as described above.

### 2.2.11. Cell viability assay

Human hepatic cancer cell line (HAK-1B) was obtained from Prof. Hirohisa Yano, Kurume University, Japan, and was grown in DMEM media with 2.5% FBS [21]. Cells were cultured in a humidified incubator at 37 °C, 5% $CO_2$. To examine the effect of IFN-α2a released from HA-Tyr hydrogels on cell proliferation, 500 μl of HAK-1B cell suspension ($1.2 \times 10^4$ cells total) was added per well of a 24-well plate and incubated for 2 days before treatment. On the day of treatment, 50 μl of hydrogels (final composition: 1.75% (w/v) of HA-Tyr conjugates, $4 \times 10^5$ IU/ml of IFN-α2a, 0.124 U/ml of HRP and 437 or 728 μM of $H_2O_2$) were prepared in a 24-well transwell insert. After 2 h of gelation, the hydrogel-loaded inserts were placed into the wells previously seeded with HAK-1B cells and 500 μl of culture medium was added to the insert. The plate was incubated for 4 days. After which the cell viability was assessed using alamarBlue assay according to the manufacturer's protocols ($\lambda_{ex}$ = 560 nm and $\lambda_{em}$ = 590 nm). The results were expressed as percentages of control (no treatment).

### 2.2.12. Caspase activity

An Apo-ONE® homogeneous caspase-3/7 kit was utilized to quantitatively measure caspase-3/7 activity in HAK-1B cells. After cells were treated with IFN-α2a-incorporated HA-Tyr hydrogels for 4 days, cells were lysed with a radio immunoprecipitation assay (RIPA) buffer (Cell Signaling, USA), followed by BCA assay to determine the total amount of proteins in each sample. Then the amount of caspase-3/7 in the samples was determined according to the manufacturer's protocol ($\lambda_{ex}$ = 499 nm and $\lambda_{em}$ = 521 nm). The caspase-3/7 activity was expressed as fluorescence intensity normalized by the protein amount (FI/μg).

### 2.2.13. Tumor regression study

To examine the anti-tumor effect of IFN-α2a delivered by HA-Tyr hydrogels, 200 μl of HAK-1B cells ($5 \times 10^7$ cells/ml) were subcutaneously injected to the back of 6-week-old female BALB/c nude mice. Seven days later, when diameter of the tumor reached 5-10 mm, the mice were divided into 4 groups (n = 7) so that the average tumor size in each group was similar. Two groups of mice were treated with hydrogels containing IFN-α2a (final compositions: 1.75% (w/v) of HA-Tyr conjugates, $1.4 \times 10^8$ IU/kg of IFN-α2a, 0.124 U/ml of HRP, and 473 or 728 μM of $H_2O_2$). Hydrogels were injected by subcutaneously once a week for 2 weeks. The remaining two groups were treated with PBS or IFN-α2a solution once a week for 2 weeks. Tumors were measured with a digital caliper and the tumor volumes ($mm^3$) were calculated from the formula: volume = (length × width$^2$)/2. The mice were sacrificed on day 20 and the tumors were resected and fixed in 4% formaldehyde solution. In a separate study, the amount of IFN-α2a delivered to the tumor was determined. Three groups of mice (n = 4) bearing HAK-1B tumors of similar sizes were injected with IFN-α2a solution or HA-Tyr hydrogels containing IFN-α2a. After 8 h, the mice were sacrificed and the tumor tissues were resected and homogenized. The supernatant of tissue lysate was stored at -20 $^oC$ until analysis. The amount of IFN-α2a in the supernatant was determined by ELISA.

### 2.2.14. Pharmacokinetics study

To examine the pharmacokinetics of IFN-α2a delivered by HA-Tyr hydrogels, 3 groups of female BALB/c nude mice (6-week-old, n = 4) were used for the study. Two groups of mice were treated with HA-Tyr hydrogels containing IFN-α2a (final composition: 1.75% (w/v) of HA-Tyr, $6 \times 10^7$ IU/ml of IFN-α2a, 0.124 U/ml of HRP and 473 or 728 μM of $H_2O_2$ in PBS). The remaining group was injected with IFN-α2a solution ($6 \times 10^7$ IU/ml in PBS) and served as the control. Injections were administered subcutaneously at the back of the mice and the injection volume was based on the weight of the mouse (200 μl per 20 g). At 1, 2, 4, 8 and 24 h post-injection, 20 μl of blood was withdrawn from the tail vein. The blood samples were mixed with 3 μl of sodium citrate (37 mg/ml) to prevent blood coagulation and then centrifuged at 4 °C, 3,000 g for 5 min. The supernatant of each sample was stored at -20 °C until the day of analysis. The amount of human IFN-α2a in the plasma of the mice was determined by ELISA.

### 2.2.15. Statistical analysis

All data are expressed as the mean ± standard deviation (SD). Differences between the values were assessed using Student's *t*-test or one-way ANOVA, and $p < 0.05$ was considered statistically significant. Data from animal studies are expressed as mean ± standard error of the mean (SEM).

## 2.3. Results and discussion

### 2.3.1. Synthesis of HA-Tyr conjugates

Tyramine was successfully conjugated to HA *via* carbodiimide-mediated coupling reaction. The resulting HA-Tyr conjugates were purified by dialysis against NaCl solution to disrupt electrostatic interactions between unconjugated tyramine and HA. Then, the HA-Tyr conjugates were dialyzed against distilled $H_2O$ before lyophilization. Yield = 80%. The degree of substitution (DS, the number of tyramine molecules per 100 repeating units of HA) was calculated from $^1$H NMR measurement and found to be 6. For long-term storage, HA-Tyr conjugates were kept at r.t. as dried products. Once dissolved in water or PBS, a solution of HA-Tyr conjugates remained stable at 4 °C for at least 3 months.

### 2.3.2. Catalytic mechanism of horseradish peroxidase (HRP)

HRP is a heme-containing enzyme found in the root of horseradish (*Armoracia rusticana)*. Heme is a complex between protoporphyrin and Fe(III). The heme iron in HRP forms a coordinate bond with the proximal His170 residue of the protein core. There are several HRP isoenzymes; the most abundant is the C isoenzyme, which is also the most widely characterized. The catalytic mechanism of HRP in the presence of $H_2O_2$ has been the subject of investigation for many years and several excellent publications are available in the literature [22, 23]. It is known that the catalytic reaction involves not only the heme group, but also the amino acid residues on the protein core, such as His42 and Arg38.

The first event in the catalytic reaction, after binding of $H_2O_2$ to the heme at its resting state, Fe(III), is a proton transfer from the α-oxygen of $H_2O_2$ to the His42 residue of HRP. The α-oxygen then forms a single bound with Fe(III), which results in a transient Fe(III)-hydroperoxy intermediate that is designated as Compound 0 [24]. Next, the α-oxygen forms a double bond with the heme iron, a process which is facilitated by the cleavage of the peroxide O-O bond and an electron transfer from the porphyrin ring to the iron. This results in a Fe(IV)=O ferryl group and a porphyrin cation radical, which together is termed Compound I

(Fig. 2-1). The residual ˙OH group of $H_2O_2$ receives the proton from the His42 residue to form a water leaving group. Compound I is two oxidation states above the resting state, hence two successive electron transfers are required to reduce it back to the resting state. This is where the reducing substrate, in this case, the tyramine moieties of HA-Tyr conjugates, comes into play. In the first reduction step, a phenolic hydrogen atom is donated to Compound I, the electron of the hydrogen atom is transferred to the porphyrin cation radical while the proton goes the His42 residue. The first reduction results in the formation of Compound II, which contains the neutralized porphyrin and the Fe(IV)=O group, and a phenolic radical. The second reduction step, which is a complex reaction involving the protonated His42 residue and an electron transfer from a phenol substrate, regenerates the Fe(III) and forms a second phenolic radical with water as a leaving group. Thus, a catalytic cycle of HRP consumes one $H_2O_2$ molecule, converts two phenols into phenolic radicals and produces two water leaving groups. The phenol radicals couple with each other through either a more common C-C linkage between the *ortho*-carbons of the aromatic ring or a C-O linkage between the *ortho*-carbon and the phenolic oxygen [25].

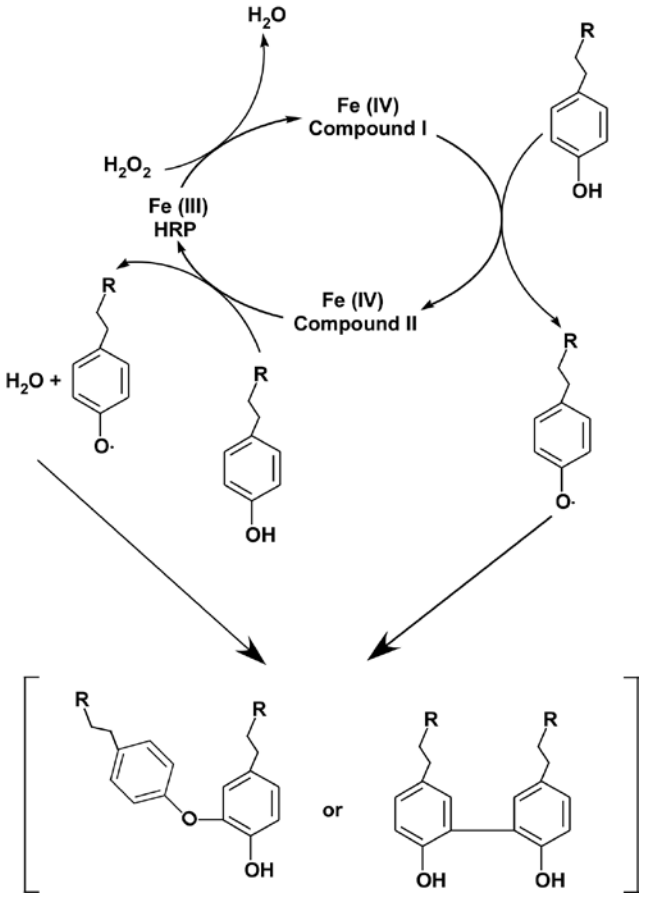


**Fig. 2-1. Coupling of phenols by HRP and $H_2O_2$.**

### 2.3.3. Rheology, swelling ratio and SEM characterization of HA-Tyr hydrogels

HA-Tyr hydrogels were formed *via* the oxidative coupling of tyramine moieties in the presence of HRP and $H_2O_2$ (Fig. 2-2). The formation of HA-Tyr hydrogels was studied using oscillatory rheometry. Fig. 2-3a shows the typical evolutions of storage modulus (G'), loss modulus (G'') and phase angle (δ) of HA-Tyr hydrogels formed with 728 μM of $H_2O_2$ and 0.025 U/ml of HRP. At the beginning of the crosslinking process, G'' was two orders of magnitude greater than G' and the phase angle was at 90°, indicating a predominantly viscous material. As time progressed, both G' and G'' increased and crossover of the two moduli occurred at 45° phase angle. This point is defined as the gel point which is known as the transition point from a viscoelastic liquid to a viscoelastic solid [26]. Herein, the time required to reach the gel point is used as an indicator of the gelation rate. After the gel point, G' continued to increase and eventually reached plateau at which the phase angle was close to zero, indicating a solid-like elastic material.

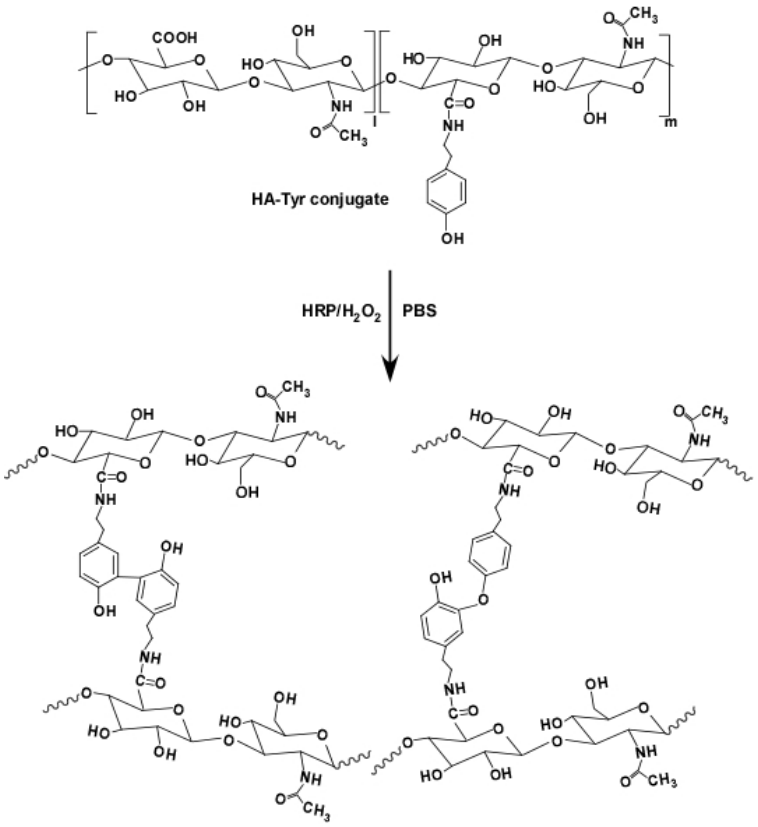


**Fig. 2-2. Formation of hydrogel composed of HA-Tyr conjugates by HRP-mediated oxidation reaction.**

Based on the catalytic mechanism of HRP, increase in the feed amount of $H_2O_2$ would generate more tyramine radicals, which in turn would form more crosslinkages. Indeed, when

the concentrations of HRP (0.062 U/ml) and HA-Tyr conjugates (1.75 % w/v) were kept constant, increasing the feed amount of $H_2O_2$ from 146 μM to 1092 μM resulted in the increase in the G' of the hydrogel, which indicates an increase in the crosslink density [13, 27] (Fig. 2-3b). The gel point remained unchanged at about 130 seconds, indicating that gelation rate was independent of $H_2O_2$ concentration. The time required for G' to reach plateau, i.e. the time needed to form all the possible tyramine crosslinks, also increased with $H_2O_2$ concentration, suggesting that HRP was continuously oxidized by $H_2O_2$ and reduced by tyramine until all $H_2O_2$ has been depleted. G' peaked at 1092 μM of $H_2O_2$, and further increase in $H_2O_2$ concentration resulted in the decline of G'. This was likely due to an excess amount of $H_2O_2$ reacting with HRP, resulting in two different types of catalytically inactive compounds being formed, namely, Compound III and IV [28]. Compound III is a reversible intermediate which will slowly revert back to the native enzyme, leading to the restoration of catalytic activity. On the other hand, Compound IV is an irreversible compound which cannot regain its catalytic activity. HRP might also be inactivated *via* attack on the protoporphyrin by phenoxyl radicals, which led to heme destruction [29]. As a result of HRP inactivation, the crosslinking reaction was inhibited.

Fig. 2-3c shows the effects of HRP concentration on hydrogel formation while $H_2O_2$ concentration was fixed at 728 μM. Both the gel point and the time required for G' to reach plateau decreased concomitantly as HRP concentration increased, indicating an inverse relationship between HRP concentration and gelation rate. At 0.124 U/ml of HRP, gelation happened so quickly that the gel point was reached within 60 seconds. At an even higher concentration of HRP (1.24 U/ml), hydrogel was formed within one second (data not shown). Interestingly, G' remained in the same order of magnitude when the HRP concentration was 0.032 U/ml and above.

To gain further understanding of the mechanical property of HA-Tyr hydrogels, the effects of frequency and strain on G' of the hydrogels were investigated. Frequency sweeps were performed on HA-Tyr hydrogels formed with various concentrations of $H_2O_2$ but fixed HRP concentration (0.062 U/ml) (Fig. 2-3d). Except for the weakest hydrogel, G' remained independent of frequencies, indicating rigid and elastic networks. Fig. 2-3e shows the strain sweeps of HA-Tyr hydrogels. G' of hydrogels formed with $H_2O_2$ concentrations between 146 and 437 μM were independent of strain, demonstrating that these hydrogels are physically stable. Above 582 μM of $H_2O_2$, the hydrogels showed a slight increase in G' at high strain. Furthermore, the hydrogel formed with 728 μM of $H_2O_2$ showed a sudden decrease in G'

beyond 60% strain, indicating a yield stress where the hydrogel was deformed irreversibly. The observed yielding is ascribed to the inherent brittle structure of hydrogels possessing high G'.

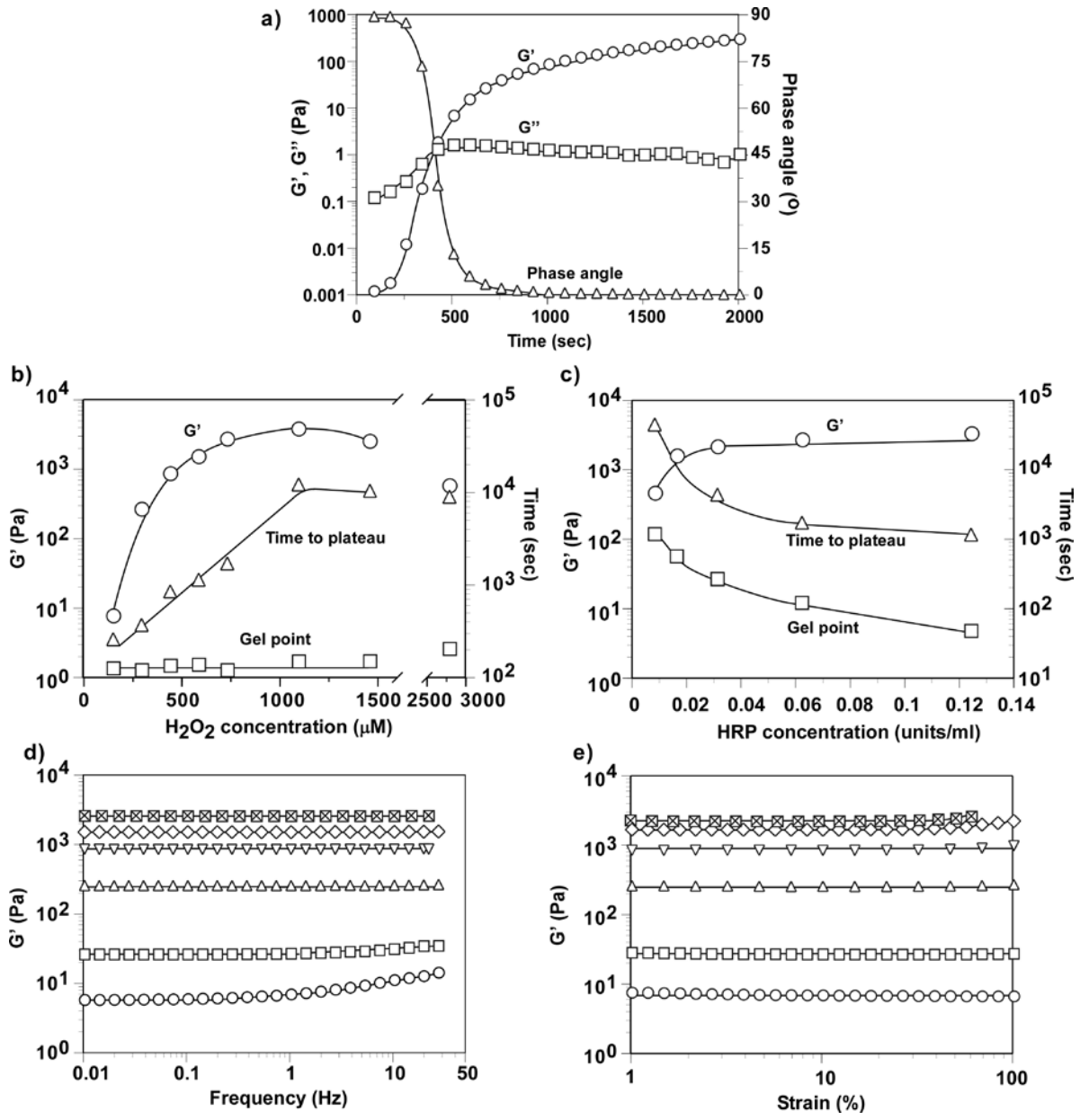


**Fig. 2-2. Rheological characterization of HA-Tyr hydrogels. (a) Typical evolutions of the storage modulus G' (○), loss modulus G'' (□) and phase angle δ (△) of HA-Tyr hydrogel formed with 0.025 U/ml of HRP and 728 μM of $H_2O_2$. Measurement was taken with a constant deformation of 1% at 1 Hz, 37 °C. Effects of (b) $H_2O_2$ and (c) HRP concentration on the G' (○), the gel point (□) and the time needed for G' to reach plateau (△). HRP and $H_2O_2$ concentrations are fixed to 0.062 U/ml for (b) and 728μM for (c), respectively. (d) Frequency sweep and (e) amplitude sweep of hydrogels formed with 0.062 U/ml of HRP and 146 (○), 160 (□), 291 (△), 437 (▽), 582 (◇), and 728 (⊠) μM of $H_2O_2$.**

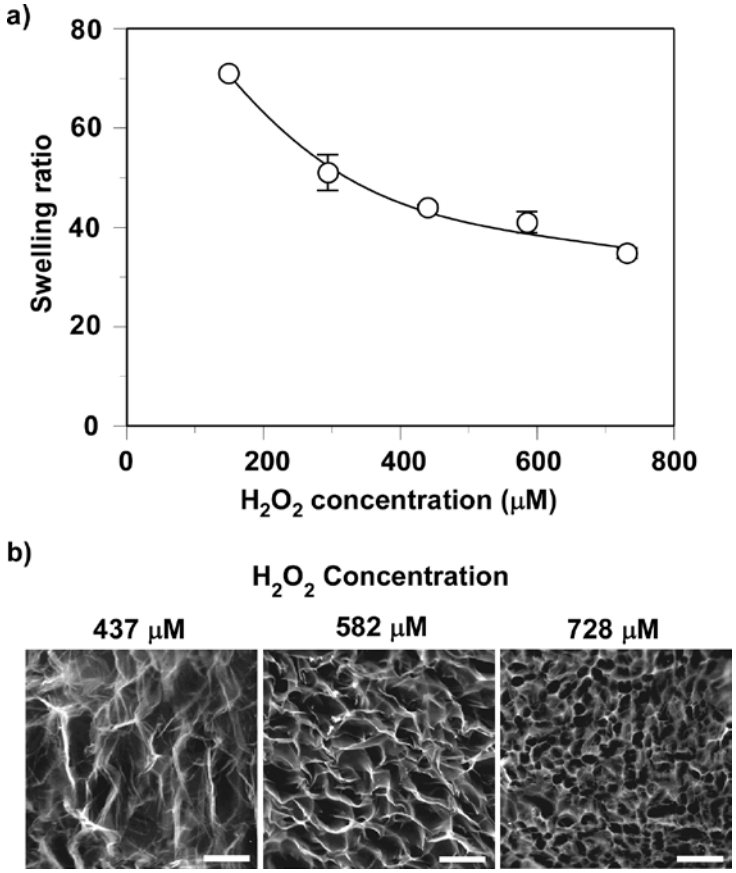


**Fig. 2-4. (a) Swelling ratios of hydrogels formed with 0.062 U/ml of HRP and various concentrations of $H_2O_2$ (n = 3). (b) SEM images of HA-Tyr hydrogels formed with 0.124 U/ml of HRP and 437, 582 and 728 μM of $H_2O_2$. Scale bar = 100 μm.**

The swelling ratio of HA-Tyr hydrogels formed with different concentrations of $H_2O_2$ is shown in Fig. 2-4a. As expected, the swelling ratio decreased with increasing concentration of $H_2O_2$, indicating that the swelling capacity was reduced due to more crosslinks. SEM images of freeze-dried hydrogels revealed that the pore size decreased with increasing $H_2O_2$ concentration, which supported the swelling ratio results (Fig. 2-4b). The rheological data, swelling ratio studies and morphological analysis demonstrated that the crosslink density and gelation rate of HA-Tyr hydrogels could be controlled independently by $H_2O_2$ and HRP concentration, respectively. The independent control of crosslink density and gelation rate allows the formation of hydrogel with different mechanical strengths at the same gelation rate.

### 2.3.4. Effects of gelation rate on hydrogel formation and protein encapsulation

Fluorescent-labeled HA-Tyr solutions with 728 μM $H_2O_2$ and different concentrations of HRP were injected subcutaneously to the back of mice. Two hours post-injection, fluorescence images were taken to detect the position of the HA-Tyr hydrogels (Fig. 2-5a, b

and c). When HA-Tyr solution was injected without HRP (Fig. 2-5a), no gel was formed and the injected solution spread out from the administered site, suggesting that the polymer solution diffused readily in the subcutaneous environment. As HRP concentration increased from 0.031 to 0.124 U/ml (gelation rate: 0.031 < 0.124 U/ml), the surface area detected with fluorescence decreased while the fluorescence intensity increased, indicating a more localized hydrogel formation at the injection site due to a faster gelation rate. Notably, the hydrogel formed with 0.124 U/ml of HRP had a more defined 3-dimensional structure compared to the hydrogel formed with 0.031 U/ml of HRP (Fig. 2-5g and h).

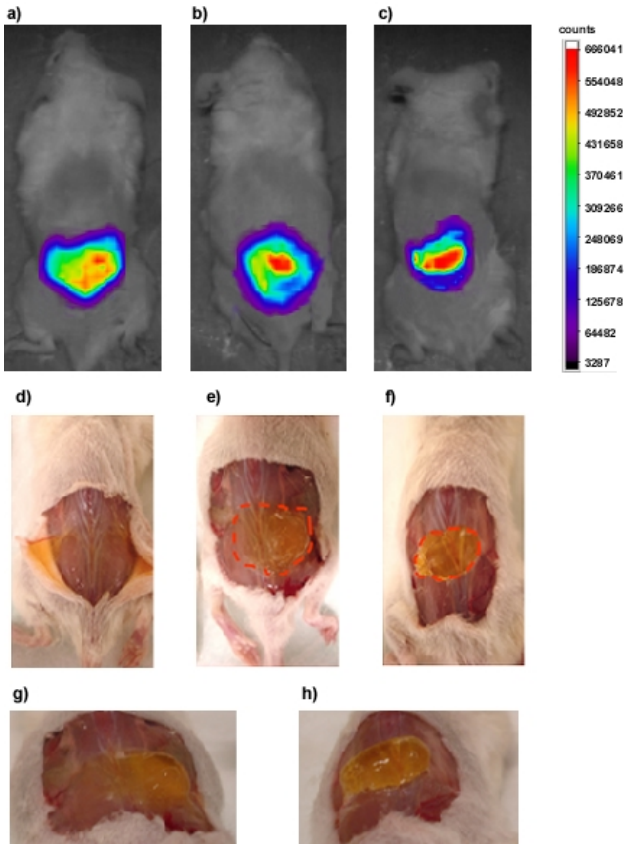


**Fig. 2-5. Effects of HRP on the subcutaneous formation of fluorescent HA-Tyr hydrogels formed with 728 μM of $H_2O_2$ and a) 0, b) 0.031 and c) 0.124 U/ml of HRP. Top (d, e and f) and side view (g and h) of the hydrogels formed with d) 0, e) and g) 0.031, and f) and h) 0.124 U/ml of HRP.**

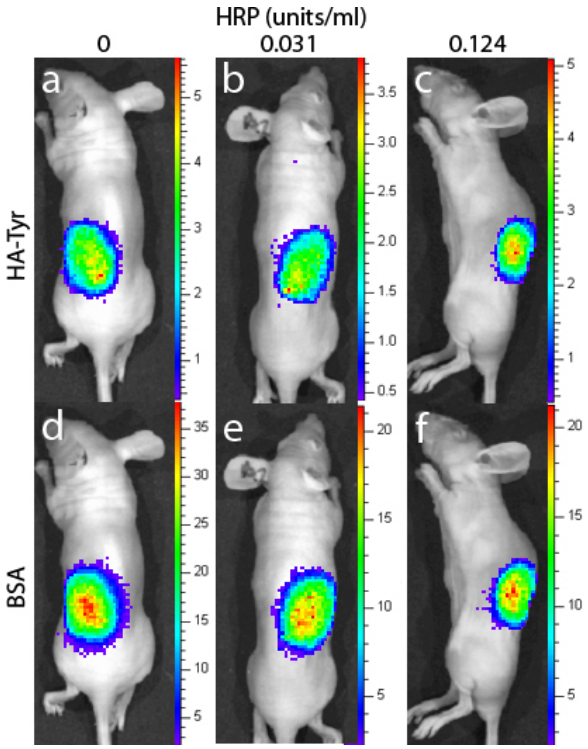


**Fig. 2.6. In vivo formation of HA-Tyr hydrogels containing BSA. $H_2O_2$ concentration was fixed to 728 μM while the concentration of HRP increased from 0 (a, d) to 0.031 (b, e) to 0.124 (c, f) U/ml. The upper row (a-c) shows the locations of HA-Tyr and the lower row (d-f) shows the location of BSA. Color bar has the unit of 109 photons/sec/cm2/steradian.**

It is crucial for an injectable hydrogel system to crosslink rapidly because slow gelation could result in delocalized gel formation due to diffusion of the gel precursors away from the injection site [13, 30]. It could also cause undesired leakage of the proteins to the surrounding tissues and compromise the therapeutic outcome. Fig. 2-6 shows the formation of HA-Tyr hydrogels containing proteins in the subcutaneous environment. Immediately after the addition of HRP (final concentration: 0, 0.031 or 0.124 U/ml) to an aqueous solution of fluorescent HA-Tyr conjugates containing $H_2O_2$ and Alexa Fluor 680-labelled BSA, the mixture was injected subcutaneously on the back of nude mice. In the absence of HRP, no network was formed and both the HA-Tyr conjugates (Fig. 2-6a) and the proteins (Fig. 2-6d) spread from the injection site, suggesting that the components diffused readily in the subcutaneous environment. When 0.031 U/ml of HRP was added, the areas detected with HA-Tyr did not reduce, suggesting that the crosslinking reaction was not sufficiently fast to confine the network at the injection site (Fig. 2-6b). It was determined that 0.124 U/ml of HRP, which had a gel point of around 1 min, was the highest concentration suitable for injection without clogging of the needle. By injecting the mixture solution containing 0.124

U/ml of HRP, both of the areas detected with HA-Tyr (Fig. 2-6c) and proteins (Fig. 2-6f) reduced, indicating that rapid gelation was required to not only localize the formation of the hydrogels and but also effectively encapsulate the proteins within the network.

### 2.3.5. Effects of crosslink density of HA-Tyr hydrogels on the rate of protein release

Crosslink density is one of the key parameters in modulating the release rate of drugs from hydrogel-based carriers [31]. As the crosslink density increases, the average molecular distance between adjacent crosslinks reduces, hence the diffusivity of drugs through the hydrogel decreases. Variations in the gel precursor concentration [2, 20, 32, 33], the molecular weight of the polymer [34, 35] and the degree of substitution of the crosslinking moiety [36] are some of the common methods to control the crosslink density. As discussed above, the crosslink density of enzymatically crosslinked HA-Tyr hydrogels could be tuned by the $H_2O_2$ concentration [13]. To examine the effect of crosslink density on protein release, HA-Tyr hydrogels incorporating α-amylase (55 kDa, pI = 5.09 [37]) were prepared by mixing the protein with the gel precursors before the additions of HRP and $H_2O_2$. Hydrogels with slab geometry were formed and immersed in 20 ml of PBS at 37°C. The aim was to investigate whether changes in the crosslink density of HA-Tyr hydrogels, through variations in $H_2O_2$ concentration, could affect the release rate of proteins. Herein, low, medium and high crosslinked hydrogels referred to HA-Tyr hydrogels formed with 0.124 U/ml of HRP and 437, 582 and 728 μM of $H_2O_2$, respectively (Table 2-1).

The release of α-amylase from HA-Tyr hydrogels exhibited a rapid release at the beginning, which was likely due to the protein concentration gradient inside and outside of the hydrogel that caused the proteins near the surface of the gel to diffuse rapidly out of the matrix (Fig. 2-7a) [38]. The release rate of proteins in the first two hours decreased significantly as the swelling ratio of the hydrogel decreased (Table 2-1). By plotting the release of α-amylase during the first few hours as a function of the square root of time, a linear plot was obtained, which indicated first order release that was typical of Fickian diffusion (Fig. 2-7a inset) [32, 33]. This was true for the low, medium and high crosslinked hydrogels up to 60, 40 and 30 % of release, respectively. After the rapid release, the release rate decreased, and 90 % of α-amylase was released in 6 h for the low crosslinked hydrogels, while approximately 75 and 41 % of proteins were released from the medium and high crosslinked hydrogels at 24 h, respectively.

**Table 2-1.** Rheological property, swelling ratio and release rate of HA-Tyr hydrogels incorporated with α-amylase[a]

| Sample | $H_2O_2$ (μM) | G' (Pa) | Gel point (s)[b] | Swelling ratio | Release rate (% / h)[c] |
|---|---|---|---|---|---|
| Low crosslinked | 437 | 848 ± 19 | 54 ± 5 | 52.7 ± 0.1 | 37.0 ± 1.0 |
| Medium crosslinked | 582 | 1675 ± 21[†] | 60 ± 8 | 43.6 ± 0.4[†] | 25.8 ± 0.5[†] |
| High crosslinked | 728 | 2602 ± 92[†‡] | 61 ± 4 | 35.8 ± 0.5[†‡] | 16.9 ± 0.2[†‡] |

[a]All samples contained 1.75 % (w/v) of HA-Tyr conjugates, 0.124 U/ml of HRP and 0.25 mg/ml of proteins. [b]Gel point is defined as the time at which the crossover of storage modulus (G') and loss modulus (G'') occurred. Herein, it is used as an indicator of the rate of gelation. There was no significant difference between the gel points of hydrogels formed with different concentrations of $H_2O_2$ (n = 2). [c]Release rate is estimated by taking the slope of the linear fit of cumulative release in the first two hours (n = 2-3). [†]Indicates that the value is significantly different from that of the low crosslinked gel ($p < 0.05$). [‡]Indicates that the value is significantly different from that of the medium crosslinked gel ($p < 0.05$).

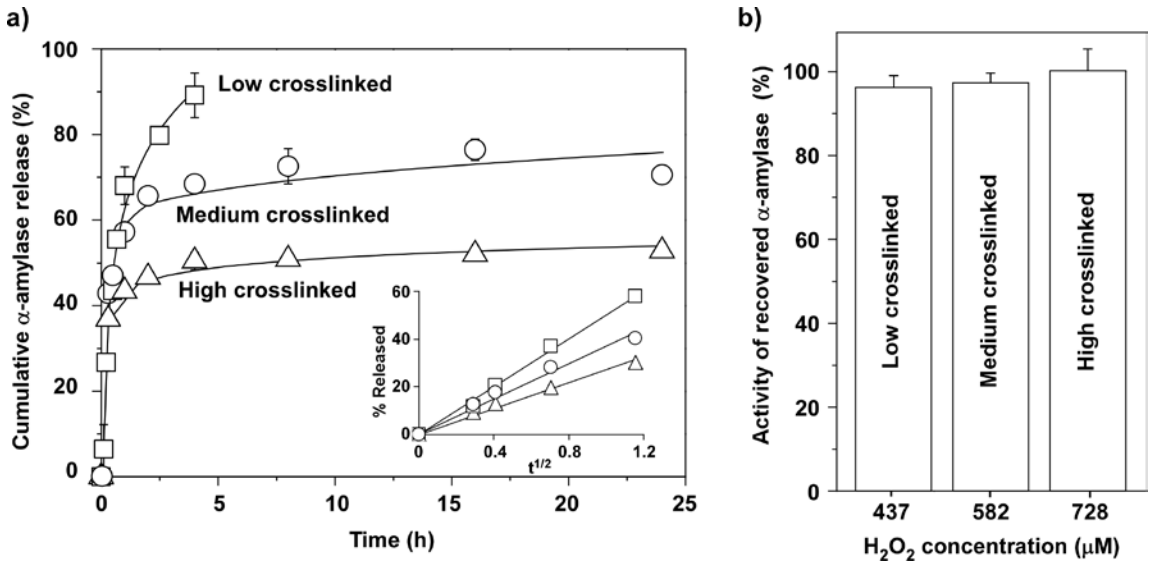


**Fig. 2-7. a) Cumulative release of α-amylase from HA-Tyr hydrogels formed with 0.124 U/ml of HRP and (□) 473, (○) 582 and (△) 728 μM of $H_2O_2$ (n = 2, mean ± SD). The inset shows the cumulative release as a function of the square root of time. b) Activities of α-amylase recovered from HA-Tyr hydrogels formed with different concentrations of $H_2O_2$. The proteins were recovered from the hydrogels by degradation of the hydrogel network in the presence of 200 U/ml of hyaluronidase for 24 h (n = 3, mean ± SD).**

It is important that a hydrogel system for protein delivery not only delivers the proteins at a controlled release rate but also maintains the activity of the proteins from the time of hydrogel preparation to the point of release. In addition, degraded products from the delivery system might cause protein denaturation, as in the case of poly(lactic-*co*-glycolic acid) (PLGA)-based systems [39, 40]. Ideally, both the gel-forming process and the degraded products of hydrogel system should not compromise the therapeutic effects of the

encapsulated proteins. Fig. 2-7b shows the activity of α-amylase recovered from HA-Tyr hydrogels with different crosslink densities by degrading the hydrogels in hyaluronidase solution. More than 95 % of the activities of α-amylase were retained regardless of the crosslink density, indicating that the enzyme-mediated crosslinking reaction and the degraded products of the hydrogels did not compromise the activity of the proteins.

### 2.3.6. Delivery of IFN-α2a using HA-Tyr hydrogels

Having established that the release rate of proteins could be tuned by controlling the crosslink density of HA-Tyr hydrogels, we proceeded to examine the delivery of a therapeutic protein using HA-Tyr hydrogels, namely, INF-α2a. Type I IFNs, such as interferon-alpha (IFN-α), are produced by host cells in response to viral infection. Binding of IFN-α to cell surface receptors leads to the activation of several interferon-stimulated genes which interfere with viral replication, protein synthesis and assembly, thus protecting the cells from viral infection [4]. IFN-α also enhances immune response by activating immune cells. Because of its anti-viral activity, IFN-α is recommended for the treatment of chronic hepatitis C [4, 5]. IFN-α is also known to induce tumor regression in cancer patients [3], and inhibit the proliferation of liver cancer cells *in vitro* [17, 18].

Two different $H_2O_2$ concentrations were used (437 and 728 μM) to form hydrogels with different crosslink densities. The effective crosslink density ($\nu_e$) and mesh size ($\xi$) were determined based on the swelling ratios of the hydrogels (Table 2-2). Hydrogels formed with 437 μM of $H_2O_2$ had a lower crosslink density and a greater mesh size compared to hydrogels formed with 728 μM of $H_2O_2$. Incorporation of IFN-α2a into the hydrogel did not affect the G', crosslink density and mesh size of the hydrogels. Hydrogels incorporated with IFN-α2a were immersed in PBS solution and the amount of proteins released over time was determined. Similar to the release profiles of α-amylase, the release rate depended on the crosslink density of the hydrogel (Fig. 2-8a). The hydrodynamic radius of IFN-α2a (2.73 nm [41]) was considerably smaller than the mesh size of HA-Tyr hydrogel (577 and 407 nm for the low and high crosslinked gels, respectively), suggesting that IFN-α2a could diffuse freely within the gel matrix. This was confirmed by plotting the release of IFN-α2a during the first 8 h as a function of the square root of time. A linear plot was obtained, which suggested Fickian diffusion with first order release kinetics (Fig. 2-8a inset). The cumulative release of IFN-α2a

from the low and high crosslinked hydrogels at 8 h were 78.5 ± 1.4% and 46.0 ± 1.7%, respectively. After which no detectable levels of proteins were released.

**Table 2-2.** Characterization of HA-Tyr hydrogels incorporated with or without IFN-α2a[a]

| Sample | $H_2O_2$ (μM) | G' (Pa) | $Q_M$ | $Q_V$ | $\nu_e$ ($10^{-6}$ mol/cm$^3$) | $\xi$ (nm) |
|---|---|---|---|---|---|---|
| Low crosslinked | 437 | 990 ± 49 | 46.1 ± 0.5 | 56.4 ± 0.7 | 1.8 ± 0.04 | 546.8 ± 7.6 |
| Low crosslinked + IFN | 437 | 898 ± 122[b] | 48.3 ± 2.5 | 59.1 ± 3.0 | 1.7 ± 0.1[c] | 576.8 ± 34.6[d] |
| High crosslinked | 728 | 3078 ± 184 | 39.3 ± 1.5 | 48.1 ± 1.9 | 2.4 ± 0.2 | 453.2 ± 20.7 |
| High crosslinked + IFN | 728 | 3028 ± 199[b] | 35.8 ± 2.3 | 43.8 ± 2.8 | 2.8 ± 0.3[c] | 406.5 ± 30.5[d] |

Note. Results are shown as the mean values ± SD (n = 3). Abbreviations: storage modulus (G'), mass swelling ratio ($Q_M$), volumetric swelling ratio ($Q_V$), effective crosslink density ($\nu_e$) and mesh size ($\xi$).
[a]Hydrogels were formed with 1.75% (w/v) of HA-Tyr conjugates and 0.124 U/ml of HRP with or without 2.5 x $10^5$ IU/ml of IFN-α2a. [b]G', [c]$\nu_e$ and [d]$\xi$ of HA-Tyr hydrogels with IFN-α2a were not significantly different from those of HA-Tyr hydrogels without IFN-α2a ($p > 0.05$).

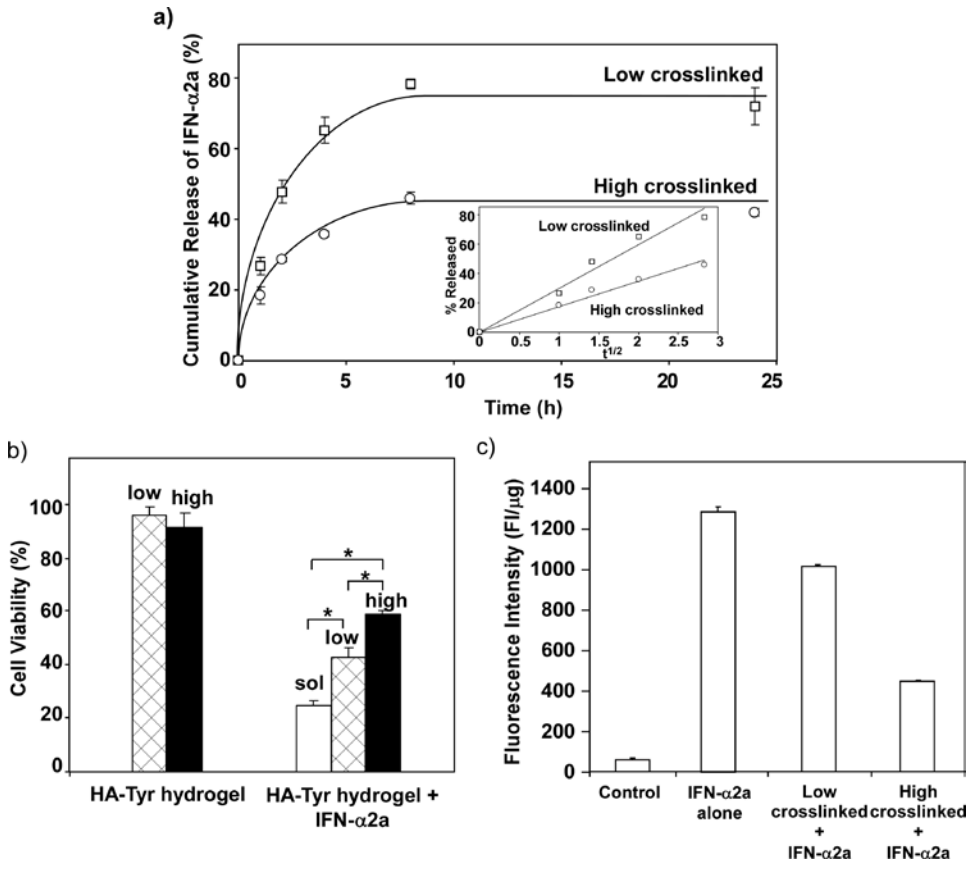


**Fig. 2-8. (a) Cumulative release of IFN-α2a from HA-Tyr-IFN hydrogels (n = 3, mean ± SD). The inset shows the cumulative release of protein as a function of the square root of time. (b) The viability of HAK-1B cells was measured after 4-day treatment of HA-Tyr hydrogels with or without 4 × $10^5$ IU/ml of IFN-α2a (*$p < 0.05$). (c) Quantitative measurement of caspase 3/7 activity in cells. The results were presented as fluorescence intensity (FI) normalized with the total protein amount (μg) in each sample (n = 3, mean ± SD).**

Next, we examined whether the IFN-α2a released from HA-Tyr hydrogels could inhibit the growth of HAK-1B cells. HAK-1B cells were established from a single nodule of hepatocellular carcinoma and have been confirmed to retain the morphological and functional characteristics of the original tumor [21]. As shown in Fig. 2-8b, after 4 days of treatment with HA-Tyr hydrogels alone (without IFN-α2a), the viability of HAK-1B cells was more than 90%, indicating that the hydrogels were non-cytotoxic. In contrast, cell viability decreased to 25% after treatment with IFN-α2a solution. Cell viability after treatment with IFN-α2a incorporated in low and high crosslinked HA-Tyr hydrogels were 42 and 59%, respectively, indicating that the released IFN-α2a negatively affect cell viability. To investigate the mechanism of decreased cell viability, Apo-ONE capspase-3/7 assay kit was used to quantify caspase-3/7 activity in HAK-1B cells after treatment. As shown in Fig. 2-8c, cells without any treatment showed low fluorescence intensity, indicating a minimal amount of active caspase-3/7. Cells treated with IFN-α2a in solution form or delivered by hydrogels showed elevated levels of caspase-3/7. Cells treated with IFN-α2a delivered from the low crosslinked hydrogels showed a higher level of caspase-3/7 compare with those treated with IFN-α2a delivered from the high crosslinked hydrogels. The results suggested that IFN-α2a delivered from hydrogels induced apoptosis in HAK-1B cells.

### 2.3.7. Effect of IFN-α2a delivered by hydrogels on tumor regression and pharmacokinetics study

The anti-cancer effect of IFN-α2a delivered by HA-Tyr hydrogels was examined *in vivo* using a nude mouse xenograft model of human liver cancer. The mice (n = 7) received a single subcutaneous injection of PBS, IFN-α2a solution, HA-Tyr hydrogels, or HA-Tyr hydrogel containing IFN-α2a once a week for two weeks. None of the mice died throughout the entire course of the experiment. Fig. 2-9a shows that HA-Tyr hydrogels alone had no effect on tumor regression, as the average tumor size was not significantly different from the control (PBS-treated). Treatment with IFN-α2a solution also failed to prevent tumor growth as the average tumor size was not significantly different from the PBS-treated group at day 20 (Fig. 2-9b). In contrast, the groups treated with HA-Tyr hydrogels containing IFN-α2 showed remarkable tumor regression. For the group treated with low crosslinked hydrogels containing IFN-α2a, the average tumor size was significantly lower than that of PBS group from day 11 onwards ($p < 0.05$). A similar trend of decreasing tumor size was also observed in mice

treated with high crosslinked hydrogel containing IFN-α2, albeit the tumor size was not statistically different from the PBS group. The results demonstrated that the delivery of IFN-α2a using low crosslinked hydrogels was more effective in inhibiting tumor growth than administering IFN-α2a as a solution.

Pharmacokinetics study of circulating IFN-α2a in the plasma was performed (Fig. 2-9c). At 1 h post-injection of IFN-α2a solution, the concentration of IFN-α2a in the plasma of mice was 105 ng/ml. In contrast, the concentrations of IFN-α2a in the plasma of mice treatment with low and high crosslinked hydrogels were 35 and 47 ng/ml, respectively. From 1 h to 4 h, the concentration of IFN-α2a in the plasma of mice administered with IFN-α2a solution decreased rapidly (65 ng/ml at 2 h and 8 ng/ml at 4 h). However, the decrease in plasma IFN-α2a concentrations was much slower when the proteins were delivered using hydrogels (low crosslinked: 30 ng/ml at 2 h and 26 ng/ml at 4 h; high crosslinked: 32 ng/ml at 2 h, 17 ng/ml at 4 h). At 8 h, the plasma concentration of IFN-α2a became negligible in mice injected with IFN-α2a solution, whereas the concentration was 8 ng/ml for mice treated with hydrogels. The amount of IFN-α2a delivered to the tumor was determined for the different treatment groups. At 8 h post injection, the amount of IFN-α2a delivered to the tumor by low crosslinked hydrogels was around 1.2 ng per gram of tumor tissue, which was three times higher than the amount found in the tumors of mice injected with IFN-α2a solution (Fig. 2-9d). The amount of IFN-α2a delivered to tumor by high crosslinked hydrogels was two-fold higher than that of injection with IFN-α2a solution alone. Taken together, the results showed that the delivery of IFN-α2a from HA-Tyr hydrogels resulted in a longer circulating life and a higher accumulation of the protein at the tumor site, which contributed to the greater anti-tumor effect compared to IFN-α2a administered as a solution.

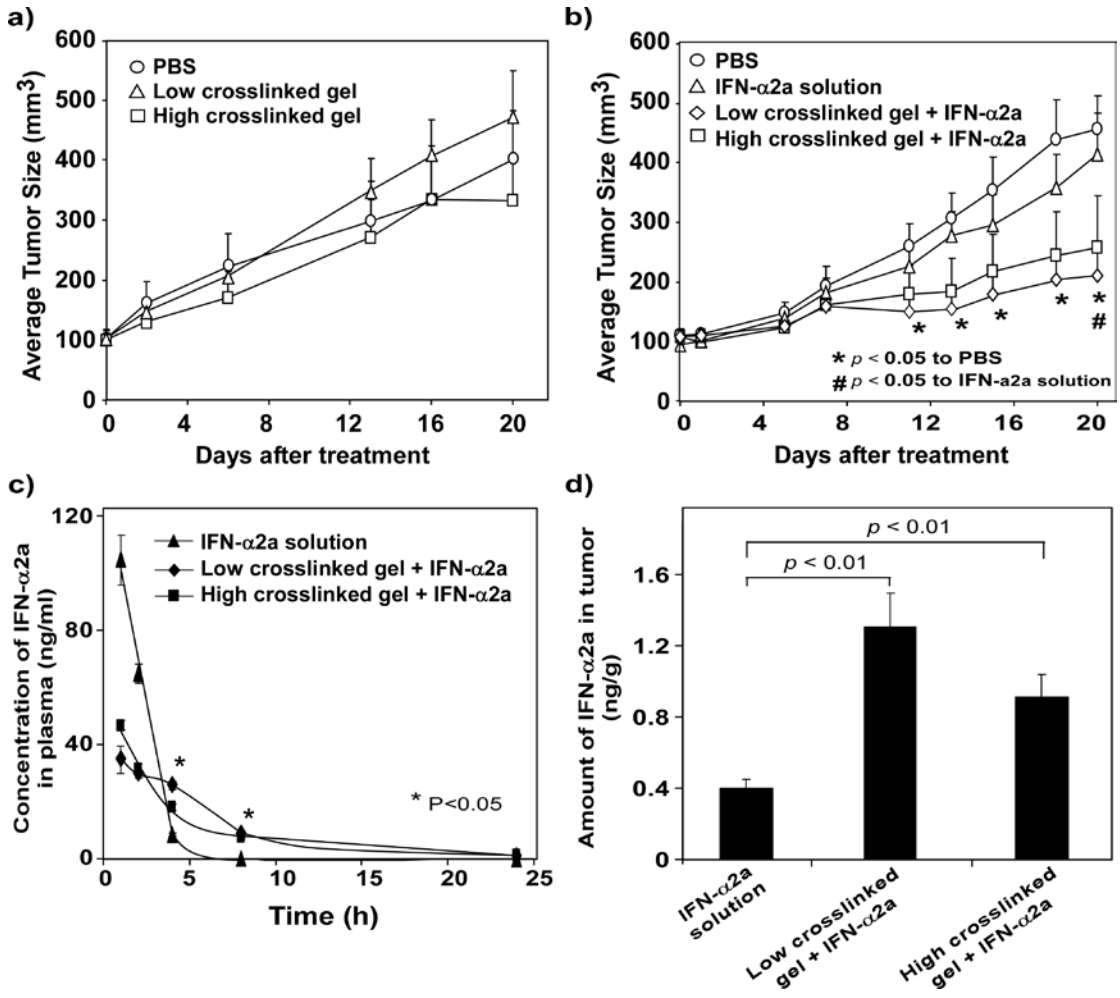


**Fig. 2-9. Tumor regression study in Balb/c nude mice xenograft model of human liver cancer. The mice were treated with (a) PBS or HA-Tyr hydrogels without IFN-α2a, and (b) IFN-α2a solution or HA-Tyr hydrogels containing IFN-α2a (n = 7, mean ± SEM). (c) Pharmacokinetics of IFN-α2a in the plasma of Balb/c nude mice. (n = 3, mean ± SEM; *$p$ < 0.05.) (d) Amount of IFN-α2a delivered to tumor tissues, which was normalized to the weight of the tumor (n = 4, mean ± SEM).**

## 2.4. Conclusions

Injectable and biodegradable HA-Tyr hydrogels were formed by the *in situ* oxidative coupling of tyramine moieties in the presence of HRP and $H_2O_2$. The crosslink density and gelation rate were tuned by $H_2O_2$ and HRP, respectively. At a constant HA-Tyr concentration, the G' could be varied from 10 to 4000 Pa by increasing $H_2O_2$ concentration while maintaining a constant and rapid gelation rate. The gelation time could be varied from 20 min to less than 1 s by increasing HRP concentration. By forming HA-Tyr hydrogels rapidly using an optimal concentration of HRP, localized hydrogel formation and efficient encapsulation of proteins were achieved. By controlling the crosslink density of HA-Tyr hydrogels through the

concentration of $H_2O_2$, the release rate of proteins could be varied. IFN-α2a released from HA-Tyr hydrogels inhibited the proliferation of HAK-1B liver cancer cells, and induced apoptosis through caspase-3/7 pathway. Comparing with IFN-α2a administered as a solution, the delivery of IFN-α2a using low crosslinked hydrogels improved the pharmacokinetics, increased the amount of IFN-α2a delivered to the tumor site, and more effectively inhibited tumor growth *in vivo*.

**References**

[1] Qiu Y, Park K. Environment-sensitive hydrogels for drug delivery. Adv. Drug Del. Rev. 2001;53:321-39.

[2] Jeong B, Bae YH, Kim SW. Drug release from biodegradable injectable thermosensitive hydrogel of PEG-PLGA-PEG triblock copolymers. J. Control. Release 2000;63:155-63.

[3] Hoffman AS. Hydrogels for biomedical applications. Adv. Drug Del. Rev. 2002;54:3-12.

[4] Hatefi A, Amsden B. Biodegradable injectable in situ forming drug delivery systems. J. Control. Release 2002;80:9-28.

[5] Kretlow JD, Klouda L, Mikos AG. Injectable matrices and scaffolds for drug delivery in tissue engineering. Adv. Drug Del. Rev. 2007;59:263-73.

[6] Brandl F, Sommer F, Goepferich A. Rational design of hydrogels for tissue engineering: impact of physical factors on cell behavior. Biomaterials 2007;28:134-46.

[7] Gupta D, Tator CH, Shoichet MS. Fast-gelling injectable blend of hyaluronan and methylcellulose for intrathecal, localized delivery to the injured spinal cord. Biomaterials 2006;27:2370-9.

[8] Zheng Shu X, Liu Y, Palumbo FS, Luo Y, Prestwich GD. In situ crosslinkable hyaluronan hydrogels for tissue engineering. Biomaterials 2004;25:1339-48.

[9] Jia X, Colombo G, Padera R, Langer R, Kohane DS. Prolongation of sciatic nerve blockade by in situ cross-linked hyaluronic acid. Biomaterials 2004;25:4797-804.

[10] Oudgenoeg G, Hilhorst R, Piersma SR, Boeriu CG, Gruppen H, Hessing M, Voragen AG, Laane C. Peroxidase-mediated cross-linking of a tyrosine-containing peptide with ferulic acid. J. Agric. Food Chem. 2001;49:2503-10.

[11] Kobayashi S, Uyama H, Kimura S. Enzymatic polymerization. Chem. Rev. 2001;101:3793-818.

[12] Kurisawa M, Chung JE, Yang YY, Gao SJ, Uyama H. Injectable biodegradable hydrogels composed of hyaluronic acid-tyramine conjugates for drug delivery and tissue engineering. Chem. Commun. (Camb.) 2005:4312-4.

[13] Lee F, Chung JE, Kurisawa M. An injectable enzymatically crosslinked hyaluronic acid-tyramine hydrogel system with independent tuning of mechanical strength and gelation rate. Soft Matter 2008;4:880-7.

[14] Hoofnagle JH, Seeff LB. Peginterferon and ribavirin for chronic hepatitis C. N. Engl. J. Med. 2006;355:2444-51.

[15] Osborn BL, Olsen HS, Nardelli B, Murray JH, Zhou JX, Garcia A, Moody G, Zaritskaya LS, Sung C. Pharmacokinetic and pharmacodynamic studies of a human serum albumin-interferon-alpha fusion protein in cynomolgus monkeys. J. Pharmacol. Exp. Ther. 2002;303:540-8.

[16] Nishiguchi S, Kuroki T, Nakatani S, Morimoto H, Takeda T, Nakajima S, Shiomi S, Seki S, Kobayashi K, et al. Randomised trial of effects of interferon-alpha on incidence of hepatocellular carcinoma in chronic active hepatitis C with cirrhosis. Lancet 1995;346:1051-5.

[17] Yano H, Iemura A, Haramaki M, Ogasawara S, Takayama A, Akiba J, Kojiro M. Interferon alfa receptor expression and growth inhibition by interferon alfa in human liver cancer cell lines. Hepatology 1999;29:1708-17.

[18] Hisaka T, Yano H, Ogasawara S, Momosaki S, Nishida N, Takemoto Y, Kojiro S, Katafuchi Y, Kojiro M. Interferon-alpha Con1 suppresses proliferation of liver cancer cell lines in vitro and in vivo. J. Hepatol. 2004;41:782-9.

[19] Harris JM, Chess RB. Effect of pegylation on pharmaceuticals. Nat. Rev. Drug Discov. 2003;2:214-21.

[20] Leach JB, Bivens KA, Patrick CW, Schmidt CE. Photocrosslinked hyaluronic acid hydrogels: Natural, biodegradable tissue engineering scaffolds. Biotechnol. Bioeng. 2003;82:578-89.

[21] Yano H, Iemura A, Fukuda K, Mizoguchi A, Haramaki M, Kojiro M. Establishment of 2 distint human hepatocellular carcinoma cell lines from a single nodule showing clonal dedifferentiation of cancer cells. Hepatology 1993;18:320-7.

[22] Veitch NC. Horseradish peroxidase: a modern view of a classic enzyme. Phytochemistry 2004;65:249-59.

[23] Rodríguez-López JN, Lowe DJ, Hernández-Ruiz J, Hiner ANP, García-Cánovas F, Thorneley RNF. Mechanism of Reaction of Hydrogen Peroxide with Horseradish Peroxidase: Identification of Intermediates in the Catalytic Cycle. J. Am. Chem. Soc. 2001;123:11838-47.

[24] Dunford HB. Peroxidases and Catalases: Biochemistry, Biophysics, Biotechnology and Physiology. 2nd ed. Hoboken, New Jersey: John Wiley & Sons, Inc.; 2010.

[25] Musso H. Phenol Oxidation Reactions. Angew. Chem. 1963;2:723-35.

[26] Winter HH, Chambon F. Analysis of linear viscoelasticity of a crosslinking polymer at the gel point. J. Rheol. 1986;30:367-82.

[27] Wang L-S, Chung JE, Pui-Yik Chan P, Kurisawa M. Injectable biodegradable hydrogels with tunable mechanical properties for the stimulation of neurogenesic differentiation of human mesenchymal stem cells in 3D culture. Biomaterials 2010;31:1148-57.

[28] Schmidt A, Schumacher JT, Reichelt J, Hecht H-J, Bilitewski U. Mechanistic and Molecular Investigations on Stabilization of Horseradish Peroxidase C. Anal. Chem. 2002;74:3037-45.

[29] Huang Q, Huang Q, Pinto RA, Griebenow K, Schweitzer-Stenner R, Weber WJ. Inactivation of Horseradish Peroxidase by Phenoxyl Radical Attack. J. Am. Chem. Soc. 2005;127:1431-7.

[30] Malkoch M, Vestberg R, Gupta N, Mespouille L, Dubois P, Mason AF, Hedrick JL, Liao Q, Frank CW, et al. Synthesis of well-defined hydrogel networks using click chemistry. Chem. Commun. (Camb.) 2006:2774-6.

[31] Lin C-C, Metters AT. Hydrogels in controlled release formulations: Network design and mathematical modeling. Adv. Drug Del. Rev. 2006;58:1379-408.

[32] Hiemstra C, Zhong ZY, van Steenbergen MJ, Hennink WE, Feijen J. Release of model proteins and basic fibroblast growth factor from in situ forming degradable dextran hydrogels. J. Control. Release 2007;122:71-8.

[33] Cadée JA, de Groot CJ, Jiskoot W, den Otter W, Hennink WE. Release of recombinant human interleukin-2 from dextran-based hydrogels. J. Control. Release 2002;78:1-13.

[34] Elbert DL, Pratt AB, Lutolf MP, Halstenberg S, Hubbell JA. Protein delivery from materials formed by self-selective conjugate addition reactions. J. Control. Release 2001;76:11-25.

[35] van de Wetering P, Metters AT, Schoenmakers RG, Hubbell JA. Poly(ethylene glycol) hydrogels formed by conjugate addition with controllable swelling, degradation, and release of pharmaceutically active proteins. J. Control. Release 2005;102:619-27.

[36] Sutter M, Siepmann J, Hennink WE, Jiskoot W. Recombinant gelatin hydrogels for the sustained release of proteins. J. Control. Release 2007;119:301-12.

[37] Borgia PT, Campbell LL. alpha-amylase from five strains of Bacillus amyloliquefaciens: evidence for identical primary structures. J. Bacteriol. 1978;134:389-93.

[38] Cai S, Liu Y, Zheng Shu X, Prestwich GD. Injectable glycosaminoglycan hydrogels for controlled release of human basic fibroblast growth factor. Biomaterials 2005;26:6054-67.

[39] Zhu G, Mallery SR, Schwendeman SP. Stabilization of proteins encapsulated in injectable poly (lactide- co-glycolide). Nat. Biotechnol. 2000;18:52-7.

[40] van de Weert M, Hennink WE, Jiskoot W. Protein instability in poly(lactic-co-glycolic acid) microparticles. Pharm. Res. 2000;17:1159-67.

[41] Dhalluin C, Ross A, Leuthold LA, Foser S, Gsell B, Muller F, Senn H. Structural and biophysical characterization of the 40 kDa PEG-interferon-alpha2a and its individual positional isomers. Bioconjug. Chem. 2005;16:504-17.

# Chapter 3

# Degradation-Triggered Release of Trastuzumab from Hyaluronic Acid-Tyramine Hydrogels for Breast Cancer Therapy

## 3.1. Introduction

Hydrogels have attracted much attention for the delivery of therapeutic proteins [1-3]. By preserving the native structure of proteins in a water-abundant matrix, hydrogels are ideal reservoirs for protein drugs. Injectable hydrogels are especially useful in clinical applications, as surgeries are not required for administration. In addition to injectability, a hydrogel should also be biodegradable because the fibrous capsules that often formed around non-biodegradable materials *in vivo* could hinder the release of drugs and potentially cause chronic inflammation [4]. Moreover, after the drugs have been released, biodegradable hydrogels do not require surgical retrieval. Importantly, the degradation rate of biodegradable hydrogels should be tunable because it can affect the rate of drug release.

In Chapter 2, an injectable hyaluronic acid-tyramine (HA-Tyr) hydrogel system formed through the oxidative coupling of Tyr moieties by horseradish peroxidase (HRP) and hydrogen peroxide ($H_2O_2$) was described. It was shown that HRP controls the gelation rate, while $H_2O_2$ controls the crosslink density. The release rate of proteins from HA-Tyr hydrogels could be controlled by tuning the crosslink density. Furthermore, it was demonstrated that the delivery of interferon-α2a (IFN-α2a) using HA-Tyr hydrogels not only resulted in a better pharmacokinetic profile compare to IFN-α2a administered in solution form, but also more effectively inhibited tumor growth in a mice xenograft model of liver cancer.

In this study, we examined the effect of crosslink density and hyaluronidase concentration on the degradation rate of HA-Tyr hydrogels. Hyaluronidase catalyzes the hydrolysis of α-*N*-acetyl-D-glucosaminidic linkages of HA. Then we incorporated lysozyme, a positively charged protein (14.3 kDa [5], isoelectric point (pI) = 11 [6]), in HA-Tyr hydrogels, and examined the protein release profiles in the presence and absence of hyaluronidase. It was found that a portion of the proteins were immobilized within the hydrogel through electrostatic interaction with the negatively charged HA. The immobilized proteins could only be released upon enzymatic degradation of the hydrogel network by hyaluronidase. Capitalizing on the electrostatic interactions between proteins and HA, we designed an injectable HA-Tyr hydrogel system for the sustained delivery of trastuzumab for breast cancer treatment (Fig. 3-1).

Trastuzumab, also known as Herceptin, is a therapeutic antibody widely used for the treatment of breast cancers [7-9] that are human epidermal growth receptor 2 (HER2)-positive

[10, 11]. It is administered once every three weeks over a period of one year for patients diagnosed with early-stage breast cancer [12]. Since trastuzumab has an pI of 8.45 [13], it can interact electrostatically with the negatively charged HA backbone under physiological conditions. The interaction is expected to minimize the initial burst release of trastuzumab from HA-Tyr hydrogels, and the release dependent on the degradation of the hydrogel network. Although hyaluronidase is present in the human body, its concentration in the plasma is only 60 ng/ml [14]. Therefore a small amount hyaluronidase was incorporated in the hydrogel to promote the hydrogel degradation, which in turn would facilitate the release of trastuzumab. The anti-proliferation effect of trastuzumab released from the hydrogels was evaluated *in vitro* using a HER2-overexpressing human breast cancer cell line, BT-474. The inhibitory effect of trastuzumab released from HA-Tyr hydrogels on tumor growth was assessed in a nude mouse xenograft model of BT-474 breast cancer. Pharmacokinetic study was performed to measure the plasma concentration of trastuzumab delivered by HA-Tyr hydrogels containing hyaluronidase. Histological and immunohistochemical analyses were utilized to examine the proliferation and apoptosis of cancer cells in the tumor tissue.

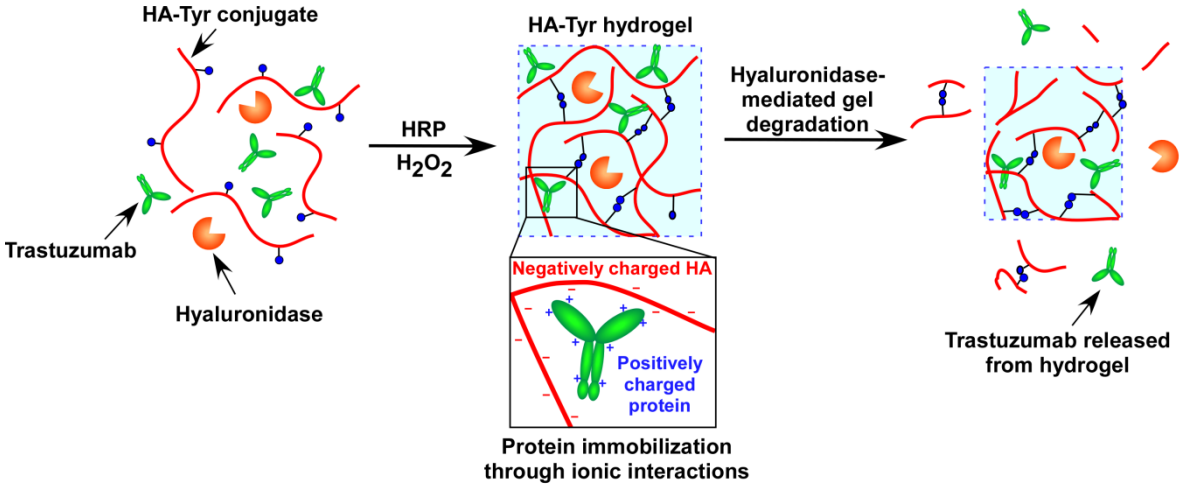


**Fig. 3-1. Design of an injectable hyaluronic acid-tyramine (HA-Tyr) hydrogel system for the sustained release of trastuzumab. Trastuzumab is immobilized in the hydrogel *via* electrostatic interaction with HA. Hyaluronidase is incorporated in the gel to promote the degradation of the hydrogel network, which facilitates the sustained release of trastuzumab.**

## 3.2. Materials and methods

### 3.2.1. Materials and cell culture

HA (90 kDa) was kindly donated by JNC Corporation (Tokyo, Japan). HA-Tyr conjugates were synthesized as described previously in Section 2.2.2 of Chapter 2. The degree of

substitution (DS, the number of tyramine molecules per 100 repeating units of HA) was 6 as determined by $^{1}$H NMR [15]. Hyaluronidase from bovine testes, lysozyme from chicken egg white, bovine serum albumin (BSA), polyoxyethylene-sorbitan monolaurate (Tween 20) and *Micrococcus lysodeikticus* were all purchased from Sigma-Aldrich. Horseradish peroxidase (HRP, 100 U/mg) was obtained from Wako Pure Chemical Industries. Polyclonal antibody to chicken lysozyme (biotin) was purchased from United States Biological. Streptavidin alkaline phosphate conjugated and *p*-nitrophenyl phosphate (*p*-NPP) were purchased from Chemicon. Alexa Fluor 680 carboxylic acid succinimidyl ester, fetal bovine serum (FBS) and alamarBlue assay kit were purchased from Life Technologies (Singapore). Trastuzumab was purchased from Roche (Basel, Switzerland). Human IgG ELISA kit was purchased from ICL lab (OR, USA). Phosphate buffer saline (PBS, 150 mM, pH 7.3) was supplied by media preparation facility in Biopolis, Singapore. Human hepatic cancer cell line (HAK-1B) was obtained from Prof. Hirohisa Yano, Kurume University, Japan, and was grown in DMEM media with 2.5% FBS [16]. BT-474 was grown in RPMI-1640 containing 10% FBS. All cells were cultured in a humidified incubator at 37 °C, 5% $CO_2$.

### 3.2.2. Enzymatic degradation of HA-Tyr hydrogels

HA-Tyr hydrogel disks were prepared as described in Section 2.2.5 of Chapter 2. The disks were swollen in PBS for 24 h to reach swelling equilibrium and then sandwiched between plastic nets to facilitate retrieval of the hydrogels during degradation experiment. The hydrogels were immersed in 20 ml of PBS containing hyaluronidase (0, 2.5, 25 or 125 U/ml) at 37 °C in an orbital shaker at 100 rpm. The extent of degradation of the hydrogels was estimated by measuring both the residual hydrogel weight and the amount of uronic acid (a degradation component of HA) in the degradation solution at specific time points. To measure the residual weight, the hydrogels were removed from the degradation solution with a pair of forceps, gently blotted dry with Kimwipe and weighed. To measure the amount of uronic acid eroded from the hydrogel, 350 μl of the degradation solution was removed and stored in microcentrifuge tubes at 4 °C until analysis. Three hundred and fifty μl of freshly prepared degradation solution were then added to maintain the total volume of 20 ml. Degradation experiments were continued until no visible signs of gel remained. It was determined that the activity of hyaluronidase remained 90 percent for 2 days (data not shown). The amount of uronic acid released from the hydrogel into the degradation medium were assayed using the previously established carbazole assay [17] with the following modifications. Three hundred

μl of samples were added to 1.5 ml of 0.025 M sodium tetraborate in sulfuric acid and heated at 100 °C for 10 minutes. After cooling to room temperature, 100 μl of carbazole (0.125% (w/w) in ethanol) was added, mixed and heated at 100 °C for 15 minutes. After cooling to room temperature, 200 μl of the solution was transferred to a 96 well plate and the absorbance of the solution was measured at 530 nm. The amount of uronic acid in each sample was estimated by comparing to the D-glucuronic acid standards.

In order to determine the swelling ratios of HA-Tyr hydrogels undergoing enzymatic degradation, hydrogels formed with 728 μM of $H_2O_2$ were swollen in PBS for 24 h to reach swelling equilibrium and then immersed in different concentrations of hyaluronidase. After incubation for 37 h in 2.5 U/ml, 10 h in 25 U/ml and 4 h in 125 U/ml of hyaluronidase, the hydrogels were removed from the degradation solution and rinsed extensively with water before swelling in MilliQ water for 2 days. Hydrogels without exposure to hyaluronidase were used as controls. The swollen disks were then gently blotted dry with Kimwipe and weighed to obtain the swollen weight. The disks were then lyophilized to obtain the dry weight. The swelling ratio is defined as a ratio of the swollen weight to the dried weight. The swelling ratio is defined as a ratio of the swollen weight to the dried weight.

### 3.2.3. Rheological measurement

Rheological measurements were performed with a HAAKE Rheoscope 1 rheometer (Karlsruhe, Germany) using a cone and plate geometry of 3.5 cm diameter and 0.949° cone angle. Briefly, 210 μl of gel precursors was applied to the bottom plate of the rheometer. The upper cone was then lowered to a measurement gap of 0.025 mm and a layer of silicon oil was carefully applied around the cone to prevent solvent evaporation during the experiment. The measurements were taken at 37 °C in the dynamic oscillatory mode with a constant deformation of 1% and frequency of 1 Hz. To avoid slippage of samples during the measurement, a roughened glass bottom plate was used.

### 3.2.4. Release of lysozyme from HA-Tyr hydrogels

HA-Tyr hydrogels loaded with 0.25 mg/ml of lysozyme were prepared by mixing 500 μl of HA-Tyr (3.5 % (w/v)) with 500 μl of protein solution (0.5 mg/ml). Then 5 μl each of HRP and $H_2O_2$ (final concentrations of HRP: 0.124 U/ml and $H_2O_2$: 437, 582 or 728 μM) was added and the mixture was vortexed gently before injected between two parallel glass plates

clamped together with 1 mm spacing. Gelation was allowed to proceed at 37 °C for one hour at which G' would have reached plateau according to the rheology results. Round gel disks with diameter of 1.6 cm were then cut out from the hydrogel slab using a circular mold. Each disk was sandwiched between a plastic net and immersed in 20 ml of release medium composed of PBS with or without 2.5 U/ml of hyaluronidase. The samples were incubated at 37 °C on an orbital shaker at 100 rpm. At selected time points, 200 μl of the release medium was drawn and stored in a microcentrifuge tube containing 200 μl of 0.1 mg/ml BSA in PBS to prevent non-specific adsorption of the model proteins to the plastic surface of the microcentrifuge tubes. Two hundred μl of solution with or without hyaluronidase was added to maintain the total release medium at 20 ml. The collected samples were stored at -20 °C.

Protein concentrations were determined by enzyme-linked immunosorbant assay (ELISA). One hundred μl of the samples thawed to room temperature was added to the wells of a 96-well MaxiSorb ELISA plate (NUNC). The proteins in the samples were bound to the well by incubation for 1.5 h and then the wells were washed three times with 300 μl of washing buffer (100 mM PBS containing 0.05 % Tween-20). After washing, the wells were blocked with 200 μl of blocking buffer (BSA 2 % (w/v) in PBS) for 30 minutes to saturate the protein-binding sites and then the wells were washed. Then, 100 μl of either biotinylated anti-lysozyme (1.67 μg/ml) antibodies diluted in blocking buffer were added to the wells and incubated for 1 h. After washing, 100 μl of streptavidin-alkaline phosphatase diluted in PBS was added and incubated for 1 h and then the wells were washed. Finally, 100 μl of *p*-NPP was added to each well and the plate was incubated for approximately 35 min. The absorbance at 405 nm was measured using Tecan Infinite 200 microplate reader. The amount of proteins contained in each sample was calculated by comparing to a set of protein standards.

### 3.2.5. Effect of ionic strength on lysozyme release

To study the effects of ionic strength of the medium on the release of lysozyme, hydrogel disks (thickness: 1 mm, diameter: 8 mm) containing 0.25 mg/ml of lysozyme were immersed in 1 ml of NaCl solution (0, 0.05, 0.15, 0.5 or 1 M) at 37 °C on an orbital shaker at 100 rpm. After four hours of incubation, 100 μl of the release medium was collected and the amount of proteins contained in the sample was measured using the micro bicinchoninic acid protein assay (microBCA, Pierce) according to the manufacturer's protocol.

### 3.2.6. Activities of lysozyme released from HA-Tyr hydrogels

Hydrogel disks (thickness: 1 mm, diameter: 8 mm) containing 5 mg/ml of lysozyme were degraded in 5 ml of 200 U/ml of hyaluronidase in PBS with 0.05 % (w/v) $NaN_3$ at 37 °C on an orbital shaker at 150 rpm. After 24 h, no visible sign of the hydrogels was observed. The activity of the released lysozyme was evaluated by mixing 20 µl of lysozyme and 100 µl of *Micrococcus lysodeikticus* (0.15 % (w/v) in PBS) in the well of a 96-well UV-starplate (Greiner Bio-one, Germany). The plate was incubated for 15 minutes on an orbital shaker at 50 rpm at room temperature. Then the absorbance at 450 nm was measured using the microplate reader. The activities retained were determined by comparing to the activities of control protein solutions which had been incubated for 24 h at 37 °C.

### 3.2.7. Incorporation and release of trastuzumab from HA-Tyr hydrogels

A mixture solution containing 1.75 % (w/v) HA-Tyr conjugates, 0.3 mg/ml trastuzumab, hyaluronidase of varying concentrations (0, 2.5 and 5 U/ml), 0.124 U/ml HRP and 437 µM $H_2O_2$ were gently mixed by pipetting and then injected between two parallel glass plates clamped 1.5 mm apart. Gelation was allowed to proceed at 37$^o$C for 2 h. Hydrogel disks with a diameter of 1.6 cm, were then cut from the hydrogel slab using a circular mold. For cumulative release studies, hydrogel disks were placed in a plastic net and immersed in 20 ml of PBS buffer containing 0.05% sodium azide and 0.5% bovine serum albumin (BSA). At selected time points, 200 µl of the release medium was withdrawn and stored in LoBind tubes (Eppendorf, Germany) at 4 °C. Then 200 µl of fresh buffer solution was added to the release medium to maintain a constant volume. The amount of trastuzumab contained in the samples was measured using a human IgG ELISA kit.

To measure the percentage of trastuzumab that can be recovered from hydrogels, another set of hydrogel disks were immersed in 3 ml PBS buffer containing 200 U/ml of hyaluronidase. Hydrogels were degraded overnight at 37$^o$C, and trastuzumab concentration was measured by ELISA.

To examine the effect of ionic strength on the release of trastuzumab from HA-Tyr hydrogels, hydrogel disks were incubated with 20 ml of buffer containing 0.05% sodium azide, 0.5% bovine serum albumin (BSA) and 0.05 or 1M NaCl. The release amount of trastuzumab at 4 h was measured by ELISA.

### 3.2.8. Cell proliferation assay

To examine the effect of trastuzumab released from HA-Tyr hydrogels on cell proliferation, 200 μl of BT-474 cell suspension containing 30,000 cells was added into a 24-well plate and incubated overnight. Next day, 50 μl of hydrogels (final composition: 1.75% (w/v) of HA-Tyr conjugates, 0.05 mg/ml of trastuzumab, 0, 2.5 or 5 U/ml of hyaluronidase, 0.124 U/ml of HRP and 437 μM of $H_2O_2$) were prepared in cell culture inserts and allowed to gel for 2 h. The hydrogel-loaded inserts were then placed into the cell-seeded wells and an additional 500 μl of culture media was added into the insert. After 4 days of incubation, cell viability was measured by alamarBlue assay according to the manufacturer's instruction. Fluorescence measurement was performed with the Infinite M200 (Tecan, Switzerland). Excitation and emission wavelengths were set at 545 and 590 nm, respectively. The results were expressed as a percentage of viability compared with untreated cells.

### 3.2.9. Tumor regression study

To examine the anti-tumor effect of trastuzumab delivered by HA-Tyr hydrogels, 200 μl of BT-474 cells ($5 \times 10^7$ cells/ml) suspended in Matrigel (BD, USA) were subcutaneously injected to the backs of 6-week-old female NCr-Fixb1$^{nu}$ (NCr) mice that were implanted with 17β-estradiol (0.72 mg/pellet, Innovative Research of America, USA). Fourteen days later, when diameter of the tumor reached 5-10 mm, the mice were divided into 5 groups (n = 7) with similar average tumor size between the groups. Each mouse (~25 g) received a single subcutaneous injection of 200 μl of hydrogels (final composition: 1.75% (w/v) of HA-Tyr conjugates, 0.63 mg/ml trastuzumab, 0.124 U/ml HRP, hyaluronidase (0, 2.5 and 5 U/ml), 0.124 U/ml of HRP and 473 μM of $H_2O_2$). The remaining two groups received a single subcutaneous injection of 200 μl of PBS or 0.5 mg/ml trastuzumab solution. The site of injection was at least 2 cm away from the tumor. Tumors were measured with a as described above. In a separate study, the effect of the hydrogels alone on tumor growth was assessed by subcutaneous injection of mixture solutions containing all the components but no trastuzumab. Subcutaneous injection of mixture solution containing 0.63 mg/ml of trastuzumab and 5 U/ml of hyaluronidase was also performed to assess the combination effect of trastuzumab and hyaluronidase on tumor growth. The care and use of laboratory animals were performed according to the protocol approved by the Institutional Animal Care and Use Committee (IACUC) at the Biological Resource Center (BRC) in Biopolis, Singapore.

### 3.2.10. Histology and immunohistochemistry

Tumor tissues were collected, fixed and stained by hematoxylin and eosin (H&E), Ki67 antibodies, and terminal deoxynucleotidyl transferase dUTP nick end labeling (TUNEL) as described previously [18]. The tissue slides were then examined with an Olympus microscope IX71. For Ki67 staining and TUNEL assay, three representative images were acquired from each group and the percentage of positive cells were quantified.

### 3.2.11. Degradation of hydrogels containing trastuzumab and hyaluronidase

For the degradation of hydrogels *in vitro*, hydrogel disk was placed in a plastic net and immersed in 20 ml PBS buffer containing 0.05% sodium azide and 0.5% BSA. At selected time points, the hydrogel disk was retrieved and blotted dry. The gel disks were weighed and then returned to the buffer solution.

For *in vivo* degradation, 200 µl of hydrogel (1.75% (w/v) of HA-Tyr, 0.63 mg/ml of trastuzumab, hyaluronidase (0, 2.5 and 5 U/ml), 0.124 U/ml of HRP, and 437 µM of $H_2O_2$) were injected into NCr mice subcutaneously. After 1, 3, 6, 14, 28 days, the remaining hydrogels retrieved and weighed.

### 3.2.12. Pharmacokinetics study

To examine the pharmacokinetics of trastuzumab released from HA-Tyr hydrogels, 6 NCr nude mice of ~25 g weight were divided into two groups (n = 3). One group received a subcutaneous injection of 200 µl hydrogels (final composition: 1.75% (w/v) of HA-Tyr conjugates, 0.63 mg/ml of trastuzumab, 5 U/ml of hyaluronidase, 0.124 U/ml of HRP and 437 µM of $H_2O_2$). The other group received a subcutaneous injection of 200 µl of 0.63 mg/ml trastuzumab solution in PBS. Blood collection, preparation and storage were performed as described above. The plasma concentration of trastuzumab was measured by a human IgG ELISA kit.

### 3.2.13. Statistical analysis

Data from *in vitro* studies are expressed as mean ± standard deviation (SD). Data from animal studies are expressed as mean ± standard error of the mean (SEM). Differences between the values were assessed using one-way ANOVA and student's *t*-test, while $p < 0.05$ was considered statistically significant.

## 3.3. Results and discussion

### 3.3.1. Enzymatic degradation of HA-Tyr hydrogels by hyaluronidase

Biodegradable hydrogels eliminate the need for surgical retrieval. It is important to characterize the degradation profile of hydrogels because it can affect the release rate of encapsulated drugs. Hydrogels formed with a fixed HRP concentration (0.124 U/ml) but various $H_2O_2$ concentrations (G' of the hydrogels: 437 < 582 < 728 μM of $H_2O_2$) were used to study the relationship between crosslink density and degradation rate. Degradations of HA-Tyr hydrogels were carried out in the presence of 2.5, 25 and 125 U/ml of hyaluronidase, and analyzed by the measurement of uronic acid production and hydrogel weight loss. Bovine testes hyaluronidase was used as the hydrolytic enzyme. Fig. 3-2 shows the amount of uronic acids in the degradation medium measured by the carbazole assay. No uronic acid was detected in the medium of the hydrogels immersed in PBS only, indicating that degradation did not occur without hyaluronidase (data not shown). In the presence of hyaluronidase, degradation rate depended on the mechanical strength of the hydrogel: stronger hydrogels degraded slower than weaker hydrogels at the same hyaluronidase concentration (degradation rate: 437 > 582 > 728 μM of $H_2O_2$). This demonstrated that the degradation rate of HA-Tyr hydrogels can be tailored by simply changing the $H_2O_2$ concentration. Furthermore, a higher concentration of hyaluronidase resulted in a faster degradation rate (degradation rate: 2.5 < 25 < 125 U/ml of hyaluronidase).

In order to investigate the degradation mode in detail, the weight of the hydrogels was measured at selected time points during the degradation period (Fig. 3-3). At 125 U/ml of hyaluronidase, the hydrogels lost weight linearly with time, in line with the trend of uronic acid production observed in the carbazole assay, suggesting surface degradation. Interestingly, at lower concentrations (2.5 and 25 U/ml) of hyaluronidase, the hydrogels swelled (negative weight loss) initially before starting to lose weight (note that all hydrogels were swollen in PBS for 24 h to reach swelling equilibrium before the degradation experiments). Swelling was most notable for the weakest hydrogel (437 μM of $H_2O_2$) at the lowest concentration (2.5 U/ml) of hyaluronidase (Fig. 3-3a). Since the hydrogels had slab geometries, the observed swelling behavior suggested the decrease in crosslink density with time as a result of bulk degradation.

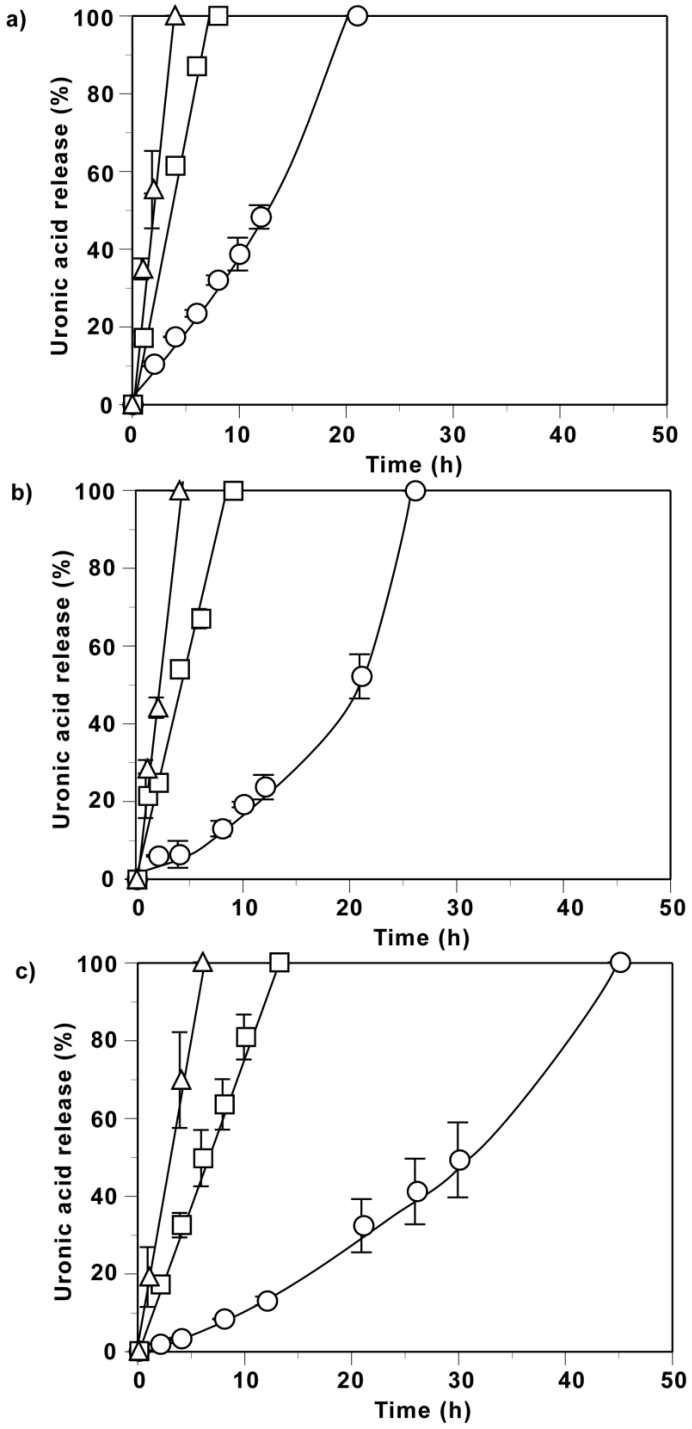


**Fig. 3-2. Uronic acids released from HA-Tyr hydrogels in the presence of 2.5 (○), 25 (□) or 125 (△) U/ml of hyaluronidase. Hydrogels were formed with 0.124 U/ml of HRP and a) 437, b) 582 and c) 728 μM of $H_2O_2$ (n = 2).**

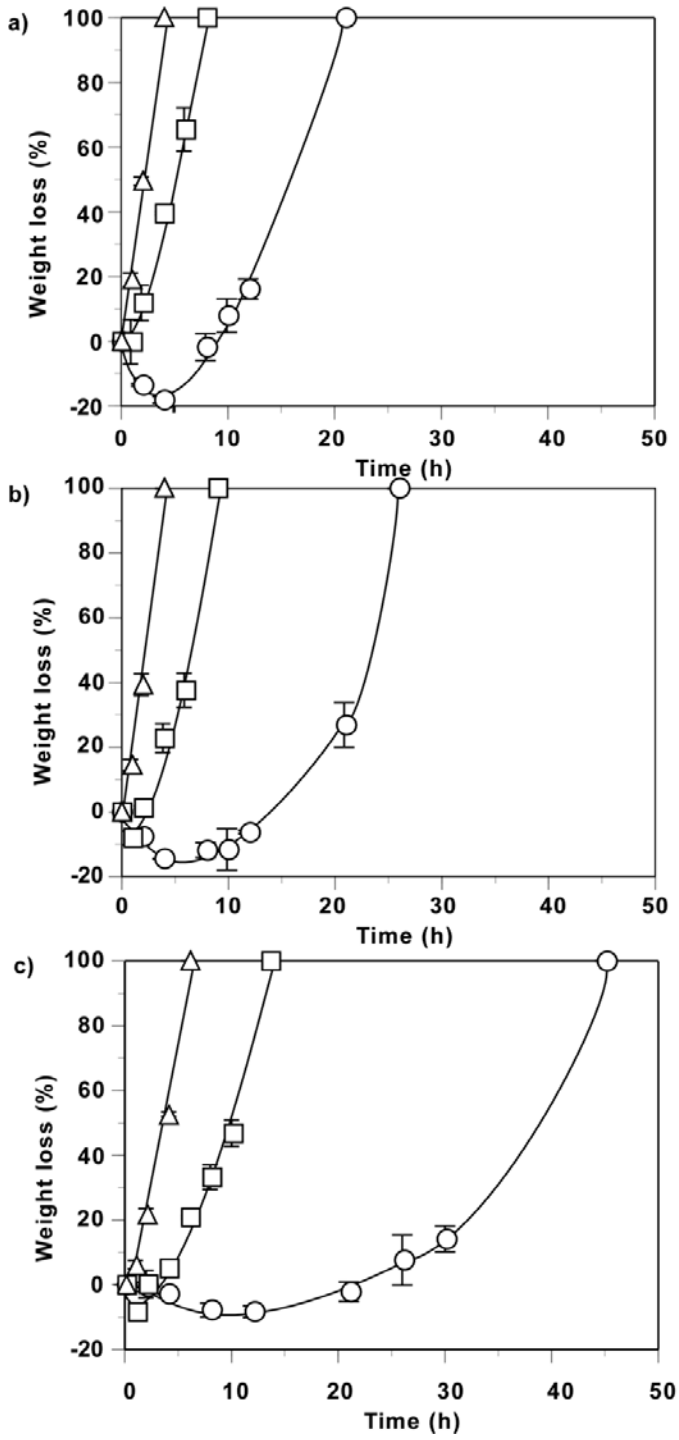


**Fig. 3-3. Weight loss of HA-Tyr hydrogels in the presence of 2.5 (○), 25 (□) and 125 (△) U/ml of hyaluronidase. Hydrogels were formed with 0.124 U/ml of HRP and a) 437, b) 582 and c) 728 μM of $H_2O_2$ (n = 2).**

We postulated that hyaluronidase diffused into the hydrogel network and hydrolyzed HA not only from the surface but also from the interior, causing a decrease in crosslink density which leads to increased water absorption by the loosened network. If the hypothesis is true, the swelling ratio of hydrogels should increase with degradation degree. The swelling ratios

of hydrogels which had lost 50% of initial weight after incubation at different concentrations of hyaluronidase were measured (Fig. 3-4). As expected, the swelling ratios of all hydrogels incubated with hyaluronidase were greater than the control which had not been exposed to hyaluronidase, proving that the swelling of hydrogels during degradation was resulted from the decrease in crosslink density due to bulk degradation. The swelling ratio increased with decreasing hyaluronidase concentration. These results implied that bulk degradation occurred in concurrence with surface degradation, the latter was more dominant at high concentrations of hyaluronidase. At low concentrations of hyaluronidase, the effect of surface degradation diminished, which allowed more time for hyaluronidase to diffuse into the hydrogel network, hence bulk degradation became more dominant.

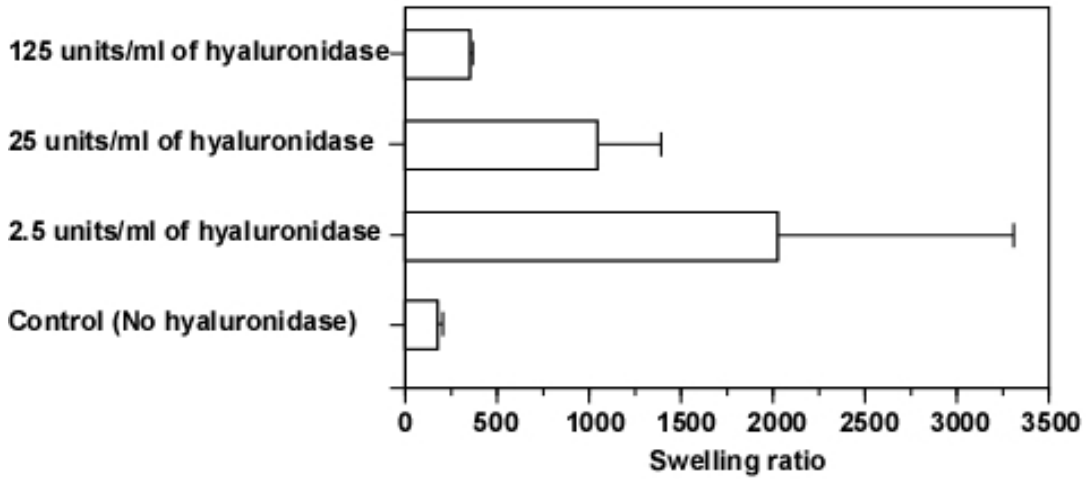


**Fig. 3-4. Swelling ratios of hydrogels under degradation conditions. The swelling ratios of hydrogels that had lost 50% of initial weight after incubation at different concentrations of hyaluronidase were measured. Hydrogels formed with 728 μM of $H_2O_2$ and 0.124 U/ml of HRP were incubated in PBS containing hyaluronidase at 2.5 U/ml for 37 h, 25 U/ml for 10 h and 125 U/ml for 4 h (n = 3).**

### 3.3.2. Release of lysozymes from HA-Tyr hydrogels in the absence and presence of hyaluronidase

HA is negatively charged under physiological pH due to the presence of carboxylic groups. This suggests that it can interact electrostatically with positively charge proteins. Lysozyme has a pI value of 11 [6], which means it is positively charged under physiological pH. Lysozymes were incorporated in HA-Tyr hydrogels formed with different concentrations of $H_2O_2$ (Table 3-1). When the hydrogels were immersed in PBS, a rapid release rate was observed in the first two hours (Fig. 3-5a), with the release rate decreased significantly as the swelling ratio of the hydrogel decreased (Table 3-1). When plotted against the square root of

time, the release in the first two hours was linear, indicating first order release that is typical of Fickian diffusion (Fig. 3-5a inset). Interestingly, after the initial phase of rapid release, the release discontinued for all the hydrogels, suggesting that the remaining lysozymes were immobilized in the HA network through electrostatic interactions. To verify this hypothesis, HA-Tyr hydrogels encapsulated with lysozymes were immersed in NaCl solutions with different ionic strengths, and the percentages of proteins released were measured by BCA protein assay. Indeed, the release of lysozyme increased together with the ionic strength of the medium, which was attributed to the disruption of electrostatic interactions (Fig. 3-5b). The hydrogels swelled at low ionic strength (0 and 0.05 M NaCl), but shrunk at high ionic strength (0.5 and 1 M NaCl) (data not shown). However, despite the swelling of hydrogels in deionized water, only 16 and 10 % of lysozymes were released from the low and high crosslinked hydrogels, indicating a strong electrostatic interaction between lysozymes and HA at low ionic strength. Similar observations of ionic strength-dependent release of lysozymes were also reported in synthetic hydrogels containing phosphate groups [19].

**Table 3-1.** Rheological property, swelling ratio and release rate of HA-Tyr hydrogels incorporated with lysozyme[a]

| Sample | $H_2O_2$ (μM) | G' (Pa) | Gel point (s)[b] | Swelling ratio | Release rate (% / h)[c] |
|---|---|---|---|---|---|
| Low crosslinked | 437 | 1162 ± 121 | 55 ± 3 | 44.0 ± 1.0 | 20.7 ± 1.8 |
| Medium crosslinked | 582 | 2029 ± 141[†] | 57 ± 3 | 41.0 ± 0.3[†] | 11.9 ± 0.5[†] |
| High crosslinked | 728 | 3068 ± 84[†‡] | 58 ± 2 | 36.8 ± 0.1[†‡] | 5.3 ± 0.5[†‡] |

[a]All samples contained 1.75 % (w/v) of HA-Tyr conjugates, 0.124 U/ml of HRP and 0.25 mg/ml of proteins. [b]Gel point is defined as the time at which the crossover of storage modulus (G') and loss modulus (G'') occurred. Herein, it is used as an indicator of the rate of gelation. There was no significant difference between the gel points of hydrogels formed with different concentrations of $H_2O_2$ (n = 2). [c]Release rate is estimated by taking the slope of the linear fit of cumulative release in the first two hours (n = 2-3). [†]Indicates that the value is significantly different from that of the low crosslinked gel ($p < 0.05$). [‡]Indicates that the value is significantly different from that of the medium crosslinked gel ($p < 0.05$).

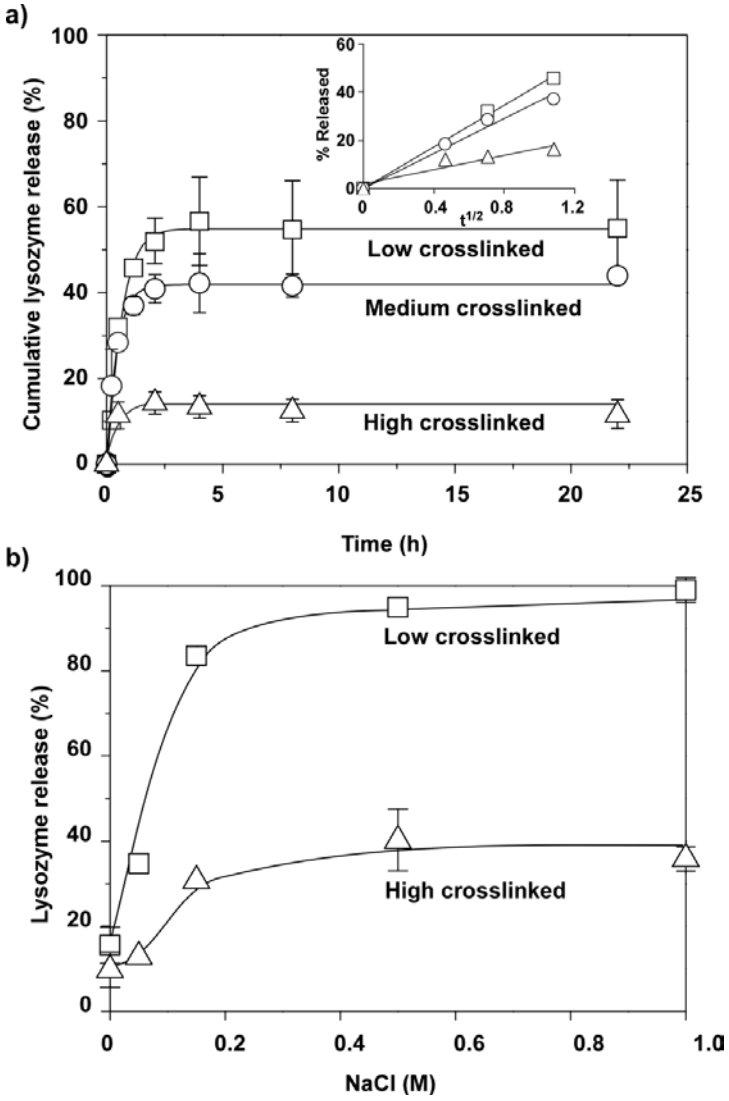


**Fig. 3-5. Release of lysozyme from HA-Tyr hydrogels formed with 0.124 U/ml of HRP and (□) 473, (○) 582 and (△) 728 μM of $H_2O_2$. a) Cumulative release against time, the inset shows cumulative release as a function of the square root of time (n = 2-3, mean ± SD). b) Percentage of lysozyme released when the hydrogels were incubated in various concentrations of NaCl for 4 h (n = 3, mean ± SD).**

In order to release all the lysozymes incorporated in HA-Tyr hydrogels, another set of hydrogels were prepared and degraded in 2.5 U/ml of hyaluronidase solution (Fig. 3-6a). Rapid release similar to the release profiles of hydrogels without enzymatic degradation was observed during the initial hours, after which lysozymes were released continuously from the hydrogels due to degradation of the matrix network. Complete release of all the lysozyme loaded in the hydrogels were achieved within one day for the low crosslinked hydrogels and two days for the medium and high crosslinked hydrogels, these time points corresponded to the time required to fully degraded the hydrogels as determined above. The activity of lysozymes released from hydrogels were found to decrease from 90 to 70 % as the $H_2O_2$

concentration increased from 437 to 728 μM, indicating that the enzymatic coupling reaction might have adverse effect the lysozyme structure (Fig. 3-6b). Hence, a low crosslinked hydrogel formed by a low concentration of $H_2O_2$ is better for maintaining the protein activity.

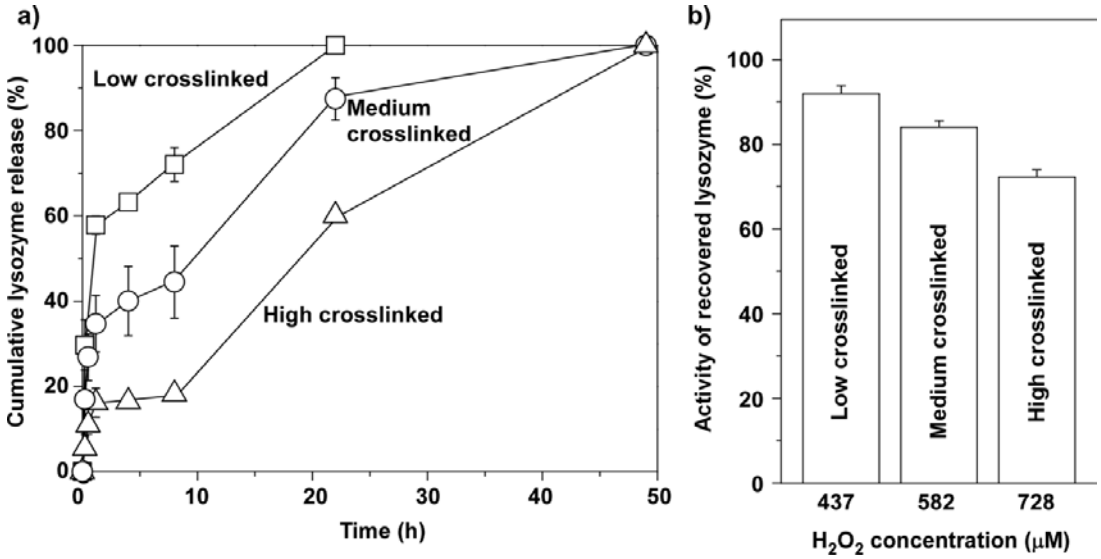


**Fig. 3-6. Cumulative release of lysozyme from HA-Tyr hydrogels in the presence of 2.5 U/ml of hyaluronidase. The hydrogels were formed with 0.124 U/ml of HRP and (□) 473, (○) 582 and (△) 728 μM of $H_2O_2$ (n = 2, mean ± SD). b) Activities of lysozyme recovered from HA-Tyr hydrogels after degradation of the hydrogel network in the presence of 200 U/ml of hyaluronidase for 24 h (n = 3, mean ± SD).**

### 3.3.3. Release of trastuzumab from HA-Tyr hydrogels containing hyaluronidase

Having confirmed that electrostatic interactions exist between negatively charged HA-Tyr hydrogel and positively charged proteins, we proceeded to incorporate trastuzumab, a therapeutic antibody with a pI of 8.45 [13], in HA-Tyr hydrogels for breast cancer treatment. Clinically, the route of administration of trastuzumab is intravenous (IV) infusion, which requires trained personnel and a dedicated infusion facility. It usually takes 30 to 90 minutes for one infusion and additional time is required for post-infusion observation. Recently, subcutaneous (SC) injection of trastuzumab was explored as an alternative method of administration. Ismael *et al.* reported in a phase III clinical trial that SC administration of trastuzumab, with human recombinant hyaluronidase (rHuPH20) [20] as an excipient, resulted in a pharmacokinetic profile with efficacy and safety that were non-inferior to intravenous administration [21]. The findings are significant because SC administration is less technically demanding compared with IV infusion and takes less than 5 minutes. Furthermore, according to one study, 88.9% of patients preferred SC administration as compared with only 9.6% that preferred IV infusion [22]. To further enhance the efficacy of trastuzumab through the SC

route, we utilized the HA-Tyr hydrogels as a delivery vehicle. Electrostatic interactions between HA and trastuzumab is expected, which could minimize the burst release and achieve the sustained release of trastuzumab through hyaluronidase-mediated degradation of the hydrogels. Towards this end, a small amount of hyaluronidase was incorporated into the hydrogel during gel preparation to promote subsequent gel degradation, as the hyaluronidase concentration in human is only is only 60 ng/ml [14].

HA-Tyr hydrogels incorporating trastuzumab and different concentrations of hyaluronidase (0, 2.5 and 5 U/ml) were abbreviated as HA-Tyr-TZB-0, HA-Tyr-TZB-2.5 and HA-Tyr-TZB-5, respectively, as shown in Table 3-2. The gel point was around 1 min for all three hydrogels. Although the G' values of the different hydrogels were not statistically different, a decrease in G' with increasing hyaluronidase concentration was observed, suggesting that the incorporation of hyaluronidase resulted in hydrogel degradation during the gel formation process. When freshly prepared hydrogels were immersed in 200 U/ml of hyaluronidase solution, the hydrogels were degraded after overnight incubation. More than 90% of trastuzumab was detected in the degradation solution by ELISA for all the hydrogels (Fig. 3-7), confirming that the majority of the incorporated trastuzumab can be recovered *via* hydrogel degradation.

**Table 3-2.** Characterization of HA-Tyr hydrogels incorporated with trastuzumab and hyaluronidase[a]

| Sample | Hyaluronidase (U/ml) | Gel point (min) | Time for G' to reach plateau (min) | G' (Pa) |
|---|---|---|---|---|
| HA-Tyr-TZB-0 | 0 | 0.93 ± 0.15 | 8.97 ± 0.32 | 500 ± 30 |
| HA-Tyr-TZB-2.5 | 2.5 | 0.95 ± 0.21[b] | 8.85 ± 0.49[b] | 476 ± 43[b] |
| HA-Tyr-TZB-5 | 5 | 1.07 ± 0.08[c] | 8.80 ± 0.14[c] | 452 ± 19[c] |

[a]All hydrogels were formed with 1.75 % (w/v) of HA-Tyr conjugates, 0.124 U/ml of HRP and 437 μM of $H_2O_2$. Results are shown as mean ± SD (n = 3). [b]Indicates that the value is not significantly different from that of HA-Tyr-TZB-0 ($p > 0.05$). [c]Indicates that the value is not significantly different from that of HA-Tyr-TZB-0 and HA-Tyr-TZB-2.5 ( $p > 0.05$).

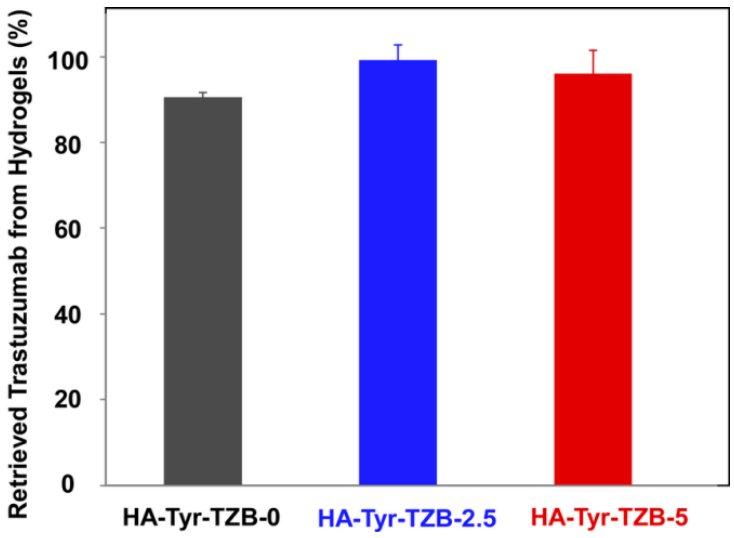


**Fig. 3-7. Percentage of trastuzumab retrieved from HA-Tyr hydrogels incorporated with trastuzumab and hyaluronidase (0, 2.5 and 5 U/ml).**

The release profiles of trastuzumab in PBS solution were shown in Fig. 3-8a. For HA-Tyr-TZB-0, 25% of trastuzumab was released in the first two days, after which no more protein was release. The incomplete release of trastuzumab from HA-Tyr-TZB-0 suggests electrostatic interactions between trastuzumab and the HA network. In contrast, when hyaluronidase was incorporated in the hydrogels, trastuzumab was released from HA-Tyr-TZB-2.5 and HA-Tyr-TZB-5 continuously for 4 weeks. The release of trastuzumab was faster from HA-Tyr-TZB-5 hydrogels compared with HA-Tyr-TZB-2.5 hydrogels. Moreover, the release of trastuzumab from the hydrogels containing hyaluronidase was accompanied by a gradual loss of hydrogel weight (Fig. 3-8b), indicating that the degradation of the hydrogel network by hyaluronidase facilitated the release of trastuzumab. When HA-Tyr-TZB-0 was immersed in 20 ml of buffer at different ionic strengths (0.05M NaCl, PBS or 1M NaCl), the amount of trastuzumab released increased with the ionic strength (Fig. 3-8c). The results confirmed that trastuzumab were immobilized in the HA-Tyr hydrogels through electrostatic interactions, and degradation of the hydrogel network was required to release the proteins.

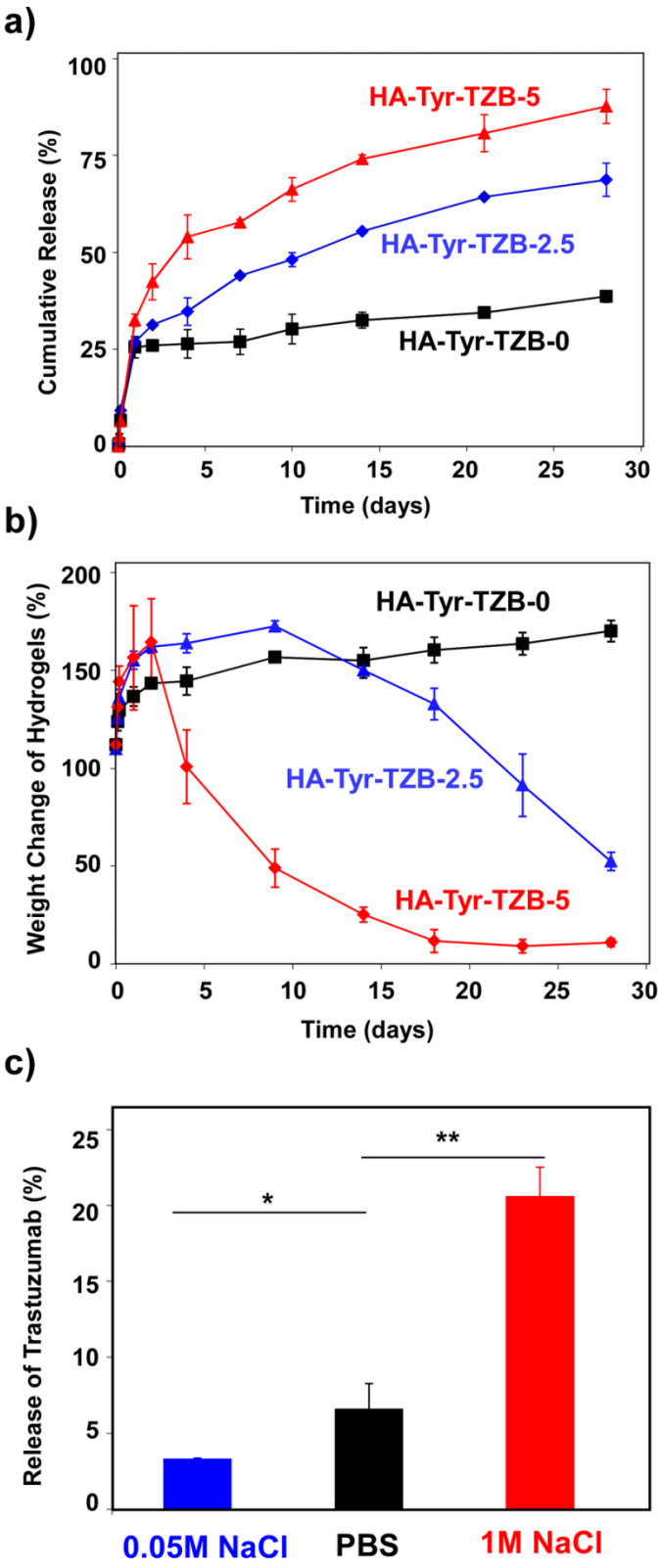


**Fig. 3-8. (a) Cumulative release of trastuzumab from HA-Tyr hydrogels incorporating both trastuzumab and hyaluronidase. (b) Degradation of the corresponding hydrogels. (c) The effect of ionic strength on the release of trastuzumab from HA-Tyr-TZB-0 (n = 3, *$p < 0.05$, **$p < 0.01$).**

### 3.3.4. Inhibition of BT-474 cell proliferation by HA-Tyr hydrogels incorporating trastuzumab and hyaluronidase

The inhibition on cell growth by trastuzumab-incorporated HA-Tyr hydrogels was examined *in vitro* using BT-474 breast cancer cells, which overexpresses human epidermal growth factor-2 (HER-2) receptor [23]. HA-Tyr hydrogels containing hyaluronidase (0, 2.5 and 5 U/ml), but no trastuzumab, did not affect cell proliferation (Fig. 3-9), which suggested that hyaluronidase and the degraded products of the hydrogels had no effect on cell growth. In contrast, hydrogels containing trastuzumab inhibited the proliferation of BT-474 cells. The percentage of growth inhibition increased further when hyaluronidase was incorporated in the hydrogels. HA-Tyr-TZB-5 inhibited cell proliferation as effectively as trastuzumab solution. The results confirmed the anti-proliferative activity of trastuzumab released from HA-Tyr hydrogels.

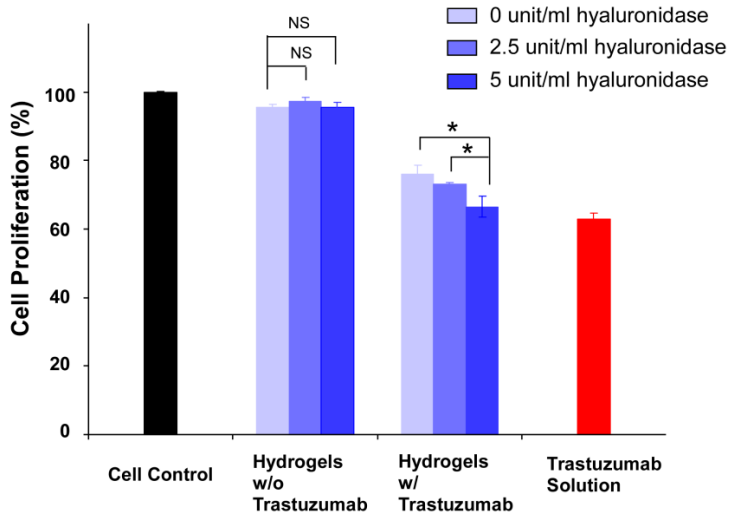


**Fig. 3-9. Proliferation of BT474 cells after treatment hydrogels containing hyaluronidase, hydrogels containing both trastuzumab and hyaluronidase, and trastuzumab solution alone. *$p < 0.05$. NS denotes not significant ($p > 0.05$).**

### 3.3.5. Tumor regression study and pharmacokinetic profile of trastuzumab delivered by HA-Tyr hydrogels

The anti-cancer effect of trastuzumab released from HA-Tyr hydrogels was examined *in vivo* using a mice xenograft model of BT-474 breast cancer cells. First, the effects of the drug carrier, i.e. the hydrogel, and hyaluronidase were examined. When mice were treated with a single administration of hydrogels incorporated with 0 or 5 U/ml of hyaluronidase (HA-Tyr-0 and HA-Tyr-5), but no trastuzumab, no significant tumor growth inhibition was observed (Fig.

3-10a). When mice were treated with a mixture solution of trastuzumab (5 mg/kg) and hyaluronidase (5 U/ml), tumor growth inhibition was observed, albeit the effect was not statistically significant. Similarly, statistically significant inhibition on tumor growth was not observed when the mice were treated with a single administration of HA-Tyr-TZB-0 or HA-Tyr-TZB-2.5 hydrogels (Fig. 3-10b). In contrast, when mice were treated with a single administration of HA-Tyr-TZB-5, starting from 15 days post-injection, tumor growth was significantly inhibited compared with PBS-treated group ($p < 0.05$). Mice of all treatment groups maintained their body weight throughout the duration of the experiment.

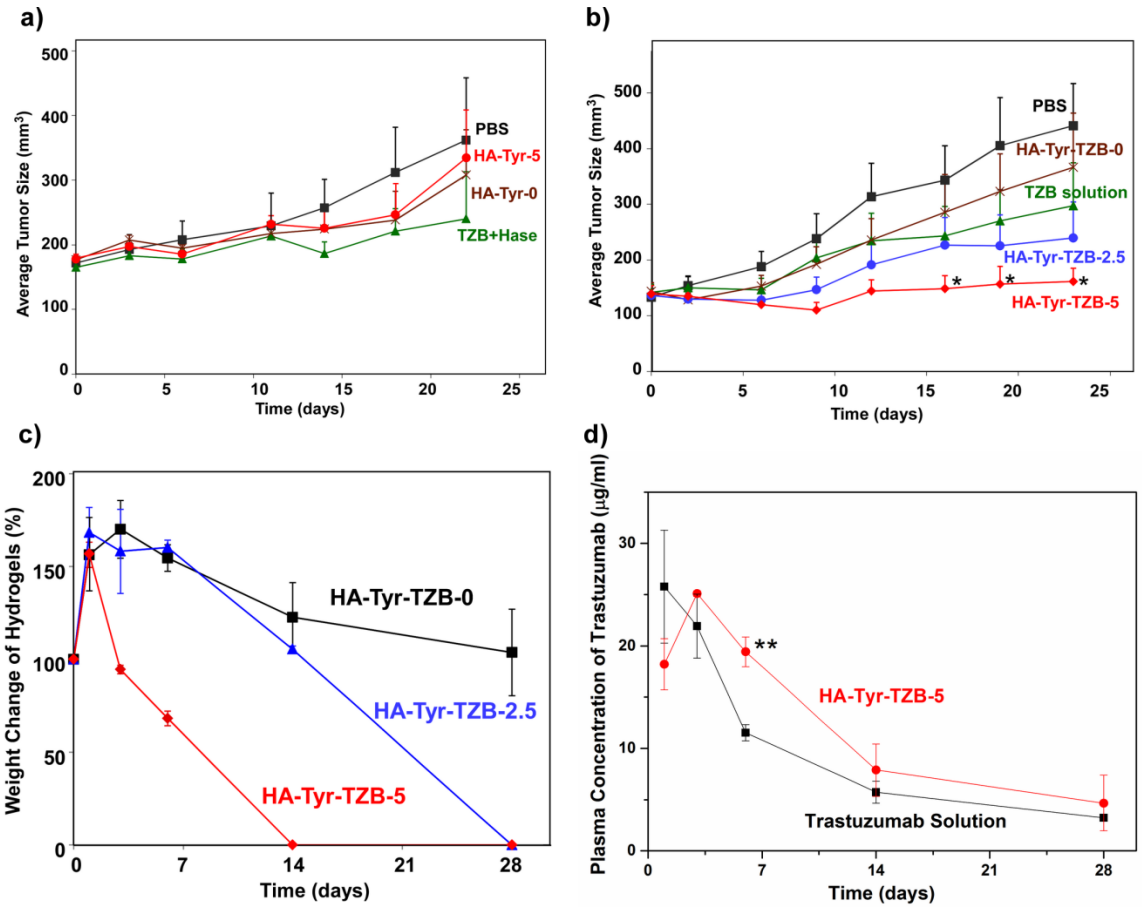


**Fig. 3-10. (a) Tumor growth in BT474-inoculated mice after treatment with PBS, HA-Tyr-0, HA-Tyr-5 and a mixture solution of trastuzumab and hyaluronidase (TZB+Hase). (b) Inhibition of tumor growth after treatment with trastuzumab solution (TZB) or HA-Tyr hydrogels incorporated with trastuzumab and hyaluronidase. (c) *In vivo* degradation of HA-Tyr hydrogels incorporated with trastuzumab and hyaluronidase. (d) Pharmacokinetics of trastuzumab in the plasma of mice after subcutaneous treatment of trastuzumab solution or HA-Tyr-TZB-5.**

Fig. 3-10c shows the degradation of hydrogels *in vivo* in terms of hydrogel weight loss. Similar to the *in vitro* degradation profiles, the weight of hydrogels increased to about 150%

in the first few days due to swelling, after which the weight started to decrease due to degradation. The weight of HA-Tyr-TZB-0 hydrogels declined slowly and returned to 100% by week 4. In contrast, HA-Tyr-TZB-2.5 hydrogels were completely degraded in 4 week, while HA-Tyr-TZB-5 hydrogels were degraded in 2 weeks. The degradation results supported the observed effect on tumor growth. The faster rate of degradation of HA-Tyr-TZB-5 ensured the continuous and complete release and trastuzumab, which in turn inhibited the growth of tumors more effectively than HA-Tyr-TZB-0 and HA-Tyr-TZB-2.5. The pharmacokinetics of trastuzumab delivered by HA-Tyr hydrogels were investigated (Fig. 3-10d). Starting from day 3, the plasma concentration of trastuzumab in mice treated with HA-Tyr-TZB-5 was consistently higher than that of mice treated with trastuzumab solution alone. Moreover, the plasma concentration was significantly higher on day 6 for mice treated with HA-Tyr-TZB-5 than trastuzumab solution. Taken together, the results indicated that the degradation-triggered release of trastuzumab from HA-Tyr hydrogels containing hyaluronidase resulted in the effective inhibition of tumor growth in a mice xenograft model of human breast cancer.

Tumor tissues were further analyzed by histology and immunohistochemistry (Fig. 3-11a). In hematoxylin and eosin (H&E) staining, we observed that tumor cells were densely packed in mice treated with PBS or trastuzumab solution, whereas cells were loosely packed in some region of tissues after the HA-Tyr-TZB-5 treatment. In immunohistochemical analyses, Ki67 and terminal deoxynucleotidyl transferase dUTP nick end labeling (TUNEL) assays were performed to detect proliferating and apoptotic cells in the tumor tissues, respectively. Ki67 is a cell proliferation marker and shows high expression in proliferating cells [24]. The Ki67 positive cells, indicated by the brown color in Fig. 3-11a, were abundant in mice treated with PBS or trastuzumab solution, whereas few cells were Ki67 positive after treatment of HA-Tyr-TZB-5. The percentage of Ki67 positive cells in HA-Tyr-TZB-5 group was significantly lower than those in PBS and HA-Tyr-TZB-0 groups (Fig. 3-11b). In the TUNEL assay [25], we did not observe any apoptotic cells in the PBS and trastuzumab solution groups; in contrast, clusters of brown-colored cells were obviously visible in the HA-Tyr-TZB-5 treated mice. The percentage of TUNEL positive cells in HA-Tyr-TZB-5 group was significantly higher than those in PBS and HA-Tyr-TZB-0 groups (Fig. 3-11c). These results confirmed that the HA-Tyr-TZB-5 treatment inhibited the proliferation and induced apoptosis of tumor cells.

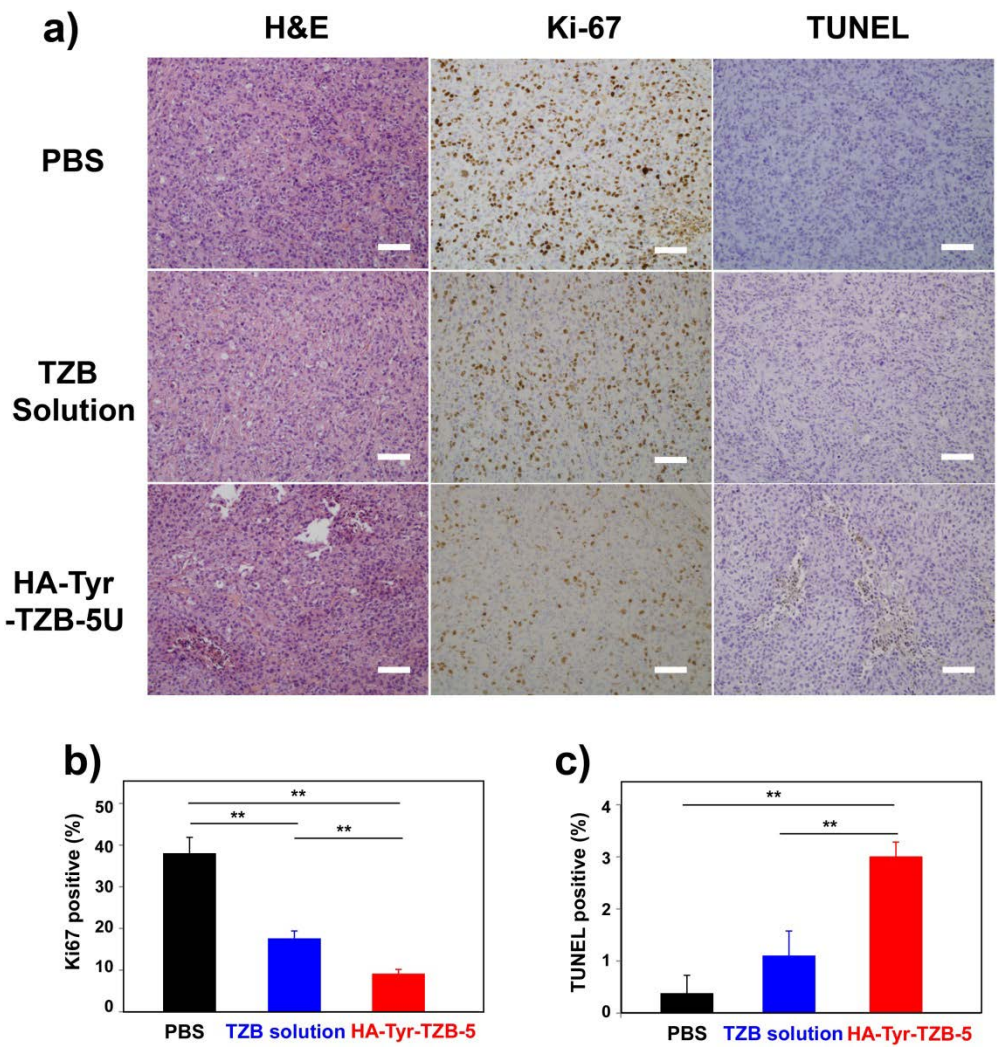


**Fig. 3-11. (a) Histological (H&E) and immunohistochemical analyses (TUNEL, brown; Ki67, brown) of tumor tissues from mice bearing BT474 tumors. The mice were treated subcutaneously with PBS, trastuzumab alone (TZB Solution) or HA-Tyr hydrogels that incorporated both trastuzumab and hyaluronidase (HA-Tyr-TZB-5U). Scale bar, 100 μm. The percentages of cells that were positive for Ki67 (b) and TUNEL (c) were quantified in the tumor tissue (** $p < 0.01$).**

## 3.4. Conclusion

In this study, the enzymatic degradation of HA-Tyr hydrogels by hyaluronidase was characterized. It was shown that the degradation rate decreased with the crosslink density of the hydrogel as well as the concentration of hyaluronidase. The injectable HA-Tyr hydrogel system was employed for the sustained delivery of positively charged proteins. It was demonstrated that proteins could interact with the negatively charged HA network *via* electrostatic interactions, resulting in protein immobilization within the hydrogel network. Hence, the release of incorporated proteins was dependent upon degradation of the hydrogel network by hyaluronidase. When positively charged trastuzumab was incorporated in the HA-

Tyr hydrogels, 25% of trastuzumab was released in the first two days, after which no more protein was release due to electrostatic interactions with the HA network. When hyaluronidase was incorporated in the hydrogels to promote gel degradation, trastuzumab was released continuously. The rate of trastuzumab release depended on the concentration of hyaluronidase incorporated in the hydrogel. HA-Tyr hydrogels containing 5 U/ml of hyaluronidase released trastuzumab at a faster rate, and showed a greater efficacy in inhibiting the proliferation of BT-474 cells, compared to HA-Tyr hydrogels 2.5 U/ml of hyaluronidase. Moreover, a single subcutaneous administration of HA-Tyr hydrogels incorporating both trastuzumab and 5 U/ml of hyaluronidase resulted in a significant inhibition of tumor growth over a period of 4 weeks. In contrast, trastuzumab administered as a solution at the same dosage failed to significantly inhibit tumor growth. The results demonstrated that the degradation-triggered release of positively charged proteins from HA-Tyr hydrogels is a promising strategy to deliver proteins over a prolonged period of time.

**References**

[1] Hoffman AS. Hydrogels for biomedical applications. Adv. Drug Del. Rev. 2002;54:3-12.

[2] Bae KH, Wang L-S, Kurisawa M. Injectable biodegradable hydrogels: progress and challenges. J. Mater. Chem. B 2013;1:5371-88.

[3] Kurisawa M, Lee F, Wang L-S, Chung JE. Injectable enzymatically crosslinked hydrogel system with independent tuning of mechanical strength and gelation rate for drug delivery and tissue engineering. J. Mater. Chem. 2010;20:5371-5.

[4] Gretzer C, Emanuelsson L, Liljensten E, Thomsen P. The inflammatory cell influx and cytokines changes during transition from acute inflammation to fibrous repair around implanted materials. J. Biomater. Sci. Polym. Ed. 2006;17:669-87.

[5] Canfield RE. The amino acid sequence of egg white lysozyme. J. Biol. Chem. 1963;238:2698-707.

[6] Pastor I, Ferrer ML, Lillo MP, Gomez J, Mateo CR. Structure and dynamics of lysozyme encapsulated in a silica sol-gel matrix. J. Phys. Chem. B 2007;111:11603-10.

[7] Piccart-Gebhart MJ, Procter M, Leyland-Jones B, Goldhirsch A, Untch M, Smith I, Gianni L, Baselga J, Bell R, et al. Trastuzumab after adjuvant chemotherapy in HER2-positive breast cancer. N. Engl. J. Med. 2005;353:1659-72.

[8] Romond EH, Perez EA, Bryant J, Suman VJ, Geyer CE, Davidson NE, Tan-Chiu E, Martino S, Paik S, et al. Trastuzumab plus adjuvant chemotherapy for operable HER2-positive breast cancer. N. Engl. J. Med. 2005;353:1673-84.

[9] Weiner LM, Surana R, Wang S. Monoclonal antibodies: versatile platforms for cancer immunotherapy. Nat. Rev. Immunol. 2010;10:317-27.

[10] Bange J, Zwick E, Ullrich A. Molecular targets for breast cancer therapy and prevention. Nat. Med. 2001;7:548-52.

[11] Sawyers C. Targeted cancer therapy. Nature 2004;432:294-7.

[12] Agency EM. Herceptin. Summary of characteristics. http://www.ema.europa.eu/docs/en_GB/document_library/EPAR_-_Product_information/human/000278/WC500074922.pdf (Feb 11, 2012)

[13] Wiig H, Gyenge CC, Tenstad O. The interstitial distribution of macromolecules in rat tumours is influenced by the negatively charged matrix components. J. Physiol. 2005;567:557-67.

[14] Frost GI, Csoka TB, Wong T, Stern R. Purification, cloning, and expression of human plasma hyaluronidase. Biochem. Biophys. Res. Commun. 1997;236:10-5.

[15] Lee F, Chung JE, Kurisawa M. An injectable enzymatically crosslinked hyaluronic acid-tyramine hydrogel system with independent tuning of mechanical strength and gelation rate. Soft Matter 2008;4:880-7.

[16] Yano H, Iemura A, Fukuda K, Mizoguchi A, Haramaki M, Kojiro M. Establishment of 2 distint human hepatocellular carcinoma cell lines from a single nodule showing clonal dedifferentiation of cancer cells. Hepatology 1993;18:320-7.

[17] Bitter T, Muir HM. A modified uronic acid carbazole reaction. Anal. Biochem. 1962;4:330-4.

[18] Xu KM, Lee F, Gao SJ, Chung JE, Yano H, Kurisawa M. Injectable hyaluronic acid-tyramine hydrogels incorporating interferon-alpha 2a for liver cancer therapy. J. Control. Release 2013;166:203-10.

[19] Nakamae K, Nishino T, Kato K, Miyata T, Hoffman AS. Synthesis and characterization of stimuli-sensitive hydrogels having a different length of ethylene glycol chains carrying phosphate groups: loading and release of lysozyme J. Biomater. Sci. Polym. Ed. 2004;15:1435-46.

[20] Frost GI. Recombinant human hyaluronidase (rHuPH20): an enabling platform for subcutaneous drug and fluid administration. Expert Opin. Drug Deliv. 2007;4:427-40.

[21] Ismael G, Hegg R, Muehlbauer S, Heinzmann D, Lum B, Kim SB, Pienkowski T, Lichinitser M, Semiglazov V, et al. Subcutaneous versus intravenous administration of (neo)adjuvant trastuzumab in patients with HER2-positive, clinical stage I-III breast cancer (HannaH study): a phase 3, open-label, multicentre, randomised trial. Lancet Oncol. 2012;13:869-78.

[22] Pivot X, Gligorov J, Muller V, Curigliano G, Knoop A, Verma S, Jenkins V, Scotto N, Osborne S, et al. Patients' preferences for subcutaneous trastuzumab versus conventional intravenous infusion for the adjuvant treatment of HER2-positive early breast cancer: final analysis of 488 patients in the international, randomized, two-cohort PrefHer study. Ann. Oncol. 2014;25:1979-87.

[23] Nahta R, Hung MC, Esteva FJ. The HER-2-targeting antibodies trastuzumab and pertuzumab synergistically inhibit the survival of breast cancer cells. Cancer Res. 2004;64:2343-6.

[24] Scholzen T, Gerdes J. The Ki-67 protein: From the known and the unknown. J. Cell. Physiol. 2000;182:311-22.

[25] Gavrieli Y, Sherman Y, Bensasson SA. Identification of programed cell-death in situ via specific labeling of nuclear-DNA fragmentation. J. Cell Biol. 1992;119:493-501.

# Chapter 4

# A Dextran-Tyramine Hydrogel System with Poly(ethylene glycol) Microdomains for the Sustained and Burst-Free Release of PEGylated Interferon-α2a

## 4.1. Introduction

Therapeutic proteins are an important class of drugs in today's medicine. They are administered mainly through the parenteral routes *via* intravenous, subcutaneous or intramuscular injections. One of the drawbacks of therapeutic proteins is their short biological half-lives, as they are rapidly cleared from the blood stream through proteolysis and renal filtration [1]. In order to prolong the circulating half-life of therapeutic proteins in the blood stream, covalent attachment of poly(ethylene glycol) (PEG) to proteins, a process known as PEGylation, has been developed. PEGylation extends the half-life of proteins by protecting them from enzymatic degradation, reducing renal filtration and avoiding recognition by the host's defense system [2, 3]. For instance, the half-life of native IFN-α2a is only 3-8 hours. In contrast, the half-life of PEGylated interferon-α2a (PEG-IFN-α2a) is 65 hours. In spite of the prolonged half-life, the use of PEG-IFN-α2a for hepatitis C treatment requires weekly injections for 12-48 weeks [1]. Frequent injection increases the cost of treatment and the risk of adverse drug reactions, and causes patient discomfort. Therefore, there exists a need for a protein delivery system that can release PEG-IFN-α2a over an extended period of time, while not compromising the therapeutic outcome.

Hydrogels are suitable candidates for the sustained delivery of proteins. As described in Chapter 2, interferon-α2a (IFN-α2a) incorporated in hyaluronic acid-tyramine (HA-Tyr) hydrogels were released sustainably for several hours, and the release rate could be tuned by the crosslink density of the hydrogel. In order to prolong the release over several days or weeks, it is necessary to introduce physical interactions between the proteins and the hydrogel networks, without which the proteins will diffuse rapidly out of the hydrogel network as the diameter of proteins is smaller than the mesh size of most hydrogels. As described in Chapter 3, electrostatic interactions between postiviely charged trastusumab and negatively charged HA-Tyr hydrogels immobilized the proteins within the hydrogels network, and the release was dependent on the degradation the hydrogel network. In addition to the short release duration, the release profiles of proteins from hydrogels typically exhibit a rapid or "burst" release at the initial phase [4], which leads to a sudden increase in the plasma concentration of the proteins that may causes side effects and results in ineffective treatments [5]. Burst release of proteins can be suppressed to some extent by increasing the crosslink density of the hydrogel. However, complete elimination is difficult to achieve. In this chapter, a novel strategy to deliver proteins using hydrogels for an extended period of time and without burst

release is described. Specifically, a dextran hydrogel system containing micrometer-sized PEG domains was designed for the sustained delivery of PEG-IFN-α2a.

Dextran (Dex) is used clinically as a plasma volume expander and an antithrombotic agent. Dex is also widely used to form hydrogels for drug delivery applications due to its hydrophilicity and biocompatibility [6]. When Dex is mixed with PEG at an appropriate concentration and temperature in aqueous condition, a cloudy mixture is formed as the two water-soluble polymers are not miscible with each other. Given enough time, the mixture solution will eventually separate into two distinct phases (Fig. 4-1), a phenomenon known as aqueous two-phase system (ATPS) [7]. We proposed that by crosslinking the Dex phase immediately after mixing the two polymers, a Dex hydrogel containing PEG microdomains could be formed. Towards this end, dextran-tyramine (Dex-Tyr) conjugates were synthesized. In the presence of horseradish peroxidase (HRP) and $H_2O_2$, a transparent Dex-Tyr hydrogels was formed through the coupling of tyramine moieties. In contrast, when PEG was mixed with Dex-Tyr conjugates prior to the addition of HRP and $H_2O_2$, an opaque Dex-Tyramine hydrogel containing PEG microdomains (Dex-Tyr/PEG) was formed. Moreover, when PEGylated proteins were present during the crosslinking process, the proteins were found to preferentially partition in the PEG microdomains rather than the Dex matrix (Fig. 4-2a). The PEG microdomains served not only as reservoirs for PEGylated proteins, but also regulated their release from hydrogels. It was shown that Dex-Tyr/PEG hydrogels released PEG-IFN-α2a over 3 months *in vitro* in a burst-free manner, and substantially extended its circulation half-life from 1.5 to 15.6 days *in vivo*. In a humanized mouse model of hepatitis C, a one-time administration of PEG-IFN-α2a-loaded Dex-Tyr/PEG hydrogels prevents HCV-induced liver injury as effectively as the clinically relevant formulation that requires eight weekly injections of PEG-IFN-α2a. The present hydrogel system can be applied for the long-term delivery of other PEGylated therapeutics for the treatment of chronic diseases.

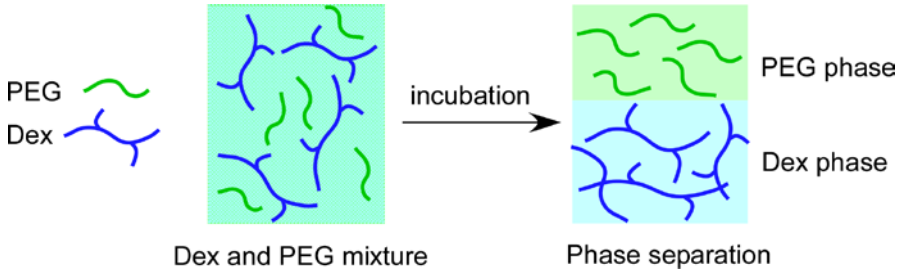


**Fig. 4-1. Phase separation of an aqueous mixture of Dex and PEG solution.**

## 4.2. Materials and Methods

### 4.2.1. Materials and cell culture

Dex (MW = 500 kDa), PEG (MW = 10 kDa), tyramine, 4-nitrophenyl chloroformate (PNC), pyridine, dextranase, bovine serum albumin (BSA), fluorescein isothiocyanate (FITC)-labelled BSA (FITC-BSA) and FITC-labelled dextran (MW = 500 kDa) were purchased from Sigma-Aldrich (Minnesota, USA). PEG-sulforhodamine (MW = 10 kDa) was purchased from Creative PEGWorks (Winston-Salem, USA). HRP (190 U/mg) was purchased from Wako Pure Chemical Industries (Osaka, Japan). $H_2O_2$ was obtained from Lancaster Synthesis (Lancashire, UK). PEG-IFN-α2a was obtained from Roche (Basel, Switzerland). Human IFN-α ELISA kit (PBL InterferonSource, USA) and luciferase assay system (Promega, Singapore) were used according to the manufacturer's instructions.

Huh-7 human hepatoma cells carrying subgenomic HCV replicon $I_{389}$luc-ubi-neo/NS3-3/5.1 with adaptive mutation (E1202G, T1280I, K1846T) were obtained from Prof. Ralf Bartenschlager (Heidelberg University, Germany). These cells were grown in DMEM media supplemented with 10% (v/v) fetal bovine serum, 1 mM non-essential amino acid and 500 μg/ml G418 (Geneticin, Merck). Adult human dermal fibroblast (Lonza, Singapore) was grown in DMEM media supplemented with 10% (v/v) fetal bovine serum and 1% penicillin/streptomycin. All cells were cultured at 37 °C in a 5% $CO_2$ atmosphere.

### 4.2.2. Synthesis of Dex-Tyr conjugate

Dex-Tyr conjugate was synthesized according to the previous report with some modifications [8]. Briefly, Dex (5 g, 92.5 mmol -OH) was dissolved in 100 ml of DMSO/pyridine mixture (1:1, v/v) for 24 h at 25 ºC. The Dex solution was then cooled at 4 ºC. PNC (1.1 g, 5.5 mmol) was slowly added into 25 ml of pyridine stirred in an ice bath. To this solution, 25 ml of DMSO was added with continuous stirring. The resulting PNC solution was added drop-wise into the Dex solution stirred in an ice bath. The reaction mixture was stirred for 24 h at 4 ºC. After the solution was added drop-wise into cold ethanol with continuous stirring, the precipitate was washed with cold ethanol, and then dried in a vacuum oven for 24 h at 25 ºC. The structure of the product was confirmed by $^1$H NMR spectroscopy. The degree of substitution (DS) is defined as the number of substituents per 100 anhydroglucose units in Dex. DS was determined to be 1.3 by comparing the relative peak area of aromatic protons of a nitrophenyl moiety (δ = 6.97 and 8.19, 4 H) and anomeric protons of Dex (δ = 5.00 and 5.35,

1 H). Yield: 98%. $^{1}$H NMR (400 MHz, $D_2O$, δ): 3.30–4.10 (m, 6 H, CH and $CH_2$), 5.00 and 5.35 (s, 1 H, CH), 6.97 and 8.19 (m, 4 H, Ar H).

The dried Dex-PNC conjugate (5 g) was dissolved in 350 ml of DMSO for 3 h at 25 ºC. To this solution, tyramine (175 mg, 1.25 mmol) dissolved in 30 ml of DMSO was added in a drop-wise manner. The mixture was stirred for 24 h at 25 ºC. Then, the solution was added drop-wise to 300 ml of cold deionized water stirred in an ice bath. The resultant Dex-Tyr conjugate was transferred to dialysis tubes with a molecular weight cutoff of 3,500 Da. The tubes were dialyzed against deionized water and then lyophilized. DS was determined to be 1.03 by comparing the relative peak area of aromatic protons of a tyramine moiety (δ=6.86 and 7.17, 4 H) and anomeric protons of Dex (δ=5.00 and 5.35, 1 H). Yield: 98%. $^{1}$H NMR (400 MHz, $D_2O$, δ): 3.30–4.10 (m, 6 H, CH and $CH_2$), 5.00 and 5.35 (s, 1 H, CH), 6.86 and 7.17 (m, 4 H, Ar H).

### 4.2.3. Preparation and characterization of Dex-Tyr/PEG hydrogels

Dex-Tyr conjugate and PEG were dissolved in 10 mM phosphate-buffered saline (PBS, pH 7.4) at a concentration of 10% and 30% (w/v), respectively. To prepare Dex-Tyr/PEG hydrogels, 270 µl of 10% (w/v) Dex-Tyr solution, 30 µl of 30% (w/v) PEG solution, and 6 µl of either PBS or PEG-IFN-α2a solution (360 µg/ml) were mixed in LoBind tubes (Eppendorf, Germany). Subsequently, 3 µl each of HRP and $H_2O_2$ solution in varying concentrations was added. The final concentration of HRP and $H_2O_2$ used to form Dex-Tyr/PEG hydrogels was 0.13-0.21 U/ml and 2.42 mM, respectively. The mixture was immediately vortexed and 210 µl of which was injected between two parallel glass plates clamped together with 1.5 mm spacing to prepare disk-shaped hydrogels. Gelation was allowed to proceed for 1 h at 37 °C on an orbital shaker at 50 rpm. For comparison, Dex-Tyr hydrogels loaded with PEG-IFN-α2a were prepared using 30 µl of PBS instead of PEG solution. Typically, 0.21 U/ml of HRP and 1.46 mM of $H_2O_2$ were used to produce Dex-Tyr hydrogels, which have storage moduli similar to that of Dex-Tyr/PEG hydrogels.

To characterize the swelling and physical properties, each hydrogel disk (12 mm diameter × 1.5 mm thick) was immersed in 10 mM PBS solution (pH 7.4) for 7 days. The swollen disks were weighed and then dried in a vacuum oven to obtain the dry weight. The mass swelling ratio and water content of hydrogels were calculated by the following equations:

$$\text{Mass swelling ratio} = \frac{M_s}{M_d}$$

$$\text{Water content (\%)} = \frac{M_s - M_d}{M_s} \times 100$$

where $M_s$ is the weight of the swollen disk and $M_d$ is the weight of the dried disk.

The volumetric swelling ratio ($Q$), effective crosslink density ($v_e$) and average mesh size ($\xi$) of hydrogels were then calculated as described in the literature [9, 10]. The rheological measurement was performed as reported previously [11]. Briefly, 270 µl of Dex-Tyr solution, 30 µl of PEG solution and 6 µl of either PBS or PEG-IFN-α2a solution (360 µg/ml) were mixed in LoBind tubes (Eppendorf, Germany). Subsequently, 3 µl each of HRP and $H_2O_2$ solution in varying concentrations was added. The mixture was immediately vortexed and 210 µl of which was applied to the bottom plate of a HAAKE Rheoscope 1 rheometer (Karlsruhe, Germany). Rheological measurement was carried out at 37 ºC in the dynamic oscillatory mode with a constant deformation of 1% and a frequency of 1 Hz, using a cone and plate geometry of 3.5 cm diameter and 1.029° cone angle. The evolution of storage modulus (G') and loss modulus (G'') was monitored as a function of time. The gel point was determined as the time at which crossover of the two moduli occurred.

### 4.2.4. Analysis of partition of proteins in Dex-PEG two-phase solution

PEGylated FITC-BSA was synthesized according to the previously reported method [12]. To determine the partition coefficient, 810 µl of 10% (w/v) Dex solution, 90 µl of 30% (w/v) PEG solution and 36 µl of protein solution were mixed in LoBind tubes. Tested proteins are listed as follows: FITC-BSA (10 mg/ml), PEGylated FITC-BSA (10 mg/ml), IFN-α2a (0.72 µg/ml) and PEG-IFN-α2a (2.16 µg/ml). The mixture was left to settle for 1 h at 4 ºC to induce phase separation. The concentration of FITC-BSA and PEGylated FITC-BSA in the PEG-rich and Dex-rich phases was assessed by measuring the fluorescence of FITC dye at an emission wavelength of 520 nm using a microplate reader (Tecan Group Ltd., Switzerland). The concentration of IFN-α2a and PEG-IFN-α2a in each phase was measured by using a human IFN-α ELISA kit. The partition coefficient of a protein was determined by dividing its concentration in the PEG-rich phase with its concentration in the Dex-rich phase. For comparison, a two-phase mixture composed of Dex-Tyr and PEG was prepared using 810 µl of 10% (w/v) Dex-Tyr solution instead of Dex solution, and then analyzed as described above.

### 4.2.5. Observation of protein partitioning and PEG domain structures in hydrogels

To examine the partition behavior of fluorescently tagged proteins in Dex-Tyr/PEG hydrogels, FITC-BSA and PEGylated FITC-BSA (2 mg) were dissolved in 270 µl of 10% (w/v) Dex-Tyr solution. To this solution, 30 µl of 30% (w/v) PEG solution and 6 µl of PBS were added. Subsequently, 3 µl each of HRP and $H_2O_2$ solution was added. The final concentration of HRP and $H_2O_2$ was fixed to 0.13 U/ml and 2.42 mM, respectively. The mixture was immediately vortexed and 80 µl of which was applied to glass-bottom microwell dishes (MatTek Corporation, USA). Gelation was allowed to proceed for 1 h at 37 °C on an orbital shaker at 50 rpm. The hydrogels were then observed by using a Zeiss LSM 5 DUO confocal laser scanning microscope (Carl Zeiss, Germany). For comparison, Dex-Tyr hydrogels were prepared using 30 µl of PBS instead of PEG solution. To observe PEG domain structures, FITC-labelled Dex and PEG-sulforhodamine were first dissolved in PBS at a concentration of 10% and 30% (w/v), respectively. Typically, 264 µl of 10% (w/v) Dex-Tyr solution, 6 µl of FITC-labelled Dex solution, 24 µl of 30% (w/v) PEG solution, 6 µl of PEG-sulforhodamine solution and 6 µl of PBS were mixed in a microcentrifuge tube in a dark place. Subsequently, 3 µl each of HRP and $H_2O_2$ solution in varying concentrations was added. The mixture was immediately vortexed and 80 µl of which was applied to microwell dishes. The produced hydrogels were observed by using a Zeiss LSM 5 DUO confocal laser scanning microscope. The average diameter of PEG domains was determined by measuring more than 250 domains in transmitted light images with an Image-Pro Plus software (Media Cybernetics, USA).

### 4.2.6. Measurement of antiviral activity of PEG-IFN-α2a incorporated in hydrogels

The antiviral activity of PEG-IFN-α2a was determined by using Huh-7 cells carrying HCV replicon, as described previously [13, 14]. Briefly, hydrogels loaded with PEG-IFN-α2a were treated with 3 ml of 10 mM PBS (pH 7.4) containing dextranase (10 U/ml) and 0.05% (w/v) BSA. The complete degradation of the hydrogels was achieved after incubation for 24 h at 37 ºC. The resultant solution was filtered through a 0.22 µm sterile syringe filter. The amount of PEG-IFN-α2a in each sample was measured by using a human IFN-α ELISA kit. The percent recovery was determined by dividing the amount of recovered proteins with the amount of proteins added to each hydrogel. For antiviral activity assay, Huh-7 cells were seeded in 6-well plates at a density of $1 \times 10^5$ cells per well. After 24 h, the cells were treated with 2 ml of DMEM media (without G418) mixed with samples at an equivalent PEG-IFN-

α2a concentration (250 pg/ml). After 72 h, the cell lysate was collected and a luciferase assay was carried out to measure the value of relative luminescence units (RLU) for each sample. The antiviral activity of PEG-IFN-α2a was calculated by the following equation:

$$\text{Relative antiviral activity}\,(\%) = \frac{\text{Log}_{10}(NC) - \text{Log}_{10}(S_n)}{\text{Log}_{10}(NC) - \text{Log}_{10}(PC)} \times 100$$

where *NC* is the value of RLU after incubation with the negative control (DMEM media alone), *PC* is the value of RLU after incubation with the positive control (PEG-IFN-α2a solution at a final concentration of 250 pg/ml), and $S_n$ is the value of RLU after incubation with samples at an equivalent IFN-α2a concentration.

### 4.2.7. *In vitro* protein release studies

Hydrogels loaded with PEG-IFN-α2a were immersed in 20 ml of 10 mM PBS (pH 7.4) containing BSA and sodium azide at a concentration of 0.05% (w/v). The samples were incubated at 37 ºC on an orbital shaker at 50 rpm. At definite time intervals, 200 µl of the release medium was collected and stored at – 20 ºC. To keep a total volume constant, 200 µl of fresh buffer solution was added to the vial. The concentration of PEG-IFN-α2a in the collected samples was measured by using a human IFN-α ELISA kit. The cumulative percentage of protein release was determined by dividing the amount of released proteins with the amount of proteins added to each hydrogel. To investigate the kinetics of protein release, the obtained release data were fitted to the zero-order, first-order and Higuchi models, respectively, as follows [15]:

$$Q_t = Q_0 - K_0 t$$

$$\ln Q_t = \ln Q_0 - K_1 t$$

$$Q_t = K_h t^{1/2}$$

where $Q_0$ is the initial amount of proteins in the hydrogels, $Q_t$ is the amount of proteins in the hydrogels at time *t*; $K_0$, $K_1$ and $K_h$ are the respective rate constants.

The protein release mechanism was analyzed by fitting the obtained release data to the Ritger-Peppas equation [16] represented as follows:

$$\frac{M^t}{M^\infty} = kt^n$$

where $M^t$ and $M^\infty$ are the amounts of proteins released at time $t$ and at equilibrium, respectively, $k$ is a proportionality constant, and $n$ is the diffusional exponent.

The antiviral activity of PEG-IFN-α2a released from hydrogels was measured as described in Section 4.2.6.

### 4.2.8. Preparation of humanized mice

Humanized mice were established by adoptive transfer of human $CD34^+$ fetal liver cells into NOD-*scid Il2rg*$^{-/-}$ (NSG) mice. Human $CD34^+$ cells were freshly isolated from aborted fetuses at 15 to 23 weeks of gestation, in accordance with the institutional ethical guidelines of the KK Women's and Children's Hospital, Singapore. Fetal liver tissues were processed as described previously [17]. $CD34^+$ cells were purified by magnetic-activated cell sorting using the EasySep CD34 positive selection kit (Stemcell Technologies) under sterile conditions, following manufacturer's protocol. The purity of the $CD34^+$ cells was >95%. NSG mice were purchased from Jackson laboratory and bred in a specific pathogen-free facility at the Biological Resource Centre in Agency for Science, Technology and Research (A*STAR), Singapore. One to three days old NSG pups were sub-lethally irradiated at 1 Gy and transplanted with $2 \times 10^5$ $CD34^+$ human fetal liver cells by intra-hepatic injections. The mice were bled 8 weeks post-transplantation to determine the human immune reconstitution level and serum human albumin level. All experimental procedures were in accordance to protocols approved by the International Animal Care and Use Committee (IACUC) at the Biological Resource Centre in A*STAR, Singapore.

### 4.2.9. Pharmacokinetics studies in humanized mice

Hydrogel disks loaded with PEG-IFN-α2a were prepared under sterile conditions according to the procedures described above. Dex-Tyr/PEG hydrogels with 3 μm domains were formed at a final concentration of 0.16 U/ml of HRP and 2.42 mM of $H_2O_2$. In the case of Dex-Tyr hydrogels, 0.21 U/ml of HRP and 1.46 mM of $H_2O_2$ were used to produce hydrogels with G' that was similar to Dex-Tyr/PEG hydrogels. Ten-week-old male humanized mice weighting approximately 25 g each were randomly divided into 3 groups consisted of 3 mice each. One group received a one-time subcutaneous (s.c.) injection of 50 μl of PEG-IFN-α2a solution at a dose of 57.6 μg/kg of body weight. The second and last group

received a one-time s.c. implantation of a Dex-Tyr and Dex-Tyr/PEG hydrogel disk containing equal amount of PEG-IFN-α2a (57.6 μg/kg) in the lateral side of mice, respectively. At selected time points, blood (30 μl) was taken from the tail vein of each mouse into microcentrifuge tubes containing 3 μl of sodium citrate solution (37 mg/ml). The blood samples were centrifuged at 7,000 × g for 10 min at 4 °C, and the plasma were stored at -20 °C. The concentration of PEG-IFN-α2a in the plasma was measured by using a human IFN-α ELISA kit. Pharmacokinetic parameters were analyzed by using a two-compartment model with the PKSolver software [18].

### 4.2.10. *In vivo* drug testing in a humanized mouse model of hepatitis C

To establish a humanized model of hepatitis C, ten-week-old humanized mice weighting approximately 25 g each were infected with $1 \times 10^6$ FFU of HCV (genotype 2a) by intravenous injection (day 0). These mice were randomly divided into 5 groups consisting of 5 mice each. On day 1 post-infection, the treatment of the infected mice was initiated. As untreated control, one group received a one-time s.c. injection of 50 μl of PBS solution. The second group received a one-time s.c. injection of 50 μl of PEG-IFN-α2a solution at a dose of 240 μg/kg of body weight. The third group received 2 doses of monthly s.c. injections of 50 μl of PEG-IFN-α2a solution (2 × 120 μg/kg) at day 1 and 29 post-infection. The fourth group received 8 doses of weekly s.c. injections of 50 μl of PEG-IFN-α2a solution (8 × 30 μg/kg). The last group received a one-time s.c. implantation of PEG-IFN-α2a-loaded Dex-Tyr/PEG hydrogel disks (240 μg/kg) in the lateral side of mice. All groups received the same total dose of PEG-IFN-α2a (240 μg/kg). A group of age-and-donor matched mice without HCV infection were used as a negative control. The blood and liver samples were harvested 8 weeks after infection. Sera were prepared from the blood samples by centrifugation at 7,000 × g for 10 min at 4 °C. The concentrations of human IFN-γ in the sera were measured by ELISA (BioLegend, USA). Serum ALT levels were measured using Cobas C111 Analyzer (Roche) in the comparative medicine in-house veterinary diagnostic laboratory, National University of Singapore (NUS). The livers were fixed with 10% formalin and embedded in paraffin. For histology, sections of 3 μm thickness were prepared from the livers. Rehydrated liver tissue sections were stained with H&E or Fast-green (Sigma) & Sirius Red (Sigma). The slides were mounted and scanned using a MIRAX MIDI system with bright field illumination (Carl Zeiss). Images were analyzed using the MIRAX viewer software.

### 4.2.11. Statistical analysis

Data are expressed as mean ± SD or mean ± SEM as indicated in the figure legends. Statistical analysis was performed using a standard Student's *t*-test. Statistical significance was determined, $p < 0.05$ is considered statistically significant.

## 4.3. Results and Discussion

### 4.3.1. Rational design of microstructured Dex hydrogels

Dex is a branched polysaccharide synthesized by bacteria. It is composed of glucopyranose units linked together through α-1,6 glycosidic bonds with branching *via* α-1,3 linkages (Fig. 1-4c, Chapter 1). Dex-Tyr conjugate was synthesized by conjugating the primary amine group of tyramine to the hydroxyl group of Dex which has been activated with *p*-nitrophenyl formate groups [8]. The DS determined by $^{1}$H NMR spectroscopy was 1.03. Dex-Tyr/PEG hydrogels were formed by enzyme-mediated crosslinking of Dex-Tyr conjugates in the presence of PEG and PEGylated proteins (Fig. 4-2a). First, Dex-Tyr conjugates, PEG, and PEGylated proteins were dissolved separately in PBS before mixing together to obtain a homogenous solution that did not show phase separation at room temperature (22 °C) (Fig. 4-2b). Subsequent addition of HRP and $H_2O_2$ catalyzed the oxidative coupling of tyramine moieties [19] (Fig. 4-2c). Although the aqueous mixture of Dex-Tyr conjugates and PEG initially existed as a single phase, intermolecular crosslinking of Dex-Tyr conjugates induced phase separation by condensing PEG molecules into PEG-rich droplets. As a result, discrete micrometer-sized PEG domains were formed in a continuous Dex phase. While Dex-Tyr hydrogels were transparent, Dex-Tyr/PEG hydrogels were opaque (Fig. 4-2d) because of light scattering by the PEG domains [20]. Micrometer-sized spherical PEG domains were clearly visible in the Dex-Tyr/PEG hydrogels when observed under an optical microscope (Fig. 4-2e). Disk-shaped hydrogels with identical thickness were fabricated for the rest of the study.

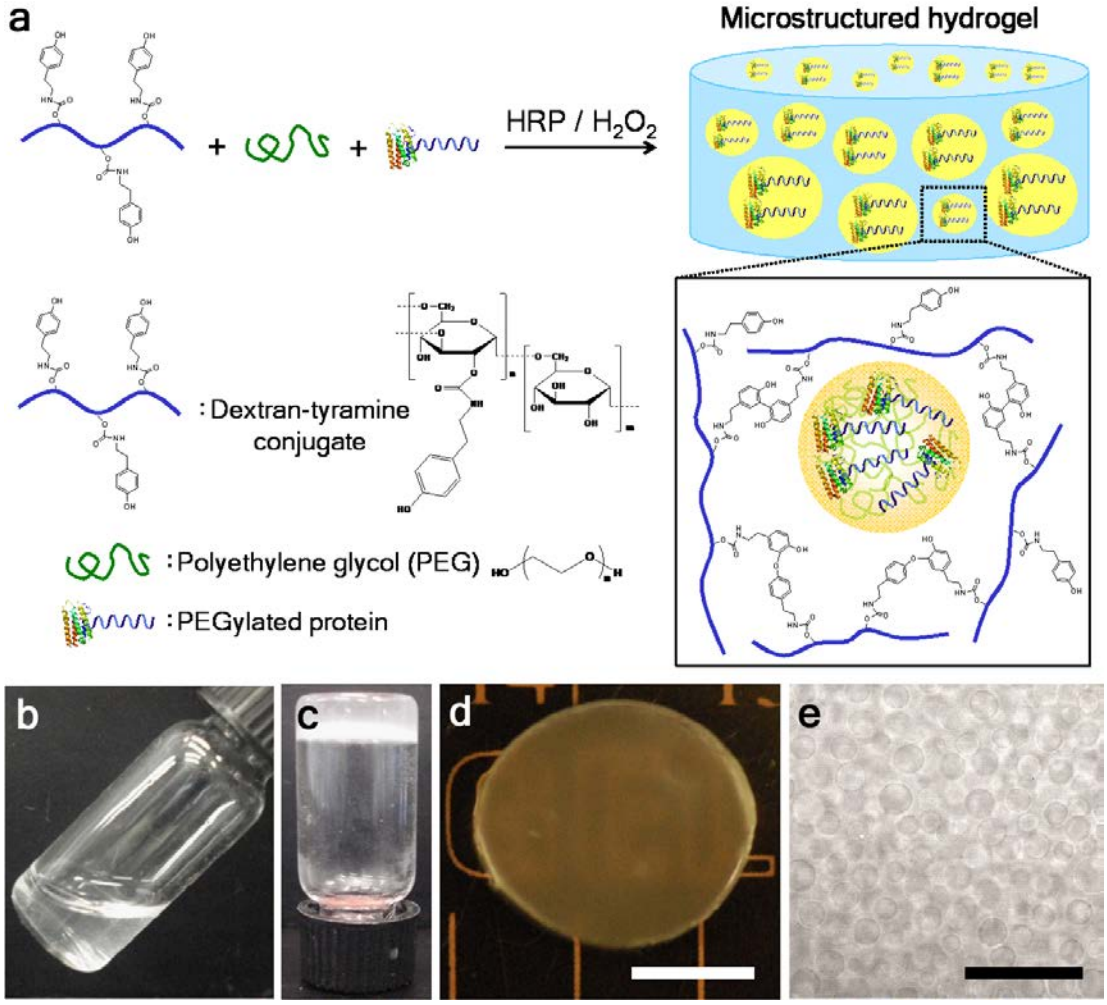


**Fig. 4-2. a) Schematic of a microstructured hydrogel for sustained release of PEGylated proteins. b-c) Photographs of aqueous solution containing Dex-tyramine (Dex-Tyr) conjugates, PEG and PEGylated proteins (b) before and (c) after addition of HRP and $H_2O_2$. d) Photograph and (e) optical microscopic image of Dex-Tyr/PEG hydrogel disks. Scale bars represent 5 mm (d) and 20 μm (e).**

### 4.3.2. Partition behavior of PEGylated proteins in microstructured hydrogels

We examined the partition behavior of proteins in the Dex-PEG two-phase solution. It is known that aqueous solutions of PEG and Dex form two immiscible phases when mixed at an appropriate concentration and temperature [7]. We found that the aqueous mixture of PEG and Dex was separated into an upper PEG-rich phase and a lower Dex-rich phase at 4 °C (Fig. 4-3a). The partition coefficient of a protein was determined as the ratio between the concentration in the PEG-rich and Dex-rich phase. The partition coefficient of IFN-α2a was smaller than 1, indicative of its preferential distribution in the Dex-rich phase. In contrast, PEG-IFN-α2a was partitioned more to the PEG-rich phase as evidenced by the large partition coefficient (7.6 ± 0.9). The presence of a PEG segment on a PEG-IFN-α2a molecule was

responsible for its partition favoring the PEG-rich phase. The observed partition behavior was in agreement with the previous report, in which PEG-modified streptavidin was highly accumulated in the PEG-rich phase within a lipid vesicle [21].

We hypothesized that the PEG domains inside Dex-Tyr/PEG hydrogels would serve as a reservoir for PEGylated proteins by encapsulating these proteins through their preferential partitioning. To test this hypothesis, we utilized FITC-BSA for fluorescent visualization of its partition behavior. As a model PEGylated protein, PEGylated FITC-BSA was prepared by conjugating FITC-BSA with PEG-succinimidyl propionate. FITC-BSA and PEGylated FITC-BSA exhibited preferential partition in the Dex-rich and PEG-rich phase, respectively (Fig. 4-3b). We then investigated the distribution of these proteins within Dex-Tyr/PEG hydrogels by confocal laser scanning microscopy. Green fluorescent FITC-BSA molecules were distributed throughout the crosslinked polymer network of Dex-Tyr/PEG hydrogels (Fig. 4-3c). On the other hand, the hydrogels containing PEGylated FITC-BSA showed intense green fluorescence from the PEG domains (Fig. 4-3d). These results revealed that PEGylated FITC-BSA was highly localized to the PEG domains *via* its preferential partitioning in the PEG-rich phase (Fig. 4-3e). Taken together, the results demonstrated that PEGylated proteins could be stably encapsulated in the reservoir structure of the PEG domains.

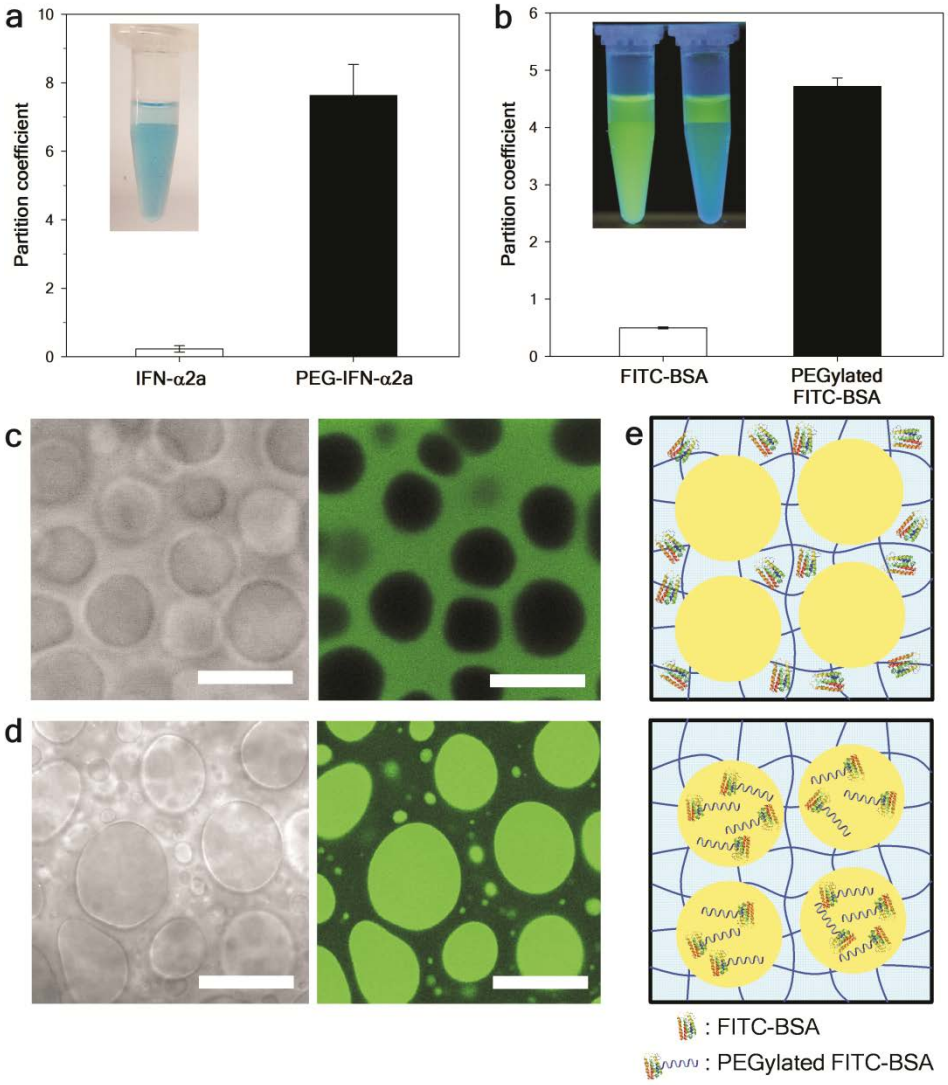


**Fig. 4-3. a) Partition coefficients of IFN-α2a and PEG-IFN-α2a in the Dex-PEG two-phase solution. The lower Dex-rich phase appears blue due to the addition of Blue Dex dyes (inset). b) Partition coefficients of FITC-BSA and PEGylated FITC-BSA in Dex-PEG two-phase solution. The inset shows a fluorescence image of the Dex-PEG two-phase solution containing FITC-BSA (left) and PEGylated FITC-BSA (right) under UV light. The green fluorescence visualizes the location of fluorescently tagged BSA proteins. c-d) Transmitted light (left) and fluorescence (right) images of Dex-Tyr/PEG hydrogels containing (c) FITC-BSA and (d) PEGylated FITC-BSA. Scale bars, 5 μm. e) Schematic illustration of the distribution of FITC-BSA (top) and PEGylated FITC-BSA (bottom) inside Dex-Tyr/PEG hydrogels. The thin blue lines show the crosslinked polymer network of Dex-Tyr/PEG hydrogels. The yellow circles represent PEG domains within the polymer network.**

### 4.3.3. Tunable PEG domain structures of microstructured hydrogels

The gelation kinetics and stiffness of Dex-Tyr/PEG hydrogels were investigated using oscillatory rheology experiments. Fig. 4-4a shows the evolution of the G' of Dex-Tyr/PEG

hydrogels prepared with various concentrations of HRP. When HRP was added at a concentration of 0.13 U/ml, the G' of Dex-Tyr/PEG hydrogels gradually increased and reached a plateau at about 22 min, indicating that the crosslinking reaction has completed. Increasing the concentration of HRP accelerated the rate of the crosslinking reaction, as evident from the shorter time required for G' to reach plateau. Although the gelation rate increased with HRP concentration, the G' at plateau were similar. Moreover, the hydrogels had similar degree of swelling and water content regardless of the HRP concentrations used (Fig. 4-4b). These results revealed that the gelation rates of Dex-Tyr/PEG hydrogels could be regulated by varying the concentration of HRP without affecting their stiffness and swelling properties.

We investigated the domain structures of Dex-Tyr/PEG hydrogels formed at various concentrations of HRP by confocal laser scanning microscopy. Green fluorescent FITC-labelled Dex and red fluorescent PEG-sulforhodamine dyes were used to visualize the Dex hydrogel matrix and PEG domains, respectively. As the HRP concentration increased from 0.13 to 0.21 U/ml, the diameter of PEG domains gradually decreased from 5.1 ± 0.9 to 2.1 ± 0.5 μm (Fig. 4-4c), with a concomitant reduction in the gel point at which crossover between G'' and G' occurs (Fig. 4-4d). The observed relationship suggests that gelation rate plays a crucial role in controlling the size of PEG domains. If gelation is slow, large PEG domains are formed because the PEG-rich droplets were allowed to grow in the continuous Dex-rich phase for a longer period of time until the transition from a liquid to a gel occurs. In contrast, rapid gelation inhibits the growth of the PEG-rich droplets, resulting in the formation of small PEG domains. Therefore, the above results demonstrated that the size of PEG domains could be tuned by HRP concentration.

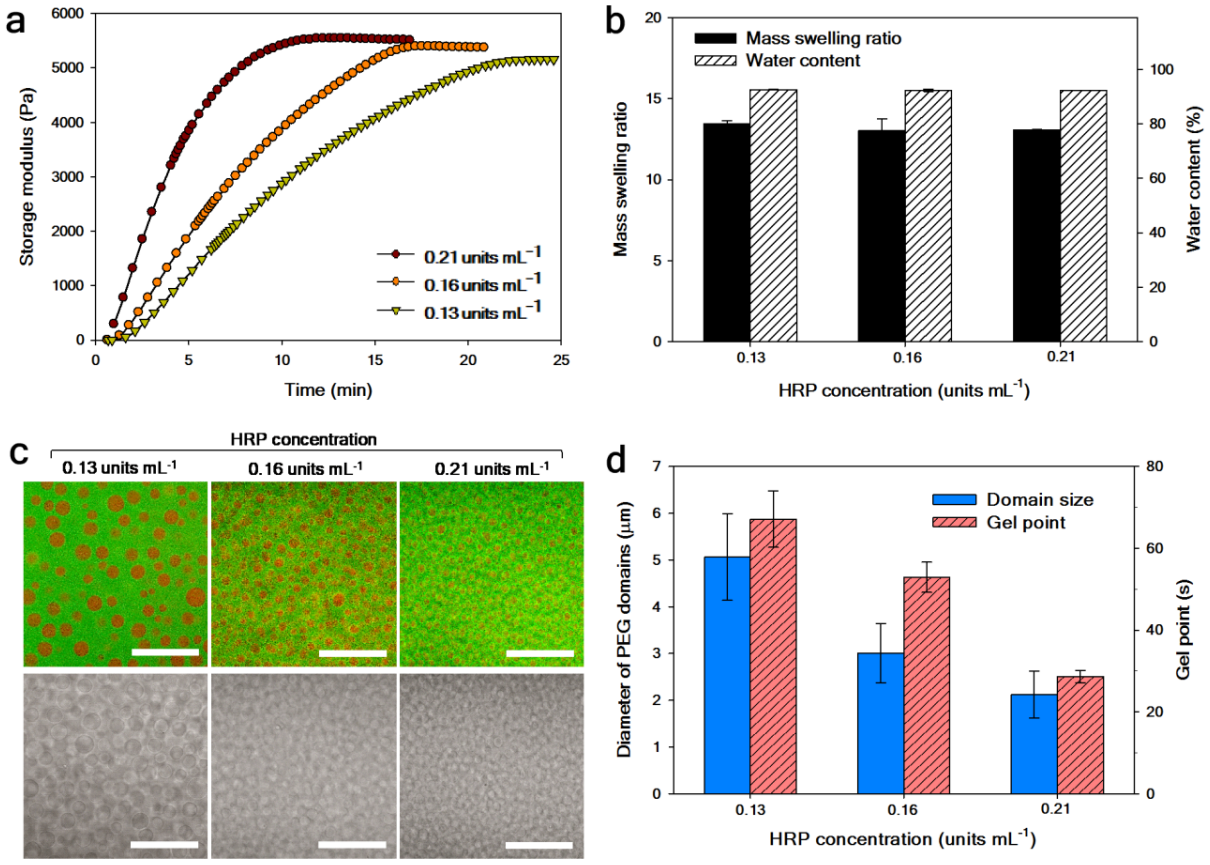


**Fig. 4-4. a) Time course of changes in the storage modulus of Dex-Tyr/PEG hydrogels prepared with various HRP concentrations (0.13, 0.16 and 0.21 U/ml). The final concentration of $H_2O_2$ was 2.42 mM. b) Mass swelling ratio and water content of Dex-Tyr/PEG hydrogels immersed in PBS solution for 7 days. c) Confocal microscopic (top panel) and transmitted light images (bottom panel) of PEG domains in Dex-Tyr/PEG hydrogels formed with various HRP concentrations (0.13, 0.16 or 0.21 U/ml). PEG domains appear red while a hydrogel matrix appears green in the confocal microscopic images. Scale bars, 20 μm. d) Diameters of PEG domains and gel points as a function of HRP concentration.**

### 4.3.4. Burst-free sustained release of PEG-IFN-α2a from microstructured hydrogels

We studied the release kinetics of PEG-IFN-α2a from Dex-Tyr/PEG hydrogels with various domain sizes (ca. 2, 3 and 5 μm). Dex-Tyr hydrogels formed with 1.46 mM of $H_2O_2$ had G' values similar to those of Dex-Tyr/PEG hydrogels, and were used as comparisons. The incorporation of PEG-IFN-α2a had minimal effect on the G' and gel points of these hydrogels. For Dex-Tyr hydrogels, burst release was observed, with around 20% of PEG-IFN-α2a liberated on the first day (Fig. 4-5a). It is known that burst release can be reduced by increasing the crosslink density of hydrogels. Therefore, the crosslink density of Dex-Tyr hydrogels was varied by changing the concentration of $H_2O_2$. As the concentration of $H_2O_2$ was increased from 1.46 to 3.64 mM, the average mesh size of Dex-Tyr hydrogels decreased

from 51.2 ± 3.9 to 37.5 ± 0.7 nm (Table 4-1). Nonetheless, decreasing the mesh size was not effective in suppressing the burst release, as more than 15% of PEG-IFN-α2a was released on the first day (data not shown). In contrast, the amount of PEG-IFN-α2a liberated from Dex-Tyr/PEG hydrogels on the first day was ~2%, suggesting that the preferential partition of PEG-IFN-α2a in PEG domains suppressed the burst release of PEG-IFN-α2a. Moreover, Dex-Tyr/PEG hydrogels with 2 and 3 μm domains released PEG-IFN-α2a in a sustained manner for 3 months (Fig. 4-5a). The observed sustained release can be explained by the repeated partitioning of PEG-IFN-α2a in the PEG domains (Fig. 4-5b). When a PEG-IFN-α2a molecule is released from a PEG domain into the Dex-rich phase, it diffuses into another PEG domain and become partitioned there. The process is repeated until the PEG-IFN-α2a molecule finally reaches the edge of the hydrogel and escapes from gel matrix. As a result, the release of PEG-IFN-α2a from Dex-Tyr/PEG hydrogels is retarded. In contrast, PEG-IFN-α2a molecules in Dex-Tyr hydrogels do not undergo repeated partitioning, and were released quickly from the gel matrix.

**Table. 4-1.** Physical properties of Dex-Tyr and Dex-Tyr/PEG hydrogels.

| **Hydrogel** | **HRP (units/ml)** | **$H_2O_2$ (mM)** | **Q**[a] | **$\nu_e$ ($10^{-6}$ mol/cm$^3$)** | **$\xi$ (nm)** |
|---|---|---|---|---|---|
| Dex-Tyr | 0.21 | 1.02 | 31.7 ± 0.4 | 4.7 ± 0.1 | 61.9 ± 1.0 |
| Dex-Tyr | 0.21 | 1.46 | 27.0 ± 1.7 | 6.2 ± 0.7 | 51.2 ± 3.9 |
| Dex-Tyr | 0.21 | 1.83 | 26.2 ± 0.08 | 6.5 ± 0.03 | 49.4 ± 0.2 |
| Dex-Tyr | 0.21 | 3.64 | 20.6 ± 0.3 | 9.7 ± 0.2 | 37.5 ± 0.7 |
| Dex-Tyr/PEG | 0.13 | 2.42 | 29.3 ± 0.4 | 5.4 ± 0.1 | 56.4 ± 0.9 |
| Dex-Tyr/PEG | 0.16 | 2.42 | 28.0 ± 0.8 | 5.8 ± 0.3 | 53.3 ± 1.8 |
| Dex-Tyr/PEG | 0.21 | 2.42 | 27.1 ± 0.2 | 6.1 ± 0.1 | 51.5 ± 0.5 |

[a]The volumetric swelling ratio (Q), effective crosslink density ($\nu_e$) and average mesh size ($\xi$) of Dex-Tyr and Dex-Tyr/PEG hydrogels are shown. The average mesh size represents the linear distance between two adjacent crosslinks in the hydrogel network. Error bars: SD, n = 3.

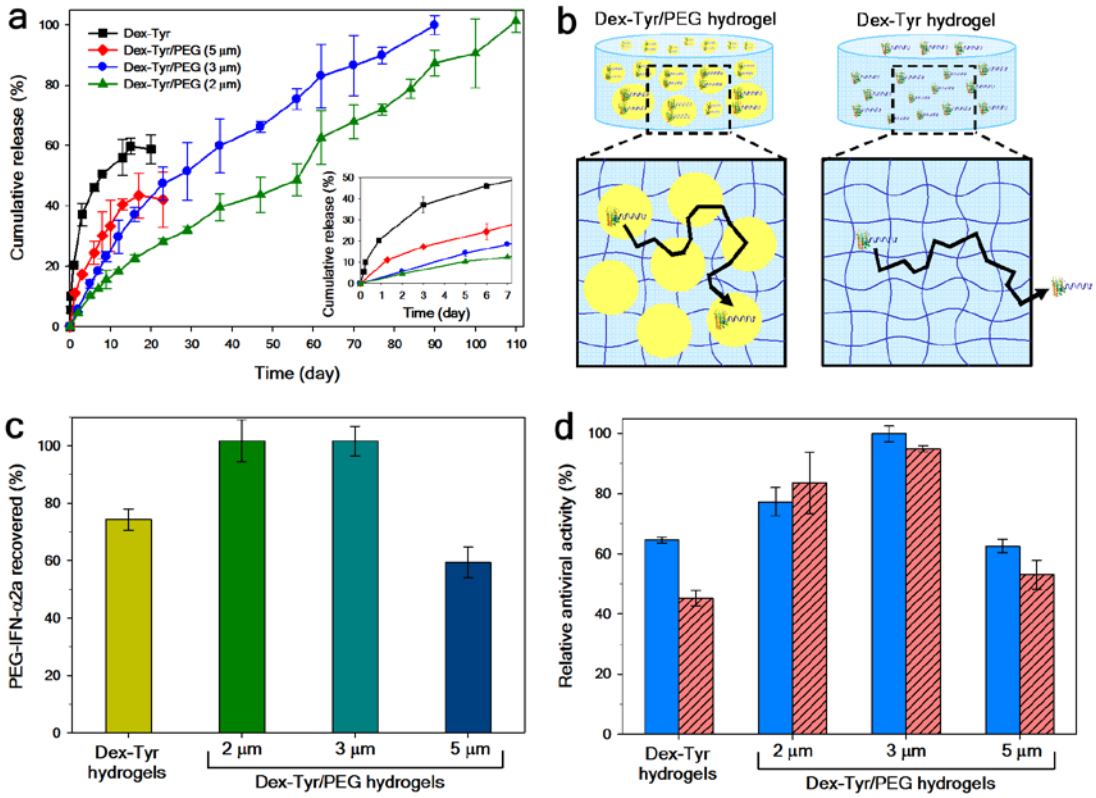


**Fig. 4-5. a) Cumulative release of PEG-IFN-α2a from Dex-Tyr hydrogels or Dex-Tyr/PEG hydrogels with various domain sizes (ca. 2, 3 or 5 μm). Dex-Tyr hydrogels and Dex-Tyr/PEG hydrogels with 5 μm domains discontinued protein release after 15 and 17 days, respectively. The inset shows protein release profiles of hydrogels for 7 days. b) A proposed model for explaining the sustained release of PEG-IFN-α2a from Dex-Tyr/PEG hydrogels. The thin blue lines show the crosslinked polymer network of Dex-Tyr/PEG hydrogels (left) and Dex-Tyr hydrogels (right). The yellow circles represent PEG domains within the polymer network. The thick black lines show hypothetical trajectories of a PEG-IFN-α2a molecule in those hydrogels at a given time. c) Percent recovery of PEG-IFN-α2a after enzymatic degradation of hydrogels. d) The relative antiviral activity of PEG-IFN-α2a retrieved from hydrogels (solid bars) and the release medium collected for 2 weeks (striped bars).**

To understand the mechanism of protein release, we determined the diffusional exponent (n) by fitting the experimental release data to the Ritger-Peppas equation [16]. The Ritger-Peppas equation relates the fractional release of drug, $M_t/M_\infty$, to the release time, t, in an exponential expression. The diffusional exponent, n, is indicative of the transport mechanism. Fickian diffusion is defined by n equal to 0.5 and non-Fickian by n greater than 0.5 [22]. The n values for Dex-Tyr hydrogels were approximately 0.5, indicating that the protein release was governed by Fickian diffusion (Table 4-2). This implies that PEG-IFN-α2a molecules would diffuse freely within the hydrogel network. Variation of the crosslink density did not affect the protein release mechanism presumably because the average mesh size of Dex-Tyr hydrogels was much larger than the hydrodynamic radius of a PEG-IFN-α protein (7.94 nm)

[23]. On the other hand, the n values for Dex-Tyr/PEG hydrogels were in the range between 0.5 and 1. This result revealed that Dex-Tyr/PEG hydrogels exhibited non-Fickian, anomalous diffusion of PEG-IFN-α2a molecules. Notably, the average mesh size of these hydrogels (51.5 ± 0.5 to 56.4 ± 0.9 nm) was comparable to that of Dex-Tyr hydrogels (Table 4-1). The observed deviation from the Fickian diffusion behavior was attributed to the increased diffusional hindrance caused by repeated partitioning of PEG-IFN-α2a in the Dex-Tyr/PEG hydrogels. It is also noteworthy that Dex-Tyr/PEG hydrogels with 2 μm domains exhibited slower protein release than those with 3 μm domains. As PEG domains became smaller, the number of the domains in a given volume increased (Fig. 5-3c). The higher number of PEG domains might contribute to the delayed release by increasing the probability of PEG-IFN-α2a moving between neighboring PEG domains.

**Table 4-2.** Evaluation of the mechanism of protein release from hydrogels.

| Hydrogel | HRP (units/ml) | $H_2O_2$ (mM) | $k$ [a] | $R^2$ | $n$ | Protein release mechanism |
|---|---|---|---|---|---|---|
| Dex-Tyr | 0.21 | 1.02 | 0.232 ± 0.019 | 0.943 ± 0.012 | 0.495 ± 0.010 | Fickian diffusion |
| Dex-Tyr | 0.21 | 1.46 | 0.188 ± 0.014 | 0.966 ± 0.010 | 0.493 ± 0.023 | Fickian diffusion |
| Dex-Tyr | 0.21 | 1.83 | 0.173 ± 0.002 | 0.969 ± 0.002 | 0.498 ± 0.021 | Fickian diffusion |
| Dex-Tyr | 0.21 | 3.64 | 0.132 ± 0.001 | 0.971 ± 0.016 | 0.507 ± 0.023 | Fickian diffusion |
| Dex-Tyr/PEG | 0.13 | 2.42 | 0.092 ± 0.003 | 0.977 ± 0.023 | 0.561 ± 0.011 | Non-Fickian transport |
| Dex-Tyr/PEG | 0.16 | 2.42 | 0.033 ± 0.001 | 0.986 ± 0.011 | 0.875 ± 0.005 | Non-Fickian transport |
| Dex-Tyr/PEG | 0.21 | 2.42 | 0.026 ± 0.003 | 0.990 ± 0.003 | 0.792 ± 0.049 | Non-Fickian transport |

[a]The proportionality constant ($k$), diffusional exponent ($n$), correlation coefficient ($R^2$) and corresponding release mechanism were analyzed by fitting the experimental release data to the Ritger-Peppas equation. Error bars: SD, n = 3.

It was observed that Dex-Tyr hydrogels released approximately 60% of their payloads in 15 days and then the release discontinued (Fig. 4-5a). To find the reason for the incomplete release, we retrieved PEG-IFN-α2a from freshly prepared Dex-Tyr hydrogels by degrading them in dextranase solution. Only 74% of the loaded proteins were recovered from these hydrogels (Fig. 4-5c), suggesting that the incomplete release was mainly caused by denaturation of PEG-IFN-α2a in the gel-forming process. It was reported previously that protein drugs might be susceptible to denaturation under the chemical stresses produced during encapsulation in hydrogels [24]. Notably, Dex-Tyr/PEG hydrogels with 2 and 3 μm domains liberated 100% of their payloads after enzymatic degradation. This result revealed

that PEG-IFN-α2a entrapped in the PEG domains was less susceptible to the chemical denaturation. This phenomenon was in agreement with literature describing the stabilizing effects of ATPS on the structure and bioactivity of the partitioned proteins [25]. Such protective effect of the PEG domains was responsible for the complete release of PEG-IFN-α2a from Dex-Tyr/PEG hydrogels with 2 and 3 μm domains. On the other hand, incomplete protein release was observed from Dex-Tyr/PEG hydrogels with 5 μm domains. Since these hydrogels were formed at a lower concentration of HRP as compared to those with 2 and 3 μm domains, the rate of $H_2O_2$ decomposition would be slower [8, 19]. The delayed decomposition of $H_2O_2$ likely contributed to the denaturation of PEG-IFN-α2a in the Dex-Tyr/PEG hydrogels with 5 μm domains.

The bioactivity of PEG-IFN-α2a was evaluated by measuring its inhibitory effects on the replication of HCV RNAs in human hepatoma cells [13]. PEG-IFN-α2a incorporated in Dex-Tyr hydrogels maintained only 65% of the original bioactivity (Fig. 4-5d). This proved that PEG-IFN-α2a was partially denatured during encapsulation in Dex-Tyr hydrogels. Its antiviral activity further dropped to ~45% after 2 weeks of release. However, denaturation of PEG-IFN-α2a was inhibited when incorporated in Dex-Tyr/PEG hydrogels with 2 and 3 μm domains. Particularly, Dex-Tyr/PEG hydrogels with 3 μm domains encapsulated PEG-IFN-α2a without compromising its bioactivity. Around 95% of antiviral activity was retained even after 2 weeks. Such protective effects of PEG domains were not observed for Dex-Tyr/PEG hydrogels with 5 μm domains, likely because the delayed decomposition of $H_2O_2$ caused protein denaturation [8]. Dex-Tyr/PEG hydrogels with 3 μm domains were chosen for *in vivo* experiments because these hydrogels enabled sustained release of PEG-IFN-α2a while preserving its bioactivity.

### 4.3.5. *In vivo* performance of microstructured hydrogels in humanized mice

We conducted pharmacokinetics and biocompatibility studies in humanized mice. These mice were established by adoptive transfer of human CD34+ fetal liver cells into NOD-scid Il2rg-/- mice [17]. Such humanized mice with a functional human immune system allow assessment of the efficacy and safety of human therapeutic proteins in a physiologically relevant manner [26, 27]. Following subcutaneous (s.c.) injection of PEG-IFN-α2a solution, its plasma concentration reached a peak within 1 day and declined to undetectable levels after 2 weeks (Fig. 4-6a). The mice implanted with Dex-Tyr hydrogels showed a similar trend, suggesting that PEG-IFN-α2a were released quickly from Dex-Tyr hydrogels and cleared

from the bloodstream. In contrast, a one-time administration of Dex-Tyr/PEG hydrogels resulted in prolonged circulation of PEG-IFN-α2a for 7 weeks. Furthermore, these hydrogels significantly increased the plasma half-life of PEG-IFN-α2a from 1.5 ± 0.2 to 15.6 ± 1.4 days (Fig. 4-6b). Therefore, these results demonstrated that Dex-Tyr/PEG hydrogels enabled continuous release of the encapsulated PEG-IFN-α2a *in vivo*.

Such sustained release formulations can improve therapeutic outcomes of PEG-IFN-α2a by maintaining its plasma concentration at therapeutically effective levels over an extended period of time [28]. These formulations can also improve patient compliance by reducing the frequency of injections and minimizing the risk of an adverse drug reaction. A substantial portion of patients receiving PEG-IFN-α2a experience harmful side effects, including flu-like symptoms, fatigue, depression and cytopenia, which necessitate dose reductions or early discontinuation of therapy [29]. In general, occurrence of such side effects is correlated with the maximum plasma concentration ($C_{max}$). Dex-Tyr/PEG hydrogels exhibited remarkably lower $C_{max}$ (44.3 ± 13.3 ng/ml) compared to PEG-IFN-α2a solution (474.0 ± 10.7 ng/ml). These hydrogels have the potential to reduce the side effects of PEG-IFN-α2a by lowering $C_{max}$ below its maximum tolerable concentration. Indeed, PEG-IFN-α2a released from Dex-Tyr/PEG hydrogels did not cause severe cytopenia and other hematological abnormalities in humanized mice (data not shown).

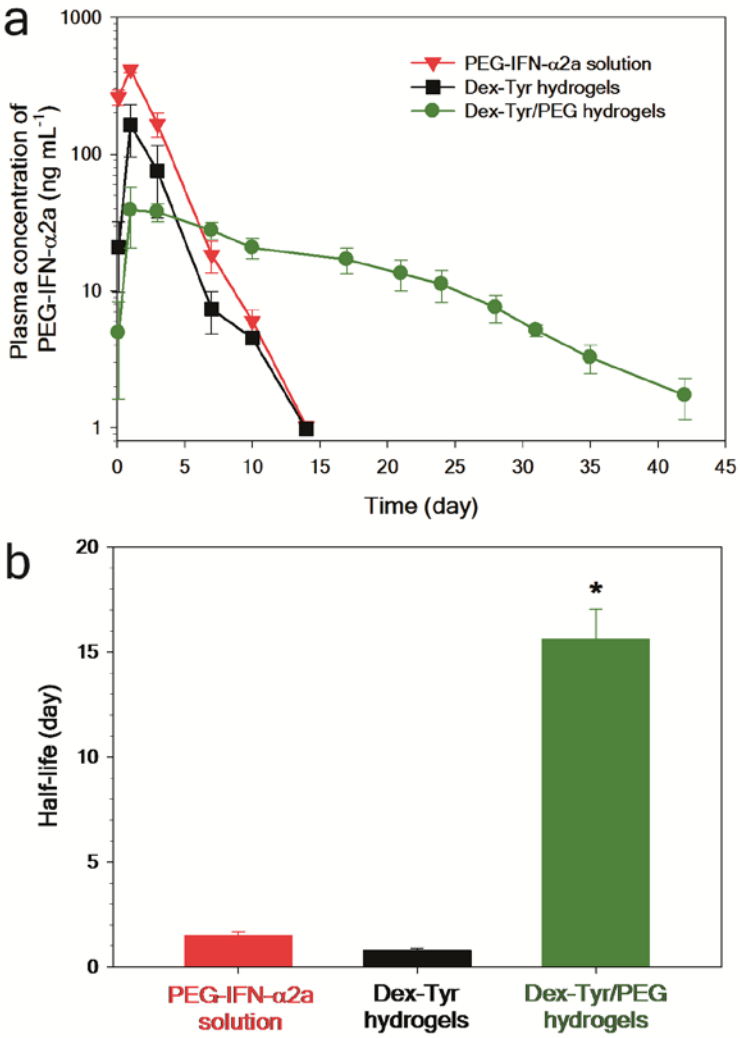


**Fig. 4-6. Pharmacokinetics of PEG-IFN-α2a in humanized mice. a) Plasma concentration-time profiles following subcutaneous administration of PEG-IFN-α2a solution, Dex-Tyr hydrogels or Dex-Tyr/PEG hydrogels with 3 μm domains. b) Plasma half-life of PEG-IFN-α2a determined from pharmacokinetics analysis. Results are presented as means ± SD (n = 3). *$p$ < 0.005 versus PEG-IFN-α2a alone and Dex-Tyr hydrogels.**

### 4.3.6. Therapeutic efficacy of microstructured hydrogels delivering PEG-IFN-α2a in HCV-infected humanized mice

We evaluated therapeutic effects of PEG-IFN-α2a-loaded Dex-Tyr/PEG hydrogels in a humanized mouse model of hepatitis C. The humanized mice infected with HCV were randomly divided into 5 groups and then treated for 8 weeks with various formulations consisting of: a one-time s.c. injection of PBS as untreated control, a one-time s.c. injection (240 μg/kg), 2 doses of monthly s.c. injections (2 × 120 μg/kg) or 8 doses of weekly s.c. injections (8 × 30 μg/kg) of PEG-IFN-α2a solution, and a one-time s.c. implantation of PEG-

IFN-α2a-loaded Dex-Tyr/PEG hydrogels (240 μg/kg). The total dose of PEG-IFN-α2a was fixed to 240 μg/kg for all formulations.

HCV infection induced severe liver inflammation and fibrosis (Fig. 4-7a and b), characterized by massive infiltration of leukocytes and collagen deposition compared to uninfected mice. After 8 weeks of treatment, weekly injections of PEG-IFN-α2a solution effectively prevented HCV-induced liver damage. In contrast, a one-time injection and monthly injections of PEG-IFN-α2a solution were less effective. This indicates that frequent injections are required to sustain the therapeutic effect of PEG-IFN-α2a for the effective treatment of hepatitis C. Importantly, a one-time administration of PEG-IFN-α2a-loaded Dex-Tyr/PEG hydrogels exhibited therapeutic effects comparable to the weekly injection formulation of PEG-IFN-α2a (i.e., 8-times repeated injection). We analyzed serum levels of alanine aminotransferase (ALT) and interferon-gamma (IFN-γ) to assess the extent of liver damage and pro-inflammatory immune responses, respectively [29]. Consistent with histological results, HCV-infected mice had elevated levels of serum ALT and IFN-γ, indicating that these mice had HCV-induced liver injury and inflammation (Fig. 4-7c and d). As expected, the serum levels of ALT and IFN-γ gradually decreased as the frequency of PEG-IFN-α2a injections increased. We found that the mice treated with 8-times repeated injection of PEG-IFN-α2a solution achieved normal ALT and IFN-γ levels. Impressively, a one-time administration of PEG-IFN-α2a-loaded Dex-Tyr/PEG hydrogels effectively normalized the serum levels of ALT and IFN-γ. The above results revealed that the sustained delivery of PEG-IFN-α2a using Dex-Tyr/PEG hydrogels significantly enhanced its therapeutic efficacy by prolonging the circulation half-life and duration of action. Consequently, our study demonstrated that Dex-Tyr/PEG hydrogels enabled the long-term sustained release of the incorporated PEG-IFN-α2a *in vivo*, resulting in the effective treatment of HCV-induced liver injury. Such sustained release formulations would be advantageous for improving patient convenience and compliance for hepatitis C therapy. The microstructured hydrogel system described here would have broad applicability for *in vivo* delivery of PEGylated protein drugs for more effective and safer treatments of diverse chronic diseases.

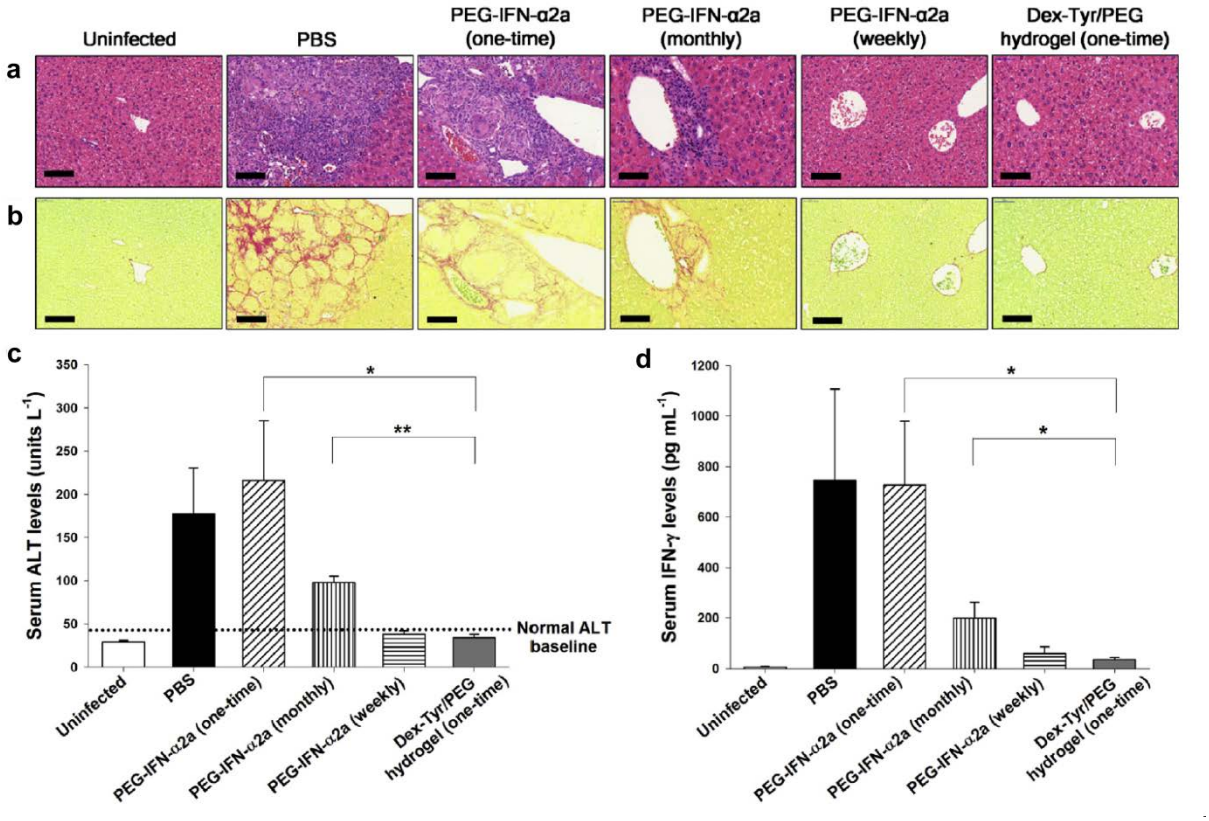


**Fig. 4-7. Therapeutic effects of PEG-IFN-α2a-loaded microstructured hydrogels in a humanized mouse model of hepatitis C. (a) H&E and (b) Sirius Red stained liver sections from uninfected humanized mice and HCV-infected humanized mice treated with PBS, PEG-IFN-α2a (a one-time, monthly or weekly subcutaneous injection) or Dex-Tyr/PEG hydrogels (a one-time subcutaneous implantation). Scale bars, 100 mm. Serum levels of (c) ALT and (d) IFN-γ in humanized mice with treatments. Results are presented as mean ± SEM (n = 5). Significance levels were set at: *$p < 0.05$ and **$p < 0.005$.**

## 4.4. Conclusions

In this chapter, a Dex-Tyr hydrogel containing PEG microdomains was designed for the sustained release of PEG-IFN-α2a. The PEG microdomains served as a reservoir for PEG-IFN-α2a *via* the preferential partition of the proteins in the PEG phase. It was demonstrated that the presence of PEG microdomains not only suppressed the burst release of PEG-IFN-α2a from hydrogels, but also enabled the sustained release of PEG-IFN-α2a for over 3 months without loss of biological activity. Moreover, the release rates of PEG-IFN-α2a could be modulated simply by tuning the size of PEG domains through variation in the gelation rate. The microstructured hydrogel system is a useful platform for the delivery of other PEGylated pharmaceuticals for the treatments of various chronic diseases.

## References

[1] Harris JM, Chess RB. Effect of pegylation on pharmaceuticals. Nat. Rev. Drug Discov. 2003;2:214-21.

[2] Tsutsumi Y, Onda M, Nagata S, Lee B, Kreitman RJ, Pastan I. Site-specific chemical modification with polyethylene glycol of recombinant immunotoxin anti-Tac(Fv)-PE38 (LMB-2) improves antitumor activity and reduces animal toxicity and immunogenicity. Proc. Natl. Acad. Sci. U. S. A. 2000;97:8548-53.

[3] Knop K, Hoogenboom R, Fischer D, Schubert US. Poly(ethylene glycol) in Drug Delivery: Pros and Cons as Well as Potential Alternatives. Angew. Chem. 2010;49:6288-308.

[4] Patil NS, Dordick JS, Rethwisch DG. Macroporous poly(sucrose acrylate) hydrogel for controlled release of macromolecules. Biomaterials 1996;17:2343-50.

[5] Kim SS, Choi YH, Han CW, Choi YD, Park Y, Lee JJ, Kim HJ, Lee IK, Lee JS, et al. DNA Methylation Profiles of MGMT, DAPK1, hMLH1, CDH1, SHP1, and HIC1 in B-Cell Lymphomas. J. Pathol. Transl. Med. 2009;43:420-7.

[6] Van Tomme SR, Hennink WE. Biodegradable dextran hydrogels for protein delivery applications. Expert Rev. Med. Devices 2007;4:147-64.

[7] Albertsson P-Å. Partition of Cell Particles and Macromolecules in Polymer Two-Phase Systems. Adv. Protein Chem. 1970;24:309-41.

[8] Jin R, Hiemstra C, Zhong Z, Feijen J. Enzyme-mediated fast in situ formation of hydrogels from dextran-tyramine conjugates. Biomaterials 2007;28:2791-800.

[9] Leach JB, Bivens KA, Patrick CW, Schmidt CE. Photocrosslinked hyaluronic acid hydrogels: Natural, biodegradable tissue engineering scaffolds. Biotechnol. Bioeng. 2003;82:578-89.

[10] Lin C-C, Metters AT. Hydrogels in controlled release formulations: Network design and mathematical modeling. Adv. Drug Del. Rev. 2006;58:1379-408.

[11] Lee F, Chung JE, Kurisawa M. An injectable hyaluronic acid-tyramine hydrogel system for protein delivery. J. Control. Release 2009;134:186-93.

[12] Hayashi Y, Milton Harris J, Hoffman AS. Delivery of PEGylated drugs from mucoadhesive formulations by pH-induced disruption of H-bonded complexes of PEG-drug with poly(acrylic acid). React. Funct. Polym. 2007;67:1330-7.

[13] Vrolijk JM, Kaul A, Hansen BE, Lohmann V, Haagmans BL, Schalm SW, Bartenschlager R. A replicon-based bioassay for the measurement of interferons in patients with chronic hepatitis C. J. Virol. Methods 2003;110:201-9.

[14] Xu KM, Lee F, Gao SJ, Chung JE, Yano H, Kurisawa M. Injectable hyaluronic acid-tyramine hydrogels incorporating interferon-alpha 2a for liver cancer therapy. J. Control. Release 2013;166:203-10.

[15] Kajjari PB, Manjeshwar LS, Aminabhavi TM. Novel blend microspheres of cellulose triacetate and bee wax for the controlled release of nateglinide. J. Ind. Eng. Chem. 2014;20:397-404.

[16] Peppas NA, Bures P, Leobandung W, Ichikawa H. Hydrogels in pharmaceutical formulations. Eur. J. Pharm. Biopharm. 2000;50:27-46.

[17] Chen Q, Khoury M, Limmon G, Choolani M, Chan JK, Chen J. Human fetal hepatic progenitor cells are distinct from, but closely related to, hematopoietic stem/progenitor cells. Stem Cells 2013;31:1160-9.

[18] Zhang Y, Huo M, Zhou J, Xie S. PKSolver: An add-in program for pharmacokinetic and pharmacodynamic data analysis in Microsoft Excel. Comput. Methods Programs Biomed. 2010;99:306-14.

[19] Kurisawa M, Chung JE, Yang YY, Gao SJ, Uyama H. Injectable biodegradable hydrogels composed of hyaluronic acid-tyramine conjugates for drug delivery and tissue engineering. Chem. Commun. (Camb.) 2005:4312-4.

[20] Moriyama K, Yui N. Regulated insulin release from biodegradable dextran hydrogels containing poly(ethylene glycol). J. Control. Release 1996;42:237-48.

[21] Long MS, Jones CD, Helfrich MR, Mangeney-Slavin LK, Keating CD. Dynamic microcompartmentation in synthetic cells. Proc. Natl. Acad. Sci. U. S. A. 2005;102:5920-5.

[22] Ritger PL, Peppas NA. A simple equation for description of solute release I. Fickian and non-fickian release from non-swellable devices in the form of slabs, spheres, cylinders or discs. J. Control. Release 1987;5:23-36.

[23] Grace MJ, Lee S, Bradshaw S, Chapman J, Spond J, Cox S, Delorenzo M, Brassard D, Wylie D, et al. Site of pegylation and polyethylene glycol molecule size attenuate interferon-alpha antiviral and antiproliferative activities through the JAK/STAT signaling pathway. J. Biol. Chem. 2005;280:6327-36.

[24] Vermonden T, Censi R, Hennink WE. Hydrogels for protein delivery. Chem. Rev. 2012;112:2853-88.

[25] Moriyama K, Ooya T, Yui N. Hyaluronic acid grafted with poly(ethylene glycol) as a novel peptide formulation. J. Control. Release 1999;59:77-86.

[26] Shultz LD, Ishikawa F, Greiner DL. Humanized mice in translational biomedical research. Nat. Rev. Immunol. 2007;7:118-30.

[27] Drake AC, Chen Q, Chen J. Engineering humanized mice for improved hematopoietic reconstitution. Cell. Mol. Immunol. 2012;9:215-24.

[28] Kim S, Kim JH, Jeon O, Kwon IC, Park K. Engineered polymers for advanced drug delivery. Eur. J. Pharm. Biopharm. 2009;71:420-30.

[29] Heathcote EJ, Shiffman ML, Cooksley WG, Dusheiko GM, Lee SS, Balart L, Reindollar R, Reddy RK, Wright TL, et al. Peginterferon alfa-2a in patients with chronic hepatitis C and cirrhosis. N. Engl. J. Med. 2000;343:1673-80.

# Chapter 5

# Formation and Stability of Interpenetrating Polymer Network Hydrogels Consist of Fibrin and Hyaluronic Acid-Tyramine Conjugate for Tissue Engineering

## 5.1. Introduction

Hydrogels have been widely used as a scaffold material in tissue engineering [1]. Among the many different hydrogel systems, fibrin gels are one of the most widely used because they support cell adhesion, proliferation, stem cell differentiation and, importantly, capillary formation (angiogenesis) [2-4]. Fibrin gels are degradable by proteases such as plasmin and matrix matelloproteinases (MMPs), permitting scaffold remodeling, and eventually, resorption by the body. Moreover, fibrinogen, the building block of fibrin gel, can be isolated from a patient's own blood, making possible to form an autologous scaffold. However, the poor mechanical properties of fibrin gels render them susceptible to contraction/compaction by cells and rapid degradation by proteases. Consequently, cell-seeded fibrin gels often shrink during *in vitro* culture [5-7] and/or degrade prematurely prior to or soon after transplantation [8, 9]. These drawbacks limit the use of fibrin gels for tissue engineering applications which require specific shape.

Several strategies have been implemented to improve the mechanical properties of fibrin gels. The most straightforward approach involves optimization of the polymerization conditions, such as pH, ionic strength, and the calcium, fibrinogen and thrombin concentrations [10, 11]. Variations in these parameters alter the fibrin fiber thickness, resulting in gels with different pore sizes and mechanical strengths. Composite materials consisting of a porous scaffold filled with fibrin gel have also been developed to achieve mechanical stability [12-15]. Porous scaffolds, typically made from synthetic polymers such as polylactic acid (PLA), poly(lactic-co-glycolic acid) (PLGA) and polycaprolactone (PCL), provide structural support, while the fibrin gel acts as a cell carrier promoting cell adhesion and growth. Alternatively, fibrinolytic inhibitors, such as aprotinin [9, 16], $\varepsilon$-aminocaproic acid [17] and tranexamic acid [18], have been utilized to stabilize fibrin by reducing the rate of proteolytic degradation. The inhibitors are supplemented in culture medium, incorporated into the fibrin gel during polymerization or, in the case of aprotinin, conjugated directly onto the fibrin gel. While fibrinolytic inhibitors can lower the rate of degradation, they do not prevent cell-induced contraction of fibrin gels. Furthermore, the use of aprotinin *in vivo* has been associated with an increased risk of complications [18].

Recently interpenetrating polymer network (IPN) hydrogels consisting of fibrin and a synthetic or natural polymer network have been developed for tissue engineering and three-dimensional (3-D) cell culture. IPNs are made of two or more polymer networks that are at

least partially interlaced on the molecular scale but without covalent bonds with each other which cannot be separated unless chemical bonds are broken [19]. Studies on IPN hydrogels composed of fibrin and poly(ethylene glycol) have demonstrated improved mechanical properties while maintaining cell growth [20]. Another study reported a fibrin-alginate IPN as a dynamic matrix for the growth of ovarian follicle cells [21]. The fibrin phase was degraded over time to facilitate follicle growth, while the alginate phase remained to provide structural support. The follicles cultured in IPN were shown to be more meiotically competent than in alginate alone.

In this chapter, IPN hydrogels composed of fibrin and hyaluronic acid (HA) for tissue engineering applications are described. As described in Chapter 1, HA is a non-sulfated glycosaminoglycan found primarily in the extracellular matrix (ECM) and HA hydrogels have been widely used as tissue engineering scaffolds due to their low-immunogenic and biodegradable properties, as well as their versatility in chemical modification [22-24]. HA also plays important roles during the process of wound healing; an increase in HA concentration in the milieu of a fibrin clot during wound healing is hypothesized to stabilize the volume and physical structure of the fibrin gel [25]. Moreover, it was previously demonstrated that contraction of collagen gels by fibroblasts could be inhibited by introducing crosslinked HA into the collagen gel [26]. While HA has previously been incorporated within fibrin gels as a natural ECM component [27-29], its potential to stabilize the shape of fibrin through the formation of a crosslinked network has not been explored. We proposed that the formation of a fibrin-HA IPN hydrogel, with the HA network being chemically crosslinked, would result in a mechanically superior scaffold compared with fibrin gels alone. The HA network is expected to provide structural reinforcement, while the fibrin network promotes cell adhesion and proliferation, as well as capillary tube formation (Fig. 5-1). To this end we utilized the hyaluronic acid-tyramine (HA-Tyr) hydrogel system to form the HA network [30]. The formation of IPN hydrogels was characterized by rheological measurement and the storage modulus (G') was tuned using the concentration of $H_2O_2$. The structure of the fibrin network in the IPN hydrogels was determined by turbidity measurement and confocal laser scanning microscopy. The ability of IPN hydrogels with different G' to maintain the shape of the scaffold in the presence of plasmin and cells was examined. In addition, the effects of IPN hydrogel rigidity on viability, spreading, and proliferation of cells embedded within the IPNs, as well as capillary tube formation, were examined.

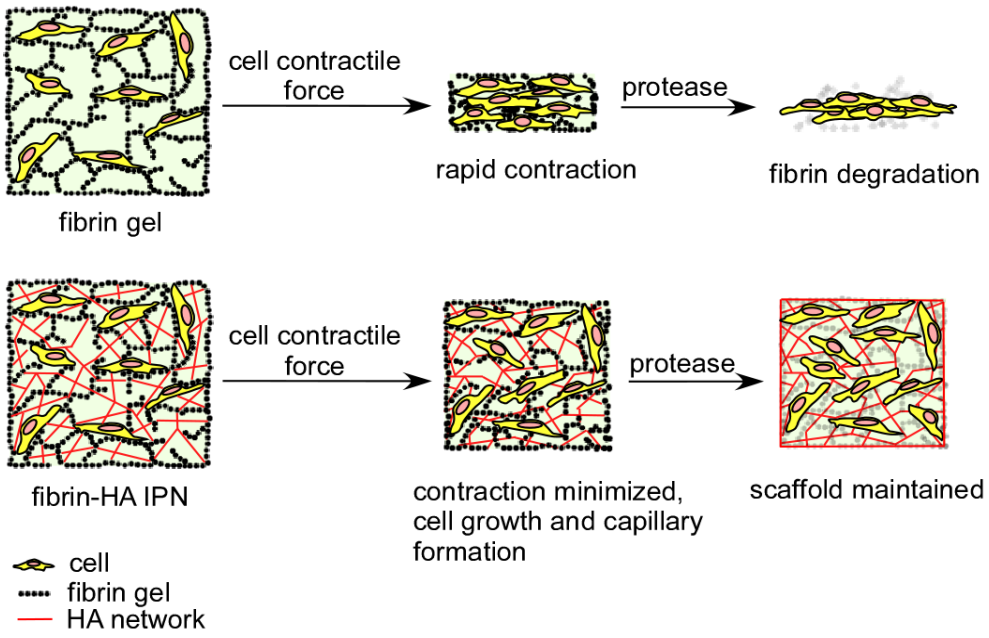


**Fig. 5-15. Fibrin gel loses its shape in the presence of cells and proteases. Fibrin-HA IPN hydrogel maintains the structure while allowing cell proliferation and capillary formation.**

## 5.2. Material and methods

### 5.2.1. Materials

Fibrinogen from bovine plasma (76.5% protein, of which 91.2% was clottable), thrombin from bovine plasma (59 NIH U/mg solid), bovine serum albumin (BSA), hydrogen peroxide ($H_2O_2$), propidium iodide, hyaluronidase from bovine testes, papain from *Papaya* latex, ethylene diamine tetraacetic acid (EDTA), L-cysteine and paraformaldehyde were all purchased from Sigma–Aldrich (Singapore). HRP (190 U/mg) was purchased from Wako Pure Chemical Industries. Sodium hyaluronate (MW 90 kDa) was kindly donated by JNC Corp. (Tokyo, Japan). Alexa Fluor 488 succinimidyl ester, fetal bovine serum (FBS), penicillin/streptomycin, calcein AM and Quant-iT™ PicoGreen® dsDNA reagent were purchased from Life Technologies (Singapore). PD-10 desalting columns and Cytodex 3 microcarriers were purchased from GE Healthcare Pte Ltd. (Singapore). Bicinchoninic acid (BCA) protein assay kits were purchased from Pierce. Mouse monoclonal primary antibody to CD31 (JC/70A) and goat F(ab′)2 polyclonal secondary antibody to mouse IgG-Fc (FITC-conjugated) were purchased from Abcam (UK). Dulbecco's modified Eagle's medium (DMEM), trypsin and phosphate-buffered saline (PBS) (150 mM, pH 7.3) were supplied by Biopolis Media Prep (Singapore).

### 5.2.2. Synthesis of HA-Tyr conjugates

HA-Tyr conjugates were synthesized as described in Chapter 2 [31] and the DS (the number of tyramine molecules per 100 repeating units of HA) was 6 as determined by $^{1}H$ NMR.

### 5.2.3. Preparation of fibrin gels and fibrin-HA-Tyr IPN hydrogels

Thrombin was prepared at a stock concentration of 100 NIH U/ml in PBS containing 0.1% (w/v) BSA. HRP was prepared at a stock concentration of 25 U/ml in PBS. Stock fibrinogen solution was prepared by dissolving 39 mg/ml in PBS. HA-Tyr conjugates were dissolved at 27.5 mg/ml in PBS. All stock solutions were sterile filtered, stored at −80 °C and used within 2 weeks. To prepare 1 ml of fibrin gel, stock fibrinogen solution was first diluted to 3.6 or 7.2 mg/ml with PBS. Three hundred and three μl of thrombin at 1.02 NIH U/ml was added to 697 μl of diluted fibrinogen solution. The final concentrations of fibrinogen and thrombin were 2.5 or 5 mg/ml and 0.31 NIH U/ml, respectively. To form 1 ml of IPN hydrogels fibrinogens and HA-Tyr conjugates were mixed together at a final concentration of 3.6 mg/ml each. Eight μl of $H_2O_2$ of various concentrations was added to 689 μl of the fibrinogen–HA-Tyr mixture, followed by 303 μl of a solution containing thrombin and HRP at 1.02 and 0.53 U/ml, respectively. The final fibrinogen and HA-Tyr concentrations were 2.5 mg/ml each and the thrombin and HRP concentrations were 0.31 and 0.16 U/ml, respectively. Both the fibrin gels and the IPN hydrogels were allowed to form for 1 h at 37 °C.

### 5.2.4. Rheological characterization

Rheological measurements were performed with a HAAKE Rheoscope 1 rheometer (Karlsruhe, Germany) as described in Chapter 2 using a cone and plate geometry of 3.5 cm diameter and 1.029 cone angle. The measurements were taken at 37 °C in dynamic oscillatory mode with a constant deformation of 0.5% and a frequency of 0.1 Hz. Fibrin gels and IPN hydrogels were prepared as described above. Immediately after adding thrombin and HRP, 210 μl of the mixture was transferred to the bottom plate. The upper cone was then lowered to a measurement gap of 0.03 mm and a layer of silicon oil was carefully applied around the cone to prevent solvent evaporation during the experiment. The measurement was allowed to proceed for 1 h at 37 °C.

### 5.2.5. Swelling ratio study

Fibrin, HA-Tyr or IPN hydrogels were prepared as described above. Immediately after adding thrombin and HRP, 400 µl of the mixture was transferred to the center of a 60 mm dish, forming gels with a hemispherical geometry. After incubation for 1 h at 37 °C, 5 ml of PBS was added to the dish and the hydrogel was detached from the dish by gently nudging with a pipette tip. After incubation overnight at room temperature, the swollen hydrogels were weighed and then lyophilized. The mass swelling ratio ($Q_M$) was taken as the swollen mass divided by the dried mass (after lyophilization). For HA-Tyr hydrogels, the volumetric swelling ratio (Qv), average molecular weight between crosslinks ($M_c$) effective crosslink density ($\nu_e$) and mesh size ($\xi$) were calculated as described in Chapter 2.

### 5.2.6. Absorbance study

Fibrin gels and IPN hydrogels were prepared as described above. Immediately after adding thrombin and HRP, 200 µl of the mixture was transferred to a 96-well plate. After incubation for 1 h at 37 °C the turbidity of the gels was determined by measuring the absorbance at 500 nm using a Tecan Infinite 200 microplate reader.

### 5.2.7. Confocal laser scanning microscopy

To visualize the structure of fibrin networks in the IPN hydrogels by confocal laser scanning microscopy fluorescent-labeled fibrinogens were prepared. Twenty-six mg of fibrinogen were dissolved in 1 ml of 0.1 M sodium bicarbonate buffer and then 0.5 mg of AlexaFluor 488 succinimidyl ester in 50 µl of DMSO was added. The mixture was incubated in the dark at room temperature for 1 h, after which the unbound fluorescent dye was removed from the labeled fibrinogen using a PD-10 desalting column following the manufacturer's instructions, with PBS as the eluent. The concentration of purified fibrinogen was determined by BCA assay and the concentration of AlexaFluor 488 conjugated to fibrinogen was determined by absorbance at 495 nm. The fluorescent dye to protein ratio was 10. A weight ratio of 1:10 of labeled to unlabeled fibrinogen was used to form the fibrin gel and IPN hydrogels. Immediately after adding thrombin and HRP, 70 µl of the mixture was deposited at the center of a glass-bottomed dish (MatTek Corporation) and a coverslip (20 × 26 mm) was placed on top so that the gel was sandwiched between two coverslips. After 1 h incubation at 37 °C the fibrin network was visualized by confocal laser scanning microscopy (Zeiss LSM 510 META).

### 5.2.8. Degradation by plasmin and hyaluronidase

Fibrin gels or IPN hydrogels were prepared as described previously. Immediately after adding thrombin and HRP, 200 µl of the mixture was deposited at the center of a 24-well plate (NUNC, untreated). The solution spread from the center and formed gels with a hemispherical geometry. The gels were left undisturbed for 5 min at room temperature before transfer to an incubator at 37 °C for 1 h. The diameters of the gels were then measured using a ruler (average diameter 11 mm). Then 700 µl of plasmin (0.1 U/ml) or hyaluronidase (50 U/ml) was added to the wells. PBS was added to a set of gels to serve as a control. The gels were then carefully detached from the wells by gently nudging with a pipette tip. After 5 h incubation at 37 °C the solution was removed and the diameters of the gels were measured. Then the gels were washed extensively with water and lyophilized to obtain the dried mass. All samples were tested in triplicate.

### 5.2.9. Cell culture

Human umbilical vein endothelial cells (HUVECs), endothelial growth medium (EGM-2) BulletKit and adult human dermal fibroblasts were purchased from Lonza Bioscience Singapore. HUVECs were maintained in EGM-2 BulletKit while fibroblasts were maintained in DMEM supplemented with 10% FBS and 1% penicillin/streptomycin. Both cell types were cultured in T75 tissue culture flasks and incubated at 37 °C in a 5% $CO_2$ atmosphere. Media were replaced every 2–3 days and the cells were subcultured at 80% confluency. Fibroblasts between passages 3 and 6 and HUVECs at passage 3 were used in this study.

### 5.2.10. Cell adhesion study

Fibrin or fibrin-HA-Tyr IPN hydrogels with a volume of 60 µl were formed as describe above in a 96-wellplate. After incubation for 1 h at 37 ºC, 5000 fibroblasts in 100 µl of serum-free medium were on top of the gels. The plate was then returned to the cell culture incubator and incubated overnight. The next day, the medium were removed and the cells were stained with 2 µM of calcein AM for 30 min in the dark at 37 ºC. Then, the staining solution was removed and the gels were washed with 100 µl of PBS for 5 min and imaged with a fluorescence microscope.

### 5.2.11. Live/Dead staining

Fibrin gels or IPN hydrogels were prepared as described previously, except that fibroblasts were included in the thrombin and HRP solution at a concentration of

$3.3 \times 10^5$ cells/ml. The final cell density in the gel was $1 \times 10^5$ cells/ml. Immediately after adding thrombin, HRP and cells 100 µl of the mixture was transferred to a 96-well plate. After incubation for 1 h at 37 °C the gels were stained with 2 µM calcein AM and 1 µM propidium iodide for 45 min in the dark at 37 °C. Then the staining solution was removed and the gels were washed with 100 µl of PBS for 5 min and imaged with a fluorescence microscope. A second set of fibrin gels and IPN hydrogels was formed, and after gelation for 1 h 100 µl of fibroblast growth medium was carefully added on top of the gel and incubated for 30 min before replacement with 100 µl of fresh medium. After 4 days culture the gels were stained and imaged as described.

### 5.2.12. Cell-induced gel contraction

Cell-embedded gels were prepared as described above. Immediately after adding thrombin, HRP and cells 100 µl of the mixture was carefully deposited at the center of a 24-well plate (untreated), forming gels with a hemispherical geometry. The gels were left undisturbed for 5 min before transfer to a cell culture incubator for 1 h. The initial diameters of the gels were measured with a ruler (average diameter 9 mm), after which 1 ml of fibroblast growth medium was added and the gels were gently detached from the bottom of the well by nudging with a pipette tip. The growth media were replaced every 2–3 days and the gels were allowed to float freely throughout the whole experiment. On selected days the media were removed, the gels were photographed and the diameters measured, after which the gels were transferred to 1.5 ml centrifuge tubes and dried under vacuum overnight. All samples were tested in triplicate.

### 5.2.13. DNA quantification

Dried gel samples from the contraction study were degraded by first incubating with 200 µl of 50 U/ml hyaluronidase in 100 mM phosphate buffer at pH 7 (sterile filtered) overnight at 37 °C. Next, 200 µl of 8 U/ml papain solution (5 mM EDTA, 5 mM L-cysteine in 100 mM phosphate buffer, pH 7) was added and incubated overnight at 60 °C. The amount of DNA was quantified by PicoGreen dsDNA reagent according to the manufacturer's protocol. Cell numbers were calculated from the amount of DNA by assuming 7.6 pg of DNA per fibroblast [5].

### 5.2.14. Capillary tube formation assay

To assess whether the IPN hydrogels permit formation of capillaries Cytodex 3 microcarriers coated with HUVECs were embedded within the IPN hydrogels and the formation of vessels was examined. Microcarriers were hydrated and autoclaved according to the manufacture's instruction. Attachment of HUVECs to the microcarriers was performed according to previously established protocols [32]. After overnight incubation of the HUVEC-coated microcarriers they were resuspended at 375 microcarriers/ml in PBS. The microcarriers were then mixed with fibrinogen or a mixture of fibrinogen and HA-Tyr conjugate solution before adding thrombin, HRP and fibroblasts. Then 250 µl of the mixture was transferred to a 48-well plate. The final concentrations of microcarriers and fibroblasts in the gels were 200 microcarriers/ml and $1 \times 10^5$ cells/ml. After incubation for 1 h at 37 °C 500 µl of EGM-2 was carefully added on top of the gels and replaced after 30 min incubation. The media were replaced every 2–3 days. Images of the microcarriers were captured on days 2 and 7. After image capture on day 7 the HUVECs in the gels were immunostained for CD31. First, the gels were washed with 1 ml of PBS for 1 h and then fixed with 1 ml of 4% paraformaldehyde for 1 h at room temperature. Then the gels were blocked with 5% (w/v) BSA in PBS overnight at 4 °C. The next day 200 µl of mouse monoclonal antibody to CD31 (1:100) in blocking buffer was added and incubated overnight at 4 °C. After washing with 1 ml of PBS (3 cycles, 1 h each on orbital shaker) 200 µl of FITC-conjugated goat polyclonal antibody to mouse IgG (1:500) was added and incubated overnight at 4 °C. Next day the gels were washed extensively with PBS and imaged with an IX70 Olympus microscope equipped with a xenon lamp. The length and width of the vessels were measured manually using the software Image-Pro Plus.

### 5.2.15. Statistical analysis

All data are expressed as mean ± standard deviation (SD). Differences between the values were assessed using Student's paired *t*-test.

## 5.3. Results and discussion

### 5.3.1. Rheological characterization

Fibrin gels are formed from fibrinogen, which is composed of two sets of three polypeptides chains joined together by disulfide bridges [4, 33]. Cleavage of fibrinogen segments, known as fibrinopeptide A and B, by thrombin converts fibrinogen to fibrin monomer. The monomers polymerize to form fibrin protofibrils, which not only grow in

length but also undergo lateral associations to form fibrin fibers. Lateral association and branching of fibrin protofibrils give rise to a fibrin gel/clot [33]. The compositions of the fibrin gels and IPN hydrogels used in this study are shown in Table 5-1. The final concentrations of thrombin and HRP in the gels were 0.31 NIH U/ml and 0.16 U/ml, respectively, as these concentrations were found to form gels at a reasonable rate for manipulation.

**Table 5-3.** Composition and physical properties of fibrin, semi-IPN and IPN hydrogels

| Sample | Fibrinogen (mg/ml) | HA-Tyr (mg/ml) | $H_2O_2$ (μM) | G' (Pa)[a] | Swelling ratio[b] |
|---|---|---|---|---|---|
| F-6Pa | 2.5 | 0 | 0 | 6.0 ± 1.5 | 73.7 ± 0.5 |
| F-24Pa | 5 | 0 | 0 | 24.2 ± 10.9 | 64.1 ± 1.0 |
| Semi-IPN | 2.5 | 2.5 | 0 | 5.2 ± 0.3 | 61.4 ± 3.8 |
| IPN-5Pa | 2.5 | 2.5 | 49 | 4.6 ± 1.3 | 86.3 ± 1.0 |
| IPN-31Pa | 2.5 | 2.5 | 98 | 30.9 ± 6.5 | 71.6 ± 0.2 |
| IPN-78Pa | 2.5 | 2.5 | 147 | 77.6 ± 3.7 | 65.4 ± 1.3 |
| IPN-55Pa | 2.5 | 2.5 | 392 | 54.5 ± 6.5 | 67.9 ± 2.4 |

[a] n = 3-5 (mean ± SD).
[b] n = 2-3 (mean ± SD).

Fig. 5-2 shows the development of the G' values of the fibrin gel, HA-Tyr hydrogel and IPN hydrogel composed of fibrin and HA-Tyr networks. The formation of fibrin networks started immediately after the addition of thrombin, as shown by the rapid increase in G'. On the other hand, the HA-Tyr hydrogel exhibited negligible change in G' initially, but it increased rapidly at around the sixth minute; the rate of increase exceeded that of the fibrin gel, as shown by the steeper slope. Due to the differential onset of the change in G' for the fibrin and HA-Tyr networks a two-phase increase was observed for the fibrin-HA-Tyr IPN hydrogel. The first phase of increase was attributed primarily to the formation of the fibrin network, while the second phase was due to the formation of both fibrin and HA-Tyr networks.

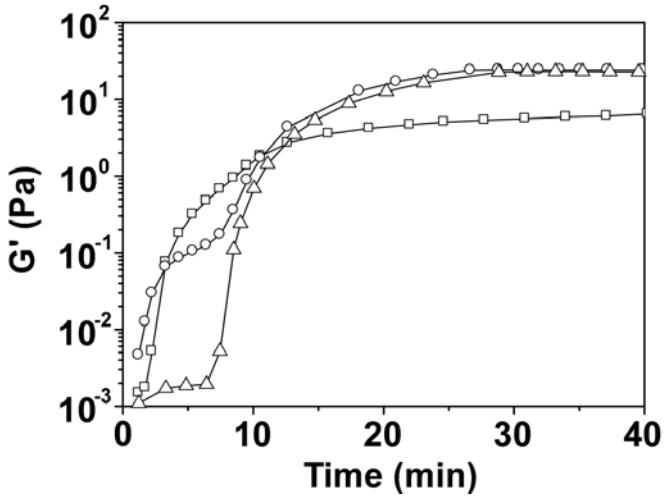


**Fig. 5-16. Development of G' of the fibrin gel (2.5 mg/ml) (□), HA-Tyr hydrogel (2.5 mg/ml) (Δ) and fibrin-HA-Tyr IPN hydrogel (2.5 mg/ml each) (○). Both the HA-Tyr hydrogels and IPN hydrogels were formed with 98 μM of $H_2O_2$. The thrombin and HRP concentrations were 0.31 NIH U/ml and 0.16 U/ml, respectively.**

After polymerization for 1h, the G' of fibrin gel formed with 5 mg/ml fibrinogen was greater than that of 2.5 mg/ml (Table 5-1). When HA-Tyr conjugates were added during the polymerization of fibrin gel in the absence of $H_2O_2$, a semi-interpenetrating network (semi-IPN) was formed and the G' remained low. When $H_2O_2$ was added to crosslink the HA-Tyr conjugates, IPN hydrogels were formed, and G' increased with increasing $H_2O_2$ concentration. $H_2O_2$ is an oxidant in the HRP-mediated coupling of tyramine moieties, hence, an increase in $H_2O_2$ concentration would increase the crosslink density of the HA-Tyr network (Table 5-2) [31, 34]. As a result of the increase in crosslink density, the swelling ratio of IPN hydrogels declined with increasing $H_2O_2$ concentration. However, a decrease in G' was observed when the $H_2O_2$ concentration was increased to 392 μM. This was attributed to excess $H_2O_2$ which adversely affected the activity of HRP [35]. Based on the G' values the fibrin gels formed with 2.5 and 5 mg/ml fibrinogen were termed F-6 Pa and F-24 Pa, respectively. Fibrin-HA-Tyr IPN hydrogels formed with $H_2O_2$ concentrations of 49, 98 and 147 μM were termed IPN-5 Pa, IPN-31 Pa and IPN-78 Pa, respectively.

**Table 5-4.** Physical properties of HA-Tyr hydrogels in PBS

| Sample | $H_2O_2$ (μM) | $Q_M$ [a] | $Q_v$ | $M_c$ ($10^6$ g/mol) | $\nu_e$ ($10^{-7}$ mol/cm$^3$) | $\xi$ (nm) |
|---|---|---|---|---|---|---|
| HA-Tyr1 | 49 | 96.4 ± 9.4 | 118.3 | 2.33 | 5.27 | 1311 |
| HA-Tyr2 | 98 | 69.5 ± 0.8 | 85.2 | 1.35 | 9.09 | 895 |
| HA-Tyr3 | 147 | 62.8 ± 1.2 | 76.9 | 1.14 | 10.78 | 794 |

[a] n = 2-3 (mean ± SD).

### 5.3.2. Effects of HA-Tyr network formation on the structure of fibrin network

Studies have shown that the turbidity of fibrin gels corresponds to the fibrin fiber thickness, i.e. turbid gels are made of thick fibrin fibers and contain large pores while clear gels have thin fibers and small pores [29, 36, 37]. To gain an insight into the structure of the fibrin network, the turbidities of the fibrin gels and IPN hydrogels were compared by determining the absorbance at 500 nm, at which the HA-Tyr network would not absorb (Fig. 5-3A). The absorbance of the fibrin gel increased with increasing fibrinogen concentration. When HA-Tyr conjugates were added during the polymerization of fibrinogen the absorbance of the resulting semi-IPN was greater than that of the fibrin gel formed with the same concentration of fibrinogen (F-6 Pa). The increase in absorbance in the presence of HA-Tyr conjugates suggested an increase in fibrin fiber thickness. Indeed, previous studies have shown that HA increased the fibrin fiber thickness, resulting in turbid gels with large pores [29, 36, 37]. Thickening of the fibrin fiber by HA is thought to be caused by non-specific volume exclusion effects or a direct interaction between HA and fibrin that leads to increased association between fibrin protofibrils [36]. It was shown previously that fibrin gels composed of thick fibers promote the migration of endothelial cells, however, the cells migrated as single cells, which resulted in decreased intercellular adhesion and formation of capillaries [29]. Hence, fibrin scaffolds with thick fibers might not be suitable for the purpose of vascularization. Interestingly, when the HA-Tyr conjugates were crosslinked by addition of HRP and $H_2O_2$, the absorbance of the IPN hydrogels decreased to lower than that of the fibrin gel alone. A slight decrease in absorbance was observed with increasing $H_2O_2$ concentration, i.e. increasing crosslink density of the HA-Tyr network. These results suggested that crosslinking HA-Tyr conjugates hinders the lateral association of fibrin protofibrils, forming thin fibrin fibers.

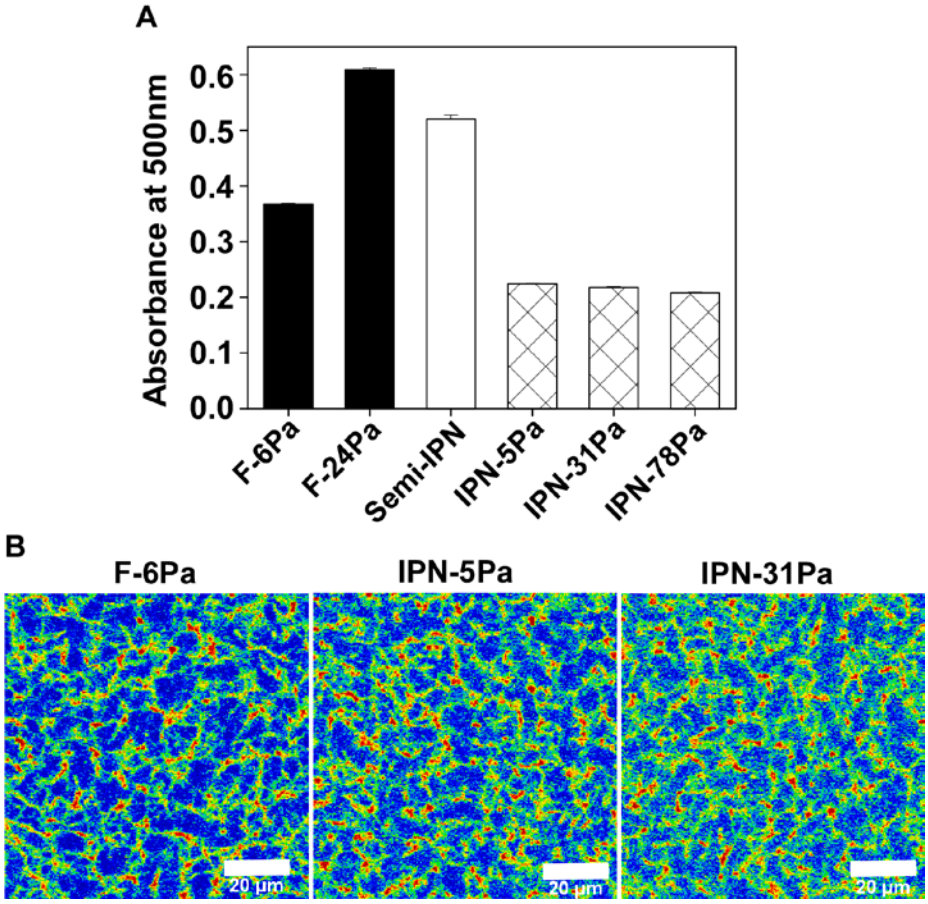


**Fig. 5-17. Fibrin structure in IPN hydrogels. (A) Turbidity of fibrin gel, fibrin-HA-Tyr semi-IPN and IPN hydrogels as determined by absorbance at 500 nm (n = 2). (B) Confocal laser scanning microscopy of the fibrin gel and IPN hydrogels containing fluorescent-labeled fibrinogen. The images were shown using a rainbow palette to highlight the differences in fluorescence intensity. Blue pixels have zero fluorescence intensity and red pixels have the strongest intensity. Scale bar 20 µm.**

To confirm that formation of a HA-Tyr network prevents lateral association of fibrin protofibrils, fluorescently labeled fibrinogen was included during gel formation and the fibrin networks were visualized by confocal laser scanning microscopy (Fig. 5-3B). The images are shown with a rainbow palette; blue pixels represent zero fluorescence intensity while red pixels have the strongest intensity. An interconnected network of non-blue pixels (fluorescence) containing blue holes (no fluorescence) was observed for the fibrin gel (F-6 Pa), indicating the formation of a fibrin network with pores. In contrast, formation of fibrin-HA-Tyr IPN hydrogels decreased the size of the pores, indicating a shorter distance between adjacent fibrin fibers. The boundary of pores also became less defined as the G' value of the IPN hydrogel increased. The results demonstrate that crosslinked HA-Tyr networks hinder the lateral associations of fibrin protofibrils, forming thin fibrin fibers (i.e. a fibrin network with

small pores). The thin fibers reduced light deflection; hence IPN hydrogels appeared less turbid than fibrin gels.

### 5.3.3. Degradation of IPN hydrogels by plasmin

To determine whether IPN hydrogels could better maintain the shape of a scaffold in the presence of proteases, fibrin gels and IPN hydrogels were incubated with plasmin. Fibrin gels were rapidly degraded by plasmin while IPN-5 Pa was dissolved after 5 h incubation, indicating that the HA-Tyr network present in IPN-5 Pa was too weak to provide structural support (Table 5-3). In contrast, the diameters of IPN-31 Pa and IPN-78 Pa did not decrease and even showed a slight increase. The dried mass of plasmin-challenged IPN-31 Pa and IPN-78 Pa corresponded to the theoretical mass of HA-Tyr conjugates used to form the IPN hydrogels (0.5 mg), suggesting that the remaining gels consisted mainly of HA-Tyr network. The results indicate that proteolytic degradation of the fibrin network would not affect the geometry of IPN-31 Pa and IPN-78 Pa, as the HA-Tyr networks could provide structural support.

**Table 5-5.** Degradation of fibrin gels and IPN hydrogels by plasmin

| Sample | Time taken to degrade (h) | Diameter remaining (%)[a] | Mass remaining (mg)[b] |
|---|---|---|---|
| F-6Pa | 2.5 | 0 | 0 |
| F-24Pa | 3.5 | 0 | 0 |
| IPN-5Pa | 5.0 | 0 | 0 |
| IPN-31Pa | - | 112.1 ± 5.2 | 0.49 ± 0.13 |
| IPN-78Pa | - | 106.1 ± 5.2 | 0.53 ± 0.04 |

[a]Remaining diameters are expressed as percentages of the initial diameters (n = 3, mean ± SD). [b]Remaining mass of degraded gels after lyophilization. The theoretical initial mass of HA-Tyr conjugates used to form the IPN hydrogels was 0.5 mg per gel (n = 3, mean ± SD).

### 5.3.4. Viability and spreading of cells in fibrin gels and IPN hydrogels

HA is known to have poor cell adhesive properties. Attachment and spreading of cells on or within HA hydrogels can be improved by incorporating cell-adhesive agents such as the RGD peptide [38, 39], fibronectin [40] or collagen [41] in the matrices. Fibrin-HA-Tyr IPN hydrogels demonstrated good cell adhesion as fibrinogen contains an endogenous RGD sequence [33] (Fig. 5-4). Furthermore, fibroblasts remained viable when embedded in the fibrin gels and IPN hydrogels (Fig. 5-5). Very few dead cells were observed and there was no notable difference in cell viability between the fibrin gels and IPN hydrogels with different G'

values immediately after gel formation and after 4 days culture (Fig. 5-5). The results indicated that IPN formation does not affect cell viability.

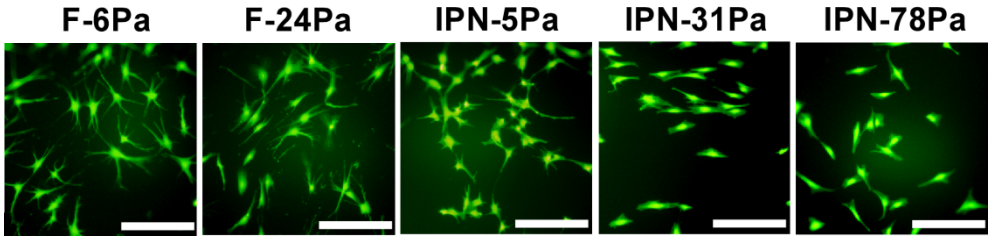


**Fig. 5-18. Adhesion of human dermal fibroblasts on fibrin gels and fibrin-HA-Tyr IPN hydrogels of different G'. Fibroblasts were able to adhere and spread on the surfaces of IPN hydrogels after 24 incubation in serum free medium. Cells adopted a dendritic morphology on the soft matrices of F-6Pa and IPN-5Pa. A mixture of both dendritic and elongated morphology was observed on F-24Pa. On stiffer matrices, i.e., IPN-31Pa and IPN-78Pa, all cells showed elongated morphology. Scale bar = 100 µm.**

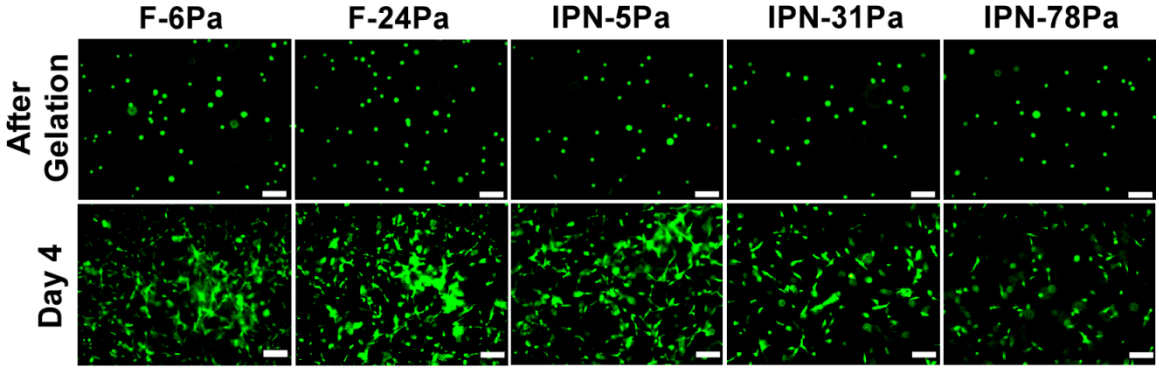


**Fig. 5-19. Live/dead staining of fibroblasts embedded within fibrin gels and IPN hydrogels immediately after gel formation (first row) and after 4 days culture (second row). The live cells were stained green while the dead cells were stained red. Scale bar 100 µm.**

However, it was observed that the number of cells that retained a spherical morphology after 4 days increased with increasing G' value of the IPN hydrogels. In a 3-D environment the matrix surrounding a cell needs to be either displaced or degraded in order to create a space into which to spread [39]. An increase in the crosslink density of the HA-Tyr network in IPN hydrogels would form a more rigid surrounding matrix, making it harder for the cells to spread. Furthermore, the crosslinked HA-Tyr networks resulted in fibrin networks containing small pores (Fig. 5-3), which would require greater cell-derived proteolytic activity to degrade the surrounding matrix. Consequently, the increase in crosslink density of the HA-Tyr network, together with the decrease in pore size of the fibrin network, resulted in a more rigid matrix that impeded matrix remodeling and cell spreading.

### 5.3.5. Contraction of fibrin gels and IPN hydrogels and cell proliferation

Fibrin gels are known to rapidly contract on contact with cells [5, 6]. Over-contraction can be problematical for applications that require specific dimensions, such as tissue engineered heart valves [5, 13]. To evaluate the resistance to cell-induced contraction, fibrin gels and IPN hydrogels were embedded with fibroblasts and maintained in a floating culture system. On selected days the culture medium was removed and the gel diameters were measured (Fig. 5-6A). F-6 Pa and F-24 Pa contracted to 35% and 65% of the initial diameter within 1 day, after which contraction continued, albeit at a slower rate. IPN-5 Pa swelled after 1 day due to hydration of the HA-Tyr networks, after which it contracted slowly, retaining 85% of its initial diameter on day 7. No contraction was observed for either IPN-31 Pa or IPN-78 Pa, and they retained a hemispherical geometry after 7 days culture (Fig. 5-6B). When comparing fibrin gels and IPN hydrogels with similar G' values, i.e. F-6 Pa with IPN-5 Pa and F-24 Pa with IPN-31 Pa, IPN hydrogels were more resistant to contraction compared with fibrin gels. When comparing IPN hydrogels with different G' values, those with higher G' values showed reduced rates of contraction. The results indicate that the formation of IPN hydrogels could inhibit fibrin gel contraction in the presence of fibroblasts. Similar findings have been reported for collagen gels by Mehra *et al*. [26]. In the study, thiol-functionalized HA derivatives (HA-DTPH) were added to collagen gels and crosslinked with polyethylene glycol diacrylate (PEGDA). The resulting collagen–HA–DTPH–PEGDA gels significantly inhibited fibroblast-mediated contraction and the extent of contraction decreased with increasing crosslink density of the HA network.

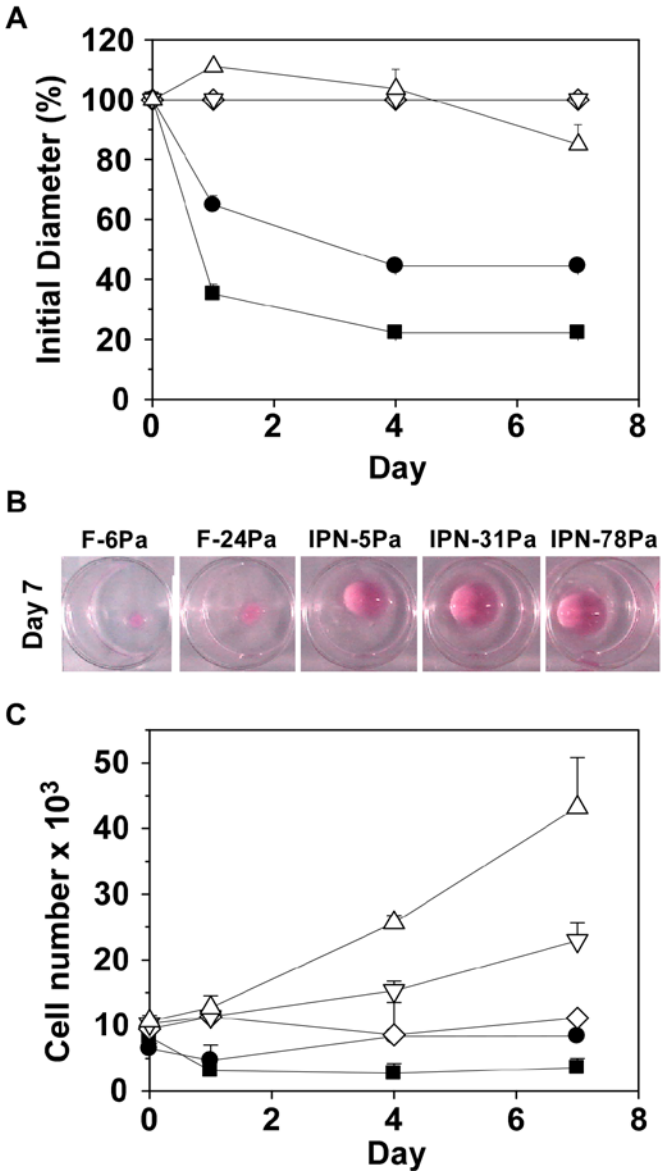


**Fig. 5-20. Floating culture of hydrogels containing fibroblasts. (A) Gel contraction by cells expressed as percentages of initial gel diameter for F-6Pa (■), F-24Pa (●), IPN-5Pa (Δ), IPN-31Pa (∇) and IPN-78Pa (◊). (B) Photographs of the gels after culture for 7 days. (C) Corresponding proliferation of fibroblasts as measured by DNA quantification (n = 3).**

The contracted gels were collected and sequentially degraded with hyaluronidase and plasmin to recover the cells. Fig. 5-6C shows the total cell number based on DNA quantification using the PicoGreen assay. After 1 day culture, both F-6 Pa and F-24 Pa showed a decrease in cell number, which could be due to cells falling out of the contracted/degraded gel matrix. After 7 days the cell number in F-6 Pa remained lower than day 0 but similar to day 1, indicating little or no cell growth. For F-24 Pa, although the cell number was higher on day 7 than day 1, the increase was small which suggested a slow rate of cell growth. The observation that contraction of fibrin gels inhibited cell growth has been

previously reported, and was also shown in contracted collagen, as well as interpenetrating collagen–fibrin matrices [7]. Based on previous studies with collagen gels, the decreased cell growth in contracted gels was due to the lack of tension generated within floating gel matrices in response to cell contractile forces. This resulted in fibroblasts with a stellate morphology, which not only became quiescent but might also undergo apoptosis due to changes in integrin engagement [42, 43].

In contrast, by maintaining the structure of the scaffold, IPN hydrogels retained the cells within the matrix and no decrease in cell number was observed after 1 day. The rate of cell proliferation in IPN hydrogels decreased as the value of G' increased. On day 7, the number of cells in IPN-5 Pa and IPN-31 Pa had increased by 4 and 2 times, respectively. The cell number remained unchanged for IPN-78 Pa. It was observed that an increase in the G' value of the IPN hydrogels prevented the embedded cells from spreading (Fig. 5-5); hence it is not surprising that cell proliferation would likewise be affected. The decrease in cell proliferation with increasing G' was attributed to the increase in crosslink density of the HA-Tyr network. Based on the gel contraction and cell proliferation studies, it was concluded that IPN-31 Pa was the best candidate to maintain the scaffold shape when embedded with cells (seeding density $1 \times 10^5$ cells/ml), while at the same time allowing the cells to proliferate.

### 5.3.6. Angiogenic sprouting and capillary tube formation in IPN hydrogels

Vascularization of engineered tissues is crucial in ensuring the survival and function of a tissue construct after transplantation. *In vitro* prevascularization, i.e. formation of a capillary network within the tissue construct before transplantation, is one of the most promising strategies to achieve rapid blood infusion *via* anastomosis with the host vasculature [44]. To examine the ability of IPN hydrogels to support capillary formation *in vitro* Cytodex microcarriers coated with HUVECs were embedded in IPN hydrogels and the invasion of cells into the surrounding matrices were observed (Fig. 5-7). Human dermal fibroblasts, which provide pro-angiogenic factors, were co-cultured within the IPN hydrogels to minimize the change in diffusive transport due to the different matrix rigidity [45]. Only IPN-31 Pa and IPN-78 Pa were included in the study, as they demonstrated shape stability when challenged by plasmin or embedded with cells.

Invasion of the gel matrices by HUVECs was observed on day 2 for both IPN hydrogels (Fig. 5-7A and B). By day 7, the capillary sprouts developed into vessels with lumens,

indicating that the IPN hydrogels could promote capillary tube formation (Fig. 5-7C and D). Immunostaining with CD 31 antibodies confirmed that these vessels were composed of endothelial cells rather than fibroblasts (Fig. 5-7E and F). A more extensive network of capillaries was observed in IPN-31 Pa compared to IPN-78 Pa. The number of vessels formed per bead, the average length and width of the vessels were significantly greater in IPN-31 Pa compared to IPN-78 Pa (Table 5-4).

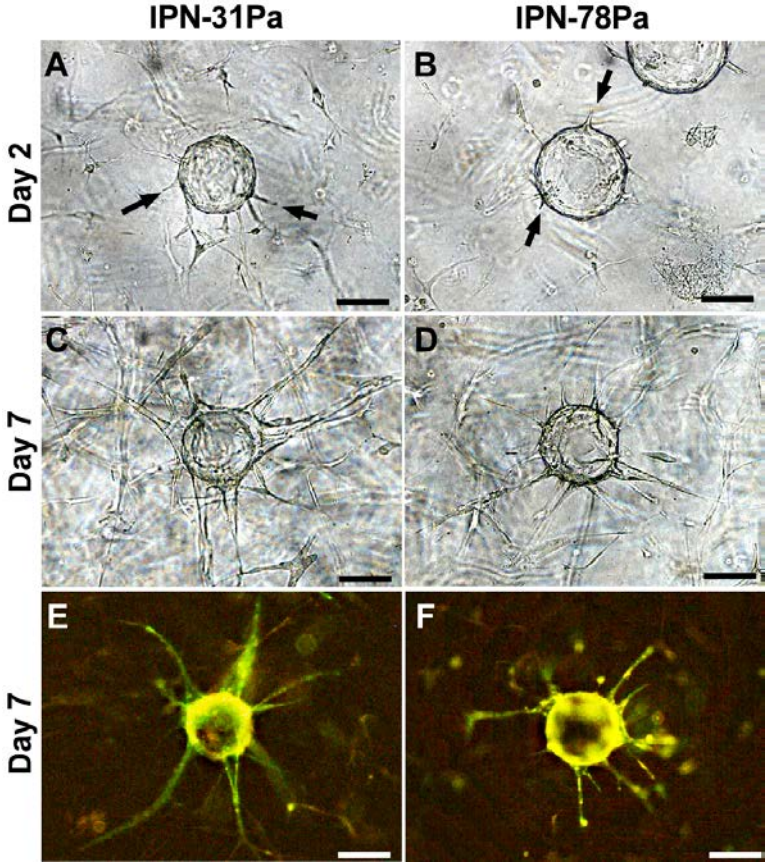


**Fig. 5-21. HUVEC vessel formation in IPN hydrogels. Representative images of beads coated with HUVECs and embedded in IPN-31Pa (A, C, and E) and IPN-78 Pa (B, D, and F). (A and B) Sprouts appeared on day 2 for both IPN hydrogels (arrows). (C and D) Vessels with lumens were observed on day 7. (E and F) Immunostaining of CD31 on day 7. Scale bar 100 µm.**

**Table 5-6.** Quantification of vessel morphology

| Sample | Vessels per bead[a] | Vessel length (µm)[b] | Vessel width (µm)[c] |
|---|---|---|---|
| IPN-31Pa | 7.7 ± 2.5[d] | 104.9 ± 13.3[e] | 6.89 ± 1.7[d] |
| IPN-78Pa | 5.3 ± 1.1 | 68.3 ± 16.5 | 5.42 ± 1.0 |

[a]Total of 10 beads were counted per sample. [b]Vessel length was determined by dividing the total vessel length with the number of vessels for each bead. 10 beads were measured. [c]Vessel width was the width at the mid point of the longitudinal length of the vessel. [d]Indicates that the value is significantly greater than IPN-78Pa ($p < 0.05$). [e]Indicates that the value is significantly greater than IPN-78Pa ($p < 0.01$).

Although fibrin gels exhibit the unique ability to induce capillary network formation by endothelial cells [46, 47], the size of the vascularized fibrin gel shrank dramatically over time due to poor mechanical properties [15]. Moreover, it has been reported that tubular structures formed by microvascular endothelial cells in turbid and porous fibrin gels disintegrated after prolonged incubation due to extensive degradation of the fibrin gel [48]. In the present study the fibrin-HA-Tyr IPN hydrogels showed improved shape stability in the presence of cells, and were able to maintain the structure of the scaffold even when the fibrin networks were fully degraded. Hence, fibrin-HA-Tyr IPN hydrogels are a promising alternative for the formation of geometrically stable and vascularized tissue constructs.

## 5.4. Conclusions

IPN hydrogels consisting of fibrin and HA-Tyr networks were formed for the purpose of improving the mechanical properties of fibrin gels while retaining the ability to promote cell proliferation and capillary tube formation. The simultaneous formation of fibrin and HA-Tyr networks resulted in fibrin-HA-Tyr IPN hydrogels. It was found that the formation of HA-Tyr networks prevented lateral association of fibrin protofibrils, resulting in fibrin networks with smaller pores compared to fibrin only gels. By tuning the amount of $H_2O_2$ added, which controlled the crosslink density of the HA-Tyr network, IPN hydrogels with different G' values were obtained. These IPN hydrogels demonstrated improved structural stability in the presence of plasmin and cell-contractile forces. The formation of IPN hydrogels did not affect the viability of the embedded cells, but cell proliferation and capillary tube formation were found to decrease with increasing G' value of the IPN hydrogels.

**References**

[1] Hoffman AS. Hydrogels for biomedical applications. Adv. Drug Del. Rev. 2002;54:3-12.

[2] Shaikh FM, Callanan A, Kavanagh EG, Burke PE, Grace PA, McGloughlin TM. Fibrin: a natural biodegradable scaffold in vascular tissue engineering. Cells Tissues Organs 2008;188:333-46.

[3] Janmey PA, Winer JP, Weisel JW. Fibrin gels and their clinical and bioengineering applications. J. R. Soc. Interface 2009;6:1-10.

[4] Ahmed TAE, Dare EV, Hincke M. Fibrin: A Versatile Scaffold for Tissue Engineering Applications. Tissue Eng. Part B Rev. 2008;14:199-215.

[5] Syedain ZH, Bjork J, Sando L, Tranquillo RT. Controlled compaction with ruthenium-catalyzed photochemical cross-linking of fibrin-based engineered connective tissue. Biomaterials 2009;30:6695-701.

[6] Tuan TL, Song A, Chang S, Younai S, Nimni ME. In vitro fibroplasia: matrix contraction, cell growth, and collagen production of fibroblasts cultured in fibrin gels. Exp. Cell Res. 1996;223:127-34.

[7] Rowe SL, Stegemann JP. Interpenetrating collagen-fibrin composite matrices with varying protein contents and ratios. Biomacromolecules 2006;7:2942-8.

[8] Meinhart J, Fussenegger M, Hobling W. Stabilization of fibrin-chondrocyte constructs for cartilage reconstruction. Ann. Plast. Surg. 1999;42:673-8.

[9] Lorentz KM, Kontos S, Frey P, Hubbell JA. Engineered aprotinin for improved stability of fibrin biomaterials. Biomaterials 2010;32:430-8.

[10] Rowe SL, Lee S, Stegemann JP. Influence of thrombin concentration on the mechanical and morphological properties of cell-seeded fibrin hydrogels. Acta Biomater. 2007;3:59-67.

[11] Eyrich D, Brandl F, Appel B, Wiese H, Maier G, Wenzel M, Staudenmaier R, Goepferich A, Blunk T. Long-term stable fibrin gels for cartilage engineering. Biomaterials 2007;28:55-65.

[12] Gundy S, Manning G, O'Connell E, Ella V, Harwoko MS, Rochev Y, Smith T, Barron V. Human coronary artery smooth muscle cell response to a novel PLA textile/fibrin gel composite scaffold. Acta Biomater. 2008;4:1734-44.

[13] Flanagan TC, Cornelissen C, Koch S, Tschoeke B, Sachweh JS, Schmitz-Rode T, Jockenhoevel S. The in vitro development of autologous fibrin-based tissue-engineered heart valves through optimised dynamic conditioning. Biomaterials 2007;28:3388-97.

[14] Mol A, van Lieshout MI, Dam-de Veen CG, Neuenschwander S, Hoerstrup SP, Baaijens FP, Bouten CV. Fibrin as a cell carrier in cardiovascular tissue engineering applications. Biomaterials 2005;26:3113-21.

[15] Lesman A, Koffler J, Atlas R, Blinder YJ, Kam Z, Levenberg S. Engineering vessel-like networks within multicellular fibrin-based constructs. Biomaterials 2011;32:7856-69.

[16] Smith JD, Chen A, Ernst LA, Waggoner AS, Campbell PG. Immobilization of aprotinin to fibrinogen as a novel method for controlling degradation of fibrin gels. Bioconjug. Chem. 2007;18:695-701.

[17] Alkjaersig N, Fletcher AP, Sherry S. xi-Aminocaproic acid: an inhibitor of plasminogen activation. J. Biol. Chem. 1959;234:832-7.

[18] Cholewinski E, Dietrich M, Flanagan TC, Schmitz-Rode T, Jockenhoevel S. Tranexamic acid--an alternative to aprotinin in fibrin-based cardiovascular tissue engineering. Tissue Eng. Part A 2009;15:3645-53.

[19] Hennink WE, van Nostrum CF. Novel crosslinking methods to design hydrogels. Adv. Drug Del. Rev. 2002;54:13-36.

[20] Akpalo E, Bidault L, Boissiere M, Vancaeyzeele C, Fichet O, Larreta-Garde V. Fibrin-polyethylene oxide interpenetrating polymer networks: new self-supported biomaterials combining the properties of both protein gel and synthetic polymer. Acta Biomater. 2011;7:2418-27.

[21] Shikanov A, Xu M, Woodruff TK, Shea LD. Interpenetrating fibrin-alginate matrices for in vitro ovarian follicle development. Biomaterials 2009;30:5476-85.

[22] Masters KS, Shah DN, Leinwand LA, Anseth KS. Crosslinked hyaluronan scaffolds as a biologically active carrier for valvular interstitial cells. Biomaterials 2005;26:2517-25.

[23] Oh EJ, Park K, Kim KS, Kim J, Yang J-A, Kong J-H, Lee MY, Hoffman AS, Hahn SK. Target specific and long-acting delivery of protein, peptide, and nucleotide therapeutics using hyaluronic acid derivatives. J. Control. Release 2010;141:2-12.

[24] Prestwich GD. Hyaluronic acid-based clinical biomaterials derived for cell and molecule delivery in regenerative medicine. J. Control. Release 2011;155:193-9.

[25] Weigel PH, Fuller GM, LeBoeuf RD. A model for the role of hyaluronic acid and fibrin in the early events during the inflammatory response and wound healing. J. Theor. Biol. 1986;119:219-34.

[26] Mehra TD, Ghosh K, Shu XZ, Prestwich GD, Clark RA. Molecular stenting with a crosslinked hyaluronan derivative inhibits collagen gel contraction. J. Invest. Dermatol. 2006;126:2202-9.

[27] Park SH, Choi BH, Park SR, Min BH. Chondrogenesis of rabbit mesenchymal stem cells in fibrin/hyaluronan composite scaffold in vitro. Tissue Eng. Part A 2011;17:1277-86.

[28] Smith JD, Melhem ME, Magge KT, Waggoner AS, Campbell PG. Improved growth factor directed vascularization into fibrin constructs through inclusion of additional extracellular molecules. Microvasc. Res. 2007;73:84-94.

[29] Nehls V, Herrmann R. The configuration of fibrin clots determines capillary morphogenesis and endothelial cell migration. Microvasc. Res. 1996;51:347-64.

[30] Kurisawa M, Chung JE, Yang YY, Gao SJ, Uyama H. Injectable biodegradable hydrogels composed of hyaluronic acid-tyramine conjugates for drug delivery and tissue engineering. Chem. Commun. (Camb.) 2005:4312-4.

[31] Lee F, Chung JE, Kurisawa M. An injectable enzymatically crosslinked hyaluronic acid-tyramine hydrogel system with independent tuning of mechanical strength and gelation rate. Soft Matter 2008;4:880-7.

[32] Nakatsu MN, Sainson RC, Aoto JN, Taylor KL, Aitkenhead M, Perez-del-Pulgar S, Carpenter PM, Hughes CC. Angiogenic sprouting and capillary lumen formation modeled by human umbilical vein endothelial cells (HUVEC) in fibrin gels: the role of fibroblasts and Angiopoietin-1. Microvasc. Res. 2003;66:102-12.

[33] Mosesson MW. Fibrinogen and fibrin structure and functions. J. Thromb. Haemost. 2005;3:1894-904.

[34] Lee F, Chung JE, Kurisawa M. An injectable hyaluronic acid-tyramine hydrogel system for protein delivery. J. Control. Release 2009;134:186-93.

[35] Huang Q, Huang Q, Pinto RA, Griebenow K, Schweitzer-Stenner R, Weber WJ. Inactivation of Horseradish Peroxidase by Phenoxyl Radical Attack. J. Am. Chem. Soc. 2005;127:1431-7.

[36] LeBoeuf RD, Gregg RR, Weigel PH, Fuller GM. Effects of hyaluronic acid and other glycosaminoglycans on fibrin polymer formation. Biochemistry 1987;26:6052-7.

[37] Hayen W, Goebeler M, Kumar S, Riessen R, Nehls V. Hyaluronan stimulates tumor cell migration by modulating the fibrin fiber architecture. J. Cell Sci. 1999;112 ( Pt 13):2241-51.

[38] Park YD, Tirelli N, Hubbell JA. Photopolymerized hyaluronic acid-based hydrogels and interpenetrating networks. Biomaterials 2003;24:893-900.

[39] Lei Y, Gojgini S, Lam J, Segura T. The spreading, migration and proliferation of mouse mesenchymal stem cells cultured inside hyaluronic acid hydrogels. Biomaterials 2011;32:39-47.

[40] Seidlits SK, Drinnan CT, Petersen RR, Shear JB, Suggs LJ, Schmidt CE. Fibronectin-hyaluronic acid composite hydrogels for three-dimensional endothelial cell culture. Acta Biomater. 2011;7:2401-9.

[41] Suri S, Schmidt CE. Photopatterned collagen-hyaluronic acid interpenetrating polymer network hydrogels. Acta Biomater. 2009;5:2385-97.

[42] Nakagawa S, Pawelek P, Grinnell F. Long-term culture of fibroblasts in contracted collagen gels: effects on cell growth and biosynthetic activity. J. Invest. Dermatol. 1989;93:792-8.

[43] Grinnell F. Fibroblast biology in three-dimensional collagen matrices. Trends Cell Biol. 2003;13:264-9.

[44] Novosel EC, Kleinhans C, Kluger PJ. Vascularization is the key challenge in tissue engineering. Adv. Drug Del. Rev. 2011;63:300-11.

[45] Ghajar CM, Chen X, Harris JW, Suresh V, Hughes CCW, Jeon NL, Putnam AJ, George SC. The effect of matrix density on the regulation of 3-D capillary morphogenesis. Biophys. J. 2008;94:1930-41.

[46] van Hinsbergh VW, Collen A, Koolwijk P. Role of fibrin matrix in angiogenesis. Ann. N. Y. Acad. Sci. 2001;936:426-37.

[47] Montano I, Schiestl C, Schneider J, Pontiggia L, Luginbuhl J, Biedermann T, Bottcher-Haberzeth S, Braziulis E, Meuli M, et al. Formation of human capillaries in vitro: the engineering of prevascularized matrices. Tissue Eng. Part A 2010;16:269-82.

[48] Collen A, Koolwijk P, Kroon M, van Hinsbergh VW. Influence of fibrin structure on the formation and maintenance of capillary-like tubules by human microvascular endothelial cells. Angiogenesis 1998;2:153-65.

# Chapter 6

# Enzymatic Conjugation of a Bioactive Peptide into an Injectable Hyaluronic Acid-Tyramine Hydrogel System to Promote the Formation of Functional Vasculature

## 6.1. Introduction

Hydrogels are suitable materials for the encapsulation of cells because the aqueous three-dimensional (3D) matrices permit the efficient exchange of nutrients and metabolites, which in turn promote the survival and proliferation of encapsulated cells. Moreover, hydrogels are also capable of presenting biological signals in the form of bioactive peptides grafted onto the gel networks, which recapitulate the extracellular matrix (ECM) of the tissue to be regenerated, and/or stimulate the encapsulated cells with specific biological cues. There are two main approaches to introduce bioactive peptides into a hydrogel network. The first is a step-wise approach in which the peptide is first conjugated to the gel precursors; then the peptide-polymer conjugates are crosslinked to form a hydrogel [1]. In the second approach, peptides containing reactive functional groups are designed for *in situ* conjugation into the hydrogel network during the crosslinking process [2-4]. For instance, exogenous bioactive peptides have been incorporated into fibrin gel *in situ* during the coagulation process by Factor XIIIa [3]. The exogenous peptides contained two different domains, a bioactive sequence of interest in one domain and a substrate for Factor XIIIa in the other domain. More recently, the HRP-mediated coupling of phenols has also been utilized for the *in situ* conjugation of bioactive peptides into a hydrogel network. Park *et al.* demonstrated the conjugation of an endothelial cell binding peptide, Ser-Val-Val-Tyr-Gly-Leu-Arg, into gelatin-PEG-tyramine (GPT) hydrogels by the enzymatic activity of HRP [5]. In the design of the endothelial cell binding peptide, a tyrosine residue was inserted at the terminus, which facilitated the coupling with tyramine moieties of GPT during the HRP-mediated crosslinking reaction.

In this chapter, a cell-adhesive peptide was designed for *in situ* conjugation into hyaluronic acid-tyramine (HA-Tyr) hydrogels during the HRP-mediated crosslinking reaction. HA is known to resist cell adhesion, which limited the use of HA-based hydrogels for tissue engineering applications. Several methods have been developed to endow HA hydrogels with cell-adhesive property, including physical incorporation of collagen [6] and fibrin [7] to form interpenetrating hydrogel networks, and chemical conjugation of fibronectin [8] and Arg-Gly-Asp (RGD) peptide [2, 9, 10] into the HA network. Among the different approaches, the use of RGD peptides is particularly attractive as RGD is a cell adhesion ligand that not only promotes integrin-mediated cell adhesion but also enhances endothelial cell migration and angiogenesis [1, 11, 12]. Herein, a RGD peptide bearing two phenol moieties ($Ph_2$-PEG-RGD) was synthesized for the conjugation to HA-Tyr hydrogels to promote cell adhesion and

vascularization of the hydrogels (Fig. 6-1). $Ph_2$-PEG-RGD was shown to conjugate into HA-Tyr hydrogels during the crosslinking reaction mediated by HRP. The RGD-modified hydrogels (HA-Tyr-RGD) were characterized in terms of rheology and water uptake, and cell adhesion, proliferation and migration. In addition, the formation of capillary-like networks by human umbilical vein endothelial cells (HUVEC) within the modified and unmodified hydrogels was examined *in vitro*. Furthermore, cell-laden hydrogels were injected into the subcutaneous environment of mice to investigate whether functional vasculatures could be formed in the hydrogels *in vivo*.

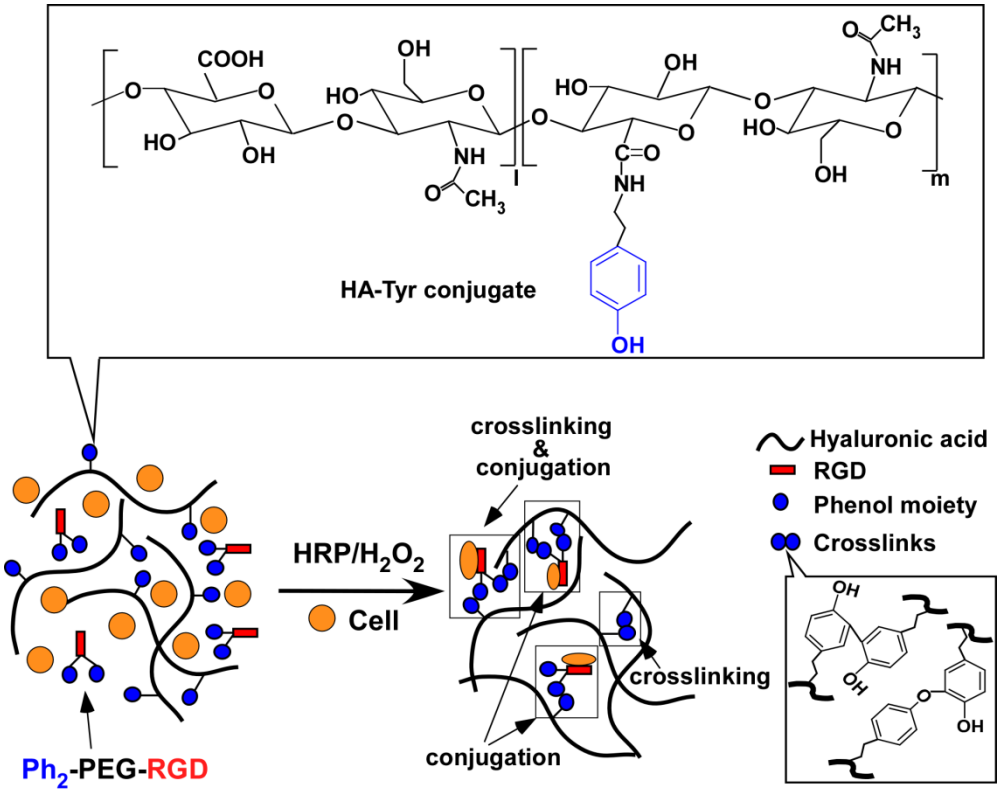


**Fig. 6-1. $Ph_2$-PEG-RGD was conjugated simultaneously onto HA-Tyr during *in situ* gel formation *via* the enzymatic oxidation reaction of HRP and $H_2O_2$. Cell could be embedded into the hydrogels to promote vascularization for tissue engineering applications.**

## 6.2. Materials and methods

### 6.2.1. Materials

Type I collagenase (246 U/mg) and Triton X-100 were purchased from Sigma-Aldrich. Dulbecco's modified Eagle medium (DMEM), fetal bovine serum (FBS), penicillin-streptomycin, Quant-iT™ PicoGreen ® dsDNA Reagent and Kits and CellTracker Green

CMFDA were provided by Life Technologies (Singapore). Actin cytoskeleton and focal adhesion staining kit containing vinculin monoclonal antibody, TRITC-conjugated phalloidin and 4',6-diamidino-2-phenylindole (DAPI) and human nuclei antibody (MAB 1281) were provided by Millipore (Singapore). Mouse monoclonal anti-CD31 antibody (ab9498) was obtained from Abcam. Anti-mouse HRP-DAB Cell & Tissue Staining Cell was purchased from R&D systems (USA). Pierce™ BCA protein assay kit was obtained from Thermo Scientific (Singapore). HA-Tyr conjugates were synthesized as described in Chapter 2. The DS was calculated from $^{1}$H NMR measurement and found to be 5.

### 6.2.2. Synthesis of (S)-2,6-bis(3-(4-hydroxyphenyl)propanamido)hexanamide (Ph2-K)

(S)-2,6-bis(3-(4-hydroxyphenyl)propanamido)hexanamide ($Ph_2$-K) was synthesized by using an automatic synthesizer Titan 357 (AAPPTEC). Fifty mg of ChemMatrix® resins (0.48 mmol/g) were swelled in *N*-methyl-2-pyrrolidone (NMP, 1 ml) for 5 min in a Reaction Vessel (RV). With the liquid drained, 20% piperidine in NMP (1 ml, v/v) was added and the RV was vortexed for 2 min. The liquid was drained and a fresh solution of 20% piperidine in NMP (1 ml, v/v) was added and the RV was vortexed for another 10 min. The resulting beads were thoroughly washed by NMP (1 ml x 2), methanol (1 ml x 2) and dichloromethane (DCM, 1 ml × 2), successively. With the resulting resins swelled with NMP (1 ml) for 15 min, Fmoc-K(Mtt)-OH (2.5 equiv, 0.2 M solution in NMP) was added to the RV, as well as *N,N,N′,N′*-tetramethyl-*O*-(benzotriazol-1-yl)uronium tetrafluoroborate (TBTU, 2.5 equiv, 0.2 M solution in NMP) and diisopropylethylamine (DIEA, 5.0 equiv, 0.5 M in NMP). The resulting mixture was vortexed for 45 min. With the liquid drained, the resulting beads were thoroughly washed by NMP (1 ml × 3). The coupling step was repeated for the coupling of 3-(4-hydroxyphenyl)propionic acid (HPA). Then, selective deprotection of 4-methyltrityl (Mtt) group was performed by reaction with 2 ml of trifluoroacetic acid (TFA)/triisopropylsilane (TIS)/DCM (3/3/94) for 2 min, 5 min and 30 min successively, using a fresh aliquot each time. Finally, another group of HPA was coupled to the exposed amine group at the residue of K. The resins were washed by NMP (1 ml × 3) and transferred in a 4 ml reactor equipped with a filter, using DCM (2 ml × 3). After the resins were dried under reduced pressure for 2 h, the peptide was cleaved in a cleavage cocktail of TFA-water-TIS (1.5 ml, 94/3/3, v/v) for 2 h on a 180-degree shaker, while all the acid-labile protective groups in the residues were also detached. The solution was collected and concentrated in a continuous flow of nitrogen and the crude peptides were precipitated in diethylether. The resulting white solid was then purified to >98% in purity by a preparative HPLC (Gilson) on a $C_{18}$ reversed phase

preparative column (Kromasil®, 21.2 mm x 250 mm) using water and acetonitrile with 0.1% trifluoroacetic acid as the mobile phase. The purified peptides showed >98% purity in high-performance liquid chromatography (HPLC). Electrospray ionization mass spectrometry (ESI-MS) of the purified product gave peaks at m/z 442.3 for $[M+H]^+$

### 6.2.3. Synthesis and characterization of $Ph_2$-PEG-RGD

Fifty mg of ChemMatrix® resins (0.48 mmol/g) was prepared following the steps described above. After the resins were swelled with NMP (1 ml) for 15 min, Fmoc-D-(OtBu)-OH (2.5 equiv, 0.2 M solution in NMP) was added to the RV, as well as *N*,*N*,*N'*,*N'*-tetramethyl-O-(benzotriazol-1-yl)uronium tetrafluoroborate (TBTU, 2.5 equiv, 0.2 M solution in NMP) and *N*,*N*-diisopropylethylamine (DIEA, 5.0 equiv, 0.5 M in NMP). The resulting mixture was vortexed for 45 min. With the liquid drained, the resulting beads were thoroughly washed by NMP (1 ml × 3). The coupling step was repeated until the desired structure attained on beads, i.e., HPA-K(Mtt)-PEG2(13atm)-R(Pbf)-G-D(OtBu). Selective deprotection of 4-methyltrityl (Mtt) group was performed as described above and another group of HPA was coupled to the exposed amine group at the residue of K. The resins were washed by NMP, dried under reduced pressure and cleaved using TFA-water-TIS following the same method as described above. The solution was collected and concentrated in a continuous flow of nitrogen and the crude peptides were precipitated in diethylether. The resulting white solid was then purified to >98% in purity by a preparative HPLC. The absorbance of $Ph_2$-PEG-RGD (0.1 mM) was measured at 276 nm using a UV–visible spectrophotometer (U-2810, Hitachi, Japan) and was compared to that of HPA (0.1 mM).

### 6.2.4. Formation and rheological properties of hydrogels

HA-Tyr conjugates (final concentration: 1% (w/v)) were dissolved in PBS and mixed with HPA, $Ph_2$-K or $Ph_2$-PEG-RGD (final concentrations: 0.1, 0.2 or 0.3 mM). Then, 1.5 µl of HRP was added to 250 µl of the mixture solution (final concentration: 0.15 U/ml) and crosslinking was initiated by adding 1.5 µl of $H_2O_2$ solution (final concentration: 0.43 mM). Rheological measurements were performed with a HAAKE Rheoscope 1 rheometer (Karlsruhe, Germany) as described in Chapter 3 using a cone and plate geometry of 3.5 cm diameter and 1.029 cone angle. The measurement parameters were determined to be within the linear viscoelastic region in preliminary experiments.

### 6.2.5. Conjugation efficiency of HPA, $Ph_2$-K and $Ph_2$-PEG-RGD and water uptake of the resulting hydrogels

To determine the amount of HPA or $Ph_2$-K conjugated into the HA-Tyr network, the hydrogels were immersed in PBS overnight to allow the unconjugated phenolic compounds to diffuse out. Then UV absorbance of the PBS solution at 274 nm was recorded and the amount of $Ph_2$-K or HPA leached out from the hydrogel was calculated based on a standard curve of HPA. To determine the percentage of $Ph_2$-PEG-RGD conjugated into the hydrogel network, the hydrogels were immersed in PBS overnight and the amount of unconjugated $Ph_2$-PEG-RGD which had diffused out of the hydrogel into the PBS solution was measured by bicinchoninic acid (BCA) assay. For water uptake study, hydrogels were swollen in PBS for 24 h. The swollen disks were then gently blotted dry with Kimwipe and weighed. Water uptake was calculated from the equation $W=(M_s-M_d)/M_d$, where $M_s$ is the weight of the hydrogel in swollen state, and $M_d$ is the dry weight of the hydrogel after lyophilization.

### 6.2.6. Cell culture

Human umbilical vein endothelial cells (HUVECs) and endothelial growth medium (EGM-2) BulletKit were purchased from Lonza Bioscience Singapore. Human foreskin fibroblast (HFF-1) cells were obtained from ATCC (USA). HUVECs were maintained in EGM-2 BulletKit while fibroblasts were maintained in Dulbecco's modified Eagle's medium (DMEM) supplemented with 15% FBS and 1% penicillin/streptomycin. Both cell types were cultured in T75 tissue culture flasks and incubated at 37 °C in a 5% $CO_2$ atmosphere. The media was changed every 2–3 days and the cells were subcultured at 80% confluency. Fibroblasts and HUVECs with passages number below 8 were used in this study.

### 6.2.7. Cell attachment and proliferation on hydrogel surface (2D)

For *in vitro* and *in vivo* studies, HA-Tyr, $Ph_2$-PEG-RGD, HRP and $H_2O_2$ solutions were filtered through 0.2 µm syringe filters. To culture cells on the surface of hydrogels, the hydrogels were prepared in a 24 well-plate as described above and incubated for 4 h after the addition of HRP and $H_2O_2$. Then 250 µl of HUVEC ($1 \times 10^5$ cells/ml) in complete growth medium was added on the hydrogels. HA-Tyr hydrogel without RGD conjugation was prepared to serve as a comparison. The culture medium was changed every 2-3 days. To visualize the focal adhesion and actin cytoskeleton, the cells were cultured for 2 days before fixing with 4% formaldehyde solution at room temperature for 20 min. After washing, the

cells were permeabilized using 0.5% Triton X-100 in PBS solution at room temperature for 5 min then blocked in 0.05% Triton X-100 containing 1% bovine serum albumin at room temperature for 1 h. The samples were then incubated with anti-vinculin in blocking buffer solution at 4 °C overnight. After washing, the cells were incubated with the FITC-conjugated secondary antibody in the dark for 30 min. For double labeling, TRITC-conjugated phalloidin was incubated simultaneously with the secondary antibody. The cell nuclei were stained with DAPI (5 mg/ml stock solution diluted 1:15,000 in water). Confocal images were taken with a confocal laser scanning microscopy (Olympus FV300, Japan). For each sample, five regions of the hydrogel surface were randomly selected and the cell spreading area was estimated by ImagePro-Plus software.

To examine the effect of RGD conjugation on cell proliferation, the cells attached to the hydrogel surfaces were harvested by incubation overnight at 37 °C with 200 µl of hyaluronidase solution (50 U/ml). The amount of DNA was quantified by PicoGreen dsDNA reagent according to the manufacturer's protocol. Briefly, cell pellets were lysed by a freeze-thaw cycle in 200 µl of DNA-free lysis buffer. Samples were then incubated with 200 µl of PicoGreen working solution and the fluorescence intensity was measured ($\lambda_{ex}$ = 480 nm and $\lambda_{em}$ = 520 nm). Four replicates were performed for each sample and the number of cells in the sample was determined by comparing the fluorescence intensity to a set of standards of known cell concentrations.

### 6.2.8. Cell migration, proliferation, capillary network formation within the hydrogel (3D)

To access the migration of HUVEC in the hydrogels, HUVECs were pre-labeled with CellTracker Green CMFDA at 25 µM for 30 min. Then the cells were embedded (final cell density: $4 \times 10^6$ cells/ml) in hydrogels (final concentration of HA-Tyr: 1% (w/v)) with or without $Ph_2$-PEG-RGD (final concentration: 0.1 or 0.2 mM). The hydrogels were prepared on the apical side of FuoroBlok inserts. EGM-2 medium with fresh VEGF and FGF (2 ng/ml) were added to lower chamber to act as chemoattractants and replaced every 24 h. EGM-2 medium without growth factors was added to the inserts on top of the cell-laden hydrogels. At predetermined time intervals, fluorescence intensity on the basal side was measured using a microplate reader in bottom-reading mode ($\lambda_{ex}$ = 492 nm and $\lambda_{em}$ = 517 nm). The fluorescence intensity relative to 0 h for each sample was recorded. The experiments were

performed in four replicates. The morphology of fluorescently labeled cells was accessed using a fluorescence microscope (Olympus, Japan).

To determine the effect of RGD conjugation on HUVEC proliferation within the hydrogels, cell-laden hydrogels were prepared as described above. The culture medium was exchanged every 2-3 days. On selected days, the hydrogels were degraded by hyaluronidase and the cell number was determined by DNA quantification assay as described previously.

To determine the effects of RGD conjugation on vascular network formation within the hydrogels, both mono and co-culture of HUVECs and HFF-1 were examined. For monoculture, only HUVECs were embedded within the hydrogels (final cell density: $4 \times 10^6$ cells/ml). Two modes of co-culture were prepared, in the first mode, HUVECs were embedded within the hydrogel ($4 \times 10^6$ cells/ml) while HFF-1 were seeded on top of the hydrogel (2D HFF-1/3D HUVEC); in the second mode, both HUVECs and HFF-1 (1:1) were embedded within the hydrogel (mixed co-culture, final cell density: $4 \times 10^6$ cells/ml). On selected days, the hydrogels were fixed and stained with FITC-conjugated secondary antibody against CD31 antibody. Confocal images were taken with a confocal laser scanning microscopy and the average length of the capillary-like network was measured.

### 6.2.9. Formation of functional human vasculature in HA-Tyr-RGD hydrogels *in vivo*

Nonobese diabetic/severe combined immunodeficiency (NOD/SCID) mice (Biological Resource Center (BRC) in Biopolis, Singapore) aged 6-8 weeks were used for this study. The cell-laden hydrogel was prepared as described above with slight modifications. Briefly, HUVEC and HFF-1 (1:1) were mixed with HA-Tyr or HA-Tyr-RGD hydrogel precursor solution at a final cell density of $1 \times 10^6$ cells/ml in a volume of 250 µl. Immediately before injection, predetermined amount of HRP and $H_2O_2$ was added to the precursor solution and then one hundred µl of the solution was injected subcutaneously through a 22-gauge needle into the backs of mice. On day 14 after the injection, 100 µl of rhodamine-dextran solution (1.5% (w/v)) was injected into the mice *via* the tail vein to illuminate the newly formed vessels in the hydrogels. The hydrogels were then harvested and photographed. Next, the hydrogels were fixed with 4% paraformaldehyde for 24 h at 4 °C and then immersed in 30% sucrose solution overnight. Next day, the samples were embedded in OCT cryostat embedding medium (Tissue-Tek®, Sakura Finetek, USA). Cryostat sections were collected on silane-coated slides and stained with hematoxylin and eosin (H&E) or immunohistostained

with human nuclei antibody. Chromogenic detection was employed to visualize the stained nuclei in brown using HRP-DAB staining kit according to manufacturer's protocol. The care and use of laboratory animals was performed according to the approved protocol of the Institutional Animal Care and Use Committee (IACUC) at the BRC in Biopolis, Singapore.

### 6.2.10. Statistical analysis

All data were expressed as mean ± standard deviation (SD). Differences between the values were assessed using one-way analysis of variance (ANOVA) test using SigmaStat software (Systat Software, Inc.). In this analysis, $p < 0.05$ was considered statistically significant.

## 6.3. Results and discussion

### 6.3.1. Effects of *in situ* conjugation of phenol-containing compounds on hydrogel formation

In the study reported by Park *et al*., an endothelial cell binding sequence that terminated with a tyrosine residue (SVVYGLRGGY) was conjugated into gelatin-poly(ethylene glycol)-tyramine (GPT) hydrogel by the HRP-mediated coupling of the tyrosine residue with the tyramine moieties of GPT [5]. Peptide conjugation resulted in the decrease of G' when the feed concentration of the peptide was increased. The decrease in G' was attributed to the consumption of tyramine moieties as the peptides were incorporated into the hydrogel network, which reduced the amount of tyramine moieties available for the crosslinking reaction. We proposed that a peptide bearing two phenol moieties could potentially act as a crosslinker, minimizing the change in G' of the hydrogel by maintaining the amount of phenols available for crosslinking. To test this hypothesis, a model compound composed of a lysine residue flanked by two phenols ($Ph_2$-K) was synthesized (Fig. 6-2). The rheology of the hydrogels and the conjugation efficiency of $Ph_2$-K into the HA-Tyr hydrogel network were studied. 3-(4-Hydroxyphenyl) propionic acid (HPA) (Fig. 6-2), which contains only one phenol moiety per molecule, was used as a comparison.

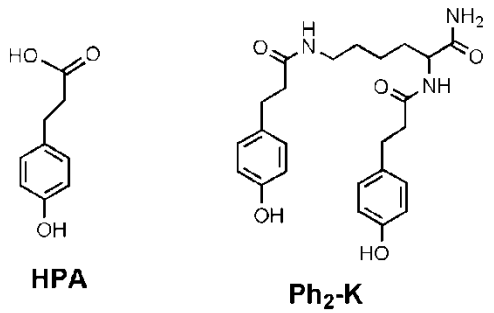


**Fig. 6-2. Chemical structures of HPA and $Ph_2$-K.**

When HPA was present in the HA-Tyr hydrogel system, the gel point (G' = G'') increased from 1.5 to 3.4 min as the feed concentration of HPA increased from 0.1 to 0.3 mM (Fig. 6-3a), indicating a decrease in gelation rate. Coupling between HPA and the tyramine moieties of the HA-Tyr conjugates reduced the number of tyramine moieties available for the crosslinking reaction; therefore the overall gelation rate decreased. Furthermore, the G' of the hydrogel decreased with increasing HPA feed concentration (Fig. 6-3b). In contrast, when $Ph_2$-K was added to the hydrogel system, the gel point remained below 1.5 min as the feed concentration of $Ph_2$-K increased from 0.1 to 0.3 M. The maintenance of gelation rate was attributed to the di-phenol structure of $Ph_2$-K. When one of the phenol moieties were coupled to HA-Tyr conjugates, the other phenol moiety would be available for crosslinking reaction. The G' of hydrogels decreased with increasing feed concentration of $Ph_2$-K. However, the G' values of $Ph_2$-K-conjugated hydrogels were higher than HPA-conjugated hydrogels at the same feed concentration. Water uptake results were in agreement with the G' values of the hydrogels (Fig. 6-3c). Hydrogels conjugated with the HPA had higher water uptake than the ones conjugated with $Ph_2$-K at the same feed concentration, indicating that the HPA-conjugated hydrogels had lower crosslink density.

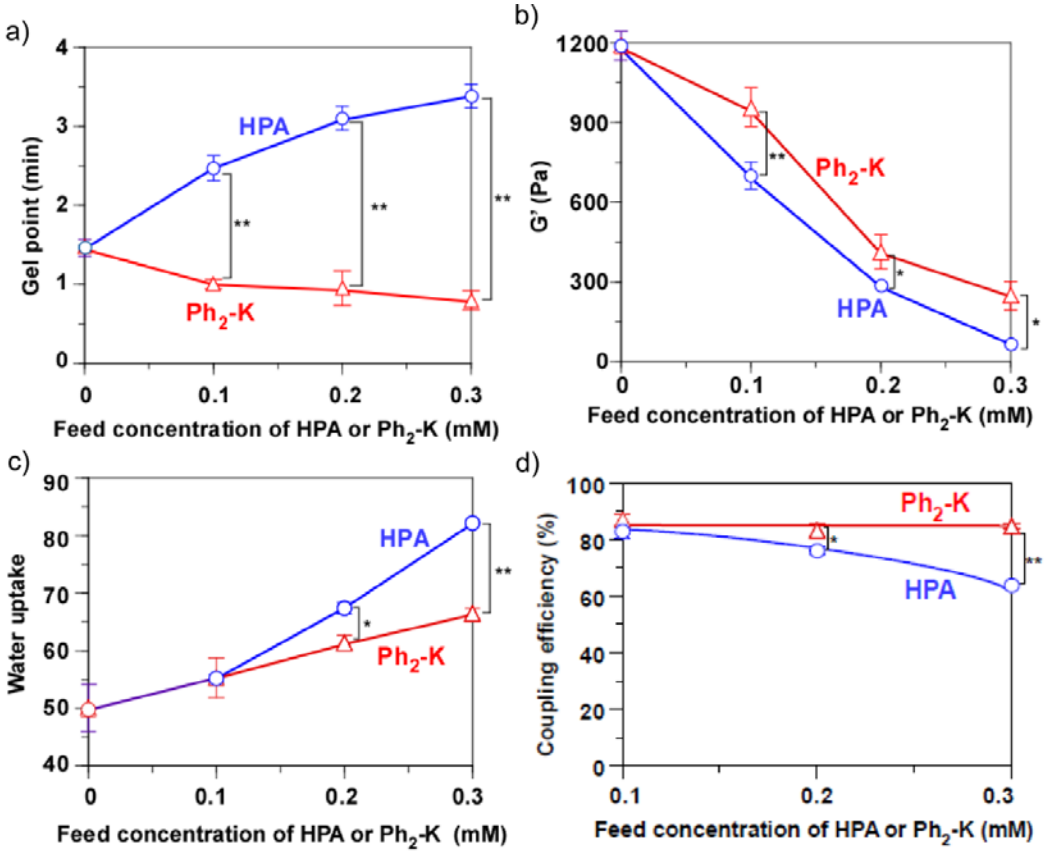


**Fig. 6-3. Effects of HPA or $Ph_2$-K feed concentration on (a) gel point, which is defined as the time at which the crossover of G' and G'' occurred, (b) G' and (c) water uptake of hydrogels. (d) Conjugation efficiency of HPA or $Ph_2$-K with different feed concentrations. All data is expressed as mean ± SD (n = 3). Difference between the values were assessed using one-way ANOVA . *$p$ < 0.05 and **$p$ < 0.01.**

Next, we examined the conjugation efficiency, defined as the percentage of the phenolic compound incorporated into the hydrogel network, of HPA and $Ph_2$-K. The conjugation efficiency decreased from 85% to 65% as the feed concentration of HPA increased from 0.1 to 0.3 mM (Fig. 6-3c). In contrast, the conjugation efficiency of $Ph_2$-K remained constant at 85%. The results indicated that $Ph_2$-K was more efficiently conjugated into the hydrogel network than HPA, which was likely due to the presence of two phenol moieties. Taken together, $Ph_2$-K was more efficiently conjugated into the HA-Tyr hydrogel network by HRP than HPA. Hydrogels conjugated with $Ph_2$-K had higher G' values and a more constant gelation rate compared to HPA-conjugated hydrogels. Therefore, a RGD peptide bearing two phenol moieties, $Ph_2$-PEG-RGD, was designed for the *in situ* conjugation into HA-Tyr hydrogels.

### 6.3.2. Synthesis and characterization of $Ph_2$-PEG-RGD

The molecular structure of $Ph_2$-PEG-RGD is shown in Fig. 6-4a. Its purity was found to be >98% as determined by HPLC (Fig. 6-4b). ESI-MS of the purified product showed peaks at m/z 487.4 for $[1]^{2+}$ and 973.5 for $[M+H]^+$, which further confirmed the successful synthesis of $Ph_2$-PEG-RGD (Fig. 6-4c). The phenol content of $Ph_2$-PEG-RGD was analyzed by UV-Vis absorbance spectroscopy. Between 250 and 280 nm, the absorbance value for $Ph_2$-PEG-RGD was approximately doubled to that of HPA at the same molar concentration. For example, at 276 nm (absorption maxima), the absorbance for $Ph_2$-PEG-RGD was 0.381 compared to 0.194 for HPA. This indicated that two HPA molecules were successfully inserted into $Ph_2$-PEG-RGD by amide bond formations between amine groups of lysine (K) residue and carboxyl groups of HPA.

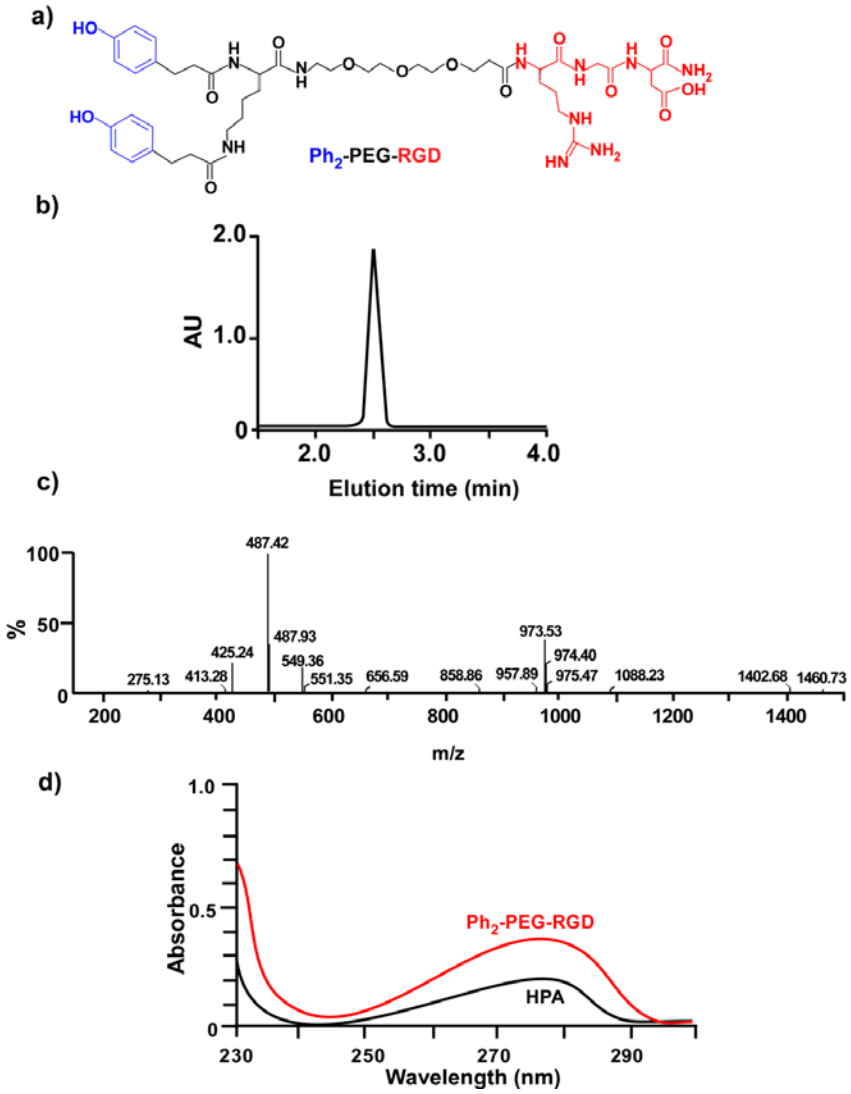


**Fig. 6-4. Synthesis and characterization of $Ph_2$-PEG-RGD. (a) Chemical structure, (b, c) LC-MS analysis, and (d) UV-VIS spectroscopy of $Ph_2$-PEG-RGD.**

### 6.3.3. Formation and characterization of HA-Tyr-RGD hydrogels

HA-Tyr-RGD hydrogels consisting of HA-Tyr and $Ph_2$-PEG-RGD were formed *via* the enzymatic coupling of phenol moieties catalyzed by HRP and $H_2O_2$ (Fig. 6-1). RGD peptide motifs were simultaneously conjugated into the hydrogel network during the gel formation process. Hydrogels without $Ph_2$-PEG-RGD, with 0.1 or 0.2 mM feed concentrations of $Ph_2$-PEG-RGD were abbreviated as HA-Tyr, HA-Tyr-RGD-0.1 and HA-Tyr-RGD-0.2, respectively. The conjugation efficiency of $Ph_2$-PEG-RGD was 74 and 71% for HA-Ty-RGD-0.1 and HA-Tyr-RGD-0.2, respectively (Table 6-1). Similar to the observations made from the test compound, $Ph_2$-K, the G' of the hydrogels decreased, and the water uptake increased, when the feed concentration of $Ph_2$-PEG-RGD was increased from 0 to 0.2 mM. The gel point of the hydrogels did not change significantly when the RGD feed concentration was increased from 0.1 to 0.2 mM.

**Table 6-7.** Preparation and characterization of HA-Tyr-RGD hydrogels[a]

| Sample | $Ph_2$-PEG-RGD (mM) | Conjugation efficiency of $Ph_2$-PEG-RGD (%) | G' (Pa) | Gel point (min)[b] | Water uptake |
|---|---|---|---|---|---|
| HA-Tyr | 0 | - | 1215 ± 31 | 1.6 ± 0.3 | 51.8 ± 3.4[c] |
| HA-Tyr-RGD-0.1 | 0.1 | 74±4 | 941 ± 152 | 1.3 ± 0.2 | 53.8 ± 0.7[c] |
| HA-Tyr-RGD-0.2 | 0.2 | 71±3 | 532 ± 36 | 1.3 ± 0.1 | 61.4 ± 1.1 |

[a]All hydrogels were prepared using 10 mg/ml of HA-Tyr conjugates, 0.15 U/ml of HRP and 0.43 mM of $H_2O_2$. Measurements were taken with constant deformation of 1% at 1Hz and 37 $^oC$. Results are shown as mean ± SD (n = 4). [b]Gel point is defined as the time at which the crossover of storage modulus (G') and loss modulus (G'') occurred. Herein, it is used as an indicator of the rate of gelation. [c]$p < 0.05$ when compared to the value of water uptake calculated for HA-Tyr-RGD-0.2

### 6.3.4. Effect of the RGD conjugation on HUVEC attachment and proliferation on hydrogel surfaces

The effects of $Ph_2$-PEG-RGD conjugation into HA-Tyr hydrogels on cell attachment and proliferation were examined. Fig. 6-5a shows the confocal fluorescence images of vinculin (green) and F-actin (red) in HUVECs (nuclei in blue) seeded on the hydrogels. The cells on HA-Tyr hydrogel were round, indicating that the unmodified gel could not support cell adhesion. In contrast, the cells adhered well on the surface of HA-Tyr-RGD hydrogels with a spread-out morphology. Moreover, the focal contact and F-actin organization of cells attached on HA-Tyr-RGD hydrogels were found to be diffused, which corresponded to previous observations of cells attached on soft substrates (G' = 0.6-2.5 kPa) [13].

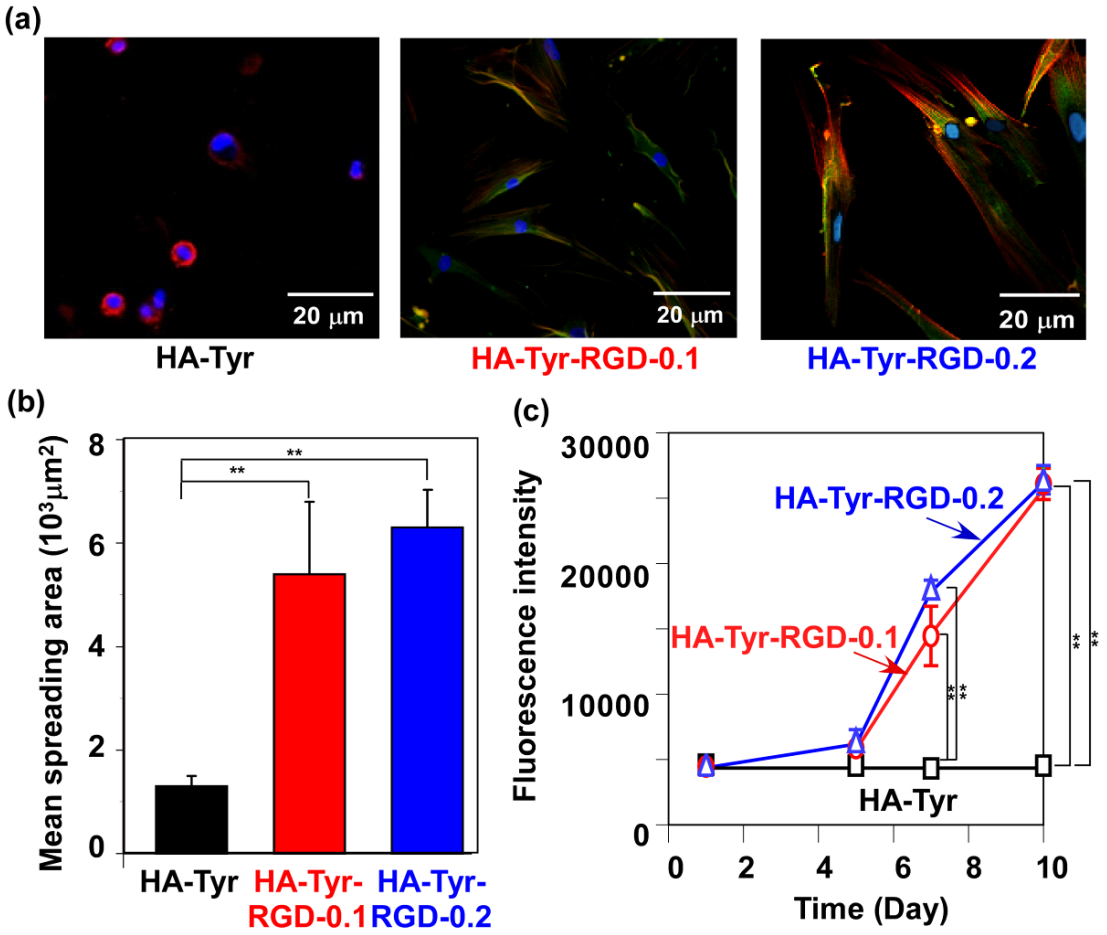


**Fig. 6-22. Attachment and proliferation of HUVECs on hydrogel surfaces. Hydrogels formed with $Ph_2$-PEG-RGD (0.1 mM or 0.2 mM) are abbreviated as HA-Tyr-RGD-0.1 and HA-Tyr-RGD-0.2, respectively. (a) Confocal fluorescence microscopy of focal adhesion and actin cytoskeleton. Vinculin, F-actin, cell nuclei were labeled green, red and blue, respectively. (b) Spreading area of HUVEC on HA-Tyr and HA-Tyr-RGD hydrogels after 24 h incubation. (c) HUVEC proliferation on the hydrogels. Results are shown as mean ± SD (n = 4). **$p < 0.01$.**

The cell spreading area was quantified using ImagePro-Plus software. The average cell spreading area of HUVECs on HA-Tyr-RGD hydrogels was four times higher (Fig. 6-5b) than the cells on unmodified HA-Tyr hydrogels. This indicated that conjugation of RGD significantly improved the cell-adhesive property of HA-Tyr hydrogels. Moreover, the improved cell adhesion led to a steady cell growth as shown in Fig. 6-5c. No statistically significant difference in cell spreading area and cell proliferation was observed between HA-Tyr-RGD-0.1 and HA-Tyr-RGD-0.2.

### 6.3.5. Effects of RGD conjugation on HUVEC migration in 3D

Fluorescence-labeled HUVECs were embedded in HA-Tyr-RGD hydrogels *in situ* by HRP and $H_2O_2$, and the migration of HUVECs from hydrogels was investigated using a Transwell® system as shown in Fig. 6-6a. The fluorescence intensity on the basal side of the insert, which correlated to the number of cells migrated out of the hydrogel and through the membrane, was recorded over a period of 48 h. Cells remained rounded in HA-Tyr hydrogels (Fig. 6-6b-i), but exhibited a more elongated morphology in HA-Tyr-RGD hydrogels (Fig.6-6b-ii and iii). Moreover, the number of cells migrated out of the hydrogels and through the membrane was significantly increased by the conjugation of RGD (Fig. 6-6b-iv, v and vi). The number of cells that migrated through the membrane increased with time, with the cells embedded in HA-Tyr-RGD hydrogels migrated more quickly compared to the cells in HA-Tyr hydrogels (Fig. 6-6c).

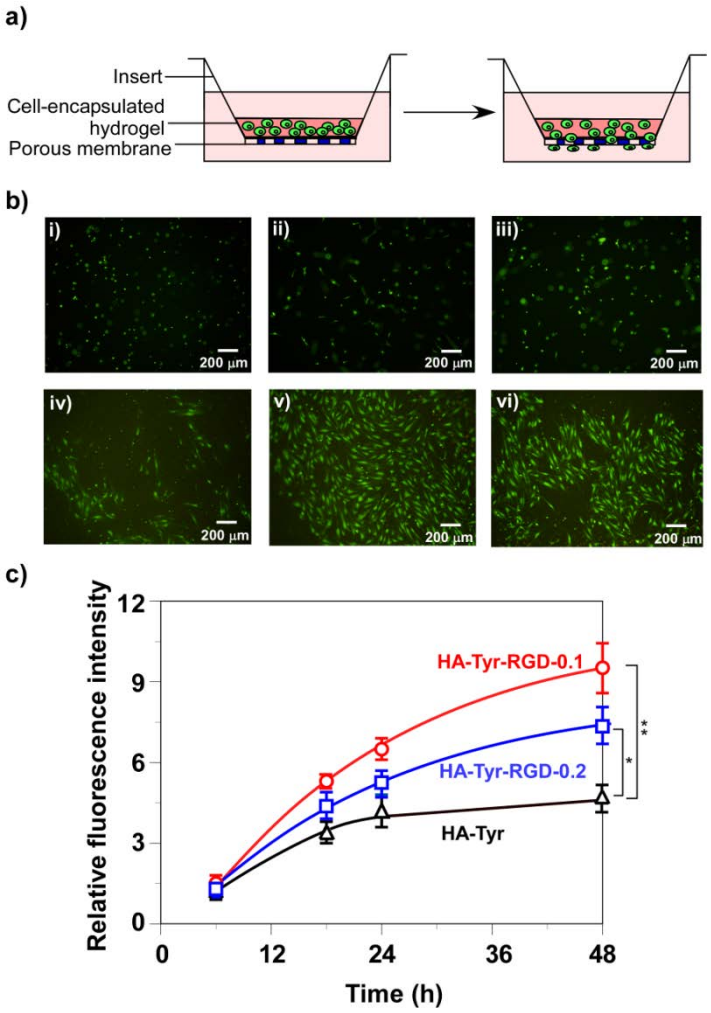


**Fig. 6-23. Migration of HUVECs in hydrogels. (a) Schematic illustration of migration study *in vitro*. (b) Representative fluorescence images of CellTracker™-labeled cells that remained in i) HA-Tyr, ii) HA-Tyr-RGD-0.1 and iii) HA-Tyr-RGD-0.2 hydrogels, or migrated through FluoroBlok membrane from iv) HA-Tyr, v) HA-Tyr-RGD-0.1 and vi) HA-Tyr-RGD-0.2 hydrogels at 24 h. (c) Fluorescence intensity**

**(relative to 0 h) of fluorescently-labeled HUVECs which had migrated through FluoroBlok membrane. Results are shown as mean ± SD *$p$ < 0.05 and **$p$ < 0.01 between groups (n = 4).**

### 6.3.6. Effects of RGD conjugation on HUVEC proliferation and capillary-like network formation within the hydrogels

HUVECs failed to proliferate in the unmodified HA-Tyr hydrogels. However, cell proliferation was observed during the first week of culture in RGD-modified hydrogels (Fig. 6-7). There was no significant difference in cell proliferation between the HA-Tyr-RGD-0.1 and HA-Tyr-RGD-0.2 ($p$ > 0.05). A decline in cell number was observed in the HA-Tyr-RGD hydrogels when the culture was extended beyond 1 week for both RGD-modified hydrogels.

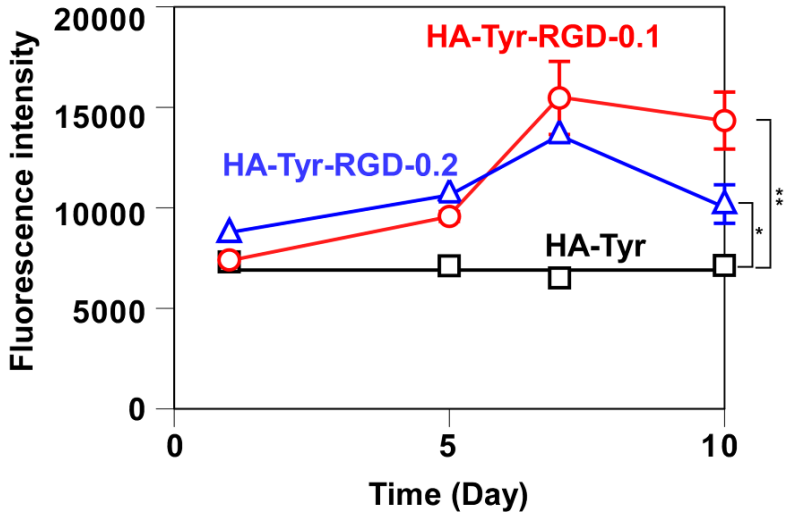


**Fig. 6-24. HUVEC proliferation in HA-Tyr and HA-Tyr-RGD hydrogels. Results are shown as mean ± SD *$p$ < 0.05 and **$p$ < 0.01 between groups (n = 6).**

Previous studies have reported that HUVECs alone was not sufficient to form stable capillary-like network, and fibroblasts and/or fibroblast-derived factors were essential in facilitating the formation and stability of capillary-like network [14, 15]. Hence, HUVECs were co-cultured with human fibroblasts (HFF-1) in the HA-Tyr-RGD hydrogels for the purpose of forming stable capillary-like networks. HA-Tyr-RGD-0.1 was used in this study and HA-Tyr hydrogel was used as a control. As shown in Fig. 6-8a, cells remained rounded in HA-Tyr hydrogels. In contrast, cells were elongated in HA-Tyr-RGD-0.1 hydrogels, and cell-cell contacts that resemble capillary structures were observed (inset of Fig 6a-iii). To ascertain that the endothelial cells were capable of forming capillary-like network in the HA-Tyr-RGD hydrogels, anti-CD31 antibody was used to label the HUVECs. The results clearly

demonstrated that the capillary-like network was composed of CD31-positive HUVECs (Fig. 6-8a-iv).

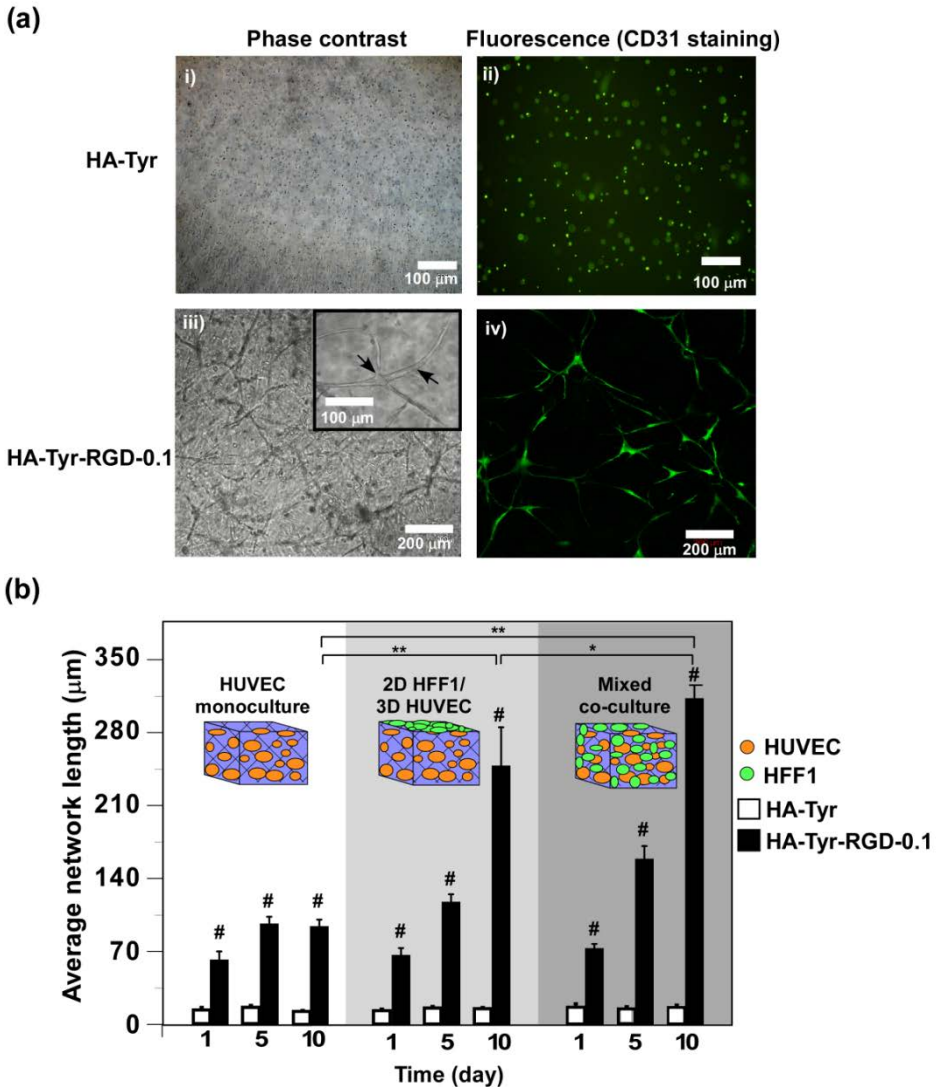


**Fig. 6-25. Formation of vascular network in the hydrogels. (a) Representative microscopic and fluorescence images of mixed co-culture of HFF-1 and HUVEC in HA-Tyr (i and ii) and HA-Tyr-RGD-0.1 hydrogels (iii and iv), respectively. Capillary-like structure with branches (black arrows) was found in HA-Tyr-RGD-0.1 hydrogels (inset in iii). Fluorescence images were acquired by labeling HUVECs with CD31 antibody. (b) Length of HUVEC capillary-like tube formed inside HA-Tyr and HA-Tyr-RGD hydrogels in three different culture modes, namely monoculture of HUVEC, 2D HFF-1/3D HUVEC and mixed co-culture of HFF-1 and HUVEC. Results are shown as mean ± SD *$p$ < 0.05 and **$p$ < 0.01 between groups, #$p$ < 0.01 when compared to the HA-Tyr group at the same experimental condition (n=6).**

Next, the effects of culture modes on HUVEC capillary-like network formation were examined. The different culture modes were monoculture, 3D culture of HUVEC with HFF-1 on the surfaces of the hydrogels (2D HFF-1/3D HUVEC), and mixed co-culture (Fig. 6-8b).

The unmodified HA-Tyr did not support the formation of the capillary-like network in 3D regardless of the culture mode. In contrast, HA-Tyr-RGD hydrogels supported capillary-like network formation, and the network length increased with time in the 2D HFF-1/3D HUVEC as well as mixed co-culture modes, but not in the monoculture mode. The network length in the mixed co-culture modes was significantly greater at the end of 10 days than in the monoculture mode ($p < 0.01$). Moreover, between the two co-culture modes, the mixed co-culture mode was found to be superior than 2D HFF-1/3D HUVEC in promoting capillary network formation and a significantly greater network length was obtained after 10 days ($p < 0.05$). This was likely due to a closer proximity between the cells, hence a better diffusion of growth factors and cellular crosstalk. The finding was also observed in a previous report in which capillary network formation was enhanced when fibroblasts were distributed throughout the fibrin gel to overcome the diffusion restriction [16].

### 6.3.7. *In vivo* vascularization of injectable HA-Tyr-RGD hydrogels

To evaluate the effect of RGD conjugation and co-culture of HUVEC and HFF-1 on the vascularization of hydrogels *in vivo*, HA-Tyr-RGD-0.1 hydrogels embedded with HUVEC alone, or a mixture of HUVEC and HFF-1 (1:1), were injected into the subcutaneous tissue of mice (Fig. 6-9a). Unmodified HA-Tyr hydrogel containing HUVEC and HFF-1 was used as a comparison. Fourteen days after the injection, rhodamine-dextran was injection *via* tail-vein and the hydrogels were harvested. Upon visual inspection, vascular structures were observed in the RGD-modified hydrogels but not in the unmodified HA-Tyr hydrogels (Fig. 6-9b). The results indicated that RGD conjugation was crucial in promoting vascularization of HA-Tyr hydrogels. Furthermore, a higher vessel density was observed in the HA-Tyr-RGD-0.1 hydrogel containing HUVEC and HFF-1 than in the hydrogel containing HUVEC alone, which underlines the importance of fibroblasts in promoting vascular formation. When the HA-Tyr-RGD-0.1 hydrogels were observed using a fluorescence microscopy, fluorescence was detected in the HA-Tyr-RGD hydrogels, indicating the presence of rhodamine-dextran (Fig. 6-9c, top row). No fluorescence was detected in the unmodified HA-Tyr hydrogels. H&E staining showed the presence of red blood cells, which were stained intensely red, in the HA-Tyr-RGD hydrogels but not in the unmodified HA-Tyr hydrogels (Fig. 6-9c, second row). The location of red blood cells observed in H&E staining corresponded to the location of fluorescent rhodamine-dextran. Immunohistochemistry analysis further confirmed that the vasculature was composed of cells of human origin (Fig. 6-9d, last row). Taken together, it

was evident that the *in situ* conjugation of $Ph_2$-PEG-RGD by HRP and the embedding of HUVECs facilitated the formation of functional vasculatures in HA-Tyr hydrogels.

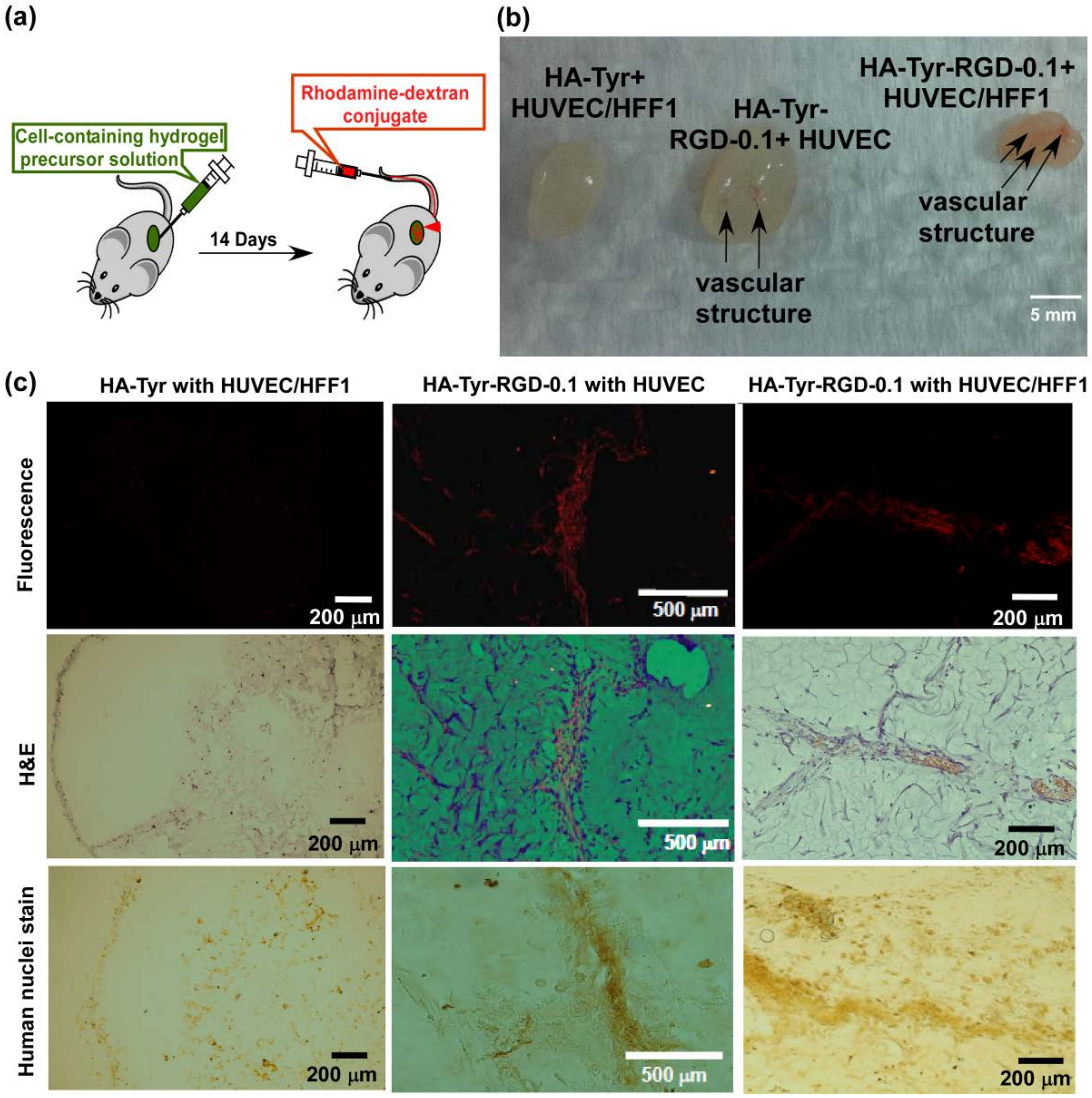


**Fig. 6-26. Effects of RGD conjugation on the formation of functional human vasculature *in vivo*. (a) Schematic representation of the experiment. (b) Photographic views of the harvested hydrogels. (c) Fluorescence images, H&E staining and immunostaining for human nuclei of hydrogel sections.**

## 6.4. Conclusions

A RGD peptide containing two phenol moieties ($Ph_2$-PEG-RGD) was synthesized for *in situ* conjugation into the HA-Tyr hydrogels by HRP. The resulting HA-Tyr-RGD hydrogels showed significant improvements in HUVEC adhesion, proliferation, migration, as well as capillary-like network formation *in vitro*. Moreover, functional vasculature was formed in HA-Tyr-RGD hydrogels that contained HUVECs. Vascularization was further improved when fibroblasts were embedded together with HUVECs in the hydrogels. The *in situ*

conjugation of RGD peptides by the enzymatic activity of HRP can be applied to introduce other bioactive peptides into HA-Tyr hydrogels for tissue engineering applications.

**References**

[1] Bidarra SJ, Barrias CC, Fonseca KB, Barbosa MA, Soares RA, Granja PL. Injectable in situ crosslinkable RGD-modified alginate matrix for endothelial cells delivery. Biomaterials 2011;32:7897-904.

[2] Shu XZ, Ghosh K, Liu YC, Palumbo FS, Luo Y, Clark RA, Prestwich GD. Attachment and spreading of fibroblasts on an RGD peptide-modified injectable hyaluronan hydrogel. J. Biomed. Mater. Res. A 2004;68A:365-75.

[3] Schense JC, Bloch J, Aebischer P, Hubbell JA. Enzymatic incorporation of bioactive peptides into fibrin matrices enhances neurite extension. Nat. Biotechnol. 2000;18:415-9.

[4] Oliviero O, Ventre M, Netti PA. Functional porous hydrogels to study angiogenesis under the effect of controlled release of vascular endothelial growth factor. Acta Biomater. 2012;8:3294-301.

[5] Park KM, Lee Y, Son JY, Bae JW, Park KD. In Situ SVVYGLR Peptide Conjugation into Injectable Gelatin-Poly(ethylene glycol)-Tyramine Hydrogel via Enzyme-Mediated Reaction for Enhancement of Endothelial Cell Activity and Neo-Vascularization. Bioconjug. Chem. 2012;23:2042-50.

[6] Suri S, Schmidt CE. Photopatterned collagen-hyaluronic acid interpenetrating polymer network hydrogels. Acta Biomater. 2009;5:2385-97.

[7] Lee F, Kurisawa M. Formation and stability of interpenetrating polymer network hydrogels consisting of fibrin and hyaluronic acid for tissue engineering. Acta Biomater. 2013;9:5143-52.

[8] Seidlits SK, Drinnan CT, Petersen RR, Shear JB, Suggs LJ, Schmidt CE. Fibronectin-hyaluronic acid composite hydrogels for three-dimensional endothelial cell culture. Acta Biomater. 2011;7:2401-9.

[9] Park YD, Tirelli N, Hubbell JA. Photopolymerized hyaluronic acid-based hydrogels and interpenetrating networks. Biomaterials 2003;24:893-900.

[10] Lei Y, Gojgini S, Lam J, Segura T. The spreading, migration and proliferation of mouse mesenchymal stem cells cultured inside hyaluronic acid hydrogels. Biomaterials 2011;32:39-47.

[11] Lutolf MP, Lauer-Fields JL, Schmoekel HG, Metters AT, Weber FE, Fields GB, Hubbell JA. Synthetic matrix metalloproteinase-sensitive hydrogels for the conduction of tissue regeneration: engineering cell-invasion characteristics. Proc. Natl. Acad. Sci. U. S. A. 2003;100:5413-8.

[12] Yu J, Gu Y, Du KT, Mihardja S, Sievers RE, Lee RJ. The effect of injected RGD modified alginate on angiogenesis and left ventricular function in a chronic rat infarct model. Biomaterials 2009;30:751-6.

[13] Wang L-S, Boulaire J, Chan PPY, Chung JE, Kurisawa M. The role of stiffness of gelatin-hydroxyphenylpropionic acid hydrogels formed by enzyme-mediated crosslinking on the differentiation of human mesenchymal stem cell. Biomaterials 2010;31:8608-16.

[14] Sukmana I, Vermette P. The effects of co-culture with fibroblasts and angiogenic growth factors on microvascular maturation and multi-cellular lumen formation in HUVEC-oriented polymer fibre constructs. Biomaterials 2010;31:5091-9.

[15] Eckermann CW, Lehle K, Schmid SA, Wheatley DN, Kunz-Schughart LA. Characterization and modulation of fibroblast/endothelial cell co-cultures for the in vitro preformation of three-dimensional tubular networks. Cell Biol. Int. 2011;35:1097-110.

[16] Ghajar CM, Chen X, Harris JW, Suresh V, Hughes CCW, Jeon NL, Putnam AJ, George SC. The effect of matrix density on the regulation of 3-D capillary morphogenesis. Biophys. J. 2008;94:1930-41.

# Chapter 7

# Enzymatically Crosslinked Hyaluronic Acid-Tyramine Hydrogel as a 3D Culture System for Controlled Propagation of Human Embryonic Stem Cells

## 7.1. Introduction

Human embryonic stem cells (hESCs) have unlimited self-renewal capability in the pluripotent state [1], and they can differentiate into specialized cell types when stimulated with appropriate growth factors and/or chemical stimuli [2-6]. Thus hESCs are an ideal cell source for tissue engineering and regenerative medicine. Currently, the propagation of hESCs *in vitro* requires the use of either mouse embryonic fibroblasts (MEF) as feeder cells [7], or feeder-free extracellular matrix (ECM) such as Matrigel (a basement membrane extracted from Engelbreth-Holm-Swarm mouse sarcoma) [8-10]. These methods of hESC propagation are not suitable for large-scale production and clinical applications due to the requirement of animal-derived components. Therefore, the controlled propagation of hESCs without animal-derived components remains a challenge. Recently, synthetic substrates with chemically defined compositions have been employed for the long-term self-renewal of human pluripotent stem cells [11-16]. However, stem cells that have been cultivated on 2D surfaces (i.e. petri-dish) need to adjust to the 3D environment after transplantation to the body, which may leads to variability in the therapeutic outcome [17]. Thus, 3D propagation systems for hESCs are preferred as they could facilitate convenience in transplantation and consistency in cell performance. In addition, 3D cultivation shows higher scalability in terms of cell numbers than 2D systems [18].

Hydrogels have been used as 3D systems for hESC propagation [19]. By attaching appropriate biomolecular clues on the polymeric networks, hydrogels could provide a 3D microenvironment that mimics the stem cell niche during embryogenesis [20]. Among the natural or synthetic hydrogel scaffolds that have been reported [21-28], hyaluronic acid (HA)-based hydrogels have attracted much interests. HA is a major constituent during early embryogenesis [29], and regulates proliferation, adhesion, metastasis and morphogenesis of hESCs [30]. HA-based photo-crosslinked hydrogels have been shown to support the undifferentiated proliferation of hESCs in conditioned medium from MEF, and retain the ability of the cells to differentiate after releasing from the hydrogels [24]. However, the effect of hydrogel stiffness on 3D cultivation of hESCs has yet to be examined. Furthermore, it is critical to use chemically-defined medium for 3D propagation of hESCs in order to meet the safety requirement for clinical applications.

In this chapter, the enzymatically crosslinked hyaluronic acid-tyramine (HA-Tyr) hydrogel system [31-33] was used for the encapsulation and propagation of hESCs together

with a chemically defined medium (Fig. 1). The advantage of HA-Tyr hydrogel system is the facile tuning of crosslink density and gelation rate, which is achieved by controlling the concentrations of $H_2O_2$ and HRP, respectively [34]. In addition, the hydrogel networks can be slowly degraded by hyaluronidase *in vivo*, leading to a smooth integration of the implants into the host tissue. The viability, proliferation and pluripotency of hESCs cultured in HA-Tyr hydrogels of different stiffness were studied and compared. Then, hESCs expanded in HA-Tyr hydrogels with compressive modulus (E) of 350 Pa were further characterized by histology, immunostaining and the expression of CD44. The ability of the released hESCs to differentiate into cells of the three different germ layers was investigated *in vitro* and *in vivo*. Finally, the genetic integrity of hESCs propagated in HA-Tyr hydrogels was characterized.

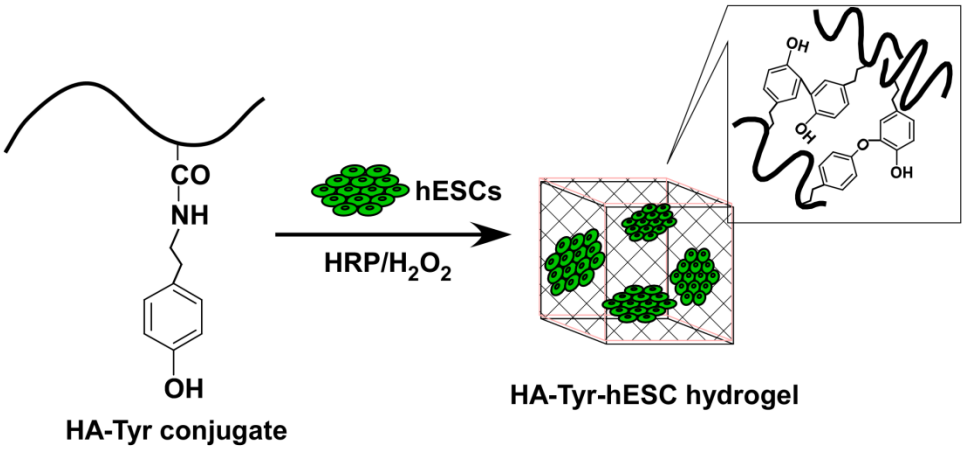


**Fig. 7-1. Schematic illustration of encapsulation of human embryonic stem cells (hESCs) in HA-Tyr hydrogels.**

## 7.2. Materials and methods

### 7.2.1. Materials

Sodium hyaluronate (HA) (MW = 90 kDa, density = 1.05 g/cm3) was kindly donated by JNC Corporation (Tokyo, Japan). Dextran (MW = 500 kDa), hydrogen peroxide ($H_2O_2$) and hyaluronidase (439 U/mg) from bovine testes were purchased from Sigma-Aldrich (Singapore). Horseradish peroxidase (HRP, 100 U/mg) was obtained from Wako Pure Chemical Industries (Osaka, Japan). Dulbecco's phosphate-buffered saline (DPBS), Hank's balanced saline solution (HBSS), Dulbecco's modified eagle medium (DMEM) and fetal bovine serum (FBS) were obtained from Life Technologies, Singapore. Hyaluronic acid-tyramine (HA-Tyr) [34] and dextran-tyramine (Dex-Tyr) [35] conjugates were synthesized as

described previously. The degree of substitution (DS) was determined by $^{1}H$ NMR. The DS (the number of tyramine molecules per 100 repeating units of HA) for HA-Tyr conjugates was 6. The DS (the number of tyramine molecules per 100 saccharide units of dextran) for Dex-Tyr conjugates was 1.3.

### 7.2.2. Maintenance of hESCs in feeder free condition

Human embryonic stem cell H1 (hESC) was purchased from WiCell (WI, USA) and maintained on a 60 mm dish pre-coated with Matrigel (hESCs qualified, BD Biosciences, USA) in chemically defined medium mTeSR1 (STEMCELL Technologies, Singapore). The hESCs were fed once a day with fresh pre-warmed medium and routinely passaged every 5 to 6 days.

### 7.2.3. Encapsulation and 3D culture of hESCs in HA-Tyr hydrogels

When the cells reached 80-90% confluency on Matrigel, the hESCs were treated with dispase I (STEMCELL Technologies, Singapore) for 7 min, washed with DPBS and scored with a P1000 micropipette in a grid-like pattern. The cell clumps were scraped and collected. A small portion of cells were treated with Accutase (STEMCELL Technologies, Singapore) for cell counting. The remaining cells were washed with DPBS and suspended in 1% (w/v) HA-Tyr solution at a concentration of 1 million cells per milliliter. HA-Tyr hydrogels were formed after HRP and $H_2O_2$ of varying concentrations were added. Similarly, the Dex-Tyr hydrogels were prepared by mixing Dex-Tyr solution (1.5% (w/v)) with HRP and $H_2O_2$. Hydrogels containing 100,000 hESCs in 100 µl were prepared in the inserts of 24-well plate, which were then submerged in mTeSR1 medium and fed once a day with fresh media. After 6–8 days, hESCs were harvested from HA-Tyr hydrogels. Briefly, hyaluronidase in HBSS (1000 U/ml) was utilized to degrade the HA-Tyr hydrogels in 2–4 h. The released hESCs can be encapsulated in HA-Tyr hydrogels again as the second passage. Up to five passages for hESCs have been studied for HA-Tyr hydrogels. In the case of Dex-Tyr hydrogels, the cells were retrieved by incubating the hydrogels in HBSS with dextranase (50 U/ml) for 4 h.

### 7.2.4. Characterization of HA-Tyr hydrogels encapsulating hESCs

Rheological measurements of the hydrogels were performed as described in Chapter 3 using a HAAKE Rheoscope 1 rheometer (Karlsruhe, Germany) equipped with a cone and plate geometry (3.5 cm diameter and 0.949° cone angle). Measurements were taken at 37 °C

in dynamic oscillatory mode with a constant deformation of 1% and frequency of 1 Hz. Rheological measurement was allowed to proceed until the storage modulus (G') reached a plateau.

Compression tests of the hydrogels were performed with Instron microtester (Model 5848P8600). Cylinder shaped hydrogels were prepared with a plastic mold, and gel dimensions were measured with calipers. Compression test was carried out with a compression module. A 50 N load cell was used with a compressive strain rate of 1 mm/min and no preload. Compressive modulus (E) was determined using the slope of the stress versus strain curve at low strains (< 20%).

For swelling ratio measurement, disk-shaped hydrogels of 1 mm thickness were prepared between two parallel glass plates clamped together with 1 mm spacing. The hydrogels were swollen in 20 ml of DPBS for 24 h and weighed ($M_s$). After lyophilization, the dried weight was measured ($M_d$). The mass swelling ratio ($Q_M$) was calculated by dividing $M_s$ with $M_d$.

### 7.2.5. Viability and proliferation of hESCs in HA-Tyr hydrogels

Calcein AM (Life Technologies, Singapore) was used to determine the viability of hESCs in the hydrogels. One, four and seven days after cell encapsulation, the hydrogels were subjected to live-dead staining with a solution of calcein AM (2 µg/ml) and propidium iodide (PI) (1 µg/ml) in mTeSR1 medium. The hydrogels were washed with DPBS three times and the fluorescence of cell clusters was observed by a confocal laser scanning microscope (Zeiss LSM 5 DUO).

CyQuant® cell proliferation assay (Life Technologies, Singapore) was utilized to study the proliferation of hESCs in the hydrogels. Briefly, hydrogels encapsulated with hESCs were prepared in 24-well plates in triplicates. After 1, 4 and 7 days of culture, the hydrogels were degraded by hyaluronidase, and hESCs were collected and stored at -80 °C. Cell lysates were prepared by adding assay lysis buffer (200 µl) to the cells. Five µl of the cell lysate was added into 210 µl of dye/lysis buffer. The fluorescence of the mixture was measured by Infinite M200 (Tecan, Switzerland) with excitation and emission wavelengths of 480 nm and 520 nm, respectively. The cell number in each sample was calculated based on a standard curve of fluorescence intensity against known concentration of cells.

### 7.2.6. Histological examination of hESCs in HA-Tyr hydrogels

HA-Tyr hydrogel-encapsulated hESCs were prepared in transwells in a 24-well plate. After 7 days of culture, hydrogels in transwells were embedded in OCT and sectioned. The sections were stained with hematoxylin & eosin (H&E). Antibody against Ki67 (cat # NCL-Ki67-MM1, NOVOcastra, UK) and secondary antibody anti-mouse HRP conjugate (NOVOcastra, UK) were used for Ki 67 staining. Terminal deoxynucleotidyl transferase dUTP nick end labeling (TUNEL) apoptosis detection kit (Millipore, Singapore) was used to stain apoptotic cells. Samples were observed in bright field using an Olympus microscope IX71 and analyzed by the software Image-Pro Plus.

### 7.2.7. Expression of CD44 and pluripotency markers of hESCs cultured in HA-Tyr hydrogels

To measure the CD44 expression of hESCs in HA-Tyr hydrogels, hESCs were retrieved from HA-Tyr hydrogel by enzymatic degradation. Single cell suspension was prepared by treating the cell clusters with TrpLE$^{TM}$ Express (Life Technologies, Singapore). Then the cells were counted and incubated with APC-conjugated CD44 antibody (BD Bioscience, Singapore) at r.t. for 15 min. The labelled cells were analyzed by a BD LSR II flow cytometer (BSF, Biopolis, Singapore).

To determine the expression of pluripotency markers, cells retrieved from hydrogels at passage 1 (P1) and passage 5 (P5) were dissociated with Accutase at 37 °C for 10 min. Then the cell suspension was passed through a 40 μm nylon membrane and labelled with antibodies (Table 7-1). The labelled cells were analyzed by a BD LSR II flow cytometer. At least 10,000 events were recorded and data were analyzed by FlowJo (Treestar, USA).

**Table 7-1.** List of antibodies for immunocytochemistry and flow cytometry

| Antibody | Type | Vendor | Dilution |
|---|---|---|---|
| Nanog | Polyclonal | Santa Cruz | 1:200 |
| Oct-4 | Monoclonal | Santa Cruz | 1:200 |
| Sox-2 | Monoclonal | Abcam | 1:200 |
| SSEA-4 | Monoclonal | Millipore | 1:200 |
| TRA-1-60 | Monoclonal | Millipore | 1:200 |
| TRA-1-81 | Monoclonal | Millipore | 1:200 |
| Nanog | Alexa Fluor® 488 conjugated | Millipore | 1:50 |
| Oct-4 | Alexa Fluor® 488 conjugated | Millipore | 1:50 |
| Sox-2 | FITC-conjugated | Millipore | 1:50 |
| Smooth muscle actin (SMA) | Monoclonal | LabSource | 1:100 |
| Foxa2 | Monoclonal | Abcam | 1:200 |
| βIII-tubulin | Monoclonal | Millipore | 1:200 |

### 7.2.8. Immunofluorescence staining of pluripotency markers of hESCs cultured in HA-Tyr hydrogels

After 7 days of culturing hESCs in HA-Tyr hydrogels, the hydrogels were degraded by hyaluronidase to retrieve the hESCs clusters. Cell clusters were plated on Matrigel and cultured for 3 days. Then the cells were fixed with 4% formaldehyde and immunostained as reported previously [36]. The primary antibodies used were listed in Table 7-1. The secondary antibodies were Alexa Fluor 488/568 anti-mouse and anti-rabbit secondary antibodies (Life Technologies, Singapore). The samples were observed with a Zeiss LSM 510 confocal microscope and processed with LSM image browser software.

### 7.2.9. Real-time PCR analysis of pluripotency markers of hESCs cultured in HA-Tyr hydrogels

HA-Tyr hydrogels encapsulated with hESCs were prepared in 24-well plates. After 7 days, cells were released from the hydrogels. Total RNA was isolated using Trizol reagent (Life Technologies, Singapore) according to manufacturer's instructions. The isolated RNAs were treated with DNase (Promega, Singapore) to remove genomic DNA, and then reverse transcribed with random hexamers (Fermentas, Singapore) as primers. Real-time PCR (RT-PCR) was performed by an iQ5 Real-Time PCR System (Bio-Rad) using TaqMan® Gene Expression assays (Life Technologies, Singapore) for Oct-4, Sox-2, Nanog and GAPDH.

### 7.2.10. Spontaneous differentiation of hESCs in HA-Tyr hydrogels *in vitro*

HA-Tyr hydrogels encapsulated with hESCs were cultured with mTeSR1 media for 7 days. Spontaneous differentiation of hESCs was initiated by exposing the cells to DMEM medium containing 20% (v/v) FBS for 14 days. Subsequently, the hydrogels were degraded and cells were harvested. The differentiated cell clusters in HA-Tyr hydrogels were released and cultured on Matrigel-coated 24 well plates. The cells were fixed with formaldehyde and immunostaining was performed to examine the differentiation of hESCs towards the three germ layers Antibodies against smooth muscle actin (SMA), Foxa2 and βIII-tubulin were used to identify mesoderm, endoderm and ectoderm lineages, respectively. Details of the antibodies used are listed in Table 7-1.

### 7.2.11. Assessment of pluripotency of hESCs cultured in HA-Tyr hydrogels by teratoma assay *in vivo*

hESCs cultured in HA-Tyr hydrogels for 7 days were released by hydrogel degradation. The cells were then mixed with Matrigel and injected into NOD-SCID mice subcutaneously to induce teratoma formation (5 million cells per mouse). After 8 weeks, the mice were euthanized and teratoma was collected. Histological analysis was performed by Histopathology Lab (Biopolis, Singapore). The care and use of laboratory animals were performed according to the approved protocols by the Institutional Animal Care and Use Committee (IACUC) at the Biological Resource Center (BRC) in Biopolis, Singapore, following the guidelines of the National Advisory Committee on Laboratory Animal Research (NACLAR).

### 7.2.12. Karyotyping analysis of hESC cultured in HA-Tyr hydrogels

hESCs cultured in HA-Tyr hydrogels were released through enzymatic degradation and subsequently cultured on Matrigel-coated glass coverslips. Chromosomal rearrangement was evaluated by G-band analysis for the cells, with at least 20 metaphase spreads observed (ParkwayHealth Laboratory Services Ltd, Singapore).

### 7.2.13. Statistical analysis

Data are expressed as mean ± standard deviation (SD). The statistical significance between two groups was determined by the unpaired Student's t-test. $p < 0.05$ was considered statistically significant.

## 7.3. Results and discussion

### 7.3.1. Encapsulation of hESCs in hydrogels and characterization of hESC-encapsulated hydrogels

Table 7-2 summarizes the rheological properties of the hydrogels. $H_2O_2$ of different concentrations (437, 728 or 1311 μM) were used to prepare HA-Tyr hydrogels of various mechanical strengths. The storage modulus (G'), which served as an indicator of the mechanical strength of a given viscoelastic material, increased significantly with increasing $H_2O_2$ concentration. When 437, 728 and 1311 μM of $H_2O_2$ concentration were used, the G' were 82, 222, and 1081 Pa, respectively. The hydrogels with different G' are abbreviated as HA-Tyr-soft-hESC, HA-Tyr-medium-hESC and HA-Tyr-stiff-hESC, respectively. The compressive modulus (E) and mass welling ratio ($Q_M$) of the hydrogels were also measured (Table 7-2). E increased as the $H_2O_2$ concentration increased, while $Q_M$ decreased. The results

confirmed that HA-Tyr hydrogels formed with a higher $H_2O_2$ concentration were stiffer and less crosslinked. Dex-Tyr hydrogels with a G' value of 83 Pa (Dex-Tyr-soft-hESC) was also prepared as a comparison for the elucidation of the role of HA in the self-renewal of hESCs. The G' of Dex-Tyr-soft-hESC was not significantly different from that of HA-Tyr-soft-hESC.

**Table 7-2.** Composition and physical properties of HA-Tyr or Dex-Tyr hydrogels encapsulating hESCs[a]

| Sample | Polymer % (w/v) | HRP (U/ml) | $H_2O_2$ (μM) | G' (Pa) | E (Pa) | $Q_M$ |
|---|---|---|---|---|---|---|
| HA-Tyr-soft-hESC | 1 | 0.124 | 437 | 82 ± 3 | 357 ± 20 | 64 ± 3 |
| HA-Tyr-medium-hESC | 1 | 0.124 | 728 | 222 ± 34[b] | 1465 ± 100[b] | 53 ± 2[b] |
| HA-Tyr-stiff-hESC | 2 | 0.248 | 1311 | 1081 ± 152[c] | 7795 ± 366[c] | 48 ± 1[c] |
| Dex-Tyr-soft-hESC | 1.5 | 0.124 | 437 | 83 ± 17[d] | 340 ± 37[d] | 24 ± 3[d] |

Note. Abbreviations: storage modulus (G'), mass swelling ratio ($Q_M$)

[a]All hydrogels were formed with $10^6$ of hESC/ml. Results are shown as the mean values ± SD (n = 3). [b]G', E and $Q_M$ of HA-Tyr-medium-hESC were significantly different from those of HA-Tyr-soft-hESC and HA-Tyr-stiff-hESC, respectively ($p < 0.01$). [c]G' , E and $Q_M$ of HA-Tyr-stiff-hESC were significantly different from those of HA-Tyr-soft-hESC and HA-Tyr-medium-hESC, respectively ($p < 0.01$). [d]G' and E of Dex-Tyr-soft-hESC were not significantly different from those of HA-Tyr-soft-hESC ($p > 0.05$).

### 7.3.2. 3D distribution, viability and self-renewal of hESCs in hydrogels with different mechanical strength

To study the distribution and viability of hESCs cultured in hydrogels, Z-stacked scanning of hydrogel-cell constructs was performed by confocal microscopy. Fig. 7-2 shows the orthogonal sections of cell clusters in HA-Tyr-soft-hESC, HA-Tyr-medium-hESC and HA-Tyr-stiff-hESC on day 1, 4 and 7. Cell viability was determined by staining with calcein AM (alive, green) and propidium iodine (dead, red). Phase contrast, green fluorescence and red fluorescence images were overlaid to obtain a composite image. On day 1, green fluorescence staining was observed for all cell clusters with no obvious red staining, suggesting that the encapsulated cell clusters were alive in all three types of hydrogels. On day 4 and 7, green fluorescence staining was observed for cell clusters in HA-Tyr-soft-hESC only, suggesting that for prolonged cultivation, the viability of the encapsulated cells was maintained only in the HA-Tyr-soft-hESC.

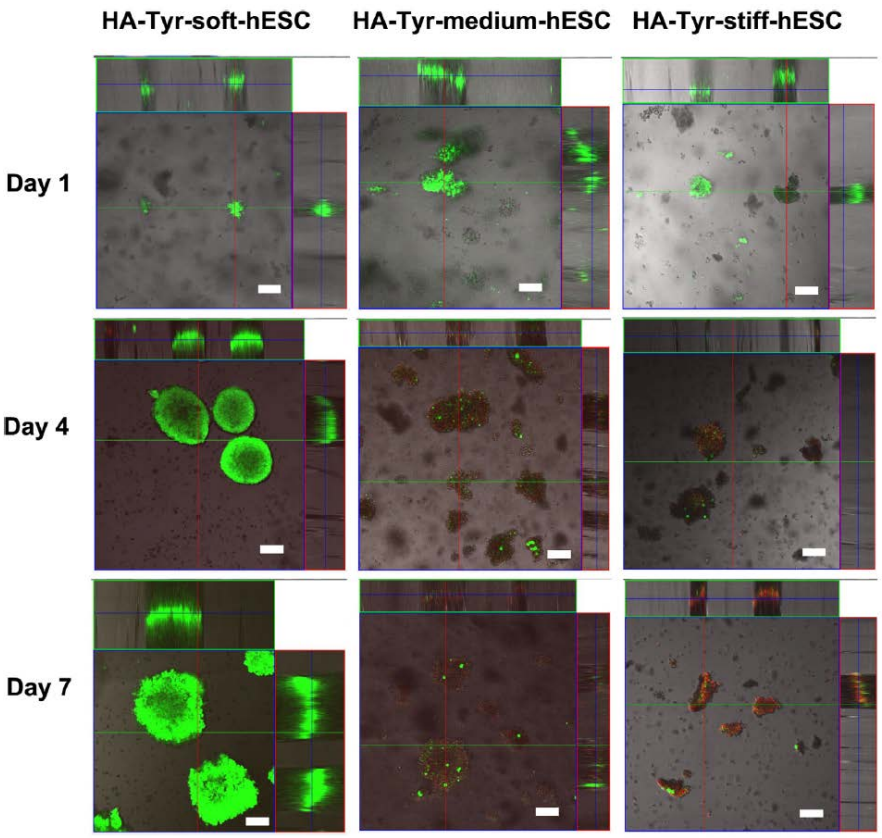


**Fig. 7-2. Confocal microscopic images hESC clusters in HA-Tyr-soft-hESC, HA-Tyr-medium-hESC and HA-Tyr-stiff-hESC after cultivation of 1, 4 and 7 days. Cell clusters in the hydrogels were stained with calcein AM and PI. Scale bar = 100 µm.**

The mechanical properties of the substrate are widely acknowledged to affect cell proliferation and differentiation in both 2D and 3D [37, 38]. To study the proliferation of hESCs in HA-Tyr hydrogels of different mechanical strengths, CyQuant® assay was utilized to determine the cell numbers in the hydrogels after culturing for 7 days. The cell number of hESCs cultured in HA-Tyr-soft-hESC hydrogels increased significantly ($p < 0.05$) after 4 and 7 days, respectively (Fig. 7-3). In contrast, hESCs in HA-Tyr-medium-hESC and HA-Tyr-stiff-hESC failed to show any increase in cell number after 7 days. Dex-Tyr-soft-hESC, which had a similar G' as HA-Tyr-soft-hESC hydrogels (Table 7-2), showed a decrease in cell number after 7 days. Since no obvious degradation of the Dex-Tyr-soft-hESC hydrogels was observed upon visual inspection, the decrease in cell number was likely due to cell death caused by the unfavorable microenvironment in the Dex-Tyr hydrogel. The result suggests that the proliferation of hESCs in 3D requires both HA as the substrate and a suitable mechanical strength.

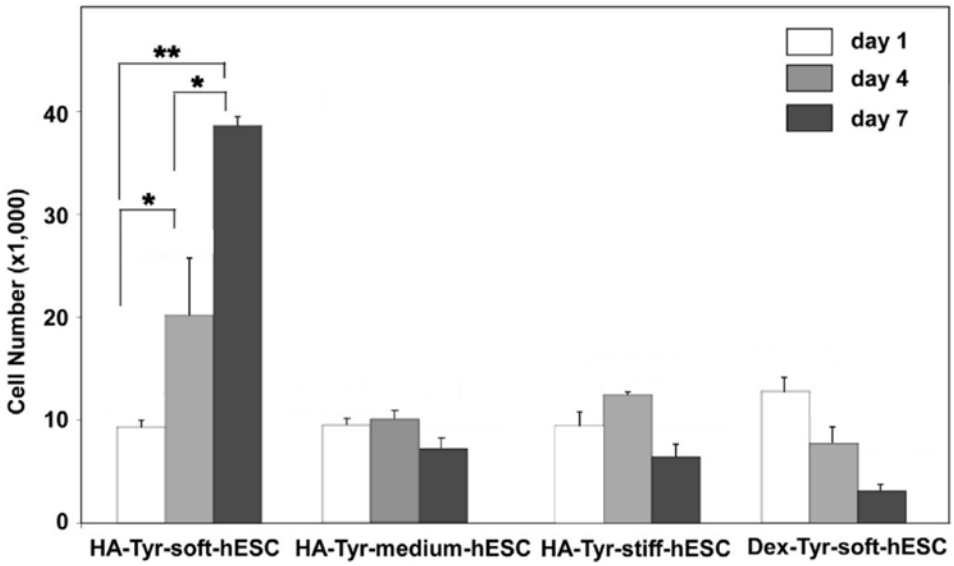


**Fig. 7-3. Proliferation of hESCs in HA-Tyr-soft-hESC, HA-Tyr-medium-hESC, HA-Tyr-stiff-hESC and Dex-Tyr-soft-hESC hydrogels. Cells were released by enzymatic degradation of hydrogel and the cell numbers were measured using CyQuant® assay (n = 3, mean ± SD). *$p < 0.05$; **$p < 0.01$.**

To further elucidate the role of substrate composition and mechanical strength on the pluripotency of hESCs cultured in HA-Tyr and Dex-Tyr hydrogels, the cells were labelled with antibodies for pluripotency markers. The percentage of cells expressing the pluripotency markers was measured by flow cytometry (Nanog, Oct-4 and Sox-2). As shown in Table 7-3, regardless of the culture medium used, the expression of pluripotency markers decreased as the mechanical strength of HA-Tyr hydrogels increased. Importantly, the expression fell below 40% when hESCs were cultured in HA-Tyr-stiff-hESC hydrogels. The results suggested that hydrogels with a lower mechanical strength are more favorable for the maintenance of pluripotency. For hESCs cultured in Dex-Tyr-soft-hESC, the expression of pluripotency markers was lower than the cells cultured in HA-Tyr-soft-hESC. Since Dex-Tyr-soft-hESCs had a similar mechanical strength as HA-Tyr-soft-hESC (Table 7-2), the result underscored the importance of HA in maintaining hESC pluripotency. As HA-Tyr-soft hydrogels showed the best performance in promoting cell proliferation and maintaining pluripotency of hESCs, hESCs were cultivated in HA-Tyr-soft-hESC for the expansion of hESCs in the following studies.

**Table 7-3.** Percentages of cells expressing pluripotency markers[a]

| Sample | mTeSR1 | | | MEF | | |
|---|---|---|---|---|---|---|
| | **Nanog (%)** | **Oct-4 (%)** | **Sox-2 (%)** | **Nanog (%)** | **Oct-4 (%)** | **Sox-2 (%)** |
| HA-Tyr-soft-hESC | 98.6 | 98.7 | 98.5 | 93.1 | 88.4 | 90.5 |
| HA-Tyr-medium-hESC | 76.8 | 88.5 | 73.4 | 70.3 | 84.5 | 60.5 |
| HA-Tyr-stiff-hESC | 15.9 | 23.1 | 38.5 | 12.9 | 35.5 | 29.9 |
| Dex-Tyr-soft-hESC | 46.3 | 70.2 | 55.3 | 6.85 | 5.89 | 3.99 |

[a]hESC cells were culture in hydrogels with specified medium for 7 days, then cell were collected after hydrogels were degraded by hyaluronidase for HA-Tyr hydrogels, or dextranase for Dex-Tyr hydrogels. Flow cytometry was used to determine the percentage of hESCs that showed positive expression of Nanog, Oct-4 and Sox-2. At least 10,000 singlet cells were analyzed after staining, and cells without staining were set as control.

### 7.3.3. Characterization of hESC clusters in HA-Tyr hydrogels

We performed cryosectioning of HA-Tyr-soft-hESC constructs and examined the morphology and biological features of hESCs *in situ* by immuno-histological analyses (H&E, Ki-67 and TUNEL). Optical images showed a round morphology of cell clusters, with a diameter of 80−100 μm (Fig. 7-4a). H&E staining confirmed that the cell clusters had a solid core with densely packed cells in each cluster (Fig. 7-4b). The results indicated that hESCs could form spheroid structures in the HA-Tyr hydrogels. The cells were stained with Ki-67, an intracellular protein marker associated with cell proliferation [39], and TUNEL, which labels apoptotic cells (Fig. 7-4c and d). Quantitative analysis revealed that the majority of cells were Ki-67-positive (~80%, Fig. 7-4e) and < 5% of cells were TUNEL-positive (Fig. 7-4f), suggesting that hESCs in the HA-Tyr-soft-hESC hydrogels were highly proliferative.

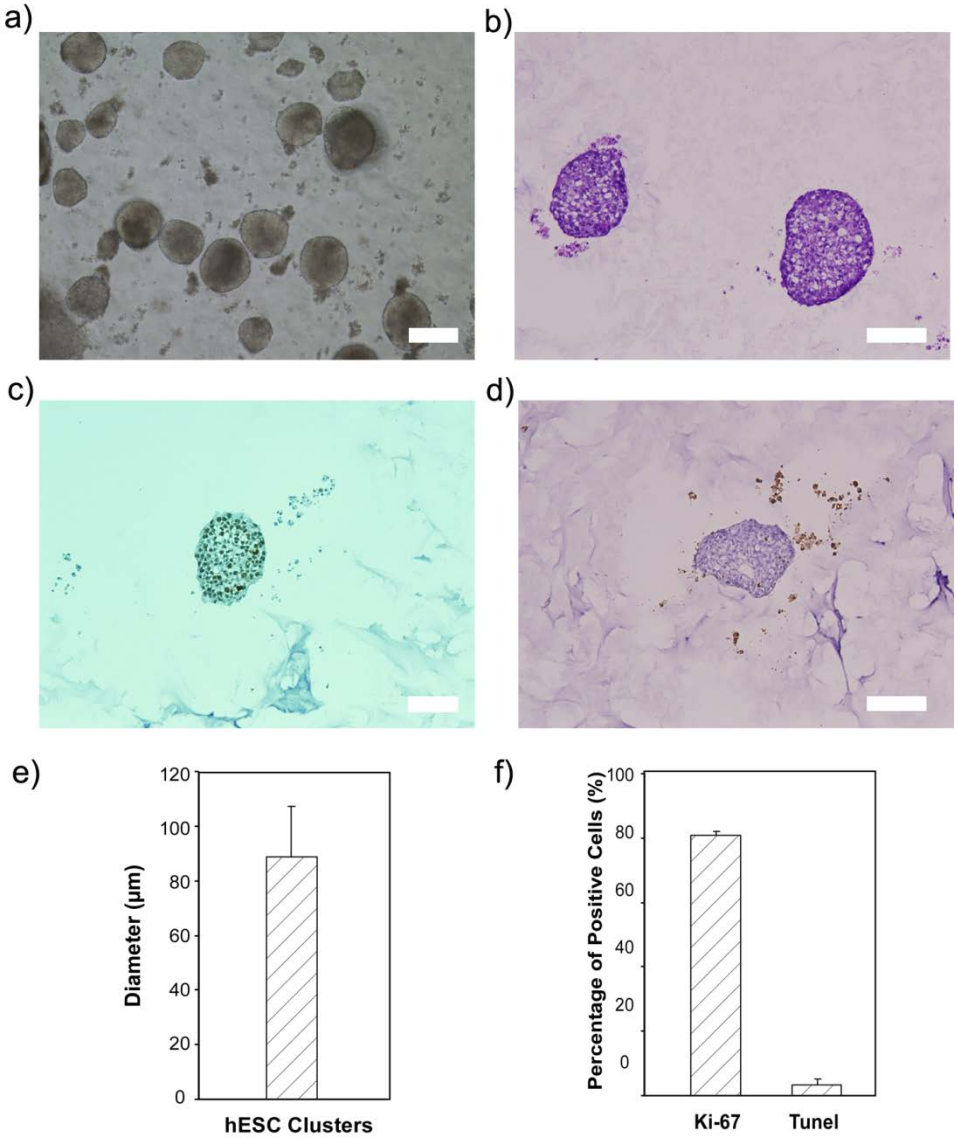


**Fig. 7-4. hESCs in HA-Tyr-soft-hESC after 7 days of cultivation. (a) Phase contrast images; (b) H&E staining; and (c) Ki-67 and (d) TUNEL staining of hESCs (representative sectioned colonies). Scale bar = 100 µm. (e) Average diameter of hESC clusters. (f) Percentage of Ki-67 and TUNEL-positive cells in hESC clusters (n = 3, mean ± SD).**

### 7.3.4. CD44 expression of hESCs cultured in HA-Tyr hydrogels

HA-Tyr hydrogels provide a 3D microenvironment that is composed of HA, a naturally occurring substrate for CD44. HA-CD44 interaction is involved in maintaining the undifferentiated state of hESCs in HA-based hydrogels [24]. Yet, it is not clear how the HA-constituted microenvironment would affect the expression of CD44. As shown in Fig. 7-5, CD44 expression was 96.0% for cells cultured in HA-Tyr-soft-hESC, which was similar to the expression of cells cultured on Matrigel (95.3%). Interestingly, the forward side scatter

(FSC), a parameter measuring the size of cells, and the CD44 expression level, were found to be less heterogenic for hESCs cultured in HA-Tyr-soft-hESC than those cultured on Matrigel. The unique 3D microenvironment in HA-Tyr hydrogels could have contributed to the reduced heterogeneity of hESC population.

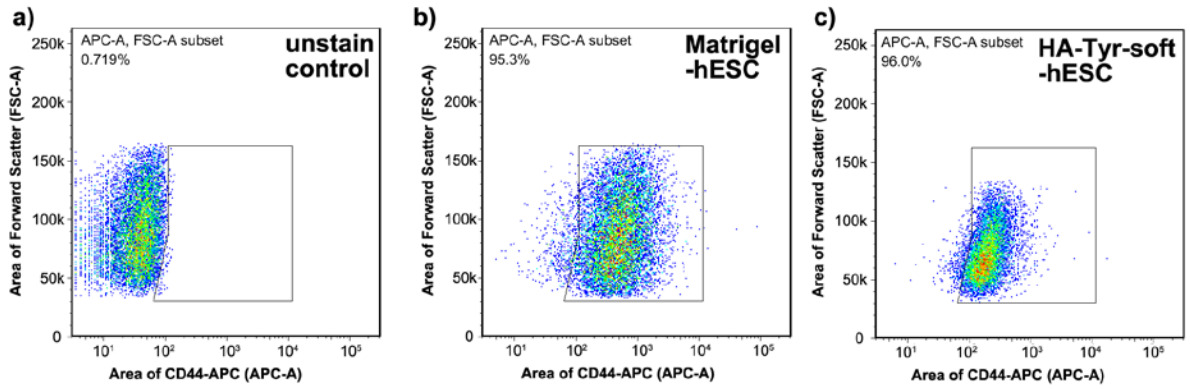


**Fig. 7-5. CD44 expression of hESCs that were cultured on Matrigel or in HA-Tyr-soft-hESC hydrogels. Cells were stained with APC conjugated CD44 antibody and analyzed by flow cytometry. For each analysis, at least 10,000 events were recorded.**

### 7.3.5. Expression of pluripotency markers in hESCs released from HA-Tyr hydrogels

It is important to maintain the pluripotency of stem cells during the controlled propagation of hESCs. hESCs were released from hydrogels by enzymatic degradation, and plated on Matrigel for immunostaining with a panel of hESC-specific proteins. Nanog, Oct-4 and Sox-2 are hESC-specific transcription factors that are important for maintaining the pluripotency of embryonic stem cells [40]. SSEA-4, TRA-1-60 and TRA-1-81 are proteoglycans that determine the phenotype of undifferentiated hESCs [41]. The pluripotency of the hESC culture is routinely assessed by the expression of these markers, and the expression of these markers is down-regulated during differentiation. The hESCs released from HA-Tyr hydrogels displayed strong expression for all the markers (Fig. 7-6), confirming that hESCs retained their pluripotent state in HA-Tyr hydrogels.

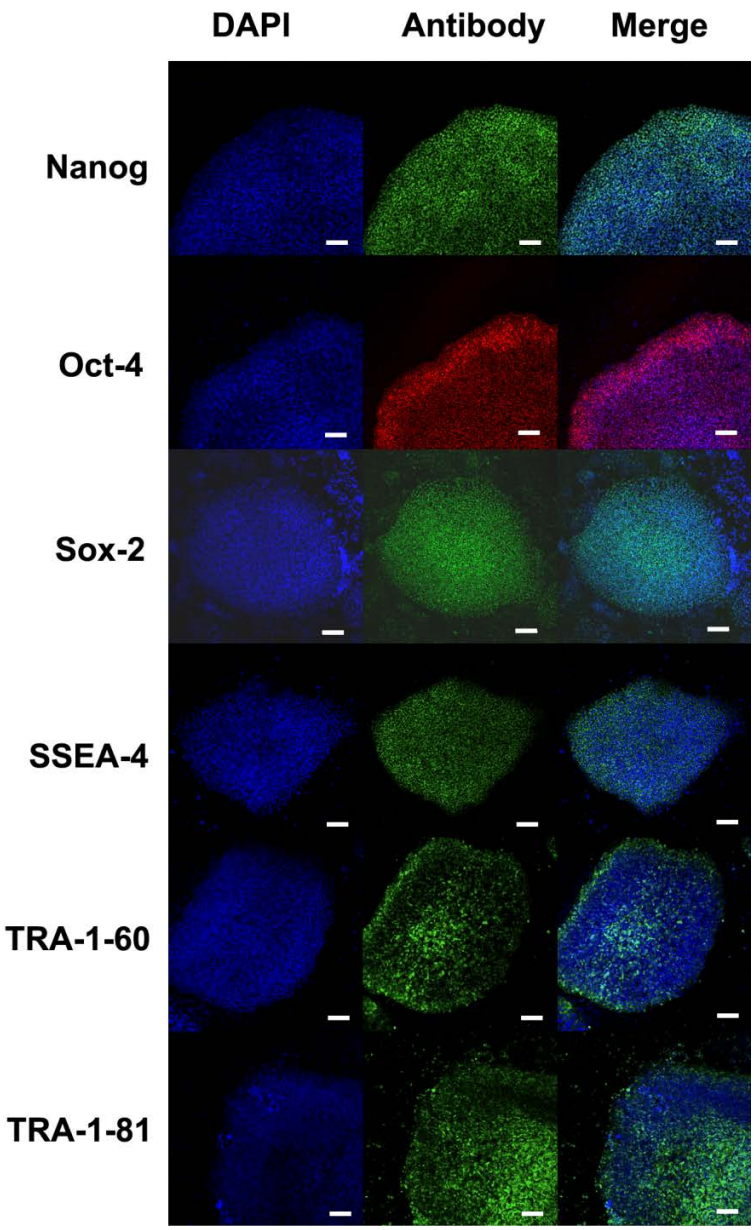


**Fig. 7-6. Confocal images of hESCs stained with antibodies against pluripotency marker proteins (Nanog, Oct-4, Sox-2, SSEA-4, TRA1-60 and TRA1-80). hESCs were released from HA-Tyr-soft-hESC hydrogels, plated on Matrigel and then labelled with primary antibodies against pluripotency markers, followed by incubation with FITC or rhodamine conjugated secondary antibodies. DAPI was used to stain the nuclei of the cells. Scale bar = 100 µm.**

Real-time PCR assays were carried out to examine the gene expression of pluripotency markers (Fig. 7-7). Gene expression analysis indicated that the expression of Nanog, Oct-4 and Sox-2 between hESCs from HA-Tyr-soft-hESC and Matrigel was not significantly different ($p > 0.05$), suggesting that the transcriptions of pluripotency genes were unaffected when hESCs were cultured in HA-Tyr hydrogels.

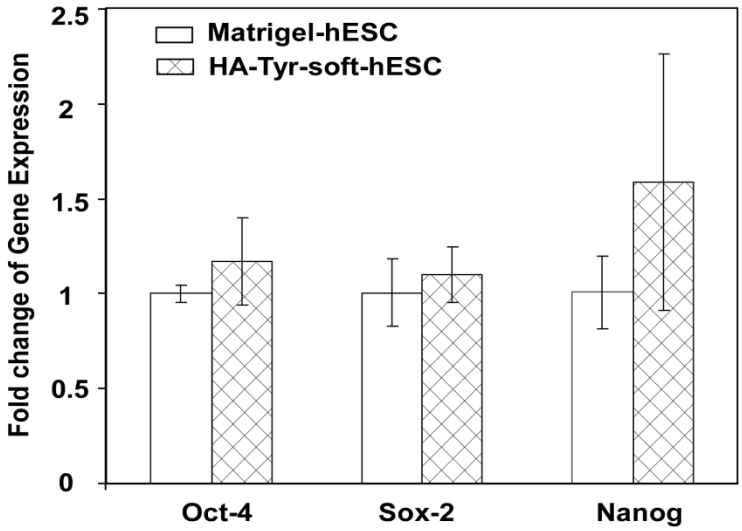


**Fig. 7-7. Gene expression of hESCs cultured on Matrigel or released from HA-Tyr-soft-hESC hydrogels. (n = 3, mean ± SD).**

### 7.3.6. Spontaneous differentiation of hESCs in HA-Tyr hydrogels *in vitro*

The ability of hESCs cultured in HA-Tyr hydrogels to differentiate into the three different germ layers were investigated by exposing the cells to DMEM containing fetal bovine serum (FBS) to induce spontaneous differentiation. Immunofluorescence staining was used to identify the expression of lineage-specific proteins. Antibodies against alpha smooth muscle actin (SMA), Foxa2 and βIII tubulin were used to detect myofibroblasts (mesoderm), hepotacytes (endoderm) and neurons (ectoderm), respectively. Positive staining was observed for all three markers (Fig. 7-8a), indicating that hESCs cultured in HA–Tyr-soft-hESC hydrogels could differentiate *in vitro* into cells of all three germ layers.

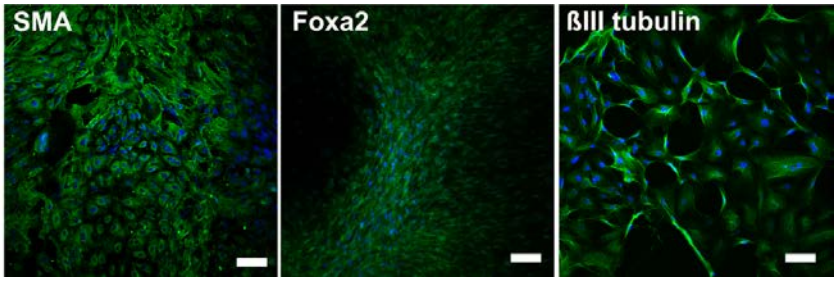


**Fig. 7-8. Immunofluorescence staining of spontaneously differentiated hESCs in HA-Tyr-soft-hESC hydrogels. Cells were fixed and labelled with antibodies against lineage specific proteins SMA, foxa2 and βIII tubulin, which correspond to cell derivatives from the mesoderm, endoderm and ectoderm, respectively. Scale bar = 100 µm.**

### 7.3.7. Formation of teratoma by hESCs from HA-Tyr hydrogels in vivo

To examine the differentiation capability of hESCs from HA-Tyr-soft-hESC hydrogels *in vivo*, cells retrieved from the hydrogels were injected subcutaneously in NOD/SCID mice. After eight to ten weeks, teratoma formation was observed in all the mice (n = 3). The teratomas were excised for histological analysis. Various tissue structures were observed in H&E staining, including blood vessels (Fig. 7-9a), muscle fibers (Fig. 7-9b), cartilage (Fig. 7-9c) and ossifying cartilage (Fig. 7-9d), which corresponded to tissues in the mesoderm. Intestinal epithelium (Fig. 7-9e) and glands (Fig. 7-9f) were also observed, which corresponded to tissues in the endoderm. Neuronal rosette (Fig. 7-9g) and pigmented cells (Fig. 7-9h) that corresponded to the ectoderm were observed as well. The result confirmed that hESCs cultured in HA-Tyr-soft-hESC hydrogels retained the ability to differentiate to multiple cell lineages.

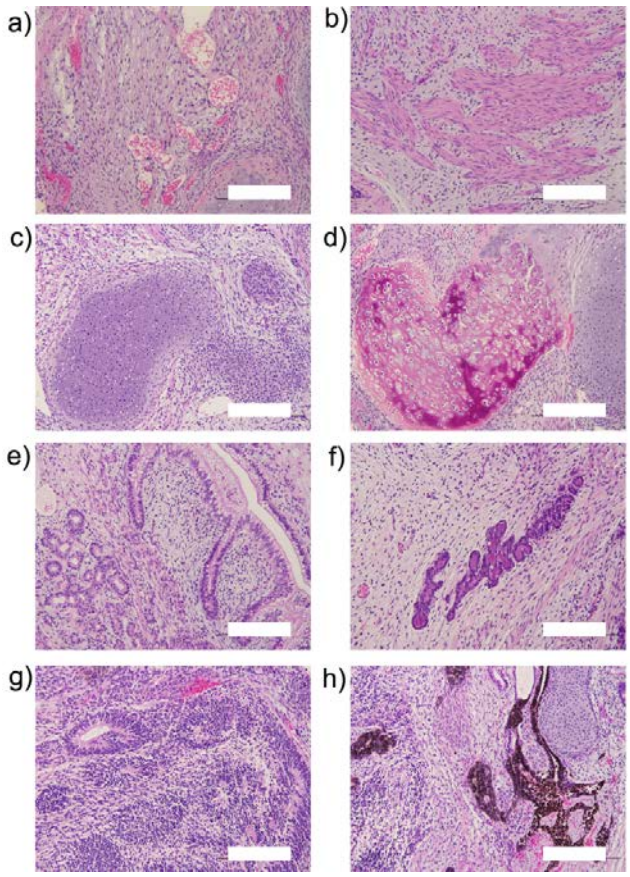


**Fig. 7-9. Histology of teratoma formed from hESCs cultured in HA-Tyr-soft-hESC hydrogels. Tissues from mesoderm: (a) blood vessel, (b) muscle fibers, (c) cartilage and (d) ossifying cartilage. Tissues from endoderm: (e) intestinal epithelium and (f) glands. Tissues from ectoderm: (g) neuronal rosette and (h) pigmented cells. Scale bar = 200 μm.**

### 7.3.8. Karyotyping analysis of hESCs released from HA-Tyr hydrogels

Karyotyping analysis was performed to confirm the genetic integrity of hESCs released from HA-Tyr-soft-hESC hydrogels. Released hESCs were plated on Matrigel and analyzed for chromosomal abnormalities by G-banding. Normal karyotype (46, XY) of hESCs without any aberration of chromosomes was observed (Fig. 7-10), indicating that the genetic integrity of hESCs was preserved.

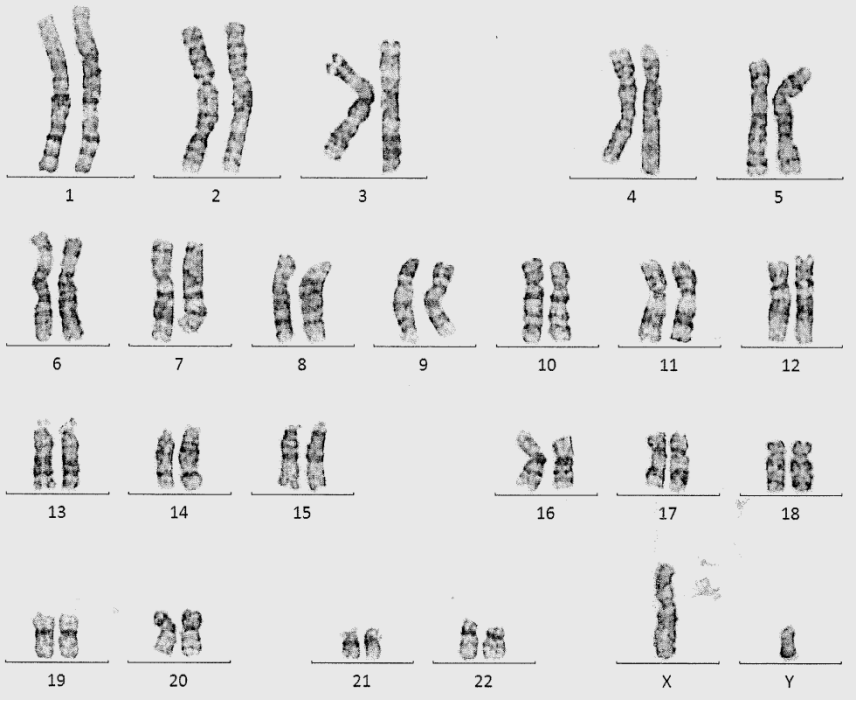


**Fig. 7-10. Karyotyping analysis of hESCs released from HA-Tyr-soft-hESC hydrogels. At least 20 metaphase spreads were screened and evaluated for chromosomal rearrangement.**

## 7.4. Conclusion

In this chapter, the enzymatically crosslinked HA-Tyr hydrogel system was used for the controlled propagation of hESCs in 3D. By comparing HA-Tyr of different mechanical strength as well as Dex-Tyr hydrogels, it was concluded that HA substrate and low mechanical strength were important factors for maintaining the viability, proliferation and pluripotency of hESCs in 3D. HA-Tyr hydrogels with a compressive modulus (E) of 350 Pa best supported the proliferation of hESCs and maintained the pluripotency. Histological analysis showed that the hESCs proliferated in soft HA-Tyr hydrogels and formed spheroid structure without undergoing apoptosis. CD44 expression was well-maintained in the HA-Tyr hydrogels. Immunostaining, flow cytometry and real-time PCR results confirmed the expression of pluripotency markers in hESCs cultured in HA-Tyr hydrogels. Moreover, hESCs cultured in HA-Tyr hydrogels could differentiate into cells of all three germ layers

both *in vitro* and *in vivo*. Karyotyping analysis of hESCs in HA-Tyr hydrogels confirmed that genetic integrity was well-preserved. In conclusion, the propagation of hESCs in HA-Tyr hydrogels is a viable approach to expand the cells in 3D for clinical applications.

**References**

[1] Brivanlou AH, Gage FH, Jaenisch R, Jessell T, Melton D, Rossant J. Setting standards for human embryonic stem cells. Science 2003;300:913-6.

[2] Kehat I, Kenyagin-Karsenti D, Snir M, Segev H, Amit M, Gepstein A, Livne E, Binah O, Itskovitz-Eldor J, et al. Human embryonic stem cells can differentiate into myocytes with structural and functional properties of cardiomyocytes. J. Clin. Invest. 2001;108:407-14.

[3] Reubinoff BE, Itsykson P, Turetsky T, Pera MF, Reinhartz E, Itzik A, Ben-Hur T. Neural progenitors from human embryonic stem cells. Nat. Biotechnol. 2001;19:1134-40.

[4] Zhang SC, Wernig M, Duncan ID, Brustle O, Thomson JA. In vitro differentiation of transplantable neural precursors from human embryonic stem cells. Nat. Biotechnol. 2001;19:1129-33.

[5] D'Amour KA, Bang AG, Eliazer S, Kelly OG, Agulnick AD, Smart NG, Moorman MA, Kroon E, Carpenter MK, et al. Production of pancreatic hormone-expressing endocrine cells from human embryonic stem cells. Nat. Biotechnol. 2006;24:1392-401.

[6] Kroon E, Martinson LA, Kadoya K, Bang AG, Kelly OG, Eliazer S, Young H, Richardson M, Smart NG, et al. Pancreatic endoderm derived from human embryonic stem cells generates glucose-responsive insulin-secreting cells in vivo. Nat. Biotechnol. 2008;26:443-52.

[7] Thomson JA, Itskovitz-Eldor J, Shapiro SS, Waknitz MA, Swiergiel JJ, Marshall VS, Jones JM. Embryonic stem cell lines derived from human blastocysts. Science 1998;282:1145-7.

[8] Xu CH, Inokuma MS, Denham J, Golds K, Kundu P, Gold JD, Carpenter MK. Feeder-free growth of undifferentiated human embryonic stem cells. Nat. Biotechnol. 2001;19:971-4.

[9] Ludwig TE, Bergendahl V, Levenstein ME, Yu J, Probasco MD, Thomson JA. Feeder-independent culture of human embryonic stem cells. Nat. Methods 2006;3:637-46.

[10] Ludwig TE, Levenstein ME, Jones JM, Berggren WT, Mitchen ER, Frane JL, Crandall LJ, Daigh CA, Conard KR, et al. Derivation of human embryonic stem cells in defined conditions. Nat. Biotechnol. 2006;24:185-7.

[11] Yao S, Chen S, Clark J, Hao E, Beattie GM, Hayek A, Ding S. Long-term self-renewal and directed differentiation of human embryonic stem cells in chemically defined conditions. Proc. Natl. Acad. Sci. U. S. A. 2006;103:6907-12.

[12] Klim JR, Li L, Wrighton PJ, Piekarczyk MS, Kiessling LL. A defined glycosaminoglycan-binding substratum for human pluripotent stem cells. Nat. Methods 2010;7:989-94.

[13] Mei Y, Saha K, Bogatyrev SR, Yang J, Hook AL, Kalcioglu ZI, Cho S-W, Mitalipova M, Pyzocha N, et al. Combinatorial development of biomaterials for clonal growth of human pluripotent stem cells. Nature Materials 2010;9:768-78.

[14] Melkoumian Z, Weber JL, Weber DM, Fadeev AG, Zhou Y, Dolley-Sonneville P, Yang J, Qiu L, Priest CA, et al. Synthetic peptide-acrylate surfaces for long-term self-renewal and cardiomyocyte differentiation of human embryonic stem cells. Nat. Biotechnol. 2010;28:606-10.

[15] Rodin S, Domogatskaya A, Strom S, Hansson EM, Chien KR, Inzunza J, Hovatta O, Tryggvason K. Long-term self-renewal of human pluripotent stem cells on human recombinant laminin-511. Nat. Biotechnol. 2010;28:611-5.

[16] Villa-Diaz LG, Nandivada H, Ding J, Nogueira-de-Souza NC, Krebsbach PH, O'Shea KS, Lahann J, Smith GD. Synthetic polymer coatings for long-term growth of human embryonic stem cells. Nat. Biotechnol. 2010;28:581-3.

[17] Passier R, van Laake LW, Mummery CL. Stem-cell-based therapy and lessons from the heart. Nature 2008;453:322-9.

[18] Mason C, Dunnill P. Quantities of cells used for regenerative medicine and some implications for clinicians and bioprocessors. Regen. Med. 2009;4:153-7.

[19] Kraehenbuehl TP, Langer R, Ferreira LS. Three-dimensional biomaterials for the study of human pluripotent stem cells. Nat. Methods 2011;8:731-6.

[20] Lutolf MP, Gilbert PM, Blau HM. Designing materials to direct stem-cell fate. Nature 2009;462:433-41.

[21] Lee ST, Yun JI, Jo YS, Mochizuki M, van der Vlies AJ, Kontos S, Ihm JE, Lim JM, Hubbell JA. Engineering integrin signaling for promoting embryonic stem cell self-renewal in a precisely defined niche. Biomaterials 2010;31:1219-26.

[22] Yang F, Cho S-W, Son SM, Hudson SP, Bogatyrev S, Keung L, Kohane DS, Langer R, Anderson DG. Combinatorial Extracellular Matrices for Human Embryonic Stem Cell Differentiation in 3D. Biomacromolecules 2010;11:1909-14.

[23] Lu HF, Narayanan K, Lim SX, Gao SJ, Leong MF, Wan ACA. A 3D microfibrous scaffold for long-term human pluripotent stem cell self-renewal under chemically defined conditions. Biomaterials 2012;33:2419-30.

[24] Gerecht S, Burdick JA, Ferreira LS, Townsend SA, Langer R, Vunjak-Novakovic G. Hyaluronic acid hydrogen for controlled self-renewal and differentiation of human embryonic stem cells. Proc. Natl. Acad. Sci. U. S. A. 2007;104:11298-303.

[25] Li Z, Leung M, Hopper R, Ellenbogen R, Zhang M. Feeder-free self-renewal of human embryonic stem cells in 3D porous natural polymer scaffolds. Biomaterials 2010;31:404-12.

[26] Ferreira LS, Gerecht S, Fuller J, Shieh HF, Vunjak-Novakovic G, Langer R. Bioactive hydrogel scaffolds for controllable vascular differentiation of human embryonic stem cells. Biomaterials 2007;28:2706-17.

[27] Hwang NS, Varghese S, Elisseeff J. Derivation of Chondrogenically-Committed Cells from Human Embryonic Cells for Cartilage Tissue Regeneration. PLoS One 2008;3:e2498.

[28] Toh WS, Lee EH, Guo X-M, Chan JKY, Yeow CH, Choo AB, Cao T. Cartilage repair using hyaluronan hydrogel-encapsulated human embryonic stem cell-derived chondrogenic cells. Biomaterials 2010;31:6968-80.

[29] Toole BP. Hyaluronan in morphogenesis. Semin. Cell Dev. Biol. 2001;12:79-87.

[30] Toole BP. Hyaluronan: from extracellular glue to pericellular cue. Nat. Rev. Cancer 2004;4:528-39.

[31] Kurisawa M, Chung JE, Yang YY, Gao SJ, Uyama H. Injectable biodegradable hydrogels composed of hyaluronic acid-tyramine conjugates for drug delivery and tissue engineering. Chem. Commun. (Camb.) 2005:4312-4.

[32] Kurisawa M, Lee F, Wang L-S, Chung JE. Injectable enzymatically crosslinked hydrogel system with independent tuning of mechanical strength and gelation rate for drug delivery and tissue engineering. J. Mater. Chem. 2010;20:5371-5.

[33] Xu KM, Lee F, Gao SJ, Chung JE, Yano H, Kurisawa M. Injectable hyaluronic acid-tyramine hydrogels incorporating interferon-alpha 2a for liver cancer therapy. J. Control. Release 2013;166:203-10.

[34] Lee F, Chung JE, Kurisawa M. An injectable enzymatically crosslinked hyaluronic acid-tyramine hydrogel system with independent tuning of mechanical strength and gelation rate. Soft Matter 2008;4:880-7.

[35] Bae KH, Lee F, Xu K, Keng CT, Tan SY, Tan YJ, Chen Q, Kurisawa M. Microstructured dextran hydrogels for burst-free sustained release of PEGylated protein drugs. Biomaterials 2015;63:146-57.

[36] Ng SLJ, Narayanan K, Gao SJ, Wan ACA. Lineage restricted progenitors for the repopulation of decellularized heart. Biomaterials 2011;32:7571-80.

[37] Wang L-S, Boulaire J, Chan PPY, Chung JE, Kurisawa M. The role of stiffness of gelatin-hydroxyphenylpropionic acid hydrogels formed by enzyme-mediated crosslinking on the differentiation of human mesenchymal stem cell. Biomaterials 2010;31:8608-16.

[38] Wang L-S, Chung JE, Pui-Yik Chan P, Kurisawa M. Injectable biodegradable hydrogels with tunable mechanical properties for the stimulation of neurogenesic differentiation of human mesenchymal stem cells in 3D culture. Biomaterials 2010;31:1148-57.

[39] Scholzen T, Gerdes J. The Ki-67 protein: From the known and the unknown. J. Cell. Physiol. 2000;182:311-22.

[40] Wang J, Rao S, Chu J, Shen X, Levasseur DN, Theunissen TW, Orkin SH. A protein interaction network for pluripotency of embryonic stem cells. Nature 2006;444:364-8.

[41] Pera MF, Reubinoff B, Trounson A. Human embryonic stem cells. J. Cell Sci. 2000;113:5-10.

# Chapter 8

# Injectable Degradation-Resistant Hyaluronic Acid Hydrogels Crosslinked via the Oxidative Coupling of Green Tea Catechin

## 8.1. Introduction

Hydrogels are physically or chemically crosslinked polymeric networks swollen in water. The 3D porous structure and aqueous environment of hydrogels rendered them particularly suitable for the encapsulation of cells and biomolecules for tissue engineering and drug delivery applications [1]. As demonstrated in the preceding chapters, the horseradish peroxidase (HRP)-mediated oxidative coupling of phenols is a highly robust reaction that can be applied for the formation of chemically-crosslinked hydrogels *in situ* [2, 3]. Indeed, various polymers have been modified with simple phenols containing one aromatic ring, such as tyramine [4-7], 3,4-hydroxyphenylpropionic acid [8] and catechol [9], for the formation of hydrogels in the presence of HRP and hydrogen peroxide ($H_2O_2$). $H_2O_2$ is an oxidant, the addition of which is an indispensable step for the HRP-mediated reaction. The advantages of HRP-mediated hydrogel formation include *in situ* gelation at physiological conditions, with the gelation time ranging from a few seconds to several minutes, and tunable crosslink density [10].

In addition to catalyzing the oxidative coupling of phenols, HRP reacts with thiols in the presence of $H_2O_2$ to form thiyl radicals, which dimerize to form disulfide bonds. It was reported that HRP induced the gelation of a solution of thiol-functionalized linear poly-(glycidol) (SH-PG) within 4 h [11]. In contrast, no hydrogel was formed in the absence of HRP. Importantly, the addition of $H_2O_2$ was not necessary in this system as it was produced during the autoxidation of thiols under aerobic condition. This greatly simplifies the gel preparation process as it only requires the mixing of two components, namely the thiol-functionalized polymers and HRP. However, HRP-mediated gelation of thiol-functionalized polymers was much slower compared with the phenol-functionalized counterpart. This was attributed in part to the lower rate constant for the reaction between HRP and thiol than that between HRP and phenol [12]. In this chapter, a hydrogel system that is formed by the HRP-mediated coupling of polyphenols is described. This hydrogel system exhibits fast gelation that is typical of hydrogels formed *via* HRP-mediated coupling of phenols, while at the same time avoids the need for exogenous $H_2O_2$.

Catechins are a group of polyphenols found in green tea, which are known for their health benefits, such as anti-cancer and anti-inflammatory properties [13]. Among the various green tea catechins, (-)-epigallocatechin-3-gallate (EGCG, Fig. 8-1) is the most abundant constituent [14, 15]. While it has been demonstrated previously that EGCG coupling occurred upon the

addition of HRP, exogenous $H_2O_2$ was added concurrently [16]. Herein, we proposed that the addition of HRP alone would be sufficient to catalyze the crosslinking of polymer-EGCG conjugates *via* coupling of EGCG moieties, as $H_2O_2$ is generated as a by-product during EGCG autoxidation under aerobic condition. To this end, a hyaluronic acid-EGCG conjugate (HA-EGCG, Fig. 8-2a) was synthesized. First, an aldehyde-mediated condensation reaction, which selectively reacts with the C-6 and C-8 positions of the A ring of EGCG, was utilized to synthesize ethylamine-bridged EGCG dimers [17, 18]. The EGCG dimers comprised of four isomers, which were characterized by HPLC, high-resolution mass spectrometry and NMR spectroscopy. Next, the amine-functionalized EGCG dimers were conjugated to HA through the formation of amide bonds using conventional carbodiimide-mediated coupling chemistry. The EGCG moieties are expected to not only serve as crosslinking moieties, but also endow the conjugates with enhanced bioactivities. Indeed, it was shown that the HA-EGCG conjugates exhibit enzyme-inhibiting, anti-proliferative and radical scavenging activities, all of which were either absent or present at a negligible level in native HA. Next, the gelation property of HA-EGCG conjugates in the presence of HRP was characterized *in vitro* and *in vivo* (Fig. 8-2b). Furthermore, it was demonstrated that hydrogels could be formed through EGCG quinone formation even in the absence of HRP.

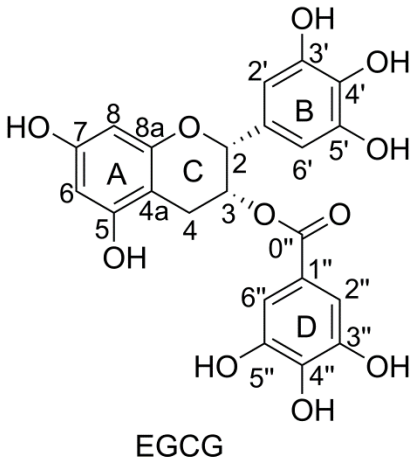


EGCG

**Fig. 8-1. Chemical structure of EGCG.**

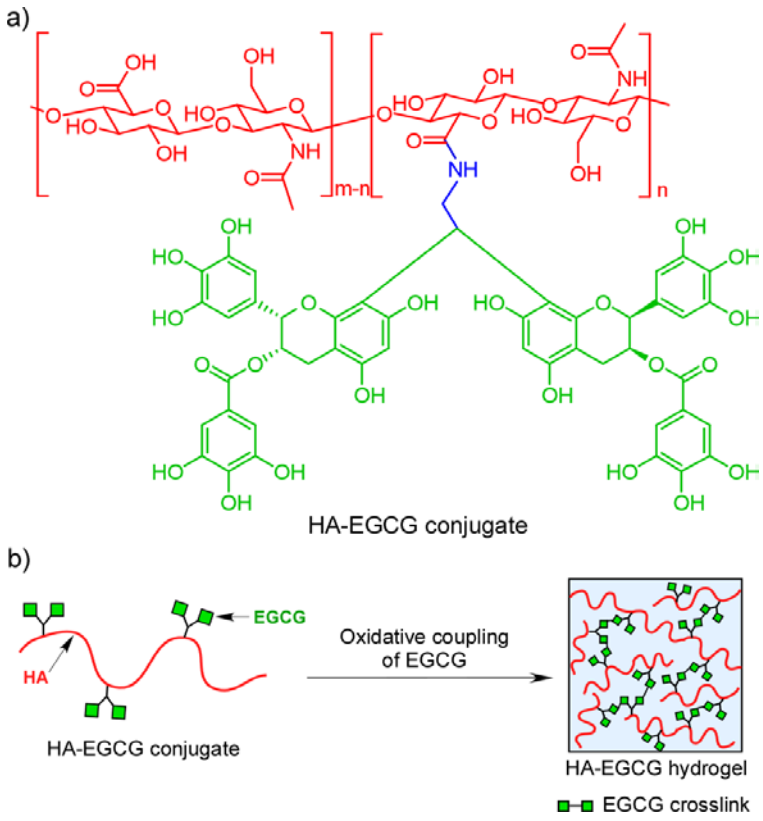


**Fig. 8-2. (a) Chemical structure of HA-EGCG conjugates. (b) Formation of hydrogels through the oxidative coupling of EGCG moieties.**

## 8.2. Materials and methods

### 8.2.1. Materials

TEAVIGO$^{TM}$ green tea extract (EGCG, minimum 90%) was purchased from DMS Nutritional Products Ltd. (Switzerland). Hyaluronic acid (HA, 90 kDa and 800 kDa) was kindly donated by JNC Corporation (Tokyo, Japan). Methanesulfonic acid (MSA), 2,2-diethoxyethylamine (DA), *N*-hydroxysuccinimide (NHS), 1-ethyl-3-(3-dimethylaminopropyl)-carbodiimide hydrochloride (EDC·HCl), xanthine, sodium nitroprusside, Greiss reagent, nitrotetrazolium blue chloride (NBT), thiobarbituric acid, 2-deoxy-D-ribose, ascorbic acid, hydrogen peroxide ($H_2O_2$), trichloroacetic acid, hyaluronidase from bovine testes (439 U/mg), hydrogen peroxide ($H_2O_2$), tyramine hydrochloride (Tyr·HCl) and sodium azide were all purchased from Sigma-Aldrich (Singapore). 2-(*N*-Morpholino)ethanesulfonic acid **(**MES), iron (II) sulfate heptahydrate ($FeSO_4·7H_2O$), *N*-acetyl-D-glucosamine, di-sodium hydrogen phosphate dihydrate ($Na_2HPO_4·2H_2O$) and sodium dihydrogen phosphate monohydrate ($NaH_2PO_4·H_2O$) were obtained from Merck (Singapore). Xanthine oxidase (XO, 0.34 U/mg) from buttermilk and horseradish peroxidase

(HRP, 190 units per mg) were purchased from Oriental Yeast Co., Ltd. (Japan). *p*-Dimethylaminobenzaldehyde (DMAB) was purchased from Wako Pure Chemical Industries (Japan). *N*,*N*-Dimethylfomamide-$d_7$ (DMF-$d_7$) was purchased from Cambridge Isotope Laboratories, Inc (USA). Human fibroblast-like synoviocytes (HFLS) derived from rheumatoid arthritis patient were obtained from Cell Applications, Inc. (USA). Fetal bovine serum (FBS), penicillin-streptomycin and PicoGreen® dsDNA quantitation assay kit were purchased from Life Technologies (Singapore). Phosphate buffer saline (PBS, pH 7.3) and RPMI 1640 were supplied by media preparation facility in Biopolis (Singapore). Deionized $H_2O$ was used in all experiments.

### 8.2.2. Synthesis of ethylamine-bridged EGCG dimers

In a glass vial containing 1.2 ml of cold MSA:THF (1:5, v/v) mixture, 145 μl of DA (1.0 mmol) was added while stirring. The mixture was transferred dropwise to EGCG (2.29 g, 5 mmol), which was dissolved in 3.8 ml of THF and 1.7 μl of MSA, and stirred overnight in the dark at ambient temperature. The resulting mixture was concentrated under reduced pressure and further dried under vacuum overnight at ambient temperature. The products were dissolved in 10 ml of $H_2O$ and the unreacted EGCG were removed by extraction with 10 ml of ethyl acetate using a separatory funnel. Unreacted EGCG moved to the organic layer while the ethylamine-bridged EGCG dimers remained in the aqueous layer. The extraction was repeated until no free EGCG was detected in the aqueous layer using a Waters Acquity UPLC-MS system. The concentration of the purified ethylamine-bridged EGCG dimer in the aqueous phase was determined by absorbance at 273 nm and was found to be 84 mg/ml (yield = 88%). HRMS-ESI calcd for $C_{46}H_{40}NO_{22}$ $[M + H]^+$ 958.2036, found 958.2062. The dimers were stored at -80 °C.

### 8.2.3. High-performance liquid chromatography (HPLC)

HPLC was performed by Waters 2695 Separation Module equipped with a Waters 2996 Photodiode Array Detector. A Spirit HPLC $C_{18}$ column (5 μm, 25 × 0.46 cm; AAPPTec) was used. The mobile phase consisted of $H_2O$ and acetonitrile with 1% acetic acid. Sample concentration was 5 mg/ml and elution was carried out at 1 ml/min flow rate, 23 °C, with a linear gradient of acetonitrile from 10 to 35% in 30 min.

### 8.2.4. Nuclear magnetic resonance (NMR) measurement

The purified EGCG dimers, which contained different isomers, were separated by a Gilson preparative HPLC system equipped with a Gilson UV/VIS-156 detector. A $C_{18}$ reversed phase preparative column (21.2 mm x 250 mm, Kromasil®) was used. The mobile phase consisted of $H_2O$ and acetonitrile with 0.1% trifluoroacetic acid. Samples were eluted at 15 ml/min, 25 °C, with 10% acetonitrile for 3 min and then gradient to 60% over 40 min. For NMR analysis, 10 mg of sample from each fraction was dissolved in 0.7 ml of DMF-$d_7$ and transferred to a Wilmad J-Young low pressure/vacuum NMR tube. Oxygen in the sample was removed by three cycles of freeze-pump-thaw. NMR experiments were performed with a Bruker Avance II (400 MHz) NMR equipped with a 5 mm PABBO probe. A series of NMR experiments were performed for each compound, including 1D $^{1}H$ and $^{13}C$ APT spectra as well as 2D $^{1}H$-$^{13}C$ HSQC and HMBC spectra using standard pulse programs. All chemical shifts are given in ppm values relative to DMF-$d_7$ ($^{1}H$: $\delta$ 2.75 ppm; $^{13}C$: $\delta$ 34.89).

### 8.2.5. Synthesis of HA-EGCG conjugates

Ethylamine-bridged EGCG dimers were conjugated to HA by a typical carbodiimide-mediated coupling reaction [19]. HA (250 mg, 0.62 mmol) was dissolved by stirring in 20.2 ml of 0.4 M MES buffer (pH 5.2) with 2.5 ml of DMF. Next, NHS (89 mg, 0.78 mmol) and ethylamine-bridged dimers (0.205 mmol in 2.33 ml of $H_2O$) were added to the reaction mixture. Then, EDC·HCl (150 mg, 0.78 mmol) was added and the pH of the reaction was adjusted to 4.7. The reaction mixture was purged vigorously with $N_2$ for 10 min and then incubated in the dark overnight under $N_2$ at ambient temperature. The HA-EGCG conjugates were purified by precipitation using a previously established method with some modifications [19, 20]. Briefly, 125 ml of $H_2O$ and 16.7 ml of 5 M NaCl solution were added to the reaction mixture and the pH was lowered to 3 with HCl solution. Then, 310 ml of ethanol was added while stirring. Under these conditions the HA-EGCG conjugates formed slurry precipitates which were collected by centrifugation (6000 rcf, 5 min). After decanting the supernatant, the precipitates were re-dissolved in 250 ml of water. Then, 33 ml of 5 M NaCl solution was added, the pH was adjusted to 3, and 620 ml of ethanol was added. The precipitates were collected by centrifugation and re-dissolved in 500 ml of $H_2O$. After adding 67 ml of 5 M NaCl solution and lowering the pH to 3, 1.24 L of ethanol was added. The precipitates were again collected by centrifugation and re-dissolved in 300 ml of $H_2O$. The conjugates were then dialyzed (Spectra/Por 7, MWCO = 3500 Da) against $H_2O$ in $N_2$ atmosphere overnight. Finally, the purified HA-EGCG conjugates were lyophilized. The yield was 185 mg (74%). For NMR analysis, the lyophilized conjugates were dissolved in $D_2O$ at 10 mg/ml. To

determine the degree of substitution (DS, the number of EGCG dimers conjugated for every 100 disaccharide units), the conjugates were dissolved at 0.5 mg/ml in water and UV-Vis spectrum was recorded with a Hitachi U-2810 spectrometer. The amount of EGCG contained in the conjugate was determined by comparing the absorbance at 273 nm with a set of EGCG standards. HA-EGCG conjugates made from 800 kDa HA were used for hyaluronidase inhibition, radical scavenging assays and hydrogel formation. HA-EGCG conjugates made from 90 kDa HA were filtered through a 0.2 μm syringe filter before lyophilization; the lyophilized products were dissolved in sterile $H_2O$ at 50 mg/ml and used for cell growth experiments.

### 8.2.6. Hyaluronidase inhibition study

HA and HA-EGCG conjugates (2 mg/ml) were treated with 0, 2.5 and 12.5 U/ml of hyaluronidase in 0.1 M sodium phosphate buffer (pH 5.7) for 20 h at 37 °C. The amount of reducing ends generated was determined by Morgan-Elson assay [21]. DMAB stock solution was prepared by dissolving 5 g of DMAB in 6.25 ml of 10 M HCl and then topped up to 50 ml with acetic acid. The DMAB reagent was diluted 10-fold with acetic acid immediately before use. The hyaluronidase-treated samples were first diluted 4-fold with $H_2O$, then 32 μl of which was mixed with 8 μl of borate solution (0.741 g of boric acid and 0.297 g of potassium hydroxide in 15 ml of $H_2O$, pH 9). The mixture was heated at 99 °C for 5 min. After cooling down to room temperature, 160 μl of DMAB was added and the mixture was then incubated at 37 °C for 20 min. One hundred and fifty μl of the solution was transferred to a 96-well plate and the absorbance at 585 nm was determined by a Tecan Infinite 200 microplate reader. The amount of reducing ends was determined by comparing to a set of *N*-acetyl-D-glucosamine standards. The dynamic viscosity was measured using a HAAKE Rheoscope 1 rheometer equipped with a cone sensor (3.5 cm in diameter and 1.029° cone angle) at a shear rate of 400/s and 25 °C.

### 8.2.7. Cell culture

Human fibroblast-like synoviocytes (HFLS) were grown in RPMI 1640 medium supplemented with 10% FBS and 1% penicillin-streptomycin. The cells were cultured in T75 tissue culture flasks and incubated at 37 °C and with 5% $CO_2$. Cells below passage 10 were used.

### 8.2.8. Cell growth assay

To determine the effect of HA, HA-EGCG conjugates and EGCG on cell growth, 2.5 x $10^3$ HFLS in 100 μl of complete growth medium were seeded on the wells of a 96-well plate. After overnight incubation, the spent medium was replaced with 50 μl of fresh complete growth medium containing 40 ng/ml of tumor necrosis factor alpha (TNFα). Next, 50 μl of HA, HA-EGCG conjugates or EGCG was added. HA/HA-EGCG conjugates and EGCG were first dissolved in water at 50 mg/ml and 2 mM, respectively, before they were diluted in RPMI 1640 and added to the wells. The final concentration of TNFα in the wells was 20 ng/ml. The final concentrations of HA or HA-EGCG conjugates were 0.2, 0.3, 0.6, 1.3 or 2.5 mg/ml. The final concentrations of EGCG were 6.3, 12.5, 25, 50 or 100 μM, which corresponded to the concentrations of EGCG contained in the HA-EGCG conjugates. The plate was incubated at 37 °C for 3 days, after which images of the cells were taken using a microscope, and the number of cells in the wells were determined by DNA quantification using PicoGreen® dsDNA assay kit. Briefly, the spent medium was removed and the cells were lysed with 20 μl of 0.2% Triton X-100 in PBS for 30 min on a shaker. Then 180 μl of PicoGreen® reagent, prepared according the manufacturer's protocol, was added to each well. The plate was placed for 5 min in the dark and then the fluorescence was measured using a microplate reader ($\lambda_{ex}$ = 480 nm and $\lambda_{em}$ = 520 nm). The amount of DNA in each well was expressed in terms of the percentage of the controls (no treatment).

### 8.2.9. Radical scavenging assays

$^{\bullet}$NO was generated by sodium nitroprusside and measured according to a previously described method [22]. Briefly, 50 μl of HA, HA-EGCG conjugates or EGCG dissolved in $H_2O$ at various concentrations was added to the wells of a 96-well plate. Then, 50 μl of sodium nitroprusside (10 mM in 0.2 M sodium phosphate buffer, pH 7.4) was added. After incubation at room temperature for 2.5 h under light, 100 μl of Greiss reagent was added. After 2 min incubation, the absorbance at 570 nm was recorded using a microplate reader. A reaction without any test sample ($H_2O$ only) was performed as control. The percentage of $^{\bullet}$NO scavenged were calculated using the following equation, where $A_{control}$ and $A_{sample}$ were the absorbance values of the control and sample, respectively:

$$\text{Radicals scavenged (\%)} = \left(\frac{A_{control} - A_{sample}}{A_{control}}\right)$$

$^{\bullet}OH$ was generated by Fenton reaction using $FeSO_4$ and $H_2O_2$. The amount of $^{\bullet}OH$ was determined by the thiobarbituric acid reaction in which the $^{\bullet}OH$ degrades 2-deoxy-D-ribose into a 3-carbon compound, malondialdehyde, which then forms a chromogen in the presence of thiobarbituric acid [23, 24]. One hundred μl of HA or HA-EGCG conjugates dissolved in $H_2O$ at various concentrations was added to microcentrifuge tubes. Then, a solution containing 2-deoxy-D-ribose (20 mM), ascorbic acid (80 μM) and $FeSO_4$ (80 μM) in 50 μl of buffer (0.2 M sodium phosphate buffer with 0.3 M NaCl, pH 7.4) was added. Next, 50 μl of $H_2O_2$ (882 μM) prepared in buffer was added to initiate Fenton reaction. After incubating at 37 °C for 1.5 h, 50 μl of the reaction mixture was mixed with 50 μl each of trichloroacetic acid (2.8%, w/v) and thiobarbituric acid (1% in 50 mM NaOH, w/v). The mixture was heated at 99 °C for 15 min. After cooling down to room temperature, 100 μl was transferred to the wells of a 96-well plate and the absorbance at 532 nm was measured using a microplate reader. The percentage of $^{\bullet}OH$ scavenged was determined by the above equation.

$^{\bullet}O_2^-$ was generated by XO and xanthine and measured by NBT reduction assay based on a previously established protocol with some modifications [25]. Stock solution of xanthine was prepared at 2.28 mg/ml in 1 M NaOH and diluted 10-fold in 0.2 M sodium phosphate buffer (pH 7.4) immediately before use. Fifty μl of HA or HA-EGCG conjugates dissolved in $H_2O$ was added to the wells of a 96-well plate. Then, 15 μl of XO (0.27 units/ml), 15 μl of NBT (0.2 mM) and 20 μl of xanthine (1.5 mM), all prepared in 0.2 M sodium phosphate buffer (pH 7.4), were added sequentially. Production of $^{\bullet}O_2^-$ was monitored by the formation of formazan dye at 560 nm using a microplate reader. Absorbance measurement was started immediately after adding xanthine and was recorded for 2 min during which the absorbance of the control (no test sample) increased linearly, suggesting a linear production of $^{\bullet}O_2^-$. The slope of the absorbance measurement during the 2 min period was determined by linear-fitting the data points using Microsoft Excel. The percentage of $^{\bullet}O_2^-$ scavenged was then determined by the following equation, where $S_{control}$ and $S_{sample}$ were the slopes of the control and sample, respectively:

$$^{\bullet}O_2^- \text{ scavenged (\%)} = \left(\frac{S_{control} - S_{sample}}{S_{control}}\right)$$

The radical scavenging activities were expressed as 50% scavenging concentration ($SC_{50}$), which was the sample concentration required to decrease in the signal intensity ($^{\bullet}NO$ and $^{\bullet}OH$) or the slope ($^{\bullet}O_2^-$) by 50% relative to the control.

### 8.2.10. Determination of $H_2O_2$ production by HA-EGCG conjugates at different pH

HA-EGCG conjugates were dissolved in $H_2O$ at 1.43 mg/ml by stirring vigorously. Seventy μl of the HA-EGCG solution was added to 230 μl of $H_2O$ and then frozen at -20 °C, this was later used to quantify the amount of $H_2O_2$ produced during the dissolution process. The pH of HA-EGCG solution was adjusted to pH 5 or 7.4 by using sodium phosphate buffer as described above, the final HA-EGCG concentration was 1 mg/ml. The HA-EGCG solutions were incubated in an orbital shaker at 80 rpm and 37°C. At selected time points, 50 μl of the samples was collected and mixed with 100 μl of 0.2 M HCl to stop the autoxidation reaction. The samples were kept frozen at -20 °C until analysis. $H_2O_2$ concentrations were determined by PeroXOquant Quantitative Peroxide Assay Kits, aqueous-compatible formulation (Pierce), according to manufacturer's protocol.

### 8.2.11. Formation of HA-EGCG hydrogels and rheological measurement

HA-EGCG conjugates were dissolved in $H_2O$ at 14.3 mg/ml. Hydrogels were formed according to the formulations shown in Table 8-1. The pH was adjusted to pH 7.4 by sodium phosphate buffer and to pH 5 by a combination of sodium phosphate buffer and HCl. The total volume was 500 μl and the final concentration of HA-EGCG conjugates was 10 mg/ml. For HRP-mediated crosslinking reaction shown in Fig. 9-2b and 2c, the final HRP concentration was 0.062 and 0.168 U/ml at pH 7.4 and pH 5, respectively. A higher concentration of HRP was used at pH 5 in order to compensate for the reduced enzymatic activity when compared with pH 7.4. In order to examine the effect of HRP concentration on gel formation at pH 7.4 (Fig. 8-12f), the final HRP concentration was varied from 0.016 to 0.125 U/ml. For HRP-mediated crosslinking reaction at pH 5 in the presence of exogenous $H_2O_2$, $H_2O_2$ was added to attain a final concentration of 0.7 mM.

**Table 8-1. Hydrogel Formulations**[a]

| Sample | HA-EGCG (μl)[b] | $H_2O$ (μl) | 1.5 M $NaH_2PO_4$ (μl) | 0.6 M $Na_2HPO_4$ (μl) | 2M HCl (μl) | HRP (μl)[c] | $H_2O_2$ (μl)[d] |
|---|---|---|---|---|---|---|---|
| pH 7.4 (-HRP) | 350 | 39.3 | 9.5 | 101.3 | 0 | 0 | 0 |
| pH 7.4 (+HRP) | 350 | 2.5 | 9.5 | 101.3 | 0 | 36.8 | 0 |
| pH 5 (-HRP) | 350 | 87.3 | 43.9 | 15.4 | 3.5 | 0 | 0 |
| pH 5 (+HRP) | 350 | 50.5 | 43.9 | 15.4 | 3.5 | 36.8 | 0 |
| pH 5 (+HRP/$H_2O_2$) | 350 | 0 | 43.9 | 15.4 | 3.5 | 36.8 | 50.5 |

[a] The total volume for each formulation was 500 μl and the final HA-EGCG concentration was 10 mg/ml. [b] 14.3 mg/ml in $H_2O$. [c] HRP was dissolved in $H_2O$. For hydrogels formed pH 7.4, the HRP feed concentration varied

from 0.22 to 1.70 U/ml. For hydrogels formed at pH 5, the HRP feed concentration was 2.28 U/ml. [d] 7.0 mM in $H_2O$.

For gel formation studies, the different gel formulations were prepared in test tubes, vortexed and then incubated at 37 °C. Digital photographs were taken on selected time points with the test tubes tilted at 90° angle. For $^1H$ NMR measurement of hydrogel formed at pH 7.4 in the absence of HRP, the formulation shown in Table 9-1 was used with the exception that the solvent was $D_2O$. The mixture was transfer to an NMR tube and allowed to gel overnight at 37 °C. Rheological measurement was performed according to the procedures described in Chapter 3 using a HAAKE Rheoscope 1 rheometer (Karlsruhe, Germany) equipped with a cone sensor (3.5 cm in diameter and 1.029° cone angle). The evolution of G' and G'' were measured for 10 h at 37 °C in the dynamic oscillatory mode with constant deformation of 1% and frequency of 1 Hz. The gel point was defined as the time taken for G' to crossover G''.

### 8.2.12. Synthesis of HA-tyramine conjugates and formation of HA-tyramine hydrogels

The synthesis of HA-tyramine conjugates was performed according to the procedures described in Chapter 2 with some modifications. Five hundred mg of HA (800 kDa) was dissolved in 45 ml of 0.4M MES buffer (pH 5.2) and 5 ml of DMF. Then NHS (179 mg, 1.55 mmol) and Tyr·HCl (71 mg, 0.41 mmol) were added. After which EDC·HCl (300 mg, 1.56 mmol) was added and the pH was adjusted to 4.7. The reaction was stirred overnight at r.t. and then the pH was adjusted to 7. The mixture was dialyzed (Spectra/Por 7 MWCO = 3500 Da) against 100 mM NaCl for two days, 25% ethanol for 1 day and $H_2O$ for 1 day and then lyophilized. The yield was 84% and the degree of substitution (the number of tyramine conjugated for every 100 disaccharide units) was determined by absorbance at 274 nm and was found to be 3. HA-tyramine hydrogels (10 mg/ml) were formed in the presence of 0.062 U/ml of HRP and 104 μM of $H_2O_2$. The G' of HA-tyramine hydrogel was 100 Pa.

### 8.2.13. *In vitro* hydrogel degradation study

HA-EGCG and HA-tyramine gel precursors (200 μl, 10 mg/ml, pH 7.4) were prepared as described above and added between two glass plates with 1.5 mm spacing. After overnight incubation at 37°C, the hydrogels were sandwiched between plastic nets and swelled in 20 ml of PBS. The next day, the swollen hydrogels were transferred to 20 ml of PBS (0.05% (w/v) sodium azide) containing 2.5 or 10 U/ml of hyaluronidase and incubated at 37°C in an orbital

shaker at 100 rpm. At selected time points, the hydrogels were removed from the degradation solution with a pair of forceps, gently blotted dry with Kimwipe and weighed.

### 8.2.14. Animal studies

Female Balb/c mice were used in the study. HA-EGCG conjugates were filtered through 0.22 μm syringe filter, lyophilized and dissolved in sterile water. Phosphate buffer, HRP and HA-tyramine solutions were sterile-filtered as well. One hundred μl of HA-EGCG or HA-tyramine gel precursors (10 mg/ml, pH 7.4) were prepared as described above and immediately injected into the subcutaneous tissue using a 25G needle. Each mouse bore two hydrogels. On day 1, 20 and 42 post-injection, the mice were euthanized by $CO_2$ and the remaining hydrogels were retrieved and weighed. The care and use of laboratory animals were performed according to the approved protocol by the Institutional Animal Care and Use Committee (IACUC) at the Biological Resource Center (BRC) in Biopolis, Singapore.

### 8.2.15. Statistics

Results were expressed as the mean ± standard deviation (SD). The difference between the values was assessed using Student's *t*-test in Microsoft Excel.

## 8.3. Results and discussion

### 8.3.1. Synthesis and characterization of ethylamine-bridged EGCG dimers

It is known that the B and D rings of EGCG are crucial for its bioactivities such as enzyme inhibition [26], induction of apoptosis [27] and scavenging of radicals [28, 29]. For instance, decreasing the number of hydroxyl groups in the B ring reduced its anti-cancer activity as a proteasome inhibitor [30]. Hence it is important to keep these sites intact during chemical modifications. Toward this goal, we utilized an aldehyde-mediated condensation reaction which selectively reacts with the A ring of EGCG (Fig. 8-3) [17]. The reaction, also known as Baeyer acid-catalyzed condensation, occurs during wine-aging in which flavanols react with aldehydes to form dimeric or oligomeric compounds [31-33]. The resulting chemical bridge between the flavanols depends on the aldehyde that is used for the reaction. In this study 2,2-diethoxyethylamine (DA), a protected aldehyde, was chosen to react with EGCG because it contains a primary amine which can form amide bond with the carboxyl groups of HA. Under acidic conditions the diethylacetal exists in equilibrium with aldehyde,

which in turn accepts nucleophilic attack by the C-6 or C-8 of EGCG. The resulting intermediate further involves another EGCG to elaborate the EGCG dimers **1, 2a, 2b**, and **3**.

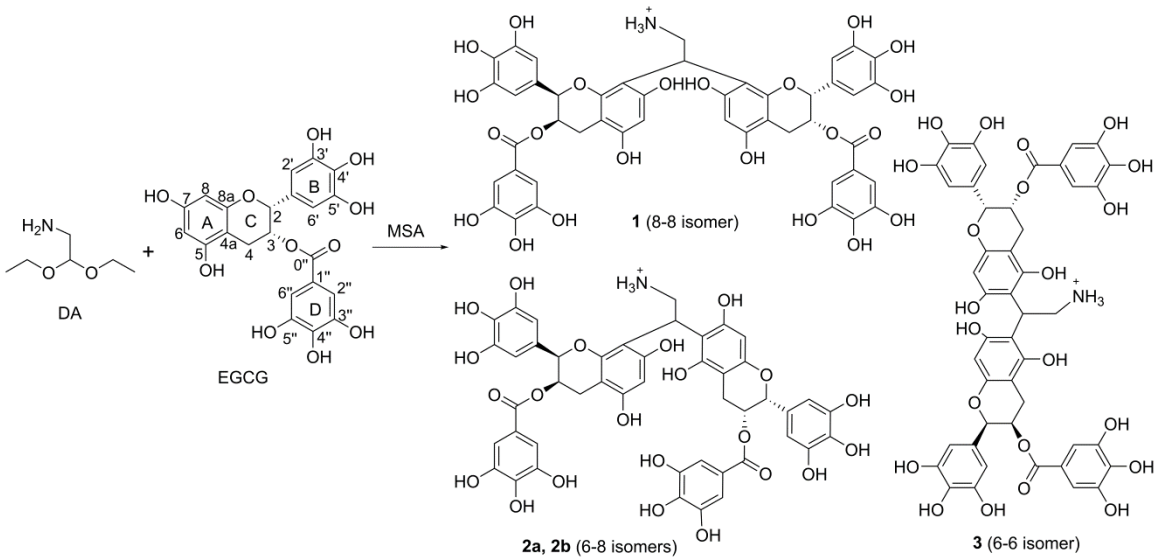


**Fig. 8-3. Synthesis of ethylamine-bridged EGCG dimers**

It was reported that the aldehyde-mediated condensation reaction of flavanols would yield four isomers with 8-8, 6-6 and two 6-8 linkages, which stems from the linkage between the two reactive sites on the A ring (C-6 and C-8) and the asymmetric carbon [32, 33]. Indeed, four major peaks were observed in HPLC analysis in which two peaks in the middle overlapped with each other (Fig. 8-4). According to previous studies the aldehyde-mediated condensation reaction is regioselective due to the sterically favorable substitution of C-8 over C-6, hence the 8-8 isomer should be generated the most while the 6-6 isomer the least [32, 34]. Based on this information, the largest peak observed in the HPLC, i.e., the first eluted peak, was assigned to **1**, the 8-8 isomer. The next two overlapping peaks accounted for **2a** and **2b**, the two 6-8 stereoisomers. The last eluted peak, which was also the smallest in area, came from **3**, the 6-6 isomer. Each isomer was isolated by preparative HPLC for NMR analysis to elucidate the chemical structures. Only three fractions were collected because the two overlapping peaks, which contained **2a** and **2b** (6-8 stereoisomers), were eluted together as one fraction. All three fractions had *m/z* of 958 as determined by LC/MS, which corresponded to $[M + H]^+$.

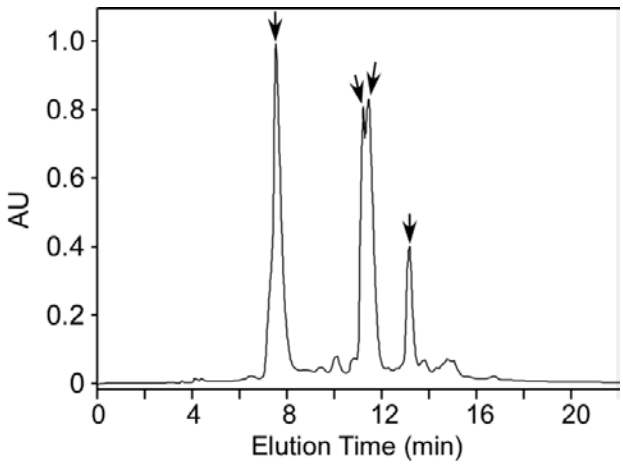


**Fig. 8-4. HPLC chromatogram (UV absorbance at 280 nm) of ethylamine-bridged EGCG dimers. Arrows indicate the major peaks which correspond to the four isomers.**

$^{1}$H NMR spectrum of the first eluted fraction, which contained **1** (8-8 isomer), revealed that the chemical shifts were paired, i.e., two peaks with equal intensity, particularly for H-2' and H-6' of the B ring and H-2" and H-6" of the D ring (Fig. 8-5a). Similarly, several of the $^{13}$C chemical shifts were paired (Table 8-2). These results imply the presence of two sets of EGCG with different resonance, which was likely caused by the formation of an ethylamine bridge between two EGCG molecules. The broad peak centered at 3.89 ppm was assigned to the $CH_2$ protons of the ethylamine bridge. The assignment was supported by the chemical shift of the corresponding carbon determined by $^{1}$H-$^{13}$C HSQC, which was negative (43.74 ppm, Fig. 8-5b), indicating either a secondary, as in this case, or a quaternary carbon. A triplet centered at 5.49 ppm was found to overlap with the chemical shifts of the H-3 proton of EGCG (Fig. 8-5a inset). This was assigned to the CH proton of the ethylamine linkage as coupling of the CH proton to the $CH_2$ protons of the ethylamine bridge would result in a triplet. Indeed, integration from 5.4 to 5.6 ppm revealed the presence of three protons, which corresponded to one CH proton and two H-3 protons. The chemical shift of the CH carbon as located by $^{1}$H-$^{13}$C HSQC (Fig. 8-5b) was positive (31.10 ppm), indicating either a primary or a tertiary carbon. The CH carbon is a tertiary carbon. Correlations between the protons of $CH_2$ and CH of the ethylamine bridge with C-8 carbon of EGCG were observed (Fig. 8-5c). The unambiguous assignment of the resonance of $CH_2$ and CH confirmed the formation of an ethylamine bridge between two EGCG molecules.

$^{13}$C NMR spectrum of **1** is shown in Fig. 8-5d. In order to assign the six carbon peaks of C-5, C-7 and C-8a which resonate closely between 154 to 156 ppm (Fig. 8-5a, inset), $^{1}$H-$^{13}$C HMBC focusing on this region was performed to obtain a high resolution spectrum. The

HMBC correlations were shown in Fig. 8-5e, and the six carbons peaks were assigned as follows. The carbons at 154.30 and 154.62 ppm, which showed correlations with the CH proton of the ethylamine bridge but not the H-6 protons of the A ring, were assigned as C-8a (Fig. 8-5f). On the contrary, the carbons at 155.38 and 155.61 ppm, which correlated with the H-6 protons but not the CH proton of the ethylamine bridge, were assigned as C-5. The remaining two carbons at 155.51 and 155.92 ppm, which exhibited correlations with both the CH proton and the H-6 protons, were assigned as C-7. Similar procedure was applied to assign the $^{1}H$ and $^{13}C$ peaks for the other isomers (Table 8-2). However, we could not assign the $^{13}C$ resonance for C-5, C-7 and C-8a of **2a** and **2b** as they were eluted together in one fraction. It is worth mentioning that the $^{1}H$ NMR spectrum of the fraction containing **2a** and **2b** showed four peaks for each of the protons of the B ring and D ring (Fig. 8-6a). On the other hand, $^{1}H$ NMR of **3** showed a single peak for each of the protons of the B and D rings (Fig. 8-6b).

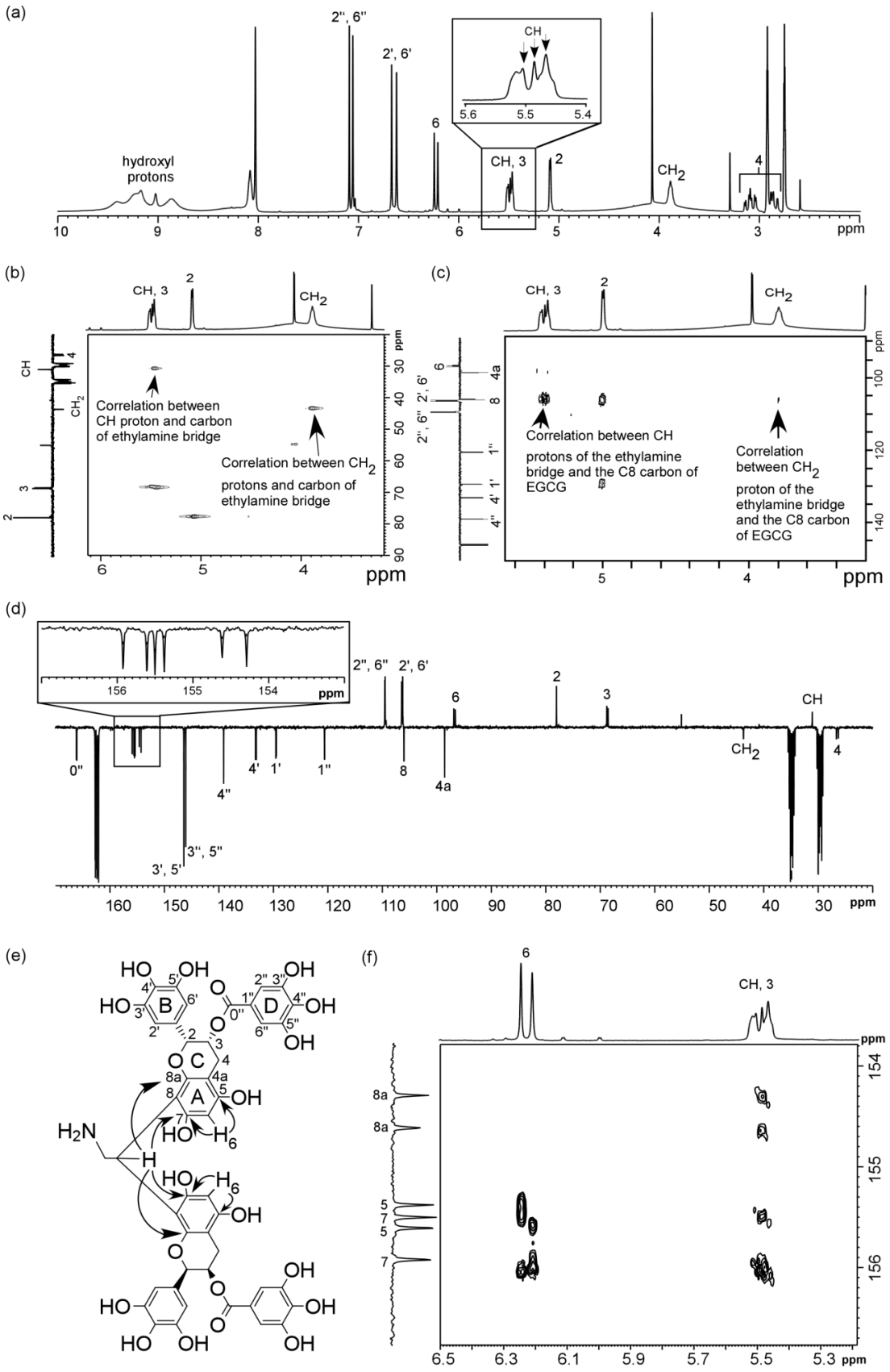


**Fig. 8-5. NMR characterization of 1 (8-8 isomer) (a) $^{1}$H NMR spectrum. The CH protons were buried within the resonance of H-3 as indicated by arrows (inset). (b) HSQC spectrum showing the correlations between the protons and carbons of ethylamine bridge. (c) HMBC spectrum showing the correlations**

**between the protons and of ethylamine bridge and C-8 of EGCG. (d) $^{13}$C NMR spectrum. (e) $^{1}$H-$^{13}$C HMBC correlations. (f) $^{1}$H-$^{13}$C HMBC spectrum.**

**Table 8-2.** $^{1}$H and $^{13}$C assignments of **1, 2a, 2b** and 3 in DMF-$d_7$ ($\delta$ in ppm, $J$ in Hz)

| No. | **1** (8-8 isomer) | | **2a, 2b** (6-8 isomers) | | **3** (6-6 isomer) | |
|---|---|---|---|---|---|---|
| | $^{1}$H | $^{13}$C | $^{1}$H | $^{13}$C | $^{1}$H | $^{13}$C |
| $CH_2$ | 3.89 | 43.73 | Buried[a] | 42.80, 43.57 | 3.90 | 42.15 |
| CH | 5.45-5.52 | 31.10 | 5.35-5.45, 5.50-5.60 | 30.73, 30.96 | 5.19 (t, $J$ = 7.5) | 31.10 |
| 2 | 5.08, 5.09 | 78.05 | 5.00-5.20 | 77.60, 78.10 | 5.0-5.1 | 77.77 |
| 3 | 5.40-5.55 | 68.57, 68.80 | 5.47 | 68.66, 68.82, 69.09, 69.21 | 5.48 | 69.06 |
| 4 | 2.80-3.20 | 26.31, 26.66 | 2.80-3.20 | 26.29, 26.90 | 2.80-3.20 | 26.89 |
| 4a | - | 98.58 | - | 99.33, 99.38, 99.69, 100.08 | - | 100.98 |
| 5 | - | 155.38, 155.61 | - | N.A.[c] | - | 154.82, 154.88 |
| 6 | 6.21, 6.24 | 96.62, 96.90 | 6.25, 6.28[b] | 107.95[b] | - | 107.20, 107.37 |
| 7 | - | 155.51, 155.92 | - | N.A.[c] | - | 154.11 |
| 8 | - | 106.04 | 6.18, 6.21[b] | 104.74, 105.26[b] | 6.24, 6.25 | 96.21, 96.38 |
| 8a | - | 154.30, 154.62 | - | N.A.[c] | - | 155.28, 155.33 |
| 1’ | - | 129.46, 129.55 | - | 129.28, 129.58, 129.63, 129.31 | - | 129.36 |
| 2’, 6’ | 6.62, 6.67 | 106.28, 106.47 | 6.60, 6.62, 6.67, 6.68 | 106.18, 106.27, 106.37, 106.20 | 6.60 | 106.16 |
| 3’, 5’ | - | 146.44 | - | 146.36, 146.38, 146.43 | - | 146.46 |
| 4’ | - | 133.14, 133.28 | - | 133.15, 133.21 | - | 133.27, 133.29 |
| 0” | - | 166.08, 166.16 | - | 165.98, 166.01, 166.06 | - | 166.02, 166.06 |
| 1” | - | 120.61, 120.64 | - | 120.52, 120.57 | - | 120.45 |
| 2”, 6” | 7.06, 7.09 | 109.50, 109.56 | 7.00, 7.03, 7.06, 7.09 | 109.31, 109.49 | 7.03 | 109.31 |
| 3”, 5” | - | 146.10 | - | 146.07, 146.12 | - | 146.17 |
| 4” | - | 139.14 | - | 139.10 | - | 139.14 |

[a]Buried in the $H_2O$ peak. [b] Values may be switched. [c] Unable to assign accurately because there are two stereoisomers in the sample.

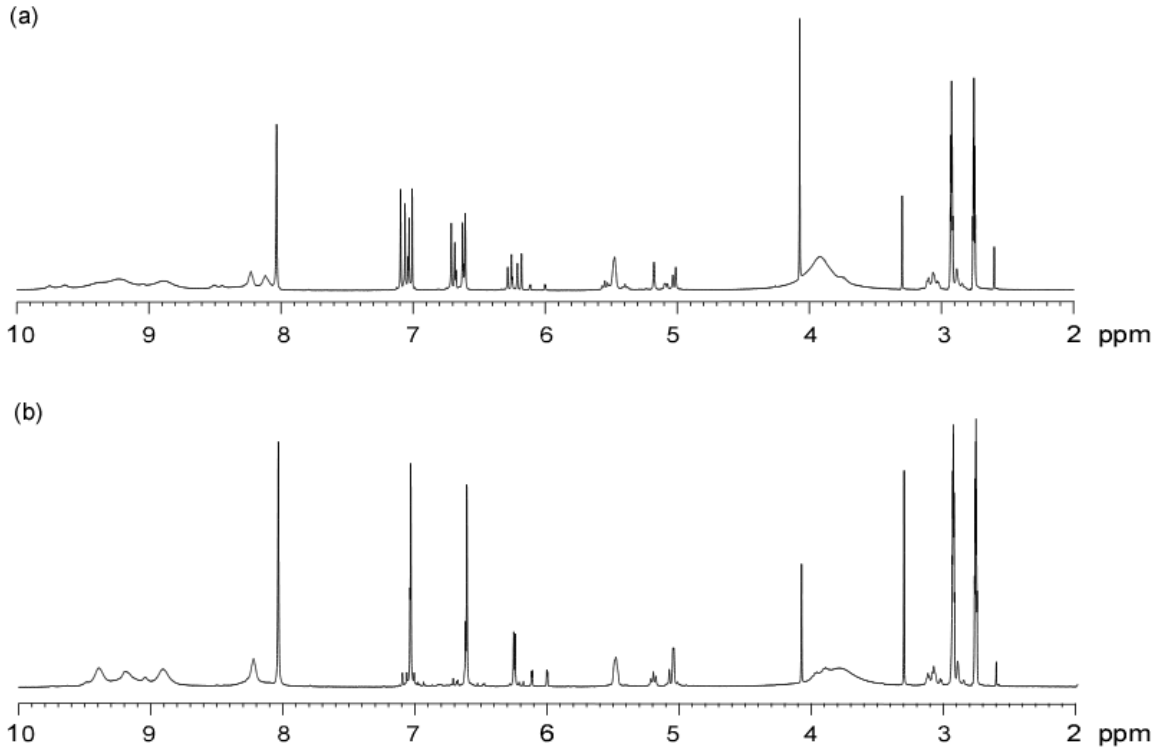


**Fig. 8-6. $^{1}$H NMR spectra of (a) 2a and 2b (6-8 isomers), and (b) 3 (6-6 isomer).**

### 8.3.2. Synthesis and characterization of HA-EGCG conjugates

Ethylamine-bridged EGCG dimers were conjugated to HA by a typical carbodiimide-mediated coupling reaction to obtain HA-EGCG conjugate (Fig. 8-7). Removal of unreacted EGCG dimers from reaction mixture by dialysis against water was attempted but found to be inefficient. Dialysis against a mixture of DMF:$H_2O$ (10:90, v/v) could remove the unreacted EGCG dimers, but the process took several days. In contrast, by precipitating the HA-EGCG conjugates with ethanol in the presence of NaCl, HA-EGCG conjugates formed slurry precipitates which could be easily collected by centrifugation. The unreacted EGCG dimers remained in the supernatant and were decanted. After lyophilization the purified HA-EGCG conjugate was dissolved in $D_2O$ and analyzed by $^{1}$H NMR (Fig. 8-8a). Although the peaks corresponding to the protons of the B and D rings could be observed (Fig. 8-8a inset), the signal to noise ratio of these peaks was too low for accurate integration. Hence absorbance measurement was employed to determine the degree of substitution. HA-EGCG conjugate showed a peak at around 273 nm (Fig. 8-8b, solid line), which corresponds to the π-π* transitions of the aromatic rings of EGCG. Ethylamine-bridged EGCG dimers also showed a peak at 273 nm (dashed line) while HA did not (dotted line). The degree of substitution (DS, the number of EGCG dimers conjugated for every 100 disaccharide units) was calculated by

comparing the absorbance at 273 nm to a set of EGCG standards. The DS of HA-EGCG conjugates made from 90 kDa and 800 kDa of HA were 0.8 and 1, respectively.

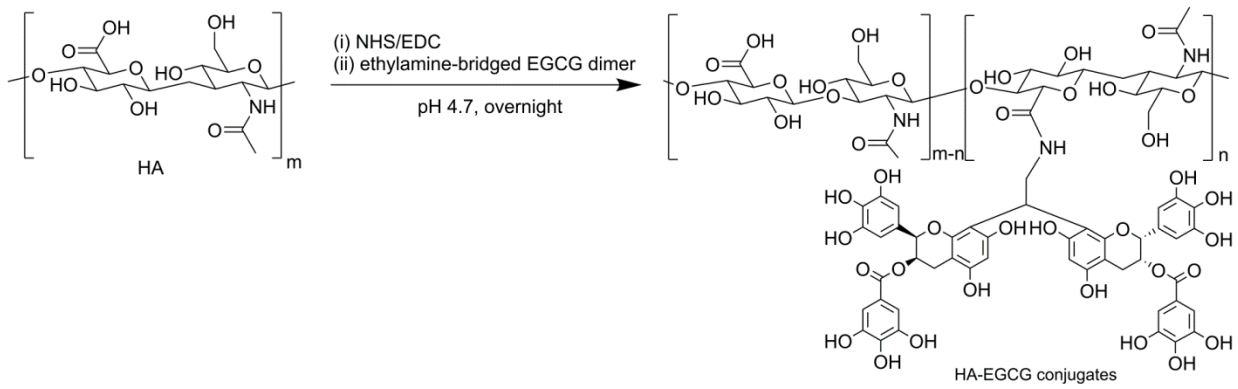


**Fig. 8-7. Synthesis of HA-EGCG conjugates.**

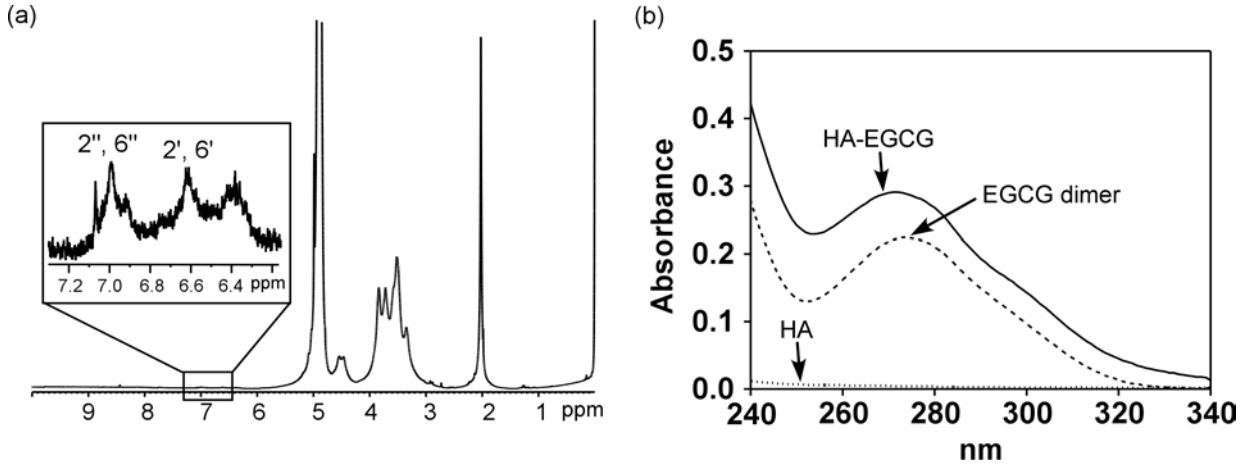


**Fig. 8-8. Characterization of HA-EGCG conjugates (800 kDa). (a) $^{1}$H NMR of 10 mg/ml of HA-EGCG conjugates in $D_2O$. Chemical shifts of H-2' and H-6' of B ring and H-2'' and H-6'' of D ring of EGCG were visible (inset). (b) Absorbance spectra of ethylamine-bridged EGCG dimer (dashed line, 10 µg/ml), HA-EGCG conjugate (solid line, 0.5 mg/ml) and unmodified HA (dotted line, 0.5 mg/ml) in $H_2O$.**

### 8.3.3. Hyaluronidase inhibition by HA-EGCG conjugates

Tea polyphenols are known to bind to proteins through hydrophobic interaction and hydrogen bonding, thereby inhibiting the activity of enzymes [35, 36]. Mammalian hyaluronidase cleaves the β-1,4-glycosidic bonds of HA, generating HA fragments with *N*-acetyl-D-glucosamine reducing ends [37]. It is expected that the EGCG moieties of HA-EGCG conjugates would inhibit hyaluronidase and reduce the rate of enzymatic degradation of the HA backbone. HA-EGCG conjugates and HA (2 mg/ml) were incubated with hyaluronidase solution for 20 h and the amount of reducing ends and the dynamic viscosity

($\eta$) of the degraded samples were measured. In the case of HA-EGCG conjugates, the reducing end concentration remained below 0.1 mM as the concentration of hyaluronidase increased from 0 to 12.5 U/ml (Fig. 8-9a). On the contrary, the reducing ends increased to more than 0.7 mM in the case of HA. Moreover, the dynamic viscosities of HA-EGCG conjugates were higher than HA after incubation with hyaluronidase (Fig. 8-9b). The results suggested that HA-EGCG conjugates were less susceptable to degradation by hyaluronidase compared with HA, likely due to the inhibition of hyaluronidase activity by the EGCG moieties.

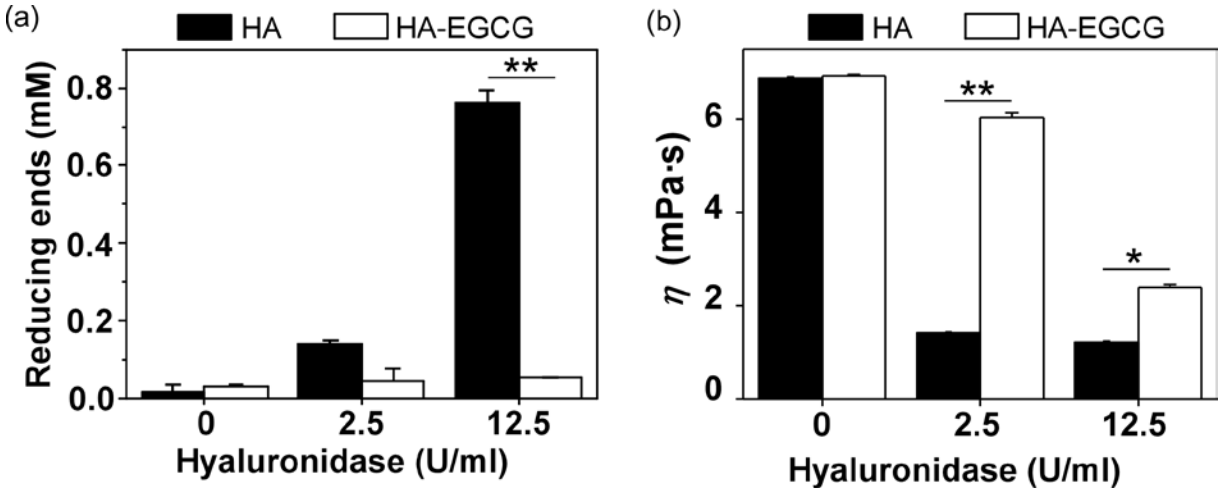


**Fig. 8-9. Inhibition of hyaluronidase activity. (a) Concentration of reducing end generated and (b) dynamic viscosity ($\eta$) of HA or HA-EGCG conjugates after treatment with hyaluronidase for 20 h at 37 °C (n = 3, mean ± SD). *$p$ < 0.05 and **$p$ < 0.005.**

Chemical modification of HA is known to disrupt hyaluronidase binding which in turn hinders degradation by the enzyme and can potentially prolong HA residence time *in vivo* [38]. In one study, the resistance to enzymatic degradation of serine-grafted HA increased as the degree of substitution increased from 40 to 100 [39]. Extensive modification of HA, however, would lead to changes in its physical and biological properties. In comparison, only 1% of the carboxyl groups of HA were substituted with EGCG dimers in the HA-EGCG conjugate, hence it was unlikely that the observed resistance to enzymatic degradation was caused by modification of HA. Rather it was the interaction between the EGCG moieties and hyaluronidase that inactivated the enzyme.

### 8.3.4. Anti-proliferative activity of HA-EGCG conjugates

EGCG is well-known for its anti-proliferative property. We examined the anti-proliferative property of HA-EGCG conjugates using an *in vitro* model of rheumatoid arthritis. Rheumatoid arthritis is an autoimmune joint disease characterized by hyperplasia of the synovial lining, which behaves like a local tumor that invades the cartilage and underlying bone, leading to joint destruction [40]. Human fibroblast-like synoviocytes (HFLS) derived from rheumatoid arthritis patient were treated with HA, HA-EGCG conjugates or EGCG while under stimulation by TNFα to simulate the inflammatory environment *in vivo*. After 3 days incubation, cells treated with HA retained healthy morphology across all the concentrations (Fig. 8-10a). Cells treated with HA-EGCG conjugates displayed normal morphology; with exception at the highest concentration of HA-EGCG conjugates, i.e., 2.5 mg/ml (containing 100 μM of EGCG). At this concentration, cells lost their elongated morphology but remained attached to the well. Cells treated with EGCG appeared apoptotic at EGCG concentrations above 50 μM. The cell number, measured in terms of the amount of DNA and expressed as a percentage of the control (no treatment), of samples treated with HA was similar to the control across the different concentrations (Fig. 8-10b). In contrast, DNA amount decreased with increasing concentrations of HA-EGCG conjugates or EGCG, suggesting the inhibition of cell growth (Fig. 8-10c). Remarkably, HA-EGCG conjugates inhibited cell growth as effectively as EGCG. The observed growth inhibition is in agreement with a previous study which reported that EGCG can downregulate uncontrolled growth and induce apoptosis in HFLS [41].

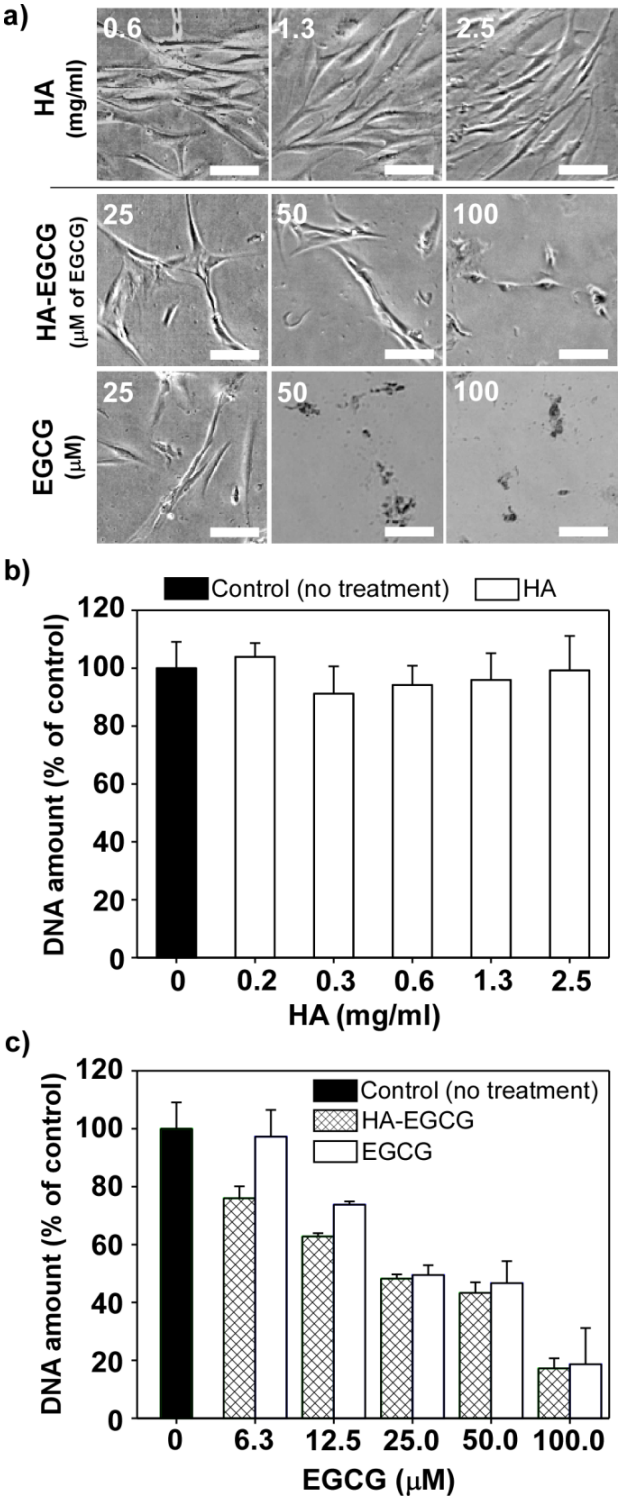


**Fig. 8-10. HFLS derived from rheumatoid arthritis patient were treated with HA, HA-EGCG conjugates or EGCG for 3 days. (a) Representative microscope images of the treated cells. Scale bar = 50 μm. (b-c) Amount of DNA, expressed in terms of percentage of the control (no treatment), for samples treated with (b) HA, (c) HA-EGCG conjugates or EGCG. HA-EGCG conjugates at 0.2, 0.3, 0.6, 1.3 and 2.5 mg/ml contained 6.3, 12.5, 25, 50 and 100 μM of EGCG, respectively (n = 4, mean ± SD).**

### 8.3.5. Radical scavenging activity of HA-EGCG conjugate

HA is known to have antioxidant activity, which is attributed to reactive oxygen species (ROS)-induced chain depolymerization and the formation of a viscous meshwork that restricts ROS movement [42, 43]. However, only high molecular weight HA (3000-6000 kDa) showed significant radical scavenging activity and little effect was observed for low molecular weight HA [42]. Indeed, we found that HA (800 kDa) showed negligible scavenging activities towards $^{\bullet}NO$, $^{\bullet}OH$ and $^{\bullet}O_2^-$ (Fig. 8-11). On the other hand, HA-EGCG conjugates showed concentration-dependent radical scavenging activities (Fig. 8-11). The concentrations at which 50% of the radicals were scavenged ($SC_{50}$) were listed in Table 8-3. The radical scavenging activity of HA-EGCG conjugates was attributed to the EGCG moieties. EGCG is one of the most potent radical scavengers among the different green tea catechins due to the high number of hydroxyl groups contained in the B ring and the galloyl moiety (D ring) [28, 44]. In addition to direct scavenging of radicals, EGCG can inhibit the generation of $^{\bullet}OH$ radicals by chelating metal ions and preventing them from participating in Fenton reaction [45]. EGCG can also bind to enzymes such as xanthine oxidase (XO) and inhibit its enzymatic activity, which in turn prevents the generation of $^{\bullet}O_2^-$ [46].

Hyaff®-11p75 (benzyl esters of HA with an approximate molecular weight of 300 kDa), a commercially available HA-derived product used in wound healing applications, was shown to scavenge $^{\bullet}O_2^-$ more effectively than high molecular weight HA (3000-6000 kDa) despite having a lower molecular weight [42]. The superior scavenging activity is attributed to the high degree of benzyl groups which offer alternative sites for $^{\bullet}O_2^-$ attack. Though Hyaff®-11p75 can scavenge $^{\bullet}O_2^-$ effectively, its physio-chemical property is quite different from that of native HA because 75% of the carboxyl groups are esterified with benzyl alcohol. As a result, Hyaff®-11p75 requires DMSO to be dissolved due to its high hydrophobicity [42]. In contrast, HA-EGCG conjugates could not only scavenge $^{\bullet}O_2^-$ but also remain soluble in water. Furthermore, HA-EGCG conjugates could scavenge $^{\bullet}OH$ whereas Hyaff®-11p75 was incapable of doing so.

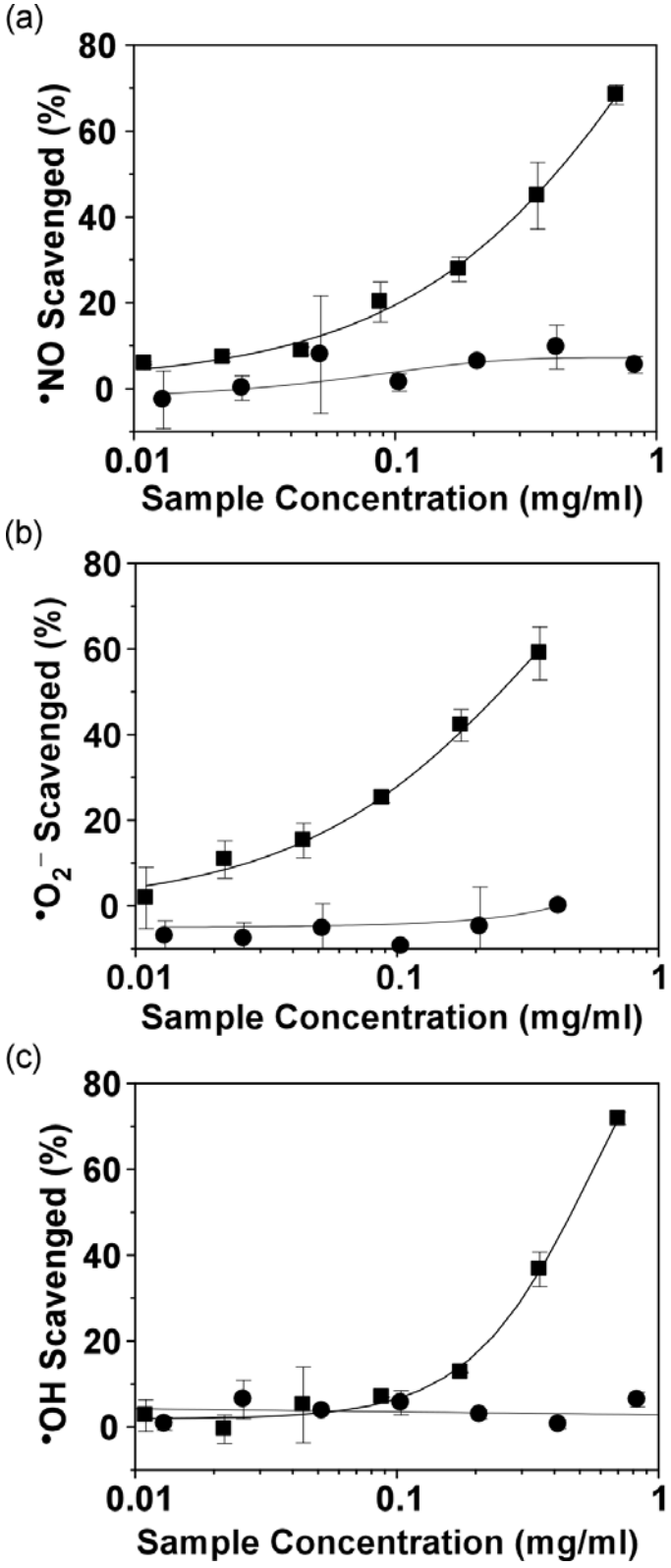


**Fig. 8-11. Radical scavenging activities of HA (●) and HA-EGCG conjugates (■) against (a) $^{\bullet}NO$, (b) $^{\bullet}O_2^-$ and (c) $^{\bullet}OH$ (n = 2, mean ± SD).**

**Table 8-3.** Radical scavenging activity of HA-EGCG conjugates and EGCG (n = 2, mean ± SD)

| Sample | $SC_{50}$ (μM) | | |
|---|---|---|---|
| | $^{\bullet}NO$ | $^{\bullet}OH$ | $^{\bullet}O_2^-$ |
| HA-EGCG conjugate[a] | 32.3 ± 3.8 | 36.3 ± 4.3 | 20.4 ± 3.8 |
| EGCG | 30.4 ± 1.4 | 18.0 ± 0.5 | 5.7 ± 1.3 |

[a]Concentration of HA-EGCG conjugates was expressed in terms of the amount of EGCG contained in the conjugates

### 8.3.6. Hydrogel formation *via* addition of HRP

Having demonstrated that HA-EGCG conjugates exhibit enhanced bioactivities compared to native HA, we proceeded to examine the gelation property of HA-EGCG conjugates. EGCG is known to couple together in the presence of HRP and $H_2O_2$, forming a symmetric dimer as the major product (Fig. 8-12a) [16]. It is known that oxidation of EGCG by molecular oxygen occurs at the trihydroxyl B ring, which results in the formation of EGCG semiquinone radical and a superoxide radical ($^{\bullet}O_2^-$). The $^{\bullet}O_2^-$ can oxidize another EGCG molecule and generate $H_2O_2$ in the process (Fig. 8-12b) [47-49]. We proposed that the generated $H_2O_2$ can serve as the oxidant in the enzymatic reaction, thus eliminate the need to add exogenous $H_2O_2$. We first measured the amount of $H_2O_2$ generated by HA-EGCG conjugates. HA-EGCG conjugates were dissolved in deionized water before mixing with phosphate buffer to bring to a specific pH. Autoxidation of EGCG is known to depend on the pH of the medium; a decrease in pH prevents acid dissociation of the hydroxyl groups of B ring [48, 49]. Thus the generation of $H_2O_2$ is inhibited at acidic condition. Indeed, $H_2O_2$ was produced by HA-EGCG conjugates at a much slower rate at pH 5 than pH 7.4 (Fig. 8-12c). The concentrations of $H_2O_2$ generated by HA-EGCG conjugates (1 mg/ml) after 24 h incubation were 15 and 150 μM at pH 5 and 7.4, respectively.

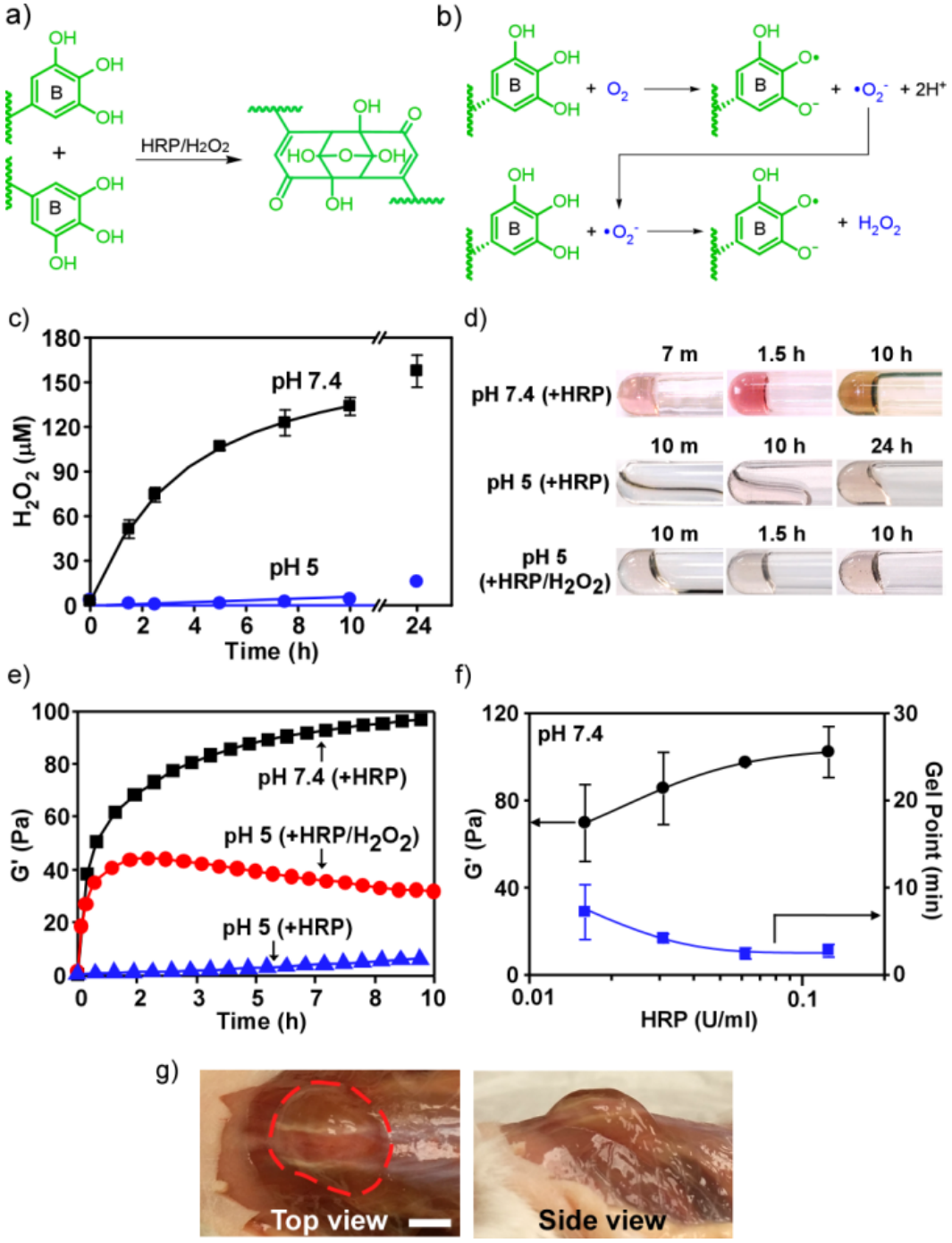


**Fig. 8-12. (a) Formation of EGCG symmetric dimer by HRP and $H_2O_2$. (b) Formation of $H_2O_2$ via EGCG autoxidation. (c) Generation of $H_2O_2$ by HA-EGCG conjugates (1 mg/ml). (d) Photographs of HA-EGCG hydrogels (10 mg/ml) formed by adding HRP at pH 7.4 (first row), pH 5 (second row), or by adding both HRP and $H_2O_2$ at pH 5 (third row). (e) Evolution of G' of the corresponding hydrogels. (f) The effects of HRP concentration on the G' and gel point of hydrogels formed at pH 7.4 (n = 3, mean ± SD). (g) *In vivo* formation of HA-EGCG hydrogel with HRP) at pH 7.4 (scale bar = 0.5 cm).**

Having confirmed that $H_2O_2$ is being produced by HA-EGCG conjugates at physiological pH, we proceeded to form hydrogels by adding HRP. When HRP was added to a solution of

HA-EGCG conjugates (10 mg/ml) at pH 7.4, a hydrogel was formed within 7 min at 37 °C (Fig. 8-12d, first row). Gelation time was determined by tilting the test tube occasionally until the solution stopped flowing. In contrast, when HRP was added at pH 5, a hydrogel was not formed until 24 h later (Fig. 8-12d, second row). On the other hand, when exogenous $H_2O_2$ was added together with HRP at pH 5, a hydrogel was formed within 10 min (Fig. 8-12d, third row). The results clearly demonstrated that the slow rate of $H_2O_2$ generation at pH 5 limited the rate of HRP-mediated crosslinking reaction. The color of the hydrogels darkened progressively. At 10 h, the hydrogel formed at pH 7.4 was reddish brown, which resembled the color of black (fermented) tea, indicating the presence of oxidized catechins. The gelation process was examined by oscillatory rheometry. The storage modulus (G') was lower than the loss modulus (G'') at the beginning of the measurement, except for the hydrogel formed at pH 7.4, in which crossover between G' and G'' occurred prior to the start of measurement. At pH 7.4, G' increased to 80 Pa in 3 h, which was followed by a slower phase of increment, reaching 100 Pa at 10 h (Fig. 8-12e). At pH 5, G' increased more rapidly when both HRP and $H_2O_2$ were added than when only HRP was added. It was reported that the gelation rate of polymer-phenol conjugates increases with increasing HRP concentration. Indeed, as the concentration of HRP increased, the gel point, defined as the crossover between G' and G'', of HA-EGCG conjugates at pH 7.4 decreased while the G' at 10 h increased (Fig. 8-12f). In order to demonstrate that the HRP-mediated gelation could likewise occur in vivo, a solution of HA-EGCG conjugates (10 mg/ml) at pH 7.4 was mixed with HRP (0.062 U/ml) and immediately injected into the subcutaneous tissue of mice. A hydrogel was successfully formed (Fig. 8-12g).

### 8.3.7. Hydrogel formation *via* EGCG quinone formation

One concern associated with HRP-mediated injectable hydrogel system is the retention of the enzyme in the gel matrix, which can potentially induce immune reaction due to its plant origin. It has been reported that autoxidation of EGCG under aerobic condition results in EGCG semiquinone radical formation. When EGCG semiquinone radical is further oxidized by oxygen, EGCG quinone is formed, which leads to EGCG coupling via a linkage at the B rings (Fig. 8-13a) [47]. This suggests that crosslinking between HA-EGCG conjugates could potentially take place without HRP. To test this hypothesis, a solution of HA-EGCG conjugates at pH 7.4, containing no HRP, was incubated at 37 °C. Gelation time was determined by tilting the tube periodically until a nonflowing gel was observed. The gelation time was 1.5 h (Fig. 8-13b). The sol-gel transition was accompanied by a gradual change in

color, from clear to pink to reddish brown, similar to hydrogels formed in the presence of HRP. However, rheological measurement showed that the G' increased at a slower rate compared with hydrogels which were formed in the presence of HRP at pH 7.4, reaching 50 Pa at 10 h (Fig. 8-13b). In contrast, a solution of HA-EGCG conjugates at pH 5 did not form a gel until 48 h (Fig. 8-13c). Despite the slower rate of gel formation in the absence of HRP, when a solution of HA-EGCG conjugates (10 mg/ml) at pH 7.4 was injected subcutaneously, a hydrogel was successfully formed (Fig. 8-13d).

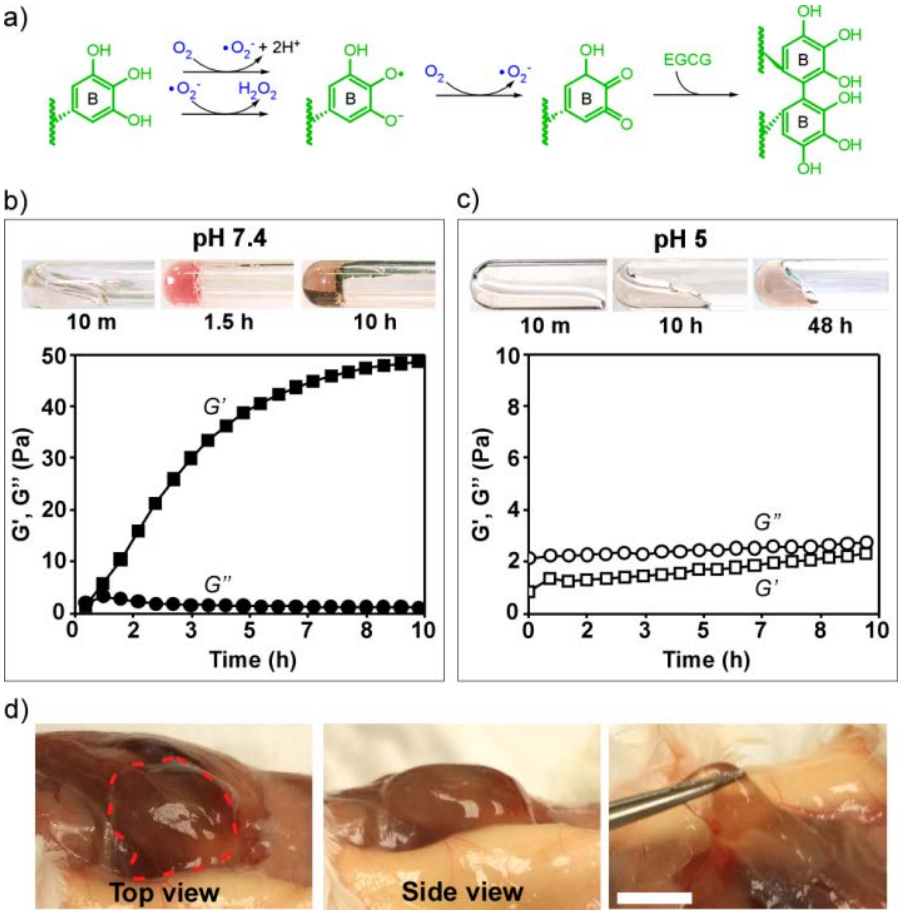


**Fig. 8-13. (a) Coupling of EGCG at the B ring via EGCG quinone formation. Photograph and rheological measurement of HA-EGCG hydrogels (10 mg/ml) formed through quinone formation at (b) pH 7.4 and (c) pH 5. (d) *In vivo* formation of HA-EGCG hydrogel at the subcutaneous environment (scale bar = 0.5 cm).**

### 8.3.8. Resistance to hyaluronidase-mediated degradation

The hydrogel degradation profiles in the presence of hyaluronidase were characterized. HA-EGCG and HA-tyramine hydrogels were prepared at pH 7.4, the latter was crosslinked by HRP/$H_2O_2$ (G' = 100 Pa) and served as a comparison. The degree of substitution of HA-tyramine conjugates was 3. In 2.5 U/ml of hyaluronidase solution, HA-EGCG hydrogels were

degraded at 33 h while HA-tyramine hydrogels were degraded within 8 h (Fig. 8-14a). When hyaluronidase concentration was increased to 10 U/ml, HA-EGCG and HA-tyramine hydrogels were degraded in 12 and 6 h, respectively (Fig. 8-14b). The longer time required for HA-EGCG hydrogels to be fully degraded suggested the inhibition of hyaluronidase activity. The degradation of HA-EGCG hydrogels was further evaluated in vivo. Forty-two days after injection into the subcutaneous tissue, the weight of HA-EGCG hydrogel formed with HRP remained close to 100% while the weight of HA-EGCG hydrogel formed without HRP decreased to 28% (Fig. 8-14c). In contrast, only 16% of the initial weight was remained for HA-tyramine hydrogel. Taken together, the *in vitro* and *in vivo* results demonstrated that the EGCG moieties endowed the hydrogels with resistance towards degradation by hyaluronidase (Fig. 8-14d).

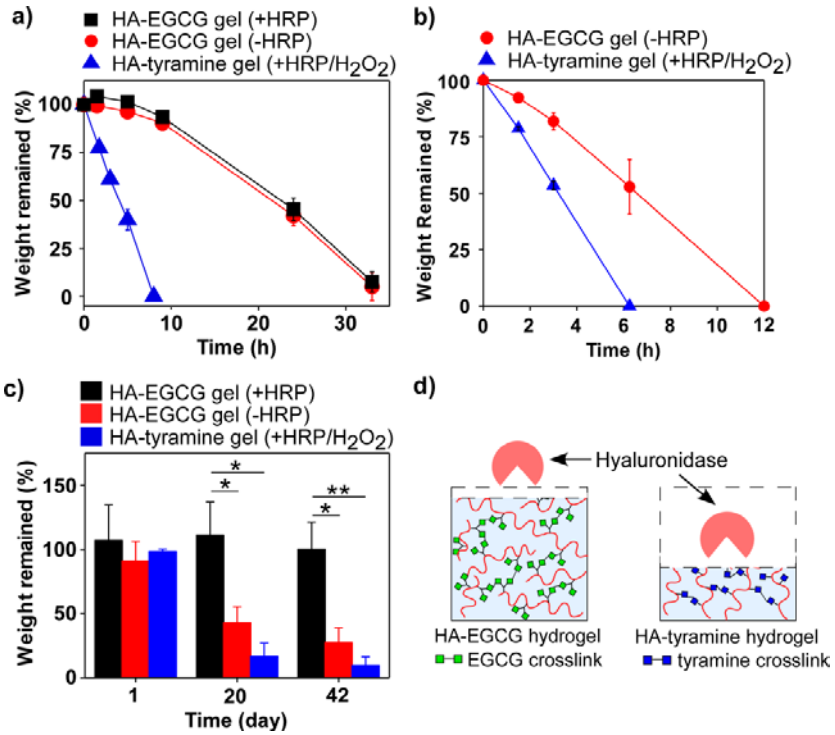


**Fig. 8-14. *In vitro* degradation of HA-EGCG and HA-tyramine hydrogels in (a) 2.5 U/ml and (b) 10 U/ml of hyaluronidase solution (n = 2, mean ± SD). (c) *In vivo* degradation of hydrogels at the subcutaneous tissue of mice (n = 6, mean ± SEM). (d) Schematic illustrating the slower rate of degradation of HA-EGCG hydrogels. *$p < 0.05$ and **$p < 0.005$.**

## 8.4. Conclusions

Ethylamine-bridged EGCG dimers were synthesized *via* aldehyde-mediated reaction with the A ring of EGCG. Four isomers were formed due to the two reactive sites on the A ring, i.e., C-6 and C-8, and the asymmetric carbon at the ethylamine linkage. The EGCG dimers

were conjugated to HA using carbodiimide-mediated coupling reaction, forming HA-EGCG conjugates. We demonstrated that the resulting HA-EGCG conjugates possess bioactivities such as resistance to hyaluronidase-mediated degradation, inhibition of cell growth and scavenging of radicals, whereas unmodified HA showed no or limited activities. Moreover, we showed that the rate of $H_2O_2$ generation *via* EGCG autoxidation at pH 7.4 was sufficiently fast that the addition of HRP resulted in gelation within a few minutes. Furthermore, coupling between EGCG moieties could also take place through EGCG quinone formation in the absence of HRP, albeit the gelation time was 1.5 h. The HRP-free gelation is an attractive approach to form hydrogels *in situ* as it circumvented the safety concern associated with HRP due to its plant origin. HA is widely used as dermal fillers for cosmetic application or as viscosupplements for osteoarthritis treatment [50]. However, in its free form, HA is rapidly degraded or drained from the injection site. The HA-EGCG hydrogel system, with *in situ* gelation and resistance towards hyaluronidase-mediated degradation, offers the advantages of injectability and prolonged residence time in the body.

**References**

[1] Hoffman AS. Hydrogels for biomedical applications. Adv. Drug Del. Rev. 2012;64, Supplement:18-23.

[2] Kurisawa M, Lee F, Wang L-S, Chung JE. Injectable enzymatically crosslinked hydrogel system with independent tuning of mechanical strength and gelation rate for drug delivery and tissue engineering. J. Mater. Chem. 2010;20:5371-5.

[3] Bae JW, Choi JH, Lee Y, Park KD. Horseradish peroxidase-catalysed in situ-forming hydrogels for tissue-engineering applications. J. Tissue Eng. Regen. Med. 2014:doi: 10.1002/term.917.

[4] Kurisawa M, Chung JE, Yang YY, Gao SJ, Uyama H. Injectable biodegradable hydrogels composed of hyaluronic acid-tyramine conjugates for drug delivery and tissue engineering. Chem. Commun. 2005:4312-4.

[5] Jin R, Hiemstra C, Zhong Z, Feijen J. Enzyme-mediated fast in situ formation of hydrogels from dextran-tyramine conjugates. Biomaterials 2007;28:2791-800.

[6] Sakai S, Hirose K, Taguchi K, Ogushi Y, Kawakami K. An injectable, in situ enzymatically gellable, gelatin derivative for drug delivery and tissue engineering. Biomaterials 2009;30:3371-7.

[7] Park KM, Shin YM, Joung YK, Shin H, Park KD. In Situ Forming Hydrogels Based on Tyramine Conjugated 4-Arm-PPO-PEO via Enzymatic Oxidative Reaction. Biomacromolecules 2010;11:706-12.

[8] Wang L-S, Chung JE, Pui-Yik Chan P, Kurisawa M. Injectable biodegradable hydrogels with tunable mechanical properties for the stimulation of neurogenesic differentiation of human mesenchymal stem cells in 3D culture. Biomaterials 2010;31:1148-57.

[9] Lee BP, Dalsin JL, Messersmith PB. Synthesis and Gelation of DOPA-Modified Poly(ethylene glycol) Hydrogels. Biomacromolecules 2002;3:1038-47.

[10] Lee F, Chung JE, Kurisawa M. An injectable enzymatically crosslinked hyaluronic acid-tyramine hydrogel system with independent tuning of mechanical strength and gelation rate. Soft Matter 2008;4:880-7.

[11] Singh S, Topuz F, Hahn K, Albrecht K, Groll J. Embedding of Active Proteins and Living Cells in Redox-Sensitive Hydrogels and Nanogels through Enzymatic Cross-Linking. Angewandte Chemie International Edition 2013;52:3000-3.

[12] Moriyama K, Minamihata K, Wakabayashi R, Goto M, Kamiya N. Enzymatic preparation of a redox-responsive hydrogel for encapsulating and releasing living cells. Chemical Communications 2014;50:5895-8.

[13] Wheeler DS, Wheeler WJ. The medicinal chemistry of tea. Drug Dev. Res. 2004;61:45-65.

[14] Nagle DG, Ferreira D, Zhou Y-D. Epigallocatechin-3-gallate (EGCG): Chemical and biomedical perspectives. Phytochemistry 2006;67:1849-55.

[15] Kanwar J, Taskeen M, Mohammad I, Huo C, Chan TH, Dou QP. Recent advances on tea polyphenols. Front. Biosci. (Elite Ed.) 2012;4:111-31.

[16] Zhu N, Sang S, Huang T-C, Bai N, Yang CS, Ho C-T. ANTIOXIDANT CHEMISTRY OF GREEN TEA CATECHINS: OXIDATION PRODUCTS OF (-)-EPIGALLOCATECHIN GALLATE AND (-)-EPIGALLOCATECHIN WITH PEROXIDASE. Journal of Food Lipids 2000;7:275-82.

[17] Chung JE, Tan S, Gao SJ, Yongvongsoontorn N, Kim SH, Lee JH, Choi HS, Yano H, Zhuo L, et al. Self-assembled micellar nanocomplexes comprising green tea catechin derivatives and protein drugs for cancer therapy. Nature Nanotechnology 2014;9:907-12.

[18] Lee F, Lim J, Reithofer MR, Lee SS, Chung JE, Hauser CAE, Kurisawa M. Synthesis and bioactivity of a conjugate composed of green tea catechins and hyaluronic acid. Polym. Chem. 2015;6:4462-72.

[19] Kuo JW, Swann DA, Prestwich GD. Chemical modification of hyaluronic acid by carbodiimides. Bioconjug. Chem. 1991;2:232-41.

[20] Homma A, Sato H, Okamachi A, Emura T, Ishizawa T, Kato T, Matsuura T, Sato S, Tamura T, et al. Novel hyaluronic acid-methotrexate conjugates for osteoarthritis treatment. Bioorg. Med. Chem. 2009;17:4647-56.

[21] Reissig JL, Strominger JL, Leloir LF. A MODIFIED COLORIMETRIC METHOD FOR THE ESTIMATION OF N-ACETYLAMINO SUGARS. J. Biol. Chem. 1955;217:959-66.

[22] Sreejayan, Rao MNA. Nitric Oxide Scavenging by Curcuminoids. J. Pharm. Pharmacol. 1997;49:105-7.

[23] Halliwell B, Gutteridge JM, Aruoma OI. The deoxyribose method: a simple "test-tube" assay for determination of rate constants for reactions of hydroxyl radicals. Anal. Biochem. 1987;165:215-9.

[24] Fernandes E, Costa D, Toste SA, Lima JLFC, Reis S. In vitro scavenging activity for reactive oxygen and nitrogen species by nonsteroidal anti-inflammatory indole, pyrrole, and oxazole derivative drugs. Free Radic. Biol. Med. 2004;37:1895-905.

[25] Shaw C-Y, Chen C-H, Hsu C-C, Chen C-C, Tsai Y-C. Antioxidant properties of scopoletin isolated from Sinomonium acutum. Phytother. Res. 2003;17:823-5.

[26] Zhang YM, Rock CO. Evaluation of epigallocatechin gallate and related plant polyphenols as inhibitors of the FabG and FabI reductases of bacterial type II fatty-acid synthase. J. Biol. Chem. 2004;279:30994-1001.

[27] Nakagawa H, Hasumi K, Takami M, Aida-Hyugaji S, Woo JT, Nagai K, Ishikawa T, Wachi M. Identification of two biologically crucial hydroxyl groups of (-)-epigallocatechin gallate in osteoclast culture. Biochem. Pharmacol. 2007;73:34-43.

[28] Nanjo F, Goto K, Seto R, Suzuki M, Sakai M, Hara Y. Scavenging effects of tea catechins and their derivatives on 1,1-diphenyl-2-picrylhydrazyl radical. Free Radic. Biol. Med. 1996;21:895-902.

[29] Nakagawa T, Yokozawa T. Direct scavenging of nitric oxide and superoxide by green tea. Food Chem. Toxicol. 2002;40:1745-50.

[30] Wan SB, Landis-Piwowar KR, Kuhn DJ, Chen D, Dou QP, Chan TH. Structure–activity study of epi-gallocatechin gallate (EGCG) analogs as proteasome inhibitors. Bioorg. Med. Chem. 2005;13:2177-85.

[31] Saucier C, Guerra C, Pianet I, Laguerre M, Glories Y. (+)-Catechin--acetaldehyde condensation products in relation to wine-ageing. Phytochemistry 1997;46:229-34.

[32] Drinkine J, Glories Y, Saucier C. (+)-Catechin-aldehyde condensations: competition between acetaldehyde and glyoxylic acid. J. Agric. Food Chem. 2005;53:7552-8.

[33] Nonier M-F, Pianet I, Laguerre M, Vivas N, Vivas de Gaulejac N. Condensation products derived from flavan-3-ol oak wood aldehydes reaction: 1. Structural investigation. Anal. Chim. Acta 2006;563:76-83.

[34] Es-Safi NE, Le Guerneve C, Cheynier V, Moutounet M. New phenolic compounds formed by evolution of (+)-catechin and glyoxylic acid in hydroalcoholic solution and their implication in color changes of grape-derived foods. J. Agric. Food Chem. 2000;48:4233-40.

[35] He Q, Lv Y, Yao K. Effects of tea polyphenols on the activities of α-amylase, pepsin, trypsin and lipase. Food Chem. 2007;101:1178-82.

[36] Wang X, Ho C-T, Huang Q. Investigation of Adsorption Behavior of (-)-Epigallocatechin Gallate on Bovine Serum Albumin Surface Using Quartz Crystal Microbalance with Dissipation Monitoring. J. Agric. Food Chem. 2007;55:4987-92.

[37] El-Safory NS, Fazary AE, Lee C-K. Hyaluronidases, a group of glycosidases: Current and future perspectives. Carbohydr. Polym. 2010;81:165-81.

[38] Picotti F, Fabbian M, Gianni R, Sechi A, Stucchi L, Bosco M. Hyaluronic acid lipoate: Synthesis and physicochemical properties. Carbohydr. Polym. 2012.

[39] Schanté CE, Zuber G, Herlin C, Vandamme TF. Improvement of hyaluronic acid enzymatic stability by the grafting of amino-acids. Carbohydr. Polym. 2011;87:2211-6.

[40] Bartok B, Firestein GS. Fibroblast-like synoviocytes: key effector cells in rheumatoid arthritis. Immunol. Rev. 2010;233:233-55.

[41] Ahmed S, Silverman MD, Marotte H, Kwan K, Matuszczak N, Koch AE. Down-regulation of myeloid cell leukemia 1 by epigallocatechin-3-gallate sensitizes rheumatoid arthritis synovial fibroblasts to tumor necrosis factor α–induced apoptosis. Arthritis Rheum. 2009;60:1282-93.

[42] Moseley R, Leaver M, Walker M, Waddington RJ, Parsons D, Chen WY, Embery G. Comparison of the antioxidant properties of HYAFF-11p75, AQUACEL and hyaluronan towards reactive oxygen species in vitro. Biomaterials 2002;23:2255-64.

[43] Šoltés L, Mendichi R, Kogan G, Schiller J, Stankovská M, Arnhold J. Degradative Action of Reactive Oxygen Species on Hyaluronan. Biomacromolecules 2006;7:659-68.

[44] Sutherland BA, Rahman RMA, Appleton I. Mechanisms of action of green tea catechins, with a focus on ischemia-induced neurodegeneration. The Journal of Nutritional Biochemistry 2006;17:291-306.

[45] Perron NR, Wang HC, DeGuire SN, Jenkins M, Lawson M, Brumaghim JL. Kinetics of iron oxidation upon polyphenol binding. Dalton Transactions 2010;39:9982-7.

[46] Lin J-K, Chen P-C, Ho C-T, Lin-Shiau S-Y. Inhibition of Xanthine Oxidase and Suppression of Intracellular Reactive Oxygen Species in HL-60 Cells by Theaflavin-3,3‘-digallate, (−)-Epigallocatechin-3-gallate, and Propyl Gallate. J. Agric. Food Chem. 2000;48:2736-43.

[47] Sang S, Yang I, Buckley B, Ho C-T, Yang CS. Autoxidative quinone formation in vitro and metabolite formation in vivo from tea polyphenol (-)-epigallocatechin-3-gallate: Studied by real-time mass spectrometry combined with tandem mass ion mapping. Free Radic. Biol. Med. 2007;43:362-71.

[48] Mochizuki M, Yamazaki S, Kano K, Ikeda T. Kinetic analysis and mechanistic aspects of autoxidation of catechins. Biochim. Biophys. Acta 2002;1569:35-44.

[49] Roginsky V, Alegria AE. Oxidation of tea extracts and tea catechins by molecular oxygen. J. Agric. Food Chem. 2005;53:4529-35.

[50] Fakhari A, Berkland C. Applications and emerging trends of hyaluronic acid in tissue engineering, as a dermal filler and in osteoarthritis treatment. Acta Biomater. 2013;9:7081-92.

# Chapter 9

# Conclusion

Hydrogels are widely used in drug delivery and tissue engineering applications. In **Chapter 1**, the various synthetic and natural polymers used to form biodegradable hydrogels were described. Among them, hyaluronic acid (HA) is one of the most widely used, for it is biocompatible, available in large-scale through bacterial fermentation, and versatile in terms of chemical modifications. The various *in situ* crosslinking strategies for forming injectable and chemically crosslinked hydrogels were also presented. Injectable hydrogel systems are preferred over conventional preformed hydrogels, as they do not require invasive techniques for implantation. The gelation rate of injectable hydrogel systems should be tunable to meet the application requirement. Fast gelation is required for drug delivery applications to prevent drug leakage, while slow gelation is more suitable for tissue engineering applications to allow time for the gel precursors to fill the irregularly shaped defects. However, the gelation rate of most existing injectable hydrogel systems is controlled by the gel precursor/crosslinker concentration or the degree of substitution (DS) of the crosslinking moiety. Changes in either parameter would also alter the crosslink density of the hydrogel, which affects the rate of drug release, the rate of hydrogel degradation, and the viability and proliferation of encapsulated cells. Lastly, the objectives of this study were stated, which was followed by an outline of this thesis.

In **Chapter 2**, an injectable hydrogel system that allows the independent tuning of gelation rate and crosslink density was designed [1]. The hydrogel was composed of hyaluronic acid-tyramine (HA-Tyr) conjugates, which crosslinked *in situ* through the oxidative coupling of tyramine moieties in the presence of horseradish peroxidase (HRP) and $H_2O_2$. When the concentrations of HA-Tyr conjugates and HRP were fixed, the storage modulus (G') of the hydrogels increased from 10 to 4000 Pa as the $H_2O_2$ concentration increased from 146 μM to 1092 μM, while the gelation point (G' = G'') remained unchanged. In contrast, when the concentrations of HA-Tyr conjugates and $H_2O_2$ were fixed, the gel point decreased from 20 min to less than 1 s with increasing HRP concentration. Although G' also increased with increasing HRP concentration, it remained in the same order of magnitude when the HRP concentration was above 0.032 U/ml. Thus, the crosslink density of HA-Tyr hydrogels could be tuned without significant changes to the gelation rate, and vice versa. The HA-Tyr hydrogel could be formed *in vivo* by injecting a solution of HA-Tyr conjugates immediately after mixing with HRP and $H_2O_2$. Importantly, rapid gelation achieved by 0.124 U/ml of HRP was needed to ensure a localized gel formation at the injection site. Protein-loaded hydrogels were formed by mixing the protein drugs with HA-Tyr conjugates, HRP and

$H_2O_2$ [2]. By tuning the crosslink density of HA-Tyr hydrogels through variation in the concentration of $H_2O_2$, the release rate of proteins could be varied. Moreover, it was shown that by injecting HA-Tyr hydrogels containing interferon-α2a (IFN-α2a) to the mice subcutaneous tissue, the time that the protein could be detected in the plasma was increased to 24 h, compared to only 8 h when the protein was injected as a solution [3]. Furthermore, sustained release of IFN-α2a from hydrogels inhibited tumor growth more effectively in a mice xenograft model of human liver cancer than administrating the protein in solution form.

In **Chapter 3**, physical interactions between the encapsulated proteins and the hydrogel network were employed to extend the protein release duration to more than 24 h. In particular, electrostatic interactions between positively charged proteins, such as lysozyme, and negatively charged HA-Tyr hydrogels were used to immobilize the proteins within the hydrogel [2]. It was shown that the release of lysozyme was dependent upon the degradation of hydrogel network by hyaluronidase. A higher concentration of hyaluronidase in the release medium resulted in a faster rate of hydrogel degradation, which in turn led to a faster rate of lysozyme release. Similarly, when trastuzumab, a positively charged therapeutic antibody, was incorporated in HA-Tyr hydrogels, 25% of the protein were released in the first few days after which no more proteins were released. The discontinued release was attributed to electrostatic interactions between trastuzumab and HA-Tyr hydrogel that immobilized the protein in the gel. When a small amount of hyaluronidase was incorporated together with trastuzumab in the hydrogel, 90% of trastuzumab were released over a period of 4 weeks [4]. Moreover, it was shown that a single subcutaneous injection of 200 µl of HA-Tyr hydrogel incorporating 0.63 mg/ml of trastuzumab and 5 units/ml of hyaluronidase effectively inhibited the growth of tumor in a mice xenograft model of human breast cancer. In contrast, the inhibition of tumor growth was not statistically significant compared to non-treated animals when trastuzumab was delivered by HA-Tyr hydrogels containing no hyaluronidase or administered as a solution.

In **Chapter 4**, a dextran-tyramine (Dex-Tyr) hydrogel containing poly(ethylene glycol) (PEG) microdomains was developed for the delivery of PEGylated proteins [5]. Dextran was chosen as the backbone polymer because it is not miscible with PEG when the two polymers are mixed at an appropriate concentration and temperature. Thus, when HRP and $H_2O_2$ were added to a mixture of Dex-Tyr conjugates and PEG, a Dex-Tyr hydrogel containing PEG microdomains (Dex-Tyr/PEG) was formed. It was shown that by increasing HRP

concentration from 0.13 to 0.21 U/ml, the diameter of PEG microdomains decreased from 5.1 to 2.1 μm. When PEGylated IFN-α2a (PEG-IFN-α2a) was added to a solution of Dex-Tyr conjugates and PEG, the protein was found to partition preferentially in the PEG microdomains after the HRP-mediated gelation. The preferential partition in the PEG microdomains resulted in sustained release of the proteins form the hydrogels. Hydrogels containing PEG microdomains (2.1 μm) released the incorporated PEG-IFN-α2a over a period of 3 months, and the bioactivity of the proteins was well preserved. In contrast, hydrogels without PEG microdomains released 60% of the proteins in the first 2 weeks, after which no more proteins were released. In a humanized mouse model of hepatitis C, a one-time administration of Dex-Tyr/PEG hydrogel containing PEG-IFN-α2a prevented hepatitis C virus-induced liver injury as effectively as the clinically relevant formulation that is composed of eight weekly injections of PEG-IFN-α2a. The Dex-Tyr/PEG hydrogel is a promising system for the long-term delivery of other PEGylated proteins.

In addition to protein delivery, the HA-Tyr hydrogel was used as a scaffold material for tissue engineering applications. In particular, methods to vascularize the hydrogel were developed, as the lack of vascularization is a major bottleneck in the engineering of thick tissues. In **Chapter 5**, interpenetrating polymer network (IPN) hydrogels consisting of fibrin and HA were developed [6]. The fibrin network was formed by fibrinogen and thrombin, while the HA network was formed by HA-Tyr conjugates, HRP and $H_2O_2$. The formation of a HA-Tyr network prevented lateral association of fibrin protofibrils, giving rise to a fibrin network consisting of smaller pores compared with fibrin only gel. By tuning the amount of $H_2O_2$, IPN hydrogels with different G' values were formed, which was attributed to the change in crosslink density of the HA-Tyr network. The IPN hydrogels demonstrated enhanced structural stability in the presence of plasmin and cell-contractile forces. Moreover, the formation of IPN hydrogels did not affect the viability of the embedded cells; although cell proliferation and capillary tube formation were found to decrease with increasing G' of the IPN hydrogels. In **Chapter 6,** a RGD peptide containing two phenol moieties ($Ph_2$-PEG-RGD) was synthesized for *in situ* conjugation into HA-Tyr hydrogels by HRP [7]. The resulting HA-Tyr-RGD hydrogels showed significant improvements in terms of cell adhesion, proliferation, migration and capillary-like network formation *in vitro*. Moreover, when HA-Tyr-RGD hydrogels containing human umbilical vein endothelial cells (HUVECs) were injected into the mice subcutaneous tissue, functional vasculatures were observed in the hydrogels two weeks post-injection. Vessel density was further improved when human

fibroblasts were embedded in the hydrogel together with HUVECs. The *in situ* coupling of phenol moieties by the enzymatic activity of HRP can be utilized to conjugate other bioactive peptides into the HA-Tyr hydrogel system for tissue engineering applications.

Another challenge associated with tissue engineering is the cell source. Human embryonic stem cells (hESCs) are a promising cell source as they have unlimited self-renewal capability and can differentiate into any cell type. Presently, hESCs are propagated on 2D surfaces with animal-derived biologics, which are not suitable for large-scale cell expansion and clinical applications. In **Chapter 7**, HA-Tyr hydrogel was investigated as a 3D culture system for the propagation of hESCs using chemically-defined culture medium [8]. It was found that HA-Tyr hydrogels with a G' of 82 Pa better supported the proliferation of hESCs than hydrogels with a higher G'. Moreover, the hESCs cultured in HA-Tyr hydrogels were able to differentiate into cell derivatives of all three germ layers. Therefore, 3D culture of hESCs in soft HA-Tyr hydrogels could potentially facilitate the large-scale expansion of hESCs of high quality for tissue engineering applications.

One concern associated with the enzyme-mediated crosslinking reaction for 3D cell culture is the use of $H_2O_2$. *In vitro* models have shown that low concentrations of $H_2O_2$ (micromolar) in the culture medium cause cell growth arrest, while high concentrations (micro to millimolar) lead to apoptosis and necrosis [9]. Besides concentration, $H_2O_2$-induced cytotoxicity also depends on the incubation time. In one study using C6 glioma cells, it was shown that the median cytotoxic concentration of $H_2O_2$ decreased from 500 to 30 μM as the incubation time increased from 1 to 24 h [10]. This suggests that the cytotoxic effect of $H_2O_2$ could be minimized if $H_2O_2$ is rapidly consumed by HRP-mediated oxidative reaction. Indeed, when human umbilical endothelial cells were cultured in growth medium containing 0.2 mM of $H_2O_2$ in the absence of HRP, less than 10% of cells remained viable after 24 h incubation [7]. In contrast, when HRP (0.15 U/ml) was added to the culture medium, close to 100% of the cells were alive after incubating for the same amount of time. Other studies have also shown that the transient exposure to $H_2O_2$ during the HRP-mediated crosslinking reaction causes minimal toxicity, with more than 90% of the embedded cells remained viable [11-13]. Moreover, it was found that the transient pre-exposure to $H_2O_2$ during the crosslinking process could endow rat adult neural stem cells (aNSCs) with resistance towards oxidative stress, resulting in a higher survival rate compared to cells without pre-exposure [12]. Based on these findings, the HRP-mediated crosslinking reaction is considered a suitable method to form cell-laden hydrogels for tissue engineering or 3D cell expansion. Nevertheless, it is

important to avoid using $H_2O_2$ concentrations that would lead to HRP inactivation. Since HRP inactivation may result in slow or incomplete consumption of $H_2O_2$, the residual of which can cause toxicity to the embedded cells. It is also advisable to mix the polymer-phenol conjugates, HRP and cells together prior to the addition of $H_2O_2$ in order to minimize the time to which the cells are exposed to $H_2O_2$.

In **Chapter 8**, a bioactive hydrogel composed of hyaluronic acid-green tea catechin conjugates was developed [14, 15]. (-)-Epigallocatechin-3-gallate (EGCG), a green tea catechin, was reacted with 2,2-diethoxyethylamine (DA) to form ethylamine-bridged EGCG dimers, which were conjugated to HA through the formation of amide bonds. The resulting HA-EGCG conjugates exhibited bioactivities that were not present in native HA, namely resistance to hyaluronidase-mediated degradation, inhibition of cell growth and scavenging of radicals. Moreover, the addition of HRP to a solution of HA-EGCG conjugates at physiological pH induced gelation in 7 min. Importantly, the addition of exogenous $H_2O_2$ was not required to catalyze the HRP-mediated coupling of EGCG, as $H_2O_2$ was produced *via* EGCG autoxidation under aerobic condition. The presence of EGCG moieties endowed the HA-EGCG hydrogels with resistance towards hyaluronidase-mediated degradation both *in vitro* and *in vivo*. Furthermore, crosslinking between HA-EGCG conjugates occurred *in situ* through EGCG quinone formation even when no HRP was added. The HRP-free gelation is an attractive approach to form injectable hydrogels because one of the concerns associated with HRP-mediated gelation is the retention of the enzyme in the hydrogel. Since HRP is a plant-derived protein, it could potentially induce immunological response when introduced into the human body as part of the hydrogel formulation. Thus the safety of HRP in human must be firmly established before clinical application of hydrogel formulations containing HRP can be realized. In order to overcome this issue, hematin-based HRP biomimetic has been developed as an alternative catalyst for the oxidative reaction [16-18]. In addition, enzyme-free hydrogels have been prepared by passing a mixture of polymer-phenol conjugates and $H_2O_2$ through a syringe packed of HRP-conjugated ferromagnetic microbeads [19]. The *in situ* formation of HA-EGCG hydrogel *via* EGCG quinone formation offers another approach to form hydrogels free of HRP.

In summary, enzymatically crosslinked hydrogels composed of polymer-phenol conjugates are promising injectable system for drug delivery and tissue engineering applications. Indeed, the HRP-mediated crosslinking reaction has attracted wide attention since the first paper from our laboratory was published in 2005 [20]. A variety of polymers

were chemically modified with phenol moieties in order to form hydrogels using the HRP-mediated crosslinking reaction, including gelatin [21, 22], dextran [23], chitosan [24], carboxymethylcellulose [25], alginate [26], xylans [27], PEG [28] and poly(amido amines) [29]. Due to the facile tuning of crosslink density and gelation rate, these hydrogels were utilized in a wide range of biomedical applications, including the differentiation of human mesenchymal stem cells [21], delivery of dexamethasone for rheumatoid arthritis treatment [22, 30], cartilage tissue engineering [31], and bone regeneration [32]. Finally, the formation of injectable hydrogels using EGCG as the crosslinking moiety offers the advantages of HRP-free gelation and resistance to hyaluronidase-mediated degradation. This development, together with the other findings presented in this thesis, contributed to the advancement of injectable hydrogels for biomedical applications.

**References**

[1] Lee F, Chung JE, Kurisawa M. An injectable enzymatically crosslinked hyaluronic acid-tyramine hydrogel system with independent tuning of mechanical strength and gelation rate. Soft Matter 2008;4:880-7.

[2] Lee F, Chung JE, Kurisawa M. An injectable hyaluronic acid-tyramine hydrogel system for protein delivery. J. Control. Release 2009;134:186-93.

[3] Xu KM, Lee F, Gao SJ, Chung JE, Yano H, Kurisawa M. Injectable hyaluronic acid-tyramine hydrogels incorporating interferon-alpha 2a for liver cancer therapy. J. Control. Release 2013;166:203-10.

[4] Xu K, Lee F, Gao S, Tan M-H, Kurisawa M. Hyaluronidase-incorporated hyaluronic acid–tyramine hydrogels for the sustained release of trastuzumab. J. Control. Release 2015;216:47-55.

[5] Bae KH, Lee F, Xu K, Keng CT, Tan SY, Tan YJ, Chen Q, Kurisawa M. Microstructured dextran hydrogels for burst-free sustained release of PEGylated protein drugs. Biomaterials 2015;63:146-57.

[6] Lee F, Kurisawa M. Formation and stability of interpenetrating polymer network hydrogels consisting of fibrin and hyaluronic acid for tissue engineering. Acta Biomater. 2013;9:5143-52.

[7] Wang L-S, Lee F, Lim J, Du C, Wan ACA, Lee SS, Kurisawa M. Enzymatic conjugation of a bioactive peptide into an injectable hyaluronic acid–tyramine hydrogel system to promote the formation of functional vasculature. Acta Biomater. 2014;10:2539-50.

[8] Xu K, Narayanan K, Lee F, Bae KH, Gao S, Kurisawa M. Enzyme-mediated hyaluronic acid–tyramine hydrogels for the propagation of human embryonic stem cells in 3D. Acta Biomater. 2015.

[9] Gardner AM, Xu F-h, Fady C, Jacoby FJ, Duffey DC, Tu Y, Lichtenstein A. Apoptotic vs. Nonapoptotic Cytotoxicity Induced by Hydrogen Peroxide. Free Radic. Biol. Med. 1997;22:73-83.

[10] Gülden M, Jess A, Kammann J, Maser E, Seibert H. Cytotoxic potency of H2O2 in cell cultures: Impact of cell concentration and exposure time. Free Radic. Biol. Med. 2010;49:1298-305.

[11] Jin R, Moreira Teixeira LS, Dijkstra PJ, Karperien M, van Blitterswijk CA, Zhong ZY, Feijen J. Injectable chitosan-based hydrogels for cartilage tissue engineering. Biomaterials 2009;30:2544-51.

[12] Lim TC, Toh WS, Wang LS, Kurisawa M, Spector M. The effect of injectable gelatin-hydroxyphenylpropionic acid hydrogel matrices on the proliferation, migration, differentiation and oxidative stress resistance of adult neural stem cells. Biomaterials 2012;33:3446-55.

[13] Toh WS, Lim TC, Kurisawa M, Spector M. Modulation of mesenchymal stem cell chondrogenesis in a tunable hyaluronic acid hydrogel microenvironment. Biomaterials 2012;33:3835-45.

[14] Lee F, Lim J, Reithofer MR, Lee SS, Chung JE, Hauser CAE, Kurisawa M. Synthesis and bioactivity of a conjugate composed of green tea catechin and hyaluronic acid. Polymer Chemistry 2015;6:4462-72.

[15] Lee F, Chung JE, Xu K, Kurisawa M. Injectable Degradation-Resistant Hyaluronic Acid Hydrogels Cross-Linked via the Oxidative Coupling of Green Tea Catechin. ACS Macro Letters 2015;4:957-60.

[16] Sakai S, Moriyama K, Taguchi K, Kawakami K. Hematin is an Alternative Catalyst to Horseradish Peroxidase for In Situ Hydrogelation of Polymers with Phenolic Hydroxyl Groups In Vivo. Biomacromolecules 2010;11:2179-83.

[17] Ryu JH, Lee Y, Do MJ, Jo SD, Kim JS, Kim B-S, Im G-I, Park TG, Lee H. Chitosan-g-hematin: Enzyme-mimicking polymeric catalyst for adhesive hydrogels. Acta Biomater. 2014;10:224-33.

[18] Byun E, Ryu JH, Lee H. Catalyst-mediated yet catalyst-free hydrogels formed by interfacial chemical activation. Chemical Communications 2014;50:2869-72.

[19] Bae JW, Kim BY, Lih E, Choi JH, Lee Y, Park KD. In situ formation of enzyme-free hydrogels via ferromagnetic microbead-assisted enzymatic cross-linking. Chem. Commun. (Camb.) 2014;50:13710-3.

[20] Kurisawa M, Chung JE, Yang YY, Gao SJ, Uyama H. Injectable biodegradable hydrogels composed of hyaluronic acid-tyramine conjugates for drug delivery and tissue engineering. Chem. Commun. (Camb.) 2005:4312-4.

[21] Wang L-S, Boulaire J, Chan PPY, Chung JE, Kurisawa M. The role of stiffness of gelatin-hydroxyphenylpropionic acid hydrogels formed by enzyme-mediated crosslinking on the differentiation of human mesenchymal stem cell. Biomaterials 2010;31:8608-16.

[22] Wang LS, Du C, Chung JE, Kurisawa M. Enzymatically cross-linked gelatin-phenol hydrogels with a broader stiffness range for osteogenic differentiation of human mesenchymal stem cells. Acta Biomater. 2012;8:1826-37.

[23] Jin R, Hiemstra C, Zhong Z, Feijen J. Enzyme-mediated fast in situ formation of hydrogels from dextran-tyramine conjugates. Biomaterials 2007;28:2791-800.

[24] Sakai S, Yamada Y, Zenke T, Kawakami K. Novel chitosan derivative soluble at neutral pH and in-situ gellable via peroxidase-catalyzed enzymatic reaction. J. Mater. Chem. 2009;19:230-5.

[25] Ogushi Y, Sakai S, Kawakami K. Synthesis of enzymatically-gellable carboxymethylcellulose for biomedical applications. J. Biosci. Bioeng. 2007;104:30-3.

[26] Sakai S, Hirose K, Moriyama K, Kawakami K. Control of cellular adhesiveness in an alginate-based hydrogel by varying peroxidase and H2O2 concentrations during gelation. Acta Biomater. 2010;6:1446-52.

[27] Kuzmenko V, HÃ¤gg D, Toriz G, Gatenholm P. In situ forming spruce xylan-based hydrogel for cell immobilization. Carbohydrate Polymers 2014;102:862-8.

[28] Park KM, Lee Y, Son JY, Bae JW, Park KD. In Situ SVVYGLR Peptide Conjugation into Injectable Gelatin-Poly(ethylene glycol)-Tyramine Hydrogel via Enzyme-Mediated Reaction for Enhancement of Endothelial Cell Activity and Neo-Vascularization. Bioconjug. Chem. 2012;23:2042-50.

[29] Sun Y, Deng Z, Tian Y, Lin C. Horseradish peroxidase-mediated in situ forming hydrogels from degradable tyramine-based poly(amido amine)s. J. Appl. Polym. Sci. 2013;127:40-8.

[30] Kim KS, Park SJ, Yang JA, Jeon JH, Bhang SH, Kim BS, Hahn SK. Injectable hyaluronic acid-tyramine hydrogels for the treatment of rheumatoid arthritis. Acta Biomater. 2011;7:666-74.

[31] Jin R, Moreira Teixeira LS, Dijkstra PJ, van Blitterswijk CA, Karperien M, Feijen J. Enzymatically-crosslinked injectable hydrogels based on biomimetic dextran-hyaluronic acid conjugates for cartilage tissue engineering. Biomaterials 2010;31:3103-13.

[32] Pek YS, Kurisawa M, Gao S, Chung JE, Ying JY. The development of a nanocrystalline apatite reinforced crosslinked hyaluronic acid-tyramine composite as an injectable bone cement. Biomaterials 2009;30:822-8.

## Appendix I: List of Publications

### Original articles

1. Lee F, Chung JE, Kurisawa M. An injectable enzymatically crosslinked hyaluronic acid-tyramine hydrogel system with independent tuning of mechanical strength and gelation rate. Soft Matter 2008;4:880-7. (IF: 4.029, Times Cited: 101)

2. Lee F, Chung JE, Kurisawa M. An injectable hyaluronic acid-tyramine hydrogel system for protein delivery. J. Control. Release 2009;134:186-93. (IF: 7.705, Times Cited: 125)

3. Lee F, Kurisawa M. Formation and stability of interpenetrating polymer network hydrogels consisting of fibrin and hyaluronic acid for tissue engineering. Acta Biomater. 2013;9:5143-52. (IF: 6.025, Times Cited: 17)

4. Xu KM, Lee F, Gao SJ, Chung JE, Yano H, Kurisawa M. Injectable hyaluronic acid-tyramine hydrogels incorporating interferon-alpha 2a for liver cancer therapy. J. Control. Release 2013;166:203-10. (IF: 7.705, Times Cited: 23)

5. Wang L-S, Lee F, Lim J, Du C, Wan ACA, Lee SS, Kurisawa M. Enzymatic conjugation of a bioactive peptide into an injectable hyaluronic acid–tyramine hydrogel system to promote the formation of functional vasculature. Acta Biomater. 2014;10:2539-50. (IF: 6.025, Times Cited: 9)

6. Lee F, Lim J, Reithofer MR, Lee SS, Chung JE, Hauser CAE, Kurisawa M. Synthesis and bioactivity of a conjugate composed of green tea catechin and hyaluronic acid. Polymer Chemistry 2015;6:4462-72. (IF: 5.52, Times Cited: 1)

7. Bae KH, Lee F, Xu K, Keng CT, Tan SY, Tan YJ, Chen Q, Kurisawa M. Microstructured dextran hydrogels for burst-free sustained release of PEGylated protein drugs. Biomaterials 2015;63:146-57. (IF: 8.557, Times Cited: 1)

8. Xu K, Narayanan K, Lee F, Bae KH, Gao S, Kurisawa M. Enzyme-mediated hyaluronic acid–tyramine hydrogels for the propagation of human embryonic stem cells in 3D. Acta Biomater. 2015;25:159–71. (IF: 6.025, Time Cited: 2)

9. Xu K, Lee F, Gao S, Tan M-H, Kurisawa M. Hyaluronidase-incorporated hyaluronic acid–tyramine hydrogels for the sustained release of trastuzumab. J. Control. Release 2015;216:47-55. (IF: 7.705, Times Cited: 1)

10. Lee F, Chung JE, Xu K, Kurisawa M. Injectable degradation-resistant hyaluronic acid hydrogels cross-linked via the oxidative coupling of green tea catechin. ACS Macro Letters 2015;4:957-60. (IF: 5.764 )

### Review articles

1. Kurisawa M, Lee F, Wang L-S, Chung JE. Injectable enzymatically crosslinked hydrogel system with independent tuning of mechanical strength and gelation rate for drug delivery and tissue engineering. J. Mater. Chem. 2010;20:5371-5. (IF: 6.626, Times Cited: 31)

2. Lee F, Bae KH and Kurisawa M. Injectable hydrogel systems crosslinked by horseradish peroxidase. Biomed. Mater. 2016;11:014101. (IF: 3.697)

## Appendix II: Conference Presentations

1. Lee F, and Kurisawa M. Formation and Stability of Interpenetrating Polymer Network Hydrogels Consisting of Fibrin and Hyaluronic Acid for Tissue Engineering, *2nd IBN International Symposium, Singapore*, Dec. 8th –9th, 2014 (poster presentation).

2. Lee F, Chung JE and Kurisawa M. Development of Hydrogels Crosslinked by Green Tea Catechin for Biomedical Applications, *International Conference on Biomaterial Sciences, Tsukuba, Ibaraki Prefecture, Japan*, Mar. 15th – 18th, 2011 (presentation in print).

3. Lee F, Chung JE and Kurisawa M. An Injectable Hyaluronic Acid-Tyramine Hydrogel System for Protein Delivery, *1st NanoToday Conference, Singapore*, Aug. 4th, 2009 (oral presentation).

4. Lee F, Chung JE and Kurisawa M. Injectable Enzymatically-Crosslinked Hyaluronic Acid Hydrogels with Rapid Gelation and Tunable Mechanical Strength, *1st Asian Biomaterial Congress, Tsukuba, Ibaraki Prefecture, Japan*, Dec. 6th - 8th, 2007 (poster presentation).

5. Lee F, Chung JE and Kurisawa M. Injectable Hyaluronic Acid-Tyramine Hydrogel for Protein Delivery, *The 3rd SBE International Conference on Bioengineering and Nanotechnology, Singapore*, Aug. 12th - 15th, 2007 (poster presentation).